~~COMPLIMENTARY COPY~~

AUSTRALIAN JOURNAL OF PHYSICS

VOLUME 13, NUMBER 3, SEPTEMBER 1960

REGISTERED IN AUSTRALIA FOR TRANSMISSION BY POST AS A PERIODICAL

AUSTRALIAN JOURNAL OF PHYSICS

Published by the Commonwealth Scientific and Industrial Research Organization. Volumes 1 to 5 of the Australian Journal of Physics and the Australian Journal of Chemistry issued as the Australian Journal of Scientific Research, Series A : Physical Sciences. Issued quarterly, £2 per annum.

BOARD OF STANDARDS

The Board of Standards for this Journal is appointed by the Commonwealth Scientific and Industrial Research Organization and the Australian Academy of Science and consists of Professor Sir Macfarlane Burnet (Chairman), Dr. N. S. Noble (Editor), Professor N. S. Bayliss, Dr. J. L. Pawsey, Professor W. P Rogers, and Professor J. S. Turner.

ADVISORY COMMITTEE

Acceptance of papers for this Journal is in the hands of an Advisory Committee appointed by the Board of Standards in consultation with the Institute of Physics (Australian Branch) and consisting of Dr. N. S. Noble (Chairman and Editor), Dr. G. H. Briggs, Emeritus Professor L. G. H. Huxley, Dr. J. L. Pawsey, and Professor H. C. Webster.

OTHER JOURNALS PUBLISHED BY C.S.I.R.O.

Australian Journal of Chemistry Australian Journal of Biological Sciences Australian Journal of Applied Science	Issued quarterly, £2 per annum
Australian Journal of Agricultural Research	Issued six times a year, £2 per annum
Australian Journal of Marine and Freshwater Research Australian Journal of Botany Australian Journal of Zoology	Not issued at regular intervals, 10/– per issue

The Organization is a signatory to the Fair Copying Declaration, details of which may be obtained from the office of the Royal Society, London.

All enquiries and manuscripts should be forwarded to :

The Editor,
Australian Journal of Physics,
Commonwealth Scientific and Industrial Research Organization,
314 Albert Street, East Melbourne, C.2, Victoria

MELBOURNE

THE CONSTANT FLUX PROBLEM IN NON-UNIFORM EXPONENTIAL MEDIA

By P. R. Wilson*

[*Manuscript received April* 4, 1960]

Summary

A description is given of radiative transfer, under conditions of constant flux, in a semi-infinite medium in which the attenuation coefficient increases exponentially with depth, and has small sinusoidal variations in a direction parallel to the surface.

The directional intensity at the surface is evaluated numerically in several cases, and the extrapolation to other cases is discussed.

I. Introduction

In astrophysical problems the equation of transfer has usually been applied to plane parallel semi-infinite media, uniform except for possible variation with depth. Recently, however, investigations of the granulation in the solar photosphere and of the structure of the umbra and penumbra of sunspots have focused attention on the need for solutions for non-uniform media. Giovanelli (1959)† investigated the problem in which the attenuation coefficient, scattering parameter, and source function are independent of depth, but exhibit small sinusoidal variations as functions of one coordinate parallel with the surface.

In any discussion of stellar atmospheres, however, it is necessary to consider the extent to which the increase of attenuation coefficient with depth affects the solution of the equation of transfer. In the present paper the solution of the constant flux problem is undertaken for a plane parallel semi-infinite medium in which the attenuation coefficient, in addition to small sinusoidal variation parallel to the surface, increases exponentially with depth.

The transfer equation is solved here in terms of the total intensity, which is then integrated numerically to obtain the directional intensity at the surface.

II. The Equation of Transfer

Consider an isotropic medium in which $\varkappa$ is the attenuation coefficient, $\varkappa\lambda$ the absorption coefficient, $\varkappa\bar{\omega}_0$ the coefficient of single scattering, and S, the source function, is the ratio of emission per unit volume and solid angle to the attenuation coefficient. For a non-uniform medium, $\varkappa$, λ, $\bar{\omega}_0$, and S are scalar functions of position. The intensity of radiation, I, is a function of position and direction, while the total intensity J, defined by

$$J=\int_{4\pi} I\mathrm{d}\Omega,$$

is a function of position only.

---

* Department of Applied Mathematics, University of Sydney.

† Giovanelli, R. G. (1959).—*Aust. J. Phys.* **12**: 164.

From the transfer equation, Giovanelli (1959) obtained an equation for J embodying an approximation similar to that of Eddington,

$$\nabla^2 J=\frac{1}{\varkappa}\nabla J.\nabla\varkappa+\varkappa^2(\lambda J-4\pi S). \quad \ldots\ldots\ldots\ldots \quad (1)$$

If the medium is in radiative equilibrium, then

$$4\pi S=\lambda J,$$

and (1) simplifies to

$$\nabla^2 J=\frac{1}{\varkappa}\nabla J.\nabla\varkappa. \quad \ldots\ldots\ldots\ldots\ldots\ldots\ldots\ldots \quad (2)$$

The following discussion is confined to this conservative case.

III. Characteristics of the Medium

If the attenuation coefficient of a semi-infinite medium increases exponentially with depth below the surface and varies sinusoidally in one direction parallel to the surface, $\varkappa$ must have the form

$$\varkappa=\varkappa_0 e^{-\nu z}(1+\alpha\cos lx), \quad \ldots\ldots\ldots\ldots\ldots \quad (3)$$

the z-axis being normal to the surface $z=0$ and positive outwards. The simple model of a stellar atmosphere, in which the attenuation coefficient tapers off exponentially to a negligibly small value, corresponds to the limiting case where $\varkappa_0$ tends to zero. A non-zero value of $\varkappa_0$, with $\varkappa=0$ for $z>0$, provides a simple model for an atmosphere whose attenuation coefficient initially increases rapidly with depth and then more slowly according to (3).

Since the horizontal structure size is determined by $2\pi/l$, and the scale height by ν^{-1}, the appearance of the medium will be found to depend largely on whether ν/l is large or small as compared with unity.

IV. Solution of the Equation of Transfer in the Conservative Case

To solve (2) for a medium in radiative equilibrium carrying constant mean flux, J is expressed in the form

$$J(x,z)=\sum_n j_n(z)\cos nlx.$$

Here $j_0(z)$ is the mean value of the total intensity at depth z, while $j_1(z)$ is the amplitude of the variations in $J(x,z)$ having the same periodicity as the structure of the medium. For $n\geqslant 2$ the functions $j_n(z)$ represent distortions in the intensity distribution, and if α is sufficiently small they may be disregarded. Then

$$J(x,z)\simeq j_0(z)+j_1(z)\cos lx, \quad \ldots\ldots\ldots\ldots\ldots \quad (4)$$

where j_1/j_0 is assumed small. Substituting (4) with (3) into (2) yields

$$j_0''(1+\alpha\cos lx)+(j_1''-l^2 j_1)\{\cos lx+\tfrac{1}{2}\alpha(1+\cos 2lx)\}=j_1.\tfrac{1}{2}\alpha l^2(1-\cos 2lx)$$
$$-\nu\{j_0'+\tfrac{1}{2}\alpha j_1'+(j_1'+\alpha j_0')\cos lx+\tfrac{1}{2}\alpha j_1'\cos 2lx\}, \quad \ldots\ldots\ldots\ldots \quad (5)$$

where $j_0'=\mathrm{d}j_0/\mathrm{d}z$ and $j''=\mathrm{d}^2j_0/\mathrm{d}z^2$. Equating the coefficients of $\cos nlx$ when $n=0$ and $n=1$ yields

$$(j_0''+\nu j_0')+\tfrac{1}{2}\alpha(j_1''+\nu j_1'-2l^2j_1)=0, \qquad \ldots\ldots\ldots\ (6)$$

and

$$\alpha(j_0''+\nu j_0')+(j_1''+\nu j_1'-l^2j_1)=0. \qquad \ldots\ldots\ldots\ (7)$$

The coefficients of $\cos 2lx$ correspond to the distortion terms and may be ignored for sufficiently small α.

Elimination of j_0 and use of the approximation $\alpha^2=0$ yield a differential equation for j_1, having the solution

$$j_1=C_1\mathrm{e}^{pz}+D_1\mathrm{e}^{qz}, \qquad \ldots\ldots\ldots\ldots\ldots\ (8)$$

where $p=\frac{1}{2}\{-\nu+\sqrt{(\nu^2+4l^2)}\}$, $Q=-\frac{1}{2}\{\nu+\sqrt{(\nu^2+4l^2)}\}$, and C_1 and D_1 are constants of integration. Substitution in (6) or (7) yields the solution for j_0,

$$j_0=C_0+D_0\mathrm{e}^{-\nu z}+\tfrac{1}{2}\alpha(C_1\mathrm{e}^{pz}+D_1\mathrm{e}^{qz}), \qquad \ldots\ldots\ldots\ldots\ (9)$$

where C_0 and D_0 are also constants of integration. Thus

$$J(x,z)=C_0+D_0\mathrm{e}^{-\nu z}+(C_1\mathrm{e}^{pz}+D_1\mathrm{e}^{qz})(\tfrac{1}{2}\alpha+\cos lx). \qquad \ldots\ (10)$$

The constants of integration C_0, C_1, D_0, and D_1 are determined by the constant flux requirement and the boundary conditions. Deep within the medium the following conditions should hold.

(i) The mean intensity j_0 may increase linearly with optical depth but at no greater rate, as may be inferred by comparison with known solutions for uniform media.

(ii) The form of $J(x,z)$ should be self preserving, i.e. $\lim\limits_{z\to-\infty} j_1/j_0$ should exist and, from (4), should be small. As $z\to-\infty$, the mean optical depth behaves as $\mathrm{e}^{-\nu z}$. However, since $\lim\limits_{z\to-\infty}\mathrm{e}^{qz}/\mathrm{e}^{-\nu z}$ is infinite, condition (i) requires $D_1=0$.

Alternatively, from (6) and (7)

$$\begin{aligned}\lim_{z\to-\infty}\frac{j_1}{j_0}&=\lim_{z\to-\infty}\frac{D_1\mathrm{e}^{qz}}{\frac{1}{2}\alpha D_1\mathrm{e}^{qz}+D_0\mathrm{e}^{-\nu z}}\\&=2/\alpha\ \text{ if } D_1\neq 0,\\&=0\quad\ \text{ if } D_1=0.\end{aligned}$$

Since α is small, condition (ii) also requires $D_1=0$.

At the surface $z=0$, the inward radiation flux is assumed zero. As usual in the treatment of the plane parallel case, this leads to the condition

$$\varkappa J(x,0)=-\tfrac{2}{3}\mathrm{d}J(x,0)/\mathrm{d}z.$$

Substituting for J at $z=0$, $\cos lx=\pm 1$, we obtain C_0 and C_1 in terms of D_0, whence finally

$$J(x,z)=D_0\left\{\frac{2}{3}\frac{\nu}{\varkappa_0}+\mathrm{e}^{-\nu z}-1-\frac{2}{3}\frac{\alpha\nu}{\varkappa_0+\frac{2}{3}p}\mathrm{e}^{pz}\cos lx\right\}. \qquad \ldots\ (11)$$

Here also terms of order α^2 have been ignored.

The flux per unit area across any layer parallel to the surface is

$$-\frac{1}{3\varkappa}\,\frac{\mathrm{d}J(x,z)}{\mathrm{d}z}.$$

Deep within the medium this has the value

$$\frac{\nu D_0}{3\varkappa_0(1+\alpha\cos lx)}$$

and, if the net flux is independent of $\varkappa_0$ and ν, (**11**) takes the form

$$J(x,z)=A\left\{\tfrac{2}{3}+\frac{\varkappa_0}{\nu}(\mathrm{e}^{-\nu z}-1)-\frac{\alpha}{3/2+p/\varkappa_0}\mathrm{e}^{pz}\cos lx\right\}, \quad \ldots\ldots \quad (\mathbf{12})$$

where the constant A replaces $D_0\nu/\varkappa_0$ and is determined solely by the mean value of the net flux. In particular, the contrast at the surface, $j_1(0)/j_0(0)$, given by (**12**), is

$$j_1/j_0=-\alpha\varkappa_0/(\varkappa_0+\tfrac{2}{3}p). \quad \ldots\ldots\ldots\ldots\ldots\ldots \quad (\mathbf{13})$$

Thus an intensity maximum is associated with an attenuation minimum.

It is of interest to note that in the limit as $\nu\rightarrow 0$ (i.e. if the medium is uniform with depth), then $p\rightarrow l$ and

$$\lim_{\nu\rightarrow 0} J(x,z)=A\left\{\tfrac{2}{3}-\varkappa_0 z-\frac{\alpha}{3/2+l/\varkappa_0}\mathrm{e}^{lz}\cos lx\right\}.$$

This is similar in form to Giovanelli's solution for a medium which is uniform with depth.

V. THE DIRECTIONAL INTENSITY AT THE SURFACE

If θ is the angle between the emergent radiation and the z-axis, and φ is the azimuthal angle referred to the x-axis, the directional intensity $I(x,z,\theta,\varphi)$ at the surface ($z=0$) is found by integrating $J(x,z)$ along a path cutting the surface at x, in a direction given by θ and φ. The position coordinate s of any point on the path measures the distance from the surface to that point along the path, and is taken as positive below the surface. This yields the relations

$$\left.\begin{aligned} z&=-s\cos\theta,\\ \Delta x&=-s\sin\theta\cos\varphi.\end{aligned}\right\} \quad \ldots\ldots\ldots\ldots\ldots \quad (\mathbf{14})$$

In a volume of the path ds at s, the radiation scattered or emitted into unit solid angle in the direction of the path is $(1/4\pi)\varkappa(s)J(s)\mathrm{d}s$, where from (**3**) and (**14**)

$$\varkappa(s)=\varkappa_0\mathrm{e}^{\nu s\cos\theta}[1+\alpha\cos l(x-cs)], \quad \ldots\ldots\ldots \quad (\mathbf{15})$$

c representing $\sin\theta\cos\varphi$. Let $\Phi_s(t)$ be the fraction of the radiation which has suffered no further scattering or absorption at a distance t from the surface. Then in a further distance $-\mathrm{d}t$,

$$\mathrm{d}\Phi_s(t)=-\Phi_s(t)\varkappa(t)(-\mathrm{d}t).$$

After integrating this equation the fraction remaining at the surface, $\Phi_s(0)$, is found to be

$$\Phi_s(0)=\exp\left(\frac{\varkappa_0}{\nu\cos\theta}[\{1+\alpha\cos\psi\cos(lx+\psi)\}-e^{\nu s\cos\theta}\{1+\alpha\cos\psi\cos(lx-lcs+\psi)\}]\right), \qquad \ldots\ldots\ldots\ldots (\mathbf{16})$$

where $\tan\psi=(l/\nu)\tan\theta$. Thus the directional intensity at the surface is

$$I(x,0,\theta,\varphi)=\frac{1}{4\pi}\int_0^\infty \Phi_s(0)\varkappa(s)J(s)\mathrm{d}s, \qquad \ldots\ldots\ldots\ldots (\mathbf{17})$$

where

$$J(s)=A\left\{\tfrac{2}{3}+\frac{\varkappa_0}{\nu}(e^{\nu s\cos 0}-1)-\frac{\alpha}{3/2+p/\varkappa_0}e^{-ps\cos\theta}\cos l(x-cs)\right\} \ldots (\mathbf{18})$$

from (**14**) and (**11**).

It will be noted from (**17**) and (**11**) that the profiles of $I(x,0,\theta,\varphi)$ and $J(x,z)$ depend only on the values chosen for the ratios $\varkappa_0/\nu$, ν/l and on the value of α. Although the structure size of each profile depends on the actual values of l and ν, every position coordinate in (**17**) and (**11**) is multiplied by l or ν (or p, where $p=\frac{1}{2}\{-\nu+\sqrt{(\nu^2+4l^2)}\}$). Thus by specifying only the ratios ν/l and $\varkappa_0/l$, and evaluating I at various values of lx, (**17**) may be applied to media of any structure size merely by using the appropriate value of l.

VI. CALCULATIONS AND DISCUSSION

In the special case of the normal intensity at the surface, $\theta=\varphi=0$ and (**17**) becomes

$$I(x,0,0,0)=\frac{A}{4\pi}\left(\tfrac{2}{3}+\frac{1}{1+\alpha\cos lx}\right)-\frac{A}{4\pi}\cdot\frac{\alpha\cos lx}{3/2+p/\varkappa_0}\int_0^\infty e^{-\tau}\left(\frac{\nu}{\varkappa'}\tau+1\right)^{-p/\nu}\mathrm{d}\tau, \qquad \ldots\ldots\ldots\ldots (\mathbf{19})$$

where $\varkappa'=\varkappa_0(1+\alpha\cos lx)$ and $\tau(s)=(\varkappa'/\nu)(e^{\nu s}-1)$. The integral in (**19**) may be related to the incomplete gamma function. In three cases approximate forms are obtained.

(i) If $\nu/l\gg1$, $-p/\nu\simeq-(l/\nu)^2\simeq0$, and

$$I\simeq\frac{5}{12}\,\frac{A}{\pi}(1-\alpha\cos lx). \qquad \ldots\ldots\ldots\ldots (\mathbf{20})$$

(ii) If $\nu/l\ll1$, $-p/\nu\simeq-l/\nu\simeq-\infty$, and

$$I\simeq\frac{5}{12}\,\frac{A}{\pi}\left(1-\frac{3}{5}\alpha\cos lx\right). \qquad \ldots\ldots\ldots\ldots (\mathbf{21})$$

(iii) If $\varkappa_0/l\ll1$, $\alpha/(3/2+p/\varkappa_0)\ll1$, and

$$I\simeq\frac{5}{12}\,\frac{A}{\pi}\left(1-\frac{3}{5}\alpha\cos lx\right). \qquad \ldots\ldots\ldots\ldots (\mathbf{22})$$

It is useful to denote the ratio of the fractional variation in the surface intensity, $\Delta I/I_0$, to the fractional x-variation in attenuation coefficient, α, by the symbol β. Thus β describes the relative contrast at the surface. In case (i) above, $\beta=1\cdot 0$, while in (ii) and (iii), $\beta=0\cdot 6$. The case (iii) ($\varkappa_0/l\ll 1$) is important in astrophysics and it may seem surprising at first that β has the value $0\cdot 6$ for all non-zero values of ν/l (the case $\nu/l\ll 1$ and $\varkappa_0/l\ll 1$ is trivial). However, it will be shown that, when the radiation emerges at an angle to the normal, the relative contrast decreases as ν/l decreases.

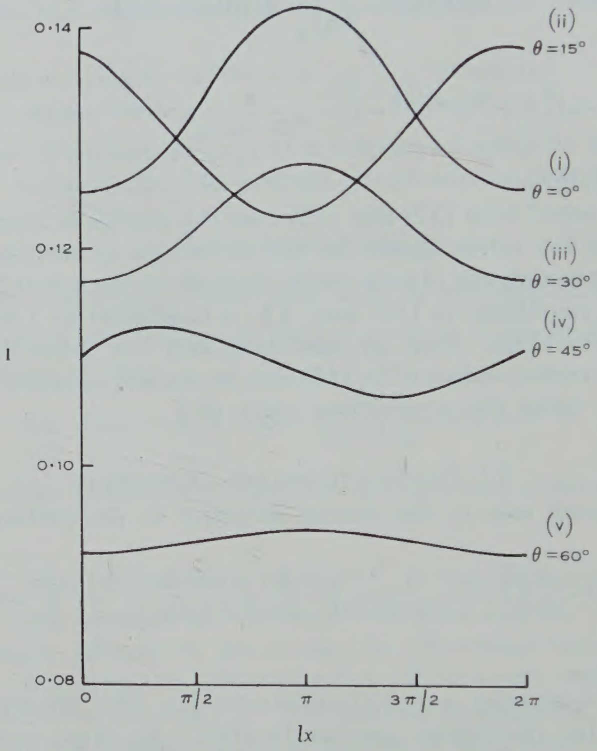

Fig. 1.—The directional intensity at the surface, $I(x,0,\theta,\varphi)$, against lx for $\varphi=0$ and (i) $\theta=0$, (ii) $\theta=15°$, (iii) $\theta=30°$, (iv) $\theta=45°$, (v) $\theta=60°$. In all cases $\varkappa_0/l=10^{-5}$, $\nu/l=1$, and $\alpha=0\cdot 1$.

For all cases involving non-zero values of θ and φ, $I(x,0,\theta,\varphi)$ must be evaluated numerically for various values of the coordinates x, θ, and φ, and of the parameters of the medium $\varkappa_0/l$, ν/l, and α. In Figures 1, 2, and 3, the results are shown for a typical case in which $\varkappa_0/l=10^{-5}$, $\nu/l=1$, and $\alpha=0\cdot 1$. The directional intensity $I(x,0,\theta,\varphi)$ is plotted against lx for various values of θ and φ. The curves obtained are obviously periodic, with wavelength $2\pi/l$. The characteristic features, the average intensity I_0, the relative contrast β, and the difference in phase between $I(\theta)$ and $I(0)$, ξ, are recorded in Table 1 for the curves of Figure 1. Also tabulated is the " darkening ", $I_0(\theta)/I_0(0)$, which is compared with Eddington's approximate relation $I_0(\theta)/I_0(0)=(2+3\cos\theta)/5$.

The contrast decreases with θ, as expected. The phase difference between $I(\theta)$ and $I(0)$ arises from the location of the source below the surface; it may easily be shown to be consistent with a simple model in which the sources of radiation are distributed over a plane parallel to the surface at about unit optical depth, varying sinusoidally in one direction. As $\varphi \to 90°$, $\xi \to 0$, as expected. The value of $\varkappa_0/l$ chosen in this case satisfies the condition for a continuously tapering medium. As expected, almost identical curves are found for $\varkappa_0/l=10^{-4}$ and 10^{-6}.

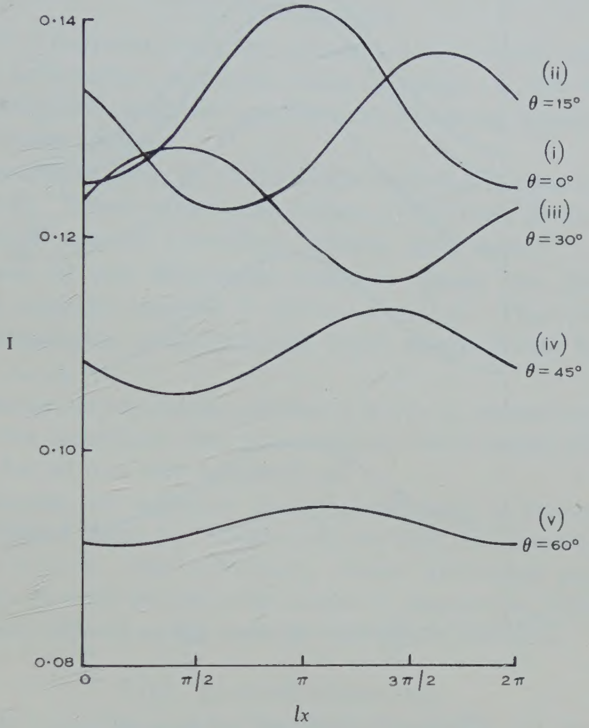

Fig. 2.—As for Figure 1, but $\varphi=45°$.

TABLE 1

FEATURES OF FIGURE 1

θ	0°	15°	30°	45°	60°
$I_0(\theta)$	0·1333	0·1305	0·1222	0·1095	0·0930
β	0·615	0·590	0·442	0·292	0·124
$\xi/2\pi$	0	0·45	1·01	1·71	2·50
$I_0(\theta)/I_0(0)$	1	0·979	0·921	0·821	0·697
$(2+3\cos\theta)/5$	1	0·980	0·920	0·824	0·700

To facilitate the extrapolation of the curves of Figures 1, 2, and 3 to other values of ν/l, many other cases have been evaluated. In Figure 4, β is plotted against γ, where $\gamma=\log_{10}\nu/l$, for $\varkappa_0/l=10^{-5}$, $\alpha=0\cdot1$, and various values of θ. For all but large values of θ, the relative contrast β is approximately $0\cdot6$ when

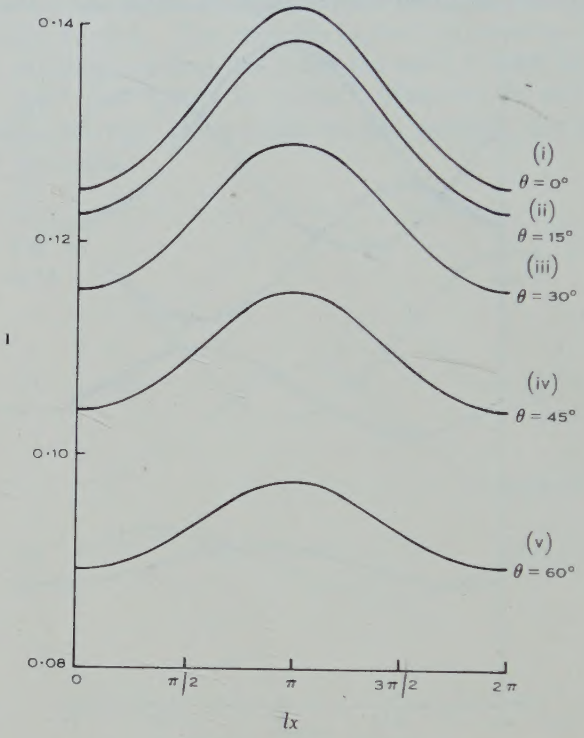

Fig. 3.—As for Figure 1, but $\varphi=90°$.

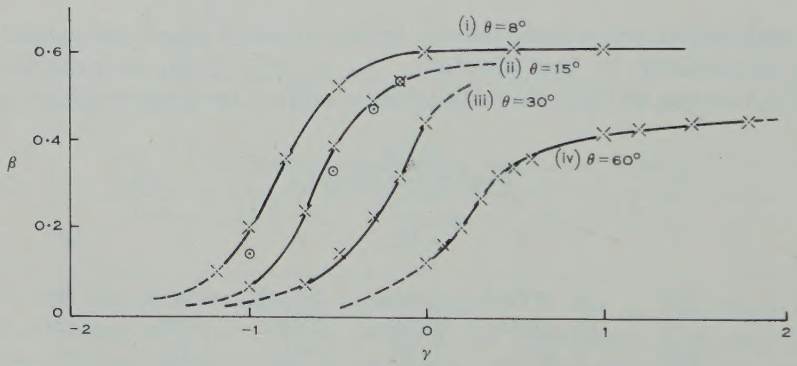

Fig. 4.—The graphs of β against γ, where $\gamma=\log_{10}\nu/l$ for $\varphi=0°$ and (i) $\theta=8°$, (ii) $\theta=15°$, (iii) $\theta=30°$, (iv) $\theta=60°$. In these cases, $\alpha=0\cdot1$ and $\varkappa_0/l=10^{-5}$. The points plotted thus, ⊙, are values of β calculated for $\alpha=0\cdot2$, $\theta=15°$, and $\varkappa_0/l=10^{-5}$.

ν/l is large (i.e. small scale heights and coarse structures), but decreases to zero as ν/l decreases; the greater the value of θ, the greater the rate of decrease. Points have also been plotted for $\theta=15°$ and $\alpha=0\cdot2$. The values of β undergo little change provided $\beta > 0 \cdot 2$. Thus the amplitude of the variations in intensity is directly proportional to the fractional variation in attenuation coefficient, α, provided α is small.

VII. CONCLUSIONS

The emission of radiation from the surface ($z=0$) of a semi-infinite medium, below which the attenuation coefficient takes the form (**3**), has been examined in the conservative case (radiative equilibrium) assuming constant flux across planes parallel to the surface.

The total intensity is given by (**12**) and the variation in total intensity across the surface by (**13**). These expressions reduce to the form given by Giovanelli (1959) in the special case of a medium uniform with depth.

The behaviour of the directional intensity across the surface may be described by the relative contrast β ($\beta = (1/\alpha)(\Delta I/I_0)$). The extent to which the increase in attenuation coefficient with depth affects β may be summarized thus:

(i) For radiation normal to the surface, $0 \cdot 6 < \beta < 1$, depending on the ratios $\varkappa_0/l$ and ν/l. In the important case of a medium which tapers off continuously ($\varkappa_0/l \ll 1$), $\beta = 0 \cdot 6$ for all non-zero values of ν/l.

(ii) The behaviour of radiation emerging obliquely is shown for a special case in Figures 1–3 and Table 1. Figure 4 shows that for a medium tapering off continuously, $0 < \beta < 0 \cdot 6$. For sufficiently coarse structures and small scale heights ($\nu/l \gg 1$), $\beta = 0 \cdot 6$ for all but large angles of emergence, while in all cases, the relative contrast falls off as the angle of emergence increases.

VIII. ACKNOWLEDGMENTS

The numerical integration of the integral of equation (**17**) was carried out on SILLIAC, the electronic digital computer of the Adolph Basser Computing Laboratory, School of Physics, University of Sydney, and the author expresses his thanks to the staff of this laboratory for their cooperation.

The author also wishes to thank Dr. R. G. Giovanelli, of the Division of Physics, C.S.I.R.O., who suggested the project and made himself available for many useful discussions.

MAGNETIC BAYS AT MACQUARIE ISLAND

By C. S. Robertson*

[*Manuscript received April* 4, 1960]

Summary

Polar magnetic bays are the most striking feature of magnetic records obtained by the Australian National Antarctic Research Expeditions at Macquarie Island. Negative bays are more numerous than positive bays and have greater amplitudes and durations. As a rule, negative bays commence about magnetic midnight whereas positive bays commence about 5 hr earlier. A daily reversal in direction of the bay-producing currents is indicated and the time at which this reversal takes place appears to vary with the seasons. During magnetically disturbed periods the ratio H bay amplitude to Z bay amplitude increases, indicating a northward movement of the bay-producing currents. At the same time auroras seen from Macquarie Island lie further north in the sky than usual.

I. Introduction

Since 1948 the Australian National Antarctic Research Expeditions have maintained a scientific station at Macquarie Island. A geomagnetic observatory, manned by officers of the Bureau of Mineral Resources, Geology and Geophysics, has operated there since 1950.

Macquarie Island (54·5° S., 159° E.) lies about 1° north of the southern auroral zone (cf. Bond and Jacka 1960) and the geomagnetic records are characteristic of that region. " Bay "-like indentations are prominent features on the magnetograms. In Figure 1 the record of October 24, 1954 is typical of " disturbed " periods while that of October 30, 1954 shows a less disturbed record. In the early part of this record a bay (or pair of bays) is formed by increase in the horizontal (H) and vertical (Z) components. Later in the day another bay is formed by decrease in H and Z. In the following discussion the first type (increase) will be termed a positive bay and the second type (decrease) a negative bay.

II. Characteristics of Bays

Most of the data used in this paper are from records of the sunspot-minimum year 1954. During that year 435 negative bays and 172 positive bays were recorded ; their distribution throughout the year is illustrated in the histograms of Figure 2. These show that most bays are recorded at or near the equinoxes—this is of course true of magnetic disturbances in general. Negative bays are more numerous and usually have amplitudes two or three times as great as those of positive bays ; in 1954 the average amplitude of negative bays was about 285 gammas. Although the beginnings and endings of many bays are poorly defined, it is possible to say that the average duration of negative bays (approximately 100 min) is roughly twice that of positive bays.

---

* Bureau of Mineral Resources, Geology and Geophysics, Melbourne.

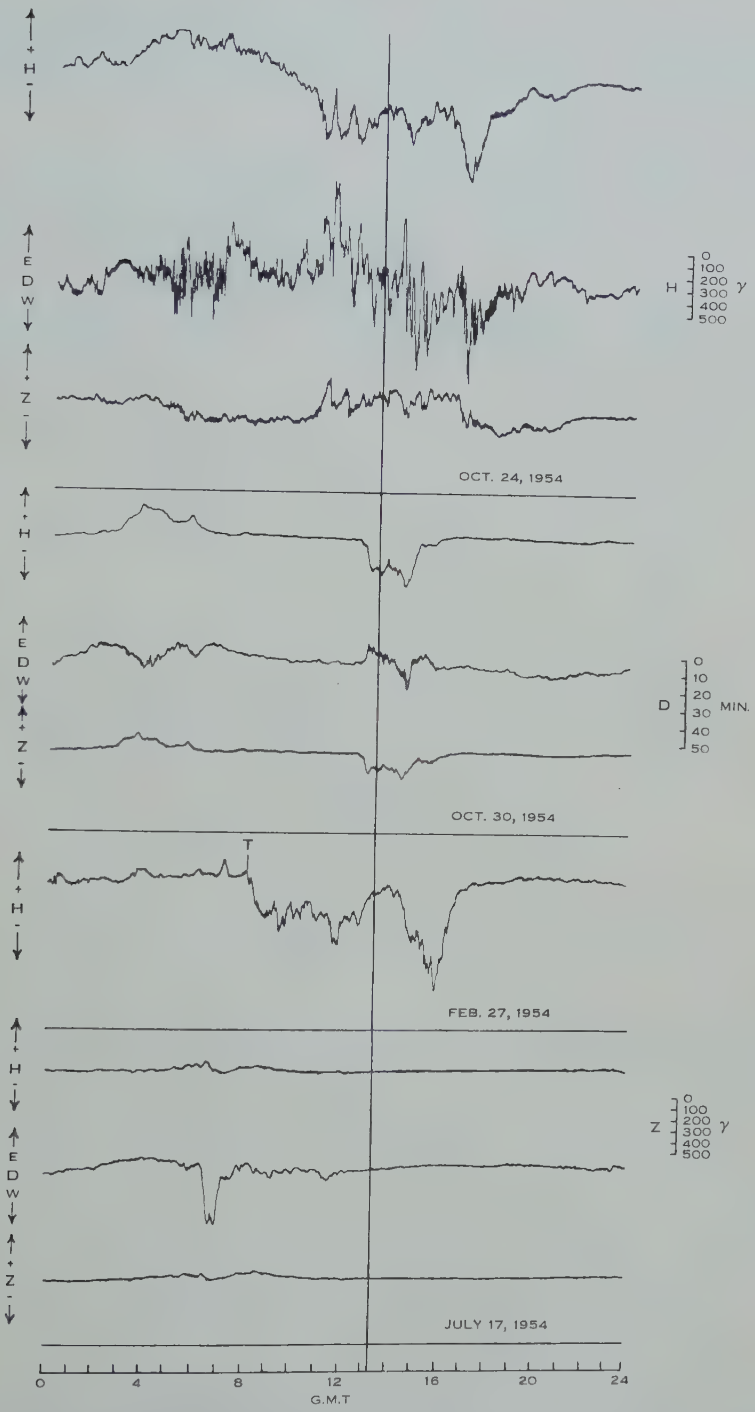

Fig. 1.—Tracings of Macquarie Island magnetograms. Scales of H, D, and Z variations are given on the right. The vertical line indicates the time (13·4 hr G.M.T.) of local midnight. For comment refer to text.

The amplitudes of all 1954 bays were plotted against their durations, to find whether these two quantities were related. Apart from the fact that most positive bays have amplitudes less than 80 gammas and durations less than 50 min, no trends could be discerned.

Figure 3 shows the variation through the year of monthly mean and extreme range of commencement times of bays recorded in 1954 ; there is an obvious grouping of the commencement times of negative bays around " magnetic midnight " (as defined by McNish (1936)). Almost all positive bays occur before magnetic midnight and most of them occur several hours before magnetic midnight. Although these diagrams suggest that there is considerable overlapping between the commencement times of negative and positive bays, it is usually found that on individual days there is no overlapping ; all bays before a certain time are positive and all bays after that time are negative. For example, on the magnetogram of February 27, 1954 (Fig. 1) there is a sudden reversal of the direction of disturbances from positive to negative at the time marked " T ". The transition is not always sudden but it is possible on about a quarter of all days to pick such a transition time by inspection of the records.

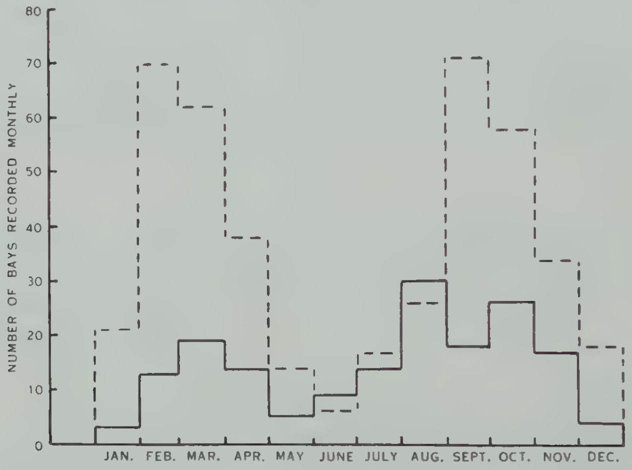

Fig. 2.—Variation of frequency of occurrence of bays in the H magnetograms through 1954 at Macquarie Island. The dashed line refers to negative bays, the full line to positive bays.

Several exceptions to this rule were recorded in the sunspot maximum period 1957–58 ; during large positive disturbances on stormy days a pronounced negative bay lasting about 1 hr sometimes occurred at about 7 or 8 hr G.M.T., some time before the general change-over to negative bays. Only one such case was observed during 1954.

Figure 4 illustrates the pattern of variation of transition times throughout the sunspot minimum year 1954 and the sunspot maximum year 1957–58. There appears to be a marked seasonal effect ; the transition from positive to negative bays is a few hours earlier at the equinoxes than at the solstices. In the data of 1954 the individual points cluster closely about the monthly mean ; in 1957–58 the scatter is much greater but the seasonal variation of monthly means is comparable.

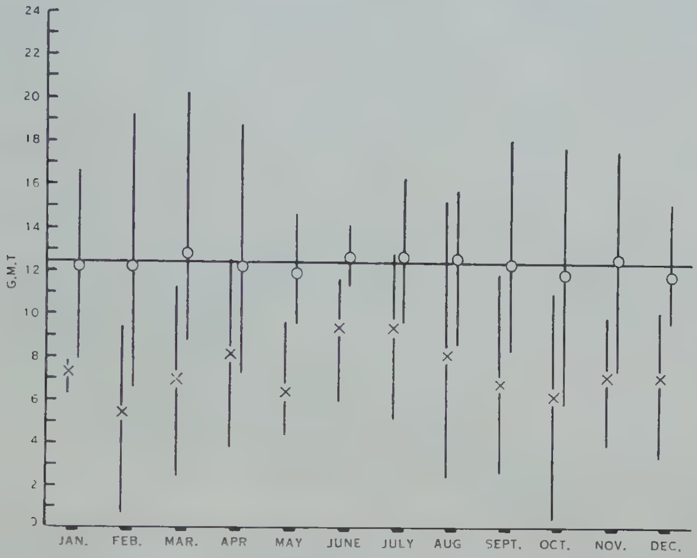

Fig. 3.—Variation of commencement times of bays in the *H* magnetograms through 1954 at Macquarie Island. Circles denote monthly means for negative bays, crosses for positive bays ; the vertical lines indicate the extreme range of commencement times. The horizontal line is at " magnetic midnight ".

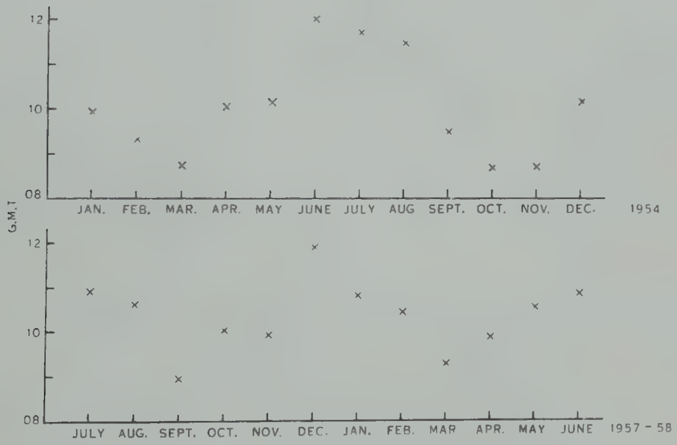

Fig. 4.—Variation through the years 1954 and 1957–58 of monthly mean times of transition from positive to negative bay activity in the *H* component at Macquarie Island.

It was thought that the transition times might be related to the degree of magnetic storminess and that the apparent seasonal effect might result from the larger number of disturbed days near the equinoxes. This could be so if the transitions occurred earlier on disturbed days than on quiet days. To test this possibility transition times were plotted against the daily K-index sums; this was done separately for equinoctial and solstice months. The plot for solstice (or other than equinoctial) months in 1954 shows some tendency for the points to form an elongated group, suggesting a correspondence between K sum and transition times. However, this tendency is not repeated in the plot for the equinoctial months of 1954, nor does it appear in either of the plots for the period July 1957 to June 1958. It seems probable then that there is a real seasonal variation in transition times.

So far this part of the paper has been concerned with magnetic bays which are evident on the H and Z component traces. Such bays are invariably accompanied by declination (D) component disturbances, but these are generally oscillatory in character and not of simple bay shape. The record of July 17, 1954 (Fig. 1) shows a different type of bay. It is evident that there is little disturbance on either H or Z but there is a pronounced negative bay in the declination component D. In 1954 about 80 such bays were recorded. All of these were negative (i.e. the westerly declination increased) and all occurred in the intervening period between the times when positive H, Z bays and negative H, Z bays were most common.

From the foregoing facts about magnetic bays at Macquarie Island it is possible to draw a number of fairly definite conclusions. It is clear from the reversal in bay sign that the bay-producing currents flowing near the southern auroral zone change direction from eastward to westward in the early evening of each day and that about this time currents often flow northward over the recording station producing bays in declination only.

These facts may be explained qualitatively by several different theories (e.g. Maeda 1957) which postulate that currents are due to an excess of ions of one sign carried along in some way by ionospheric winds. It appears that the bay-producing current system rotates so that it presents the same general pattern as viewed from the Sun. This could result from a wind pattern fixed relative to the Sun while bay-producing ionization takes place in bursts, giving rise to considerable variation in current intensity. The normal diurnal variation may be produced by less intense but more regular ionization operating in conjunction with the same wind system. The large excess of negative bays over positive bays indicates a preponderance of bay-producing ionization on the night side of the Earth. The apparent seasonal variations in the change-over times from positive to negative bays suggests that magnetic bay studies may make useful contributions to the understanding of upper atmospheric wind systems.

III. Correlation between Bays and Auroras

It has long been recognized that the polar bay type of magnetic disturbance is often accompanied by visible aurora. Some aspects of the relation between the two phenomena have been investigated.

The magnetic records and records of auroral observations for the year 1954 were studied closely to determine whether simultaneous onset of magnetic bays and the auroras generally occurred. Of 77 nights on which the sky was clear and it was possible to decide whether the first bay activity coincided with the first auroral activity, good agreement was noted on 35 nights. On 16 more nights there was agreement in the absence of both magnetic and auroral activity; as absence of activity is comparatively rare in each phenomenon the probability of chance coincidence is low. Of the remaining 26 nights 14 would have shown agreement but for the observation of auroral glow at a time when there was no magnetic bay activity. Glows are frequently the upper limits of very distant auroras so that the magnetic effects of currents associated with them may be very weak; these cases cannot be regarded as conclusive.

Summarizing these findings:

Bays and auroras commenced together	35 nights
Neither was recorded all night	16
Results inconclusive	14
Only one recorded, or times disagree	12
Total	77

It is clear that in most cases magnetic bays and auroras do commence at about the same time.

Once bays have begun, magnetic fluctuations are usually so frequent that further correlation with the auroras is more difficult. It seems likely that a burst of ionization impinging on the ionosphere in the auroral zone produces the visible aurora and at the same time creates the condition in the ionosphere necessary for a bay, which commences simultaneously with or soon after the visible aurora. Arcs and bands are the auroral forms most frequently associated with the commencement of bays.

Observations at Macquarie Island also demonstrate that the bay-producing currents and the aurora are more or less coincident in space. On most days the Z component trace closely resembles the H component trace, as for example on October 31, 1954 (Fig. 1). Easterly or westerly currents several degrees polewards of the recording station would account for this. However, on many magnetically disturbed days the H and Z traces are observed to be quite dissimilar: a general increase in the value of the H component may be accompanied by a general decrease in the value of the Z component or vice versa. These effects would be caused by easterly or westerly currents situated equatorwards of the recording station. For example, on the magnetogram for October 24, 1954 (Fig. 1) a positive bay or series of bays between about 5 and 10·5 hr is accompanied by depressed values in Z. After 10·5 hr a series of pronounced negative H bays occurs and is accompanied by generally increased values of Z lasting until about 17·5 hr, after which H disturbances again tend to be positive and Z disturbances negative.

It may be noted that, although the Z component trace shows an average increase between 10·5 and 17·5 hr, it exhibits small variations which correspond in form and sign to bays in H. This suggests the continued presence of a varying current located polewards from the recording station in addition to a current situated equatorwards from the station.

In 1954 there were 15 days on which the Z trace remained neutral or became generally positive during negative H bays. All except one of the 15 days were very disturbed magnetically and, during all on which the night sky was clear, auroras were observed overhead or to the north of the island, rather than only to the south as was normal. Moreover, these 15 days include the times when all the most brilliant auroral displays of the year were seen.

These observations at Macquarie Island strongly support the view that magnetic bay-producing currents and the aurora are closely related in both time and space.

IV. ACKNOWLEDGMENTS

The author wishes to thank the Bureau of Mineral Resources, Geology and Geophysics of the Department of National Development, for permission to use data from the magnetic observatory at Macquarie Island. Thanks are due also to the Antarctic Division of the Department of External Affairs for supplying auroral data.

V. REFERENCES

BOND, F. R., and JACKA, F. (1960).—*Aust. J. Phys.* **13** : 610.
MCNISH, A. G. (1936).—*Terr. Magn.* **41** : 37.
MAEDA, H. (1957).—*J. Geomagn. Geoelect., Kyoto* **9** : 119.

MOTION OF THE AURORA AND MAGNETIC BAYS

By F. R. Bond*

[*Manuscript received April 4, 1960*]

Summary

Observations from the ANARE station at Macquarie Island show that the development of an auroral display is characterized by a slow northward drift, east to west longitudinal motion, and an associated positive bay in the horizontal component magnetogram in the evening hours. This is followed by a sudden change in structure of the aurora and appearance of a negative bay. The negative bay persists for some hours, accompanied by west to east longitudinal motion and slow southward drift of the aurora.

The co-latitude of the northern limits of the aurora is shown to be strongly dependent on level of geomagnetic disturbance.

It is suggested that the observed motions are the mass motions of electrons which constitute the magnetic bay producing current within the boundaries of the auroral form.

I. Introduction

The data used in this paper are from the records of visual observations of the aurora at the Australian National Antarctic Research Expeditions' (ANARE) station at Macquarie Island and from volunteer observers' reports in eastern Australia collected by the Auroral Data Centre.

The auroras considered were located on or to the north of the southern auroral zone which lies approximately 1° south of Macquarie Island (Bond and Jacka 1960). In this region auroras are usually aligned or extended roughly along parallels of geomagnetic latitude. The observations were recorded mainly during the period of the International Geophysical Year 1957–58.

Attention is confined to the large-scale motions of the aurora as a whole across the sky and associated geomagnetic disturbance. Changes of internal structure such as movements of rays along an "arc" or "band" are not considered.

II. Magnetic Bays

A study of magnetic bays recorded at Macquarie Island during 1954 has been reported by Robertson (1960). Examination of the magnetic records for 1958 showed trends similar to the records for 1954.

Positive bays in the horizontal component H occurred less frequently than negative bays, their duration was shorter and their amplitude less. Many positive bays commenced during daylight, mainly between $14^{\mathrm{h}}\,30^{\mathrm{m}}$ and $18^{\mathrm{h}}\,30^{\mathrm{m}}$ local time; while negative bays occurred during the night hours, commencing mainly between $18^{\mathrm{h}}\,30^{\mathrm{m}}$ and $04^{\mathrm{h}}\,30^{\mathrm{m}}$. The time of change-over from positive bay to negative bay most frequently occurred between $21^{\mathrm{h}}\,00^{\mathrm{m}}$ and $22^{\mathrm{h}}\,00^{\mathrm{m}}$.

---

* Antarctic Division, Department of External Affairs, Melbourne.

III. Motion of the Aurora

(a) *Typical Development of a Display*

Climatic conditions at Macquarie Island are extremely unfavourable for auroral observing; the sky is very rarely clear for more than a few hours at a time. However, an examination of the Macquarie Island observations over the period 1951–1959 indicates that the main pattern of auroral behaviour may be described in terms of two phases.

The first phase commences as a succession of one or more arcs or bands appearing above the southern horizon. Aligned roughly along parallels of geomagnetic latitude, these arcs or bands may show rayed structure of intensity 1 or 2 and very rarely intensity 3 (on the usual 0–4 scale). There is, then, a general northwards progression of the display. This may be a continuous drift, sometimes with a succession of advances or retreats; or it may be a discontinuous progression involving fading of the aurora at one position and a new appearance at another. A new arc or band may form in advance of an existing display. An arc or band may disappear only to be replaced by another further to the south and the advance be repeated. When this phase has a duration exceeding 30 min it is almost invariably associated with a positive bay in the H magnetogram.

In general, the northward drift continues until the beginning of the second phase which is characterized by a quite sudden increase in intensity and development of bright rayed structure. This may be followed by flaming. The discrete structure is replaced by moving diffuse rayed forms and pulsating and diffuse surfaces which latter slowly drift or progress to the south. This second phase is always associated with a negative bay in the H magnetogram.

This main sequence may be halted at any stage and one or more stages may be absent. Occasionally after the second phase has begun arcs reappear for a short time interval and the whole or part of a sequence may be repeated one or more times.

The lateral drifts of individual forms and lateral progression of the display as a whole referred to above, take place typically at a rate of a few degrees of latitude per hour (cf. Jacka 1953) corresponding to speeds of the order of 100 m/sec. Canadian observations by Kim and Currie (1958) on individual auroral forms show a modal value of north-south drift speed of 50–100 m/sec. They also find some evidence for an increase of drift speed with increase in geomagnetic disturbance.

During times of very marked geomagnetic disturbance the complicated auroral situation over Macquarie Island is difficult to interpret in detail, but in these cases the pattern of the aurora as described above seems to apply to the observations from southern Tasmania and, for the major magnetic storms, to the observations from further north in Australia.

The patterns of the auroral display as observed at Macquarie Island appear to be very similar to those described by Heppner (1954) and Elvey (1957) for the approximately magnetically conjugate location, College, Alaska Heppner notes that in general the first appearing arcs and bands approximately coincide in time with the recording of a positive bay in H, while the change-over to a negative bay is associated with the appearance of bright rayed structure and subsequent break up in the arc nearest the equator.

The Macquarie Island 1958 aurora records were examined in detail, in conjunction with the magnetograms to see to what extent a detailed correspondence, similar to that recorded by Heppner, existed.

Auroral reports for 62 nights were examined. It was found that on 11 nights auroral behaviour was quiet and positioned well to the south of Macquarie Island; these were all nights of little magnetic activity. On 46 nights, auroral behaviour and magnetic behaviour did not contradict the Heppner patterns, although in some cases the auroral record was somewhat meagre. Of the remaining 5 nights, on 3 of them the auroral behaviour is difficult to classify, while on 2 nights bright rayed displays occurred at times when the magnetograms showed positive bays. On both occasions these bright rayed displays were at least 1° of latitude to the south, rather than overhead or to the north, which is more usual.

(b) *Co-latitude of Auroras and* K_p

Using data obtained during the I.G.Y., synoptic maps have been prepared showing, at 15-min intervals, the distribution of auroras in the region of Macquarie Island and eastern Australia. Auroral positions were computed from recorded elevations and azimuths of points on the lower border, assumed at a constant height of 105 km.

From the maps the co-latitude of the most northerly lower border crossing geographic longitude 152° E. was extracted for each quarter hour and tabulated against the prevailing K_p-index. These data are represented in Figure 1, which shows clearly the equatorwards appearance of the northernmost auroral form with increasing magnetic disturbance. Over the range of K_p values 1–7, the mean co-latitudes in Figure 1 are comparable with those reported for homogeneous arcs at Macquarie Island by Jacka (1953). A similar relation with the K-index recorded at Macquarie Island is apparent in the radio-echo observations tabulated by Gadsden (1959*a*).

(c) *Longitudinal Motion*

Observations of longitudinal motion of auroras were made by G. Cowling, a member of the ANARE at Macquarie Island in 1958. Mr. Cowling also carried out a preliminary analysis.

Measurements of elevation and azimuth to points on the lower border were made using an open sights theodolite and successive positions of the aurora were plotted on grids showing reference lines for elevation and azimuth. When, due to rapid movement of the auroral form, measurements were not possible, the initial position of the aurora was estimated and the direction of movement noted. Longitudinal motion, that is, motion in the direction in which the aurora is aligned or extended, was recorded in 33 cases.

Of these 33 cases, 6 were of east to west motion and 27 of west to east motion. The former occurred at or before $22^{h}\ 36^{m}$, the latter between $22^{h}\ 01^{m}$ and $06^{h}\ 01^{m}$ local time. In 5 cases only was it possible to estimate speeds of longitudinal motion; these estimates lay in the range 200–1000 m/sec. Comparable speeds are reported by Kim and Currie (1958), who also find an increase in speed with increase in magnetic disturbance.

Direction of longitudinal motion of auroral forms was compared at corresponding times with the H component magnetogram. In general it was found that positive departures $(+\Delta H)$ from the quiet-day curve corresponded with east to west motions of the aurora, while negative departures $(-\Delta H)$ corresponded with west to east motions. This trend is illustrated in Table 1.

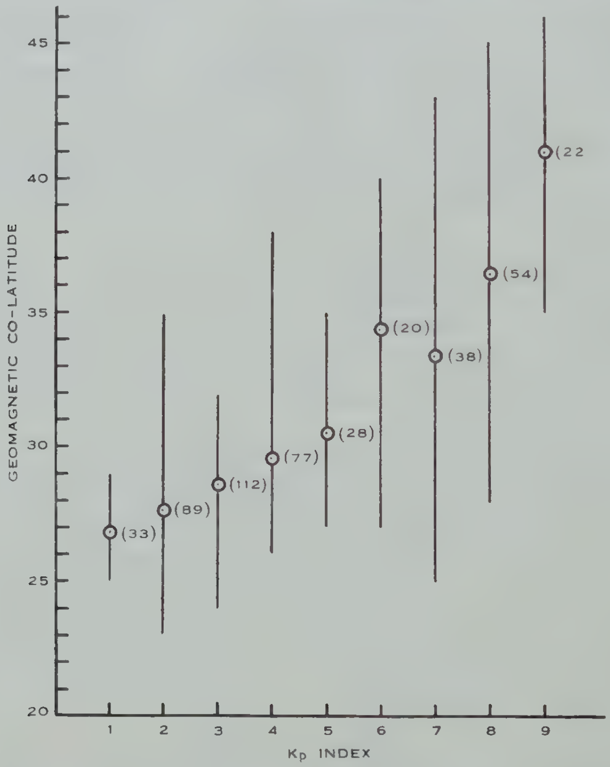

Fig. 1.—Co-latitude of the northernmost auroral lower border versus K_p. The circle represents the mean, the line represents the total range, of co-latitude, and the numbers give the total of quarter-hourly observations, for each value of K_p. (Data from gg. longitude 152 °E.)

It should be noted that in the arc or band type of aurora present during a positive bay, longitudinal motion is virtually along itself and can be recognized only when a discontinuity can be discerned. Discontinuities of recognizable size or shape are not of frequent occurrence. Moreover, it has already been noted that a proportion of positive bays commence during daylight, and that positive bays are of shorter average duration than negative bays. It is presumably for these reasons that the number of recorded cases of east to west motion is small.

These limitations are not present when radio-echo methods are used to trace the motion of ionization at auroral heights. Unwin (1959) has reported such motions over Macquarie Island and has shown that the echoes come from a layer, a few to 25 km thick, centred between a height of 110 km and a little more than 120 km. Unwin found that east to west moving echoes occurred between about $15^h\ 30^m$ and $01^h\ 30^m$ local time, while west to east moving echoes occurred between about $18^h\ 30^m$ and $09^h\ 30^m$ local time. On any one occasion the change from westerly to easterly motion was quite distinct. Velocities ranged from about 200 to 4000 m/sec. Unwin reports a distinct increase in velocity with increasing values of the Macquarie Island K-index.

A summary of some observations of auroral motion and motion of auroral ionization in the northern hemisphere is given in Table 2. The marked similarity with the data of this paper and with those of Unwin is clear.

TABLE 1

MOTION OF THE AURORA, MACQUARIE ISLAND 1958

Direction of Auroral Motion	Number of Cases		
	$+\Delta H$	$-\Delta H$	No Departure
East to west	4	1*	1
West to east	—	27	—

* Value -15γ, a small value for this station.

IV. DISCUSSION

The results of this and quoted works may be summarized as follows. Northward lateral drift or progression and westward longitudinal motion of auroral luminosity and auroral ionization are each associated with positive magnetic bays. Southward drift or progression and eastward longitudinal motion are associated with negative bays. Whether there is a direct association of lateral drift and longitudinal motion of individual auroral forms cannot be ascertained from the present data. These are not precise enough to enable detection of slow lateral drift during the relatively short time intervals in which longitudinal motion is usually discernible. Speeds of longitudinal motion are an order of magnitude greater than lateral drift speeds.

Positive magnetic bays and associated auroral movements northwards and westwards are characteristic of the evening hours. Negative bays and associated movements are characteristic of the night and early morning hours. The transition is usually rapid and may occur within a time range of several hours (but usually within a range of about 1 hr) centred a little before midnight.

The maximum co-latitude and the speed of longitudinal motion and possibly of lateral drift increase with geomagnetic disturbance.

It is apparent that the longitudinal motion takes place in the direction of an electron current which would produce the observed sign of magnetic bays.

TABLE 2

LONGITUDINAL MOTION OF THE AURORA AND MAGNETIC BAYS—SUMMARY

Observers' Location	Approx. Gm. Lat. of Auroras	Time of E. to W. Movement	Time of W. to E. Movement	Type of Bay during Movement		Longitudinal Speed (m/sec)	Reference
				E. to W.	W. to E.		
Yerkes	53 °N	Prior to $24^h\ 00^m$	After $24^h\ 0\ ^m$			100–1400	Meinel and Schulte (1953)
Saskatoon	61 °N	Prior to $02^h\ 00^m$	Throughout the night				Meek (1954)
College	65 °N	$16^h\ 00^m$–$02^h\ 00^m$	$23^h\ 00^m$–$08^h\ 00^m$		—		Heppner (1954)
Ithaca	61 °N	Early in the night	Late in the night				Bless, Gartlein, and Kimball (1955)
Jodrell Bank	55 °N	Prior to $21^h\ 00^m$–$22^h\ 00^m$	After $21^h\ 00^m$–$22^h\ 00^m$	+	—	0–2800	Bullough *et al.* (1957) Bullough and Kaiser (1955)
College	65 °N	Mainly prior to $22^h\ 00^m$	Mainly after $22^h\ 00^m$	+	—	350–2000	Nichols (1957)
Saskatoon Flin Flon Uranium City	61 °N 64 °N 56 °N	$18^h\ 00^m$–$02^h\ 00^m$	$22^h\ 00^m$–$04^h\ 00^m$			90–1183	Kim and Currie (1958)
Saskatoon	61 °N	Mainly prior to $24^h\ 00^m$	Mainly after $24^h\ 00^m$	+	—	0–670	Lyon and Kavadas (1958)
Invercargill	61 °S	$15^h\ 30^m$–$01^h\ 30^m$	$18^h\ 30^m$–$09^h\ 30^m$			200–4000	Unwin (1959)
Macquarie Island	61 °S	Prior to $22^h\ 30^m$	$22^h\ 00^m$–$06^h\ 00^m$	+	—	200–1000	This paper

Gadsden (1959*b*) has shown that the occurrence of auroral ionization (giving rise to radar echoes) and of visible auroral luminosity are statistically independent events. However, the morphologies of these phenomena are similar.

The simplest hypothesis consistent with the observations is that the radio and optical methods detect different attributes (produced by different causes, either of which may be absent) of the one basic auroral phenomenon. This is characterized by a slow lateral drift and more rapid longitudinal motion. This motion of patterns of ionization and/or luminosity is identified with the mass motion of electrons which constitutes a magnetic bay producing electric current within the narrow confines of the auroral phenomenon. At any one time several such phenomena, generally roughly parallel to one another, may be observable from the one station.

V. Acknowledgments

The writer acknowledges the benefit of discussions with Dr. F. Jacka, Chief Physicist, and Mr. K. D. Cole of the Antarctic Division, Department of External Affairs, and also with members of ANARE. The Macquarie Island magnetograms were made available by the Bureau of Mineral Resources, Geology and Geophysics, Department of National Development.

VI. References

Bless, R. C., Gartlein, C. W., and Kimball, D. S. (1955).—*Astrophys. J.* **122** : 205.

Bond, F. R., and Jacka, F. (1960).—*Aust. J. Phys.* **13** : 610.

Bullough, K., and Kaiser, T. R. (1955).—*J. Atmos. Terr. Phys.* **6** : 198.

Bullough, K., Davidson, T. W., Kaiser, T. R., and Watkins, C. (1957).—*J. Atmos. Terr. Phys.* **11** : 237.

Elvey, C. T. (1957).—*Proc. Nat. Acad. Sci., Wash.* **43** : 63.

Gadsden, M. (1959*a*).—*Ann. Géophys.* **15** : 395.

Gadsden, M. (1959*b*).—*Ann. Géophys.* **15** : 403.

Heppner, J. P. (1954).—Thesis, California Institute of Technology.

Jacka, F. (1953).—*Aust. J. Phys.* **6** : 219.

Kim, J. S., and Currie, B. W. (1958).—*Canad. J. Phys.* **36** : 160.

Lyon, G. F., and Kavadas, A. (1958).—*Canad. J. Phys.* **36** : 1661.

Meek, J. H. (1954).—*Astrophys. J.* **120** : 602.

Meinel, A. B., and Schulte, D. H. (1953).—*Astrophys. J.* **117** : 454.

Nichols, B. (1957).—Sci. Rep. No. 1, Air Force Contract No. AF 19(604)—1859, Geophysical Institute, University of Alaska.

Robertson, C. S. (1960).—*Aust. J. Phys.* **13** : 470.

Unwin, R. S. (1959).—*Nature* **183** : 1044.

A DYNAMO THEORY OF THE AURORA AND MAGNETIC DISTURBANCE*

By K. D. Cole†

[*Manuscript received April* 4, 1960]

Summary

A model of an aurora regarded as a plane slab of highly ionized air parallel to the geomagnetic field within the ionosphere is examined. The model is stable in the presence of a wind of neutral molecules which, blowing the slab across the geomagnetic field, generates an electric polarization field perpendicular to its faces and a current along its length. This current is concentrated in a small height range and is chiefly due to electron drift.

The aurora moves normal to itself with a speed of the same order as the wind speed, while the drift carries its luminosity and ionization pattern along its length at a speed an order of magnitude greater. Measurement of these speeds will permit determinations of collision frequencies of ions and electrons within the aurora.

Assuming, in the equatorial vicinity of the auroral zone, an equatorwards wind in the evening and a polewards wind in the night and morning hours it is possible to explain the major movements of the aurora and associated bay type magnetic disturbances. It is suggested that the magnetic disturbance indices K and K_p are indicators of wind speed. A likely mechanism of maintenance of luminosity and ionization in the aurora is outlined. The general features of magnetic disturbance current systems within the auroral zone are briefly considered in relation to the theory and it is suggested that auroras are visible manifestations of the current flow.

Qualitative speculation on a possible source of energy for winds in the polar dynamo region leads to a unified account of the Van Allen radiation belts, auroras, and some (low latitude) airglow.

I. INTRODUCTION

Two parameters are required to define the atmospheric dynamo problem, namely, the conductivity of the ionosphere and the velocity of the wind. The quiet daily variations in the geomagnetic field can be explained in terms of the conductivity of the quiet ionosphere in conjunction with the velocity of wind inferred from atmospheric tidal oscillations (Baker and Martyn 1953). To define a model for the explanation of geomagnetic disturbance one has, in the absence of other criteria, the choice of specifying a disturbed conductivity pattern (Obayashi and Jacobs 1957) and/or a disturbed wind velocity (Maeda 1957).

The present paper does not attempt to explain the world-wide distribution of magnetic disturbance, but rather considers a highly probable local situation. A model of the aurora is defined and its properties examined. These are compared with observational data, especially on large-scale movements of the aurora and associated magnetic disturbance.

---

* Preliminary accounts of this work were presented at ANZAAS, Perth, August 1959, and at the Antarctic Symposium, Buenos Aires, November 1959.

† Antarctic Division, Department of External Affairs, Melbourne.

Although a one-to-one correspondence has not been established between the luminosity, magnetic, and radar observations of the aurora, these are here treated as aspects of the one phenomenon (Bond 1960) supposed as having the form of the common auroral " arcs " and " bands ". These are typically long (thousands of kilometres) compared to their vertical extent (tens to hundreds of kilometres) and to their thicknesses (a few kilometres).

II. THEORY

The current density at any point in an ionized gas is given by

$$\mathbf{j}=\sigma_0\mathbf{E}_{||}+\sigma_1\mathbf{E}_{\perp}+\sigma_2(\mathbf{H}\times\mathbf{E}_{\perp})/H, \quad \ldots\ldots\ldots\ldots \quad (1)$$

where $\mathbf{E}$ is the electric field and $||$ and $\perp$ indicate components parallel and perpendicular to the magnetic field $\mathbf{H}$. σ_0, σ_1, σ_2 are the direct (parallel to $\mathbf{H}$), Pedersen (transverse), and Hall conductivities respectively.

In a lightly ionized gas

$$\begin{aligned}\sigma_0&=Ne^2(1/m_i\nu_i+1/m_e\nu_e),\\ \sigma_1&=Ne^2(t_i+t_e),\\ \sigma_2&=-Ne^2(h_i-h_e),\end{aligned}$$

where N=electron density, e=charge on electron,

$$\begin{aligned}t_{e,i}&=\nu_{e,i}/m_{e,i}(\nu^2_{e,i}+\omega^2_{e,i}),\\ h_{e,i}&=\omega_{e,i}/m_{e,i}(\nu^2_{e,i}+\omega^2_{e,i})\,;\end{aligned}$$

where $\nu_{e,i}$, $\omega_{e,i}$, and $m_{e,i}$ are the collision frequencies (with neutral particles), gyro frequencies, and masses of electrons and ions respectively. The assumption is made that the mobilities t and h are independent of ionization density N.

In general σ_0 is much larger than σ_1 or σ_2; however, our first considerations are restricted to situations in which $\mathbf{E}_{||}$ is zero. Later (in Section III (*b*)) limited consideration is given to the effects of a non-zero $\mathbf{E}_{||}$.

(*a*) *The Model*

(i) *The Steady State*.—Clemmow, Johnson, and Weekes (1955) have examined the motion of a cylindrical irregularity in an ionized medium. We investigate another elementary model now proposed. As with Clemmow, Johnson, and Weekes, dissipative effects such as diffusion and recombination are neglected here.

Given a homogeneous, unbounded, weakly ionized neutral gas with ionization density N (ions) in the presence of uniform and steady orthogonal electric and magnetic fields $\mathbf{E}^0$, $\mathbf{H}$, is there a steady state solution for which an infinite plane slab parallel to H and of ionization density N' (ions) persists in the gas without change of form?

The unit normal ($\mathbf{n}$) outward from the slab makes an angle α with $\mathbf{E}^0$. Rectangular axes $0(x, y, z)$ with unit vectors $\mathbf{e}_1$, $\mathbf{e}_2$, $\mathbf{e}_3$, have the directions of $\mathbf{E}^0\times\mathbf{H}$, $\mathbf{E}^0$, and $\mathbf{H}$ respectively (see Fig. 1). The superscript 0 is used for quantities in the undisturbed state in the absence of the slab and the superscript p

for the incremental quantities resulting from polarization charge. The total electric field is $\mathbf{E}^0+\mathbf{E}^p$. The geometry of the model will make $\mathbf{E}^p$ orthogonal to $\mathbf{H}$. Drift velocities of electrons (negative ions are neglected) and positive ions (assumed singly charged) are given, respectively, by

$$\mathbf{v}_e=-e\left(t_e\mathbf{E}_\perp+h_e\frac{\mathbf{H}\times\mathbf{E}_\perp}{H}\right), \qquad \text{(2a)}$$

$$\mathbf{v}_i=e\left(t_i\mathbf{E}_\perp-h_i\frac{\mathbf{H}\times\mathbf{E}_\perp}{H}\right). \qquad \text{(2b)}$$

A prime is used to indicate quantities inside the slab. Then, if $\mathbf{V}$ denotes the velocity of the faces of the slab, the condition that the electronic and positive ion currents should separately be continuous yields two relations which must be satisfied on the surface of the slab, namely,

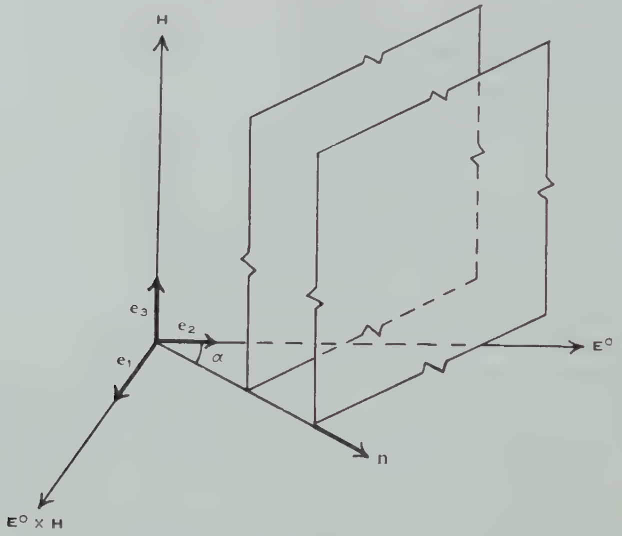

Fig. 1.—Gas between the parallel planes differs in electron density from that of its surroundings. Magnetic field **H** is parallel to the planes and orthogonal to $\mathbf{E}^0$ (an applied electric field). $\mathbf{e}_1$, $\mathbf{e}_2$, $\mathbf{e}_3$ are unit vectors in the direction of $\mathbf{E}^0\times\mathbf{H}$, $\mathbf{E}^\circ$, and **H**, and **n** is an outward unit normal to the parallel planes.

$$\mathbf{n}.(\mathbf{v}_e^0+\mathbf{v}_e^p-\mathbf{V})N=\mathbf{n}.(\mathbf{v}_e^0+\mathbf{v}_e^{p'}-\mathbf{V})N', \qquad \text{(3a)}$$

$$\mathbf{n}.(\mathbf{v}_i^0+\mathbf{v}_i^p-\mathbf{V})N=\mathbf{n}.(\mathbf{v}_i^0+\mathbf{v}_i^{p'}-\mathbf{V})N'. \qquad \text{(3b)}$$

From equations (2) and (3) it follows that

$$\mathbf{V}.\mathbf{n}=\frac{[\omega_e/\nu_e+\omega_i/\nu_i]eE^0\sin\alpha}{\{(\nu_e^2+\omega_e^2)/\nu_e\}m_e+\{(\nu_i^2+\omega_i^2)/\nu_i\}m_i}. \qquad \text{(4)}$$

It is thus shown that a steady state is possible in which the slab does not change form and that this state is independent of electron density either inside or outside the slab.

If $\mathbf{E}^0$ is due to a wind of velocity $-U\mathbf{e}_1$ and δ is the angle between $-U\mathbf{e}_1$ and $\mathbf{n}$, then $\sin\delta=-\cos\alpha$. Then, in a frame of reference moving with the wind,

$$\mathbf{V}.\mathbf{n}=\frac{-(\omega_e/\nu_e+\omega_i/\nu_i)\,U\cos\delta}{\omega_e/\nu_e+\nu_e/\omega_e+\omega_i/\nu_i+\nu_i/\omega_i}. \quad \ldots\ldots\ldots\ldots \quad (5)$$

Now in the ionosphere $\omega_e/\nu_e>\omega_i/\nu_i$, hence*

$$\mathbf{V}.\mathbf{n}\approx-U\cos\delta/(1+\nu_e\nu_i/\omega_e\omega_i). \quad \ldots\ldots\ldots\ldots \quad (6)$$

In a frame of reference in which the wind velocity is $\mathbf{U}$ (i.e. a rest frame on the ground) the velocity of the faces is given by

$$V_s=\mathbf{n}.(\mathbf{U}+\mathbf{V}). \quad \ldots\ldots\ldots\ldots\ldots\ldots \quad (7)$$

The ratio $V_s/\mathbf{U}.\mathbf{n}$ is plotted in Figure 2 as a function of ω_e/ν_e, assuming with Baker and Martyn (1953) that $(\omega_e/\nu_e).(\nu_i/\omega_i)=1650$.

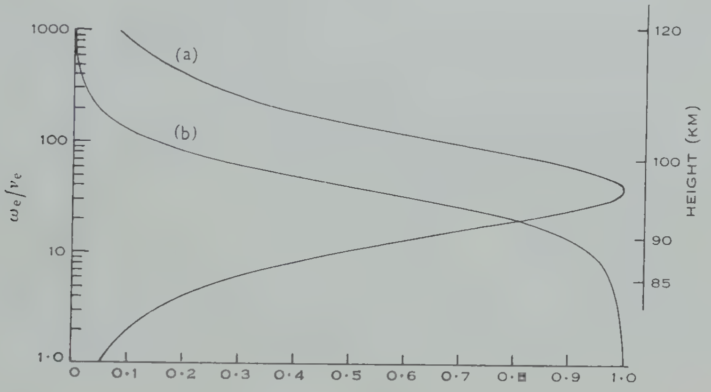

Fig. 2.—Curve (*a*), $(\sigma_2/\sigma_1)/(\sigma_2/\sigma_1)_{\text{max.}}$ as a function of ω_e/ν_e. Note: $(\sigma_2/\sigma_1)_{\text{max.}}\approx 20$. Curve (*b*), $V_s/\mathbf{U}.\mathbf{n}$ as a function of ω_e/ν_e. Height scale is approximate.

(ii) *Current Flow.*—We now investigate the current flowing in the slab. The polarization field will be entirely internal and normal to the slab faces. The rate of accumulation of electrons on a face of the slab is

$$\partial n_e/\partial t=eN'\mathbf{n}.(\mathbf{v}_e^0+\mathbf{v}_e^{p'}-\mathbf{V})-eN\mathbf{n}.(\mathbf{v}_e^0-\mathbf{V}),$$

whilst the rate of accumulation of positive charge on a face is

$$\partial n_i/\partial t=eN'\mathbf{n}.(\mathbf{v}_i^0+\mathbf{v}_i^{p'}-\mathbf{V})-eN\mathbf{n}.(\mathbf{v}_i^0-\mathbf{V}).$$

Thus the rate of charge (q) accumulation is

$$\partial q/\partial t=eN'\mathbf{n}.(\mathbf{v}_i^0-\mathbf{v}_e^0+\mathbf{v}_i^{p'}-\mathbf{v}_e^{p'})-eN\mathbf{n}.(\mathbf{v}_i^0-\mathbf{v}_e^0).$$

---

* After completion of this work a recent paper by Clemmow and Johnson (1959) came to hand. Equation (6) is almost identical with their equation (61) for the velocity of propagation of an irregularity.

Now the polarization field $\mathbf{E}^{p'}$ is $-4\pi q\mathbf{n}$, hence

$$(-1/4\pi)\partial E^{p'}/\partial t = (N'-N)e^2(t_i+t_e)E^0\cos\alpha + N'e^2(t_i+t_e)E^{p'} \\ +(N'-N)e^2(h_i-h_e)E^0\sin\alpha.$$

Thus,

$$E^{p'} = \frac{N-N'}{N'}E^0\left(\cos\alpha + \frac{h_i-h_e}{t_i-t_e}\sin\alpha\right)[1-\exp\{-4\pi N'e^2(t_i+t_e)t\}].$$

Let us resolve the total current density $\mathbf{j}$ into two components, $\mathbf{j}_n$ normal to the slab and $\mathbf{j}_p$ parallel to the slab in the direction $\mathbf{n}\times\mathbf{H}$. It follows, since $\mathbf{j}=N_e(\mathbf{v}_i-\mathbf{v}_e)$, that

$$j_n' = \sigma_1 E^0\cos\alpha - \sigma_2 E^0\sin\alpha \\ +\sigma_1' \frac{N'-N}{N'}E^0\left(\cos\alpha - \frac{\sigma_2}{\sigma_1}\sin\alpha\right)\exp(-4\pi\sigma_1' t), \quad \ldots\ldots \quad \mathbf{(8a)}$$

$$j_p' = -\sigma_3' E^0\sin\alpha - \sigma_2 E^0\cos\alpha + \frac{\sigma_2^2}{\sigma_1}E^0\sin\alpha \\ -\sigma_2' \frac{N'-N}{N'}E^0\left(\cos\alpha - \frac{\sigma_2}{\sigma_1}\sin\alpha\right)\exp(-4\pi\sigma_1' t), \quad \ldots \quad \mathbf{(8b)}$$

$$j_n = \sigma_1 E^0\cos\alpha - \sigma_2 E^0\sin\alpha, \quad \ldots\ldots\ldots\ldots \quad \mathbf{(8c)}$$

$$j_p = -\sigma_1 E^0\sin\alpha - \sigma_2 E^0\cos\alpha, \quad \ldots\ldots\ldots\ldots \quad \mathbf{(8d)}$$

where

$$\sigma_3 = \sigma_1 + \sigma_2^2/\sigma_1.$$

Thus the exponential time constant for approaching the steady state is $1/4\pi\sigma_1'$. If $\mathbf{E}^0$ arises from a wind with speed U of neutral particles in the direction opposite to $\mathbf{e}_1$, the internal current in the steady state is given by

$$j_n' = \sigma_1 UH\sin\delta + \sigma_2 UH\cos\delta, \quad \ldots\ldots\ldots\ldots \quad \mathbf{(9a)}$$

$$j_p' = \sigma_3' UH\cos\delta - \sigma_2 UH\sin\delta - \frac{\sigma_2^2}{\sigma_1}UH\cos\delta, \quad \ldots\ldots \quad \mathbf{(9b)}$$

and the polarization field by

$$E^{p'} = \frac{N-N'}{N'}UH\left(\sin\delta + \frac{\sigma_2}{\sigma_1}\cos\delta\right). \quad \ldots\ldots\ldots\ldots \quad \mathbf{(10)}$$

This polarization field has a maximum (in the case of $N\to 0$) of

$$|E^{p'}|_{\max.} = UH\sqrt{(\sigma_3/\sigma_1)} \quad \ldots\ldots\ldots\ldots \quad \mathbf{(11)}$$

when $\delta = \frac{1}{2}\pi - \tan^{-1}\sigma_2/\sigma_1$. Clearly $|E^{p'}|_{\max.}$ may be much greater than UH, the maximum electrostatic field derivable from the movement of an isotropic conductor across a magnetic field (Alfvén 1950).

(b) *Acceleration of Charged Particles*

Under the influence of an electric field $\mathbf{E}$ and magnetic field $\mathbf{H}$, charged particles move in trochoidal paths between collisions. The energies of the particles continually oscillate by virtue of movement to and fro along $\mathbf{E}$. It may be shown from the equations of Chapman and Cowling (1953, p. 324) that in the absence of collisions the distance d travelled to and fro by a particle of mass m and charge e is $2(v/\omega+eE/m\omega^2)$ where ω is its gyro frequency and v its speed prior to the application of E. In the field $|E^{p'}|_{\text{max.}}$ given by equation (**11**),

$$d=2\left(\frac{v}{\omega}+\frac{eUH}{m\omega^2}\sqrt{\frac{\sigma_3}{\sigma_1}}\right). \qquad \textbf{(12)}$$

Thus the maximum change in energy of the particle over a half cycle is

$$\Delta\xi=2|\pm mvU\sqrt{(\sigma_3/\sigma_1)}+mU^2(\sigma_3/\sigma_1)|, \qquad \textbf{(13)}$$

the sign + or − being used accordingly as the charge of the particle is positive or negative. Except for gas particles of initially very high velocities and for even moderate values of U, equation (**13**) becomes

$$\Delta\xi\approx 2mU^2(\sigma_3/\sigma_1). \qquad \textbf{(14)}$$

In an isotropic gas $\sigma_3/\sigma_1=1$, of course. In a lightly ionized tenuous gas (e.g. ionospheric F region) $\sigma_3/\sigma_1\approx 1$. In the ionospheric E region σ_3/σ_1 may reach a value of about 400 (Baker and Martyn 1953). In stellar atmospheres values greater than 10^{10} are common (Piddington 1954).

In the dynamo region of the Earth's atmosphere significant values of U may arise through the action of a neutral particle wind; the effects of such winds are considered in later sections. In stellar atmospheres U may attain significant values through the action of radiation pressure of the Milne kind (Milne 1926).

It appears likely that the movement of the Earth's exosphere through the interplanetary magnetic field or the solar system through a galactic magnetic field may produce significant electrostatic fields which would manifest themselves as anisotropies in cosmic ray intensities. Such fields may also accelerate individual charged dust particles.

III. APPLICATION TO THE AURORA AND MAGNETIC DISTURBANCE

Baker and Martyn (1953) have calculated the conductivities as functions of height in a model ionosphere. It is seen from their work that the bulk of atmospheric dynamo current flows between 90 and 120 km height. Also between the same height limits Hall currents far outweigh Pedersen currents. Thus a good approximation in the dynamo region is

$$\sigma_3\approx\sigma_2.\sigma_2/\sigma_1. \qquad \textbf{(15)}$$

Weekes (1956) exhibits graphs of the mobilities of electrons and ions separately as functions of height. From these graphs it is seen that in the dynamo region the Hall current due to electrons dominates that due to ions. Hence throughout the greater part of the dynamo region we may say

$$\sigma_2\approx\sigma_{2(\text{electrons})}=\frac{Ne^2}{m_e}\,\frac{\omega_e}{\nu_e^2+\omega_e^2}.$$

Since $\omega_e/\nu_e\gg 1$ in the region considered,

$$\sigma_2\approx Ne/H. \qquad \textbf{(16)}$$

Since electrons dominate the flow of current,

$$\mathbf{j} \approx -Ne\mathbf{v}_d, \quad \ldots\ldots\ldots\ldots\ldots\ldots\ldots \quad (\mathbf{17})$$

where $\mathbf{v}_d$ represents the drift velocity of electrons.

We now identify the model described in Section II (*a*) above with an aurora immersed in the ionosphere and identify $\mathbf{U}$ with the velocity of horizontal wind perpendicular to the (near vertical) polar geomagnetic field. The current flow within an aurora is given by equations (**9**). From equations (**9b**), (**15**), (**16**), (**17**), we obtain for the drift velocity of the electrons within the auroral mode

$$v_d \approx -(\sigma_2/\sigma_1)U \cos \delta \quad \ldots\ldots\ldots\ldots\ldots \quad (\mathbf{18})$$

in the direction $+\mathbf{n}\times\mathbf{H}$. (It is assumed that $N' \gg N$ so that the first term of equation (**9b**) is the dominant one.)

Figure 2 shows the variation of σ_2/σ_1 as a function of ω_e/ν_e and height. The ratio σ_2/σ_1 reaches a maximum value of about 20 in the dynamo region (cf. Baker and Martyn 1953). The maximum value depends on the value chosen for the ratio of collision frequencies of ions and of electrons. This point will be discussed below (Section III (*c*)).

We now identify the speed V_s given by (**7**) with the horizontal movement of an aurora normal to its length and the velocity of drift of electrons $\mathbf{v}_d$ with that along the aurora of large-scale features of the luminosity pattern and of the ionization pattern producing radio echoes. This is justified when $N' \gg N$, for $E^{p'}$ (equation (**10**)) and hence v_e (equation (**2a**)) and v_d become independent of N'. The theory predicts that for the lower portion of the ionosphere V_s is of order U and v_d of order $10U$ (see Fig. 2).

(*a*) *Auroral Movements and Magnetic Disturbance*

If we now suppose that patterns of ionization established within the auroral zone are blown by a neutral particle wind it is possible to account for a number of observations on auroral morphology. Appropriate wind speeds, generally 10–100 m/sec and sometimes more, are observed in the dynamo region (Elford 1959*a*, 1959*b*).

In the vicinity of and equatorwards of the auroral zone, auroras are oriented on the average roughly east-west. If then the wind in this region has a diurnal variation, being equatorwards in the evening and polewards later in the night and morning, one would expect a similar movement of auroras. This is observed (cf. Bond 1960). Similarly we explain the diurnal variation of latitude of arcs reported by Jacka (1953). Equations (**17**) and (**18**) also explain Robertson's (1960) observation on the occurrence of positive bays in the evening and negative bays later in the night and morning.

The drifts of auroral ionization (Unwin 1959) and luminosity patterns (Bond 1960) along the aurora with speeds an order of magnitude greater than typical wind speeds are explained by equation (**18**). The diurnal variation in ionization drift speed (Kaiser 1958) is explained by the cos δ term in (**18**).

Heppner (1954) shows that the bulk of the magnetic bay producing current does in fact flow in or near auroras. This indicates that $N \ll N'$. To estimate the magnitude of a magnetic bay we take account now of only the current flowing in visible auroras (equation (**9b**)). The currents flowing outside an aurora indicated by equations (**8c**) and (**8d**) may contribute significantly to disturbance if they occupy a great enough region. At Macquarie Island when the magnetic K-index is 6 there is a magnetic disturbance of order 500 gamma and auroras typically fill the whole sky. Thus the total effective (latitude) thickness of auroras is of order 100 km. Recent rocket measurements of electron densities in auroras give values of 10^6–10^7 per cm^3 (Jackson and Seddon 1959). If the auroral dynamo be 10 km thickness in height and at 100 km above the ground, then a disturbance at the ground of over 500 gamma is easily explicable.

It has been observed (Zaborshchikov and Fediakina 1958) that during positive magnetic bays $h_{\text{min.}}E_s$ is generally above 100 km, whilst during negative bays $h_{\text{min.}}E_s$ is generally below 100 km. Moreover, increased absorption of extraterrestrial radio waves is more associated with negative than with positive bays. These observations can be qualitatively explained by a modification of the theory which will not impair the foregoing conclusions.

We consider the effect of allowing for the inclination of the Earth's magnetic field to the vertical. Figure 3 illustrates a cross section of an aurora in the magnetic meridional plane with the wind blowing equatorwards. Positive charges will gather on the leading face of the aurora and negative ones on the trailing face. Thus in this situation electrons will tend to be lifted out of the lower regions of the ionosphere so that their effect on absorption is lessened. Apparently they are lifted to a region where their horizontal drift velocity is less (namely, above the peak in drift velocity near 100 km, cf. Fig. 2). However, when the wind is polewards electrons will be depressed into lower regions where their effect on absorption is increased yet the bulk of them still occupy a region of high drift speed. This also explains Robertson's (1960) observation that negative bays are of larger amplitude in general than positive bays.

The two physically distinct components of velocity of an aurora are V_s and v_d. Since v_d is of order 10 and more times V_s, the arbitrary resolution of the movements of auroras north-south and east-west will not in general give information about V_s and v_d unless the orientation is known. However, as mentioned above, near the auroral zone the average orientation of auroras is east-west, so that on the average we may associate north-south movement with V_s and east-west movement with v_d. Now Bond (1960) exhibits a graph for the latitude of auroras as a function of K_p, whilst Unwin (1959) exhibits a graph for the drift velocity of auroral ionization as a function of K at Macquarie Island. The average values from these two sets of data are plotted in Figure 4. (The fit is achieved by choosing the same ordinate for the drift 3000 m/sec and 41° gm. co-lat. at K_p, $K=9$ and $K_p=0$ corresponding to 100 m/sec and 27° gm co-lat.) In terms of the present theory, the correspondence revealed in Figure 4 suggests that K and K_p are indicators of wind speed.

Thus, though changes in ionization density are important, it appears that the wind in the polar dynamo region is a prime factor in determining the morphology of auroras and magnetic disturbance. A source of energy for this wind will be discussed later (Section IV).

(*b*) *Luminosity of Auroras*

In the model presented in Section II the only electric field available for the acceleration of charged particles is that given by (**10**), which is orthogonal to *H*. The maximum energy acquired by a charged particle which does not suffer collision is given by equation (**13**). Thus a 100 m/sec wind may accelerate charged nitrogen and oxygen molecules to energies of approximately 1 eV. Under favourable circumstances this field may contribute to the luminosity of auroras.

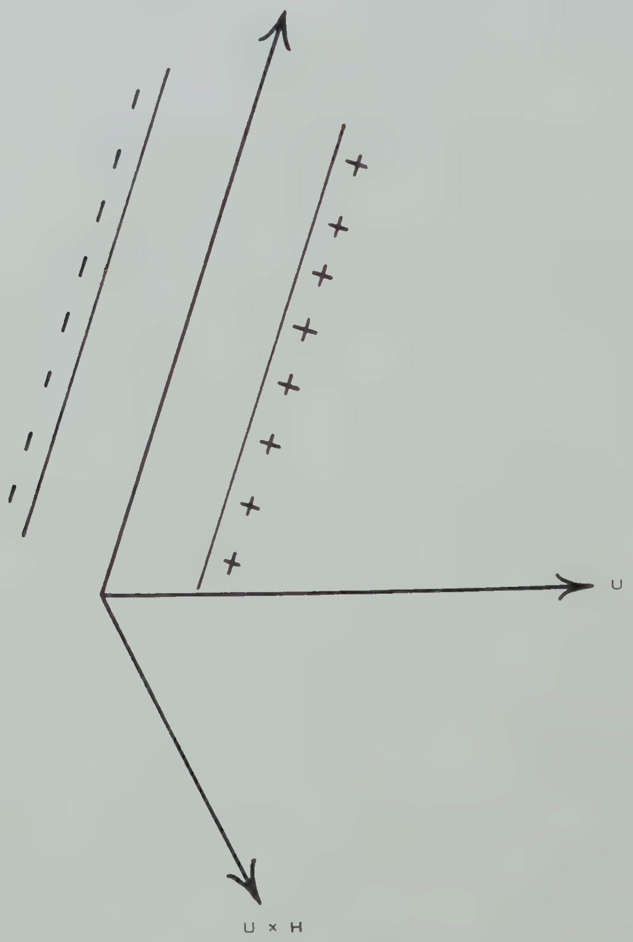

Fig. 3.—Effect of inclined magnetic field.

However, in a real aurora significant electric fields may develop parallel to the geomagnetic field. For conductivity is a function of height and therefore the build-up of polarization at the faces of the aurora will not be uniform at all heights. Under these conditions current must flow along **H**—this is equivalent to creating an electric field parallel to **H**. The effect of this current flow along **H** will be to delay the steady state suggested by equation (**9**). An upper limit to this electric field parallel to **H** may be obtained by assuming that in the initial stages of luminosity development all the current which flows in the direction of the normal **n** (see Fig. 1) is redirected along the geomagnetic field lines. Thus from equations (**1**) and (**8a**) (putting $t=0$, $E^0=UH$, $\delta=\frac{1}{2}\pi+\alpha$ and $N'\gg N$)

$$E_{||}\approx r(\sigma_1' UH \sin\delta+\sigma_2' UH \cos\delta)/\sigma_0', \qquad \ldots\ldots\ldots \ (\mathbf{19})$$

where r is the ratio of the height extent and the latitude extent of the dynamo section of an aurora. An auroral dynamo may be 20 km in height extent and less than 1 km thick. Since in the dynamo region $(\sigma_2/\sigma_0)_{\text{max.}}$ and $(\sigma_1/\sigma_0)_{\text{max.}}$ are about 10^{-2} (Baker and Martyn 1953), it may be shown that $E_{||}$ values of order 10^{-5} V/cm are obtainable from a wind of 30 m/sec. Chamberlain (1955) in a study of auroral rays concludes that an electric field of order 10^{-5} V/cm is adequate to explain their luminosity.

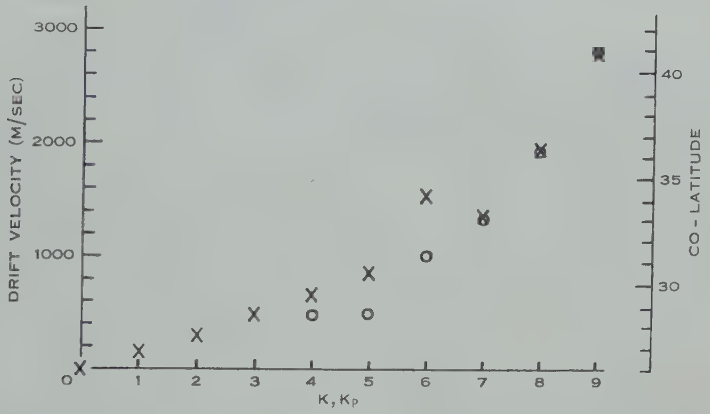

Fig. 4.—Superposition of two sets of data: (○) the EWE average drift speed of auroral ionization as a function of K-index at Macquarie Island (Unwin 1959); (×) the average maximum co-latitude of auroras as a function of K_p (Bond 1960).

The luminosity of an aurora appears to move with the same velocity at all heights. This observation does not conflict with the theory. The electric field causing luminosity at great heights moves with a speed dictated by the electron flow at the base of the aurora in the dynamo region. The auroral dynamo may occupy only a small height range and so only a small range of values of V_s and v_d may be effective in determining the speed of luminosity. It appears that the values of V_s and v_d associated with the bulk of " dynamo " electrons will dominate and that values of V_s and v_d associated with other electrons may contribute to diffuseness at the edges of auroral luminosity.

As mentioned above, the leakage of charge along the field lines increases the time to reach the steady state (maximum) electron drift (v_d) in an aurora. It is thus expected that the luminosity peak of an aurora should precede the associated magnetic disturbance at the ground, as has been reported by Bless *et al.* (1959).

(*c*) *The Collision Frequencies of Ions and Electrons with Neutral Particles*

From equation (**18**) it follows that $\sigma_2/\sigma_1 \approx v_d/U \cos \delta$. It can be seen from the equations of Baker and Martyn (1953) that when $\nu_i/\nu_e \gtrsim 10$ (as is presumably the case in the ionosphere), then $(\sigma_2/\sigma_1)_{\text{max.}} \approx \frac{1}{2}(\nu_i/\nu_e)$ (to within 1 per cent.). Thus

$$\frac{\nu_i}{\nu_e} \approx 2\left(\frac{v_d}{U \cos \delta}\right)_{\text{max.}} . \qquad \ldots\ldots\ldots\ldots\ldots\ldots \quad (\mathbf{20})$$

Also it may be shown that

$$\frac{V_s}{(\sigma_2/\sigma_1)\, U \cos \delta} \approx \frac{\nu_e}{\omega_e} .$$

Therefore, from equation (**18**)

$$\nu_e/\omega_e \approx V_s/v_d . \qquad \ldots\ldots\ldots\ldots\ldots\ldots \quad (\mathbf{21})$$

Thus the collision frequencies of electrons and ions may be determined by ground-based observations of wind and auroral movements.

(*d*) *World-wide Magnetic Disturbance*

Dynamo theory of world-wide magnetic disturbance (Maeda 1957 ; Obayashi and Jacobs 1957) in its usual form argues from a diffuse continuously (spatially) varying current. It does not envisage structural discontinuities of the kind discussed here. It may be capable of explaining on a world scale average magnetic disturbance but would fail to draw out the small-scale and short-term detail.

It is suggested that auroras are just visible lines of the magnetic disturbance current system. This is a natural outcome of the above theory and is supported by observations as follows. At Macquarie Island (just outside the auroral zone, Bond and Jacka (1960)) the orientation of auroras is generally east-west (Bond 1960) ; at Mawson (just inside the zone) the aurora often shows large-scale curvature (as distinct from relatively small-scale convolutions and kinks which appear as a general feature of auroras in most places) (ANARE records) ; at Scott Base (well inside the zone) the aurora often takes the form of complete loops in the sky (Carter Observatory 1957, 1958) ; at Dumont d'Urville (well inside the zone) the orientation of arcs in 1954 generally lagged the orientation of the Sun-Earth line by an acute angle (Weill 1958). These observations are qualitatively what could be expected following inspection of diagrams for disturbance current systems (see Figs. 227–240 of Vestine *et al.* 1947).

The polar disturbance current system (Vestine *et al.* 1947) could be explained in terms of a wind system with a source at the centre of the " afternoon " current cells and a sink at the centre of the " morning " current cells. The lines of flow of the wind would be roughly orthogonal to the current lines, hence across the polar cap wind in the dynamo region would blow from the afternoon sector to the morning sector.

IV. ENERGY SOURCE FOR THE WIND SYSTEM

Corpuscular bombardment of the Earth may be effected by a solar wind (Parker 1959) or hydromagnetic shock waves (Singer 1957) or weak hydromagnetic waves (Cole 1959). Let us consider the last mentioned. Hydromagnetic waves can deliver energy in two modes ; the extraordinary and the ordinary mode.

The extraordinary mode travels with the Alfvén speed V_A in all directions, whilst the ordinary mode travels with the phase velocity $V_A \cos \psi$, where ψ is the angle between the wave normal and the magnetic field (Piddington 1955).

In the case of hydromagnetic waves coming all the way from the Sun or being generated at the interface of the Earth's outer atmosphere and the interplanetary medium, the energy of the ordinary mode will accumulate principally in high magnetic latitudes and in the lines of force connected to them, whilst the energy of the extraordinary mode may be expected to accumulate in low magnetic latitudes and in the lines of force connected to them because of the curvature of the geomagnetic field lines. This would explain in a simple unified fashion the occurrence of the two maxima in the radiation intensity at heights above the Earth's surface (Van Allen 1959). This mechanism is without the difficulties of the actual transmission of particles. For, whereas disruption of the Earth's magnetic field must be invoked to explain how low energy extraterrestrial particles become trapped in the Earth's magnetic field, no such disruption is necessary for the capture of energy from hydromagnetic waves. The latter is merely a function of the geometry of the capturing system.

Let us consider the effect of hydromagnetic waves of all wavelengths coming either from the Sun or from interplanetary space near the Earth. Waves of length less than the scales of inhomogeneities (e.g. in density or magnetic field) in the Earth's exosphere would retain their character as waves and suffer damping and loss of energy, as demonstrated by Piddington (1959). However, waves of length greater than the scales of inhomogeneities would soon degenerate into a system of gyrating particles in the Earth's field. These particles will lose energy chiefly at their mirror points by collision ; in this way ionization is established and energy is delivered to the dynamo region. Also the polar dynamo region may receive energy from low energy cosmic rays.

One would expect an " auroral zone " associated with each of the naturally occurring radiation belts, just as a temporary " auroral zone " was associated with the man-made radiation belts of the Argus experiments (Christofilos 1959). This would account for the maximum of intensity of the airglow observed near gm. lat. 35° by Nakamura (1958) as the " auroral zone " of the inner Van Allen radiation belt. Also Sandford (1959) has observed that " the intensity of the O_I lines 5577 Å and 6300 Å in the airglow and aurora vary as similar functions of the K_p-index and therefore suggests that the increased O_I emissions in the airglow during periods of increased magnetic activity are essentially the same phenomena as aurora ". This supports the above thesis.

V. Discussion

The above theory correlates many widely dispersed observations. The application of the dynamo idea to the theory of auroras is not new ; Vestine (1954) quotes references to work up to that time. However, the present approach is new.

The theory leads to the inference that the " weather " of the polar dynamo region is under the control of corpuscular or hydromagnetic wave bombardment ; these effects dominate the effects of tidal oscillation.

The following picture of an aurora has evolved from consideration of the above theory. Some agency, probably charged particles from the outer Van Allen radiation belt or hydromagnetic waves directly from interplanetary space, establishes a wind system in the polar dynamo region. The wind blows an established pattern of ionization across the magnetic field. This generates electric fields, in the region of high electric conductivity, which drive currents and cause luminosity and maintain ionization for very much longer times than would be permitted by " quiet " ionospheric conditions.

To test the theory simultaneous observations of wind velocity (by the meteor trail drift method) and auroral orientation, movement, and height are required. These are required to check that indeed the speed of an elongated aurora normal to itself is just V_s. If this were established, the aurora would become a very valuable visible adjunct to the study of winds in the polar dynamo region.

VI. Acknowledgments

The author thanks Dr. F. Jacka, Chief Physicist, Major F. R. Bond, and Mr. G. Cowling of the Antarctic Division for stimulating discussion. To Dr. Jacka thanks are due for help in presentation of the final manuscript. Miss J. Cummings-Wright performed the numerical calculations and drew the graphs.

VII. References

Alfvén, H. (1950).—" Cosmical Electrodynamics." (Clarendon Press: Oxford.)

Baker, W. G., and Martyn, D. F. (1953).—*Phil. Trans.* A **246**: 281.

Bless, R. C., Gartlein, C. W., Kimball, D. S., and Sprague, G. (1959).—*J. Geophys. Res.* **64**: 949.

Bond, F. R. (1960).—*Aust. J. Phys.* **13**: 477.

Bond, F. R., and Jacka, F. (1960).—*Aust. J. Phys.* **13**: 610.

Carter Observatory (1957, 1958).—Log of Auroral Display, C.O.A.7, Scott Base 1957, 1958.

Chamberlain, J. W. (1955).—" The Airglow and the Aurora." p. 206. (Pergamon Press: London.)

Chapman, S., and Cowling, T. G. (1953).—" Mathematical Theory of Non-uniform Gases." 2nd Ed. (Cambridge Univ. Press.)

Christofilos, N. C. (1959).—*J. Geophys. Res.* **64**: 869.

Clemmow, P. C., and Johnson, M. A. (1959).—*J. Atmos. Terr. Phys.* **16**: 21.

Clemmow, P. C., Johnson, M. A., and Weekes, K. (1955).—" The Physics of the Ionosphere." p. 136. (Phys. Soc.: London.)

Cole, K. D. (1959).—*Planet. Space Sci.* **1**: 319.

Elford, W. G. (1959*a*).—*Planet. Space Sci.* **1**: 94.

Elford, W. G. (1959*b*).—Antarctic Symposium, Buenos Aires. November 1959.

Heppner, J. P. (1954).—Thesis, California Institute of Technology 1958. D.R.B. Canada Rep. No. DR135.

Jacka, F. (1953).—*Aust. J. Phys.* **6**: 219.

Jackson, J. E., and Seddon, J. C. (1959).—IGY Bulletin No. 28, October. National Academy of Sciences.

Kaiser, T. R. (1958).—*Ann. Géophys.* **14**: 1.

Maeda, H. (1957).—*J. Geomagn. Geolect., Kyoto* **9**: 119.

Milne, E. A. (1926).—*Mon. Not. R. Astr. Soc.* **86**: 459, 578.

Nakamura, J. (1958).—*Rep. Ionosph. Res. Japan* **12**: 419.

Obayashi, T., and Jacobs, J. A. (1957).—*J. Geophys. Res.* **62**: 589.

Parker, E. N. (1959).—*Proc. Inst. Radio Engrs., N.Y.* **47**: 239.

Piddington, J. H. (1954).—*Mon. Not. R. Astr. Soc.* **114**: 638.

Piddington, J. H. (1955).—*Mon. Not. R. Astr. Soc.* **115**: 671.

Piddington, J. H. (1959).—*Geophys. J. R. Astr. Soc.* **2** : 173.

Robertson, C. S. (1960).—*Aust. J. Phys.* **13** : 470.

Sandford, B. P. (1959).—*Ann. Géophys.* **15** : 445.

Singer, S. F. (1957).—*Trans. Amer. Geophys. Un.* **38** : 175.

Unwin, R. S. (1959).—*Nature* **183** : 1044.

Van Allen, J. A. (1959).—*J. Geophys. Res.* **64** : 1683.

Vestine, E. H. (1954).—*J. Geophys. Res.* **59** : 93.

Vestine, E. H., Laporte, L., Lange, I., and Scott, W. E. (1947).—" The Geomagnetic Field, its Description and Analysis." Carnegie Institute of Washington. Publication 580.

Weekes, K. (1956).—Polar Atmosphere Symposium, Part 2, p. 12.

Weill, G. W. (1958).—Rapport d'Activité des Expéditions Antarctiques Françaises. AGI Sous-Comité Antarctique Français.

Zaborschikov, F. Ya., and Fediakina, N. I. (1958).—Defence Research Board, Canada. Translation No. T288R.

RAYLEIGH WAVE DISPERSION FOR A SINGLE LAYER ON AN ELASTIC HALF SPACE

By B. A. Bolt* and J. C. Butcher*

[*Manuscript received May 3, 1960*]

Summary

Numerical solutions of the period equation for Rayleigh waves in a single surface layer were calculated using the SILLIAC computer at the University of Sydney. Values of the phase and group velocities for both the fundamental and first higher mode are tabulated against period for eleven models. These related models allow a sensitivity analysis of the effect of variation in the seismic parameters.

I. Introduction

The complicated algebraic form of the period equation for Rayleigh wave propagation in a semi-infinite layered solid elastic medium discourages manual computation and only a few solutions for fairly simple cases have been calculated in this way (Ewing, Jardetsky, and Press 1957). Recently, solutions for the fundamental mode in three cases, each with three layers, have been obtained on EDSAC (Stoneley 1954); and IBM 650 machines have been used to evaluate the fundamental, first, and second higher mode velocities for a 3-layered model, and two 4-layered models (Oliver, Dorman, and Sutton 1959).

In the present paper solutions for the fundamental and first higher mode have been obtained for 11 related 2-layered models. Values of the elastic constants were chosen to fit the seismic velocities determined for the Western Australian crust (Bolt, Doyle, and Sutton 1958), so that the solutions are relevant to studies of the crustal structure of Australia. Computations were carried out on SILLIAC at the Basser Computing Department, the University of Sydney.

II. The Period Equation

Consider plane waves of length $2\pi/\varkappa$, phase velocity c, propagated in a homogeneous perfectly elastic medium, 1, of uniform thickness H, welded to the plane boundary of a semi-infinite similar medium, 2.

In such media, the velocities α, β of compressional and shear waves are

$$\alpha^2=(\lambda+2\mu)/\rho,\quad \beta^2=\mu/\rho, \quad \ldots\ldots\ldots\ldots\ldots \quad (1)$$

where ρ is the density and λ, μ the Lamé parameters.

---

* Department of Applied Mathematics, University of Sydney.

As a convenient notation (Stoneley, loc. cit.) we define

$$r_i^2=\varkappa^2(1-c^2/\alpha_i^2),$$
$$s_i^2=\varkappa^2(1-c^2/\beta_i^2),$$
$$b_i=(\varkappa^2+\rho_i^2)/\varkappa^2=2-c^2/\beta_i^2,\ (i=1,2),$$

$\cosh r_1H\equiv Cr_1$, $\sinh r_1H\equiv Sr_1$, $\cosh s_1H\equiv Cs_1$, $\sinh s_1H\equiv Ss_1$, $\mu=\mu_2/\mu_1$, where subscripts indicate the particular medium.

From the equations of motion and boundary conditions it may be shown (Sezawa 1927) that Rayleigh surface waves exist so long as

$$\Delta\equiv\begin{vmatrix}\begin{array}{l}(\varkappa b_1/r_1)Sr_1+(\varkappa b_1/r_2)Cr_1\\ \quad-(2s_1/\varkappa)Ss_1-(2\varkappa/r_2)Cs_1\end{array} & \begin{array}{l}2Cr_1+(2r_1/r_2)Sr_1\\ \quad-b_1Cs_1-(\varkappa^2b_1/r_2s_1)Ss_1\end{array} & s_2/\varkappa-\varkappa/r_2\\ 2b_1(1-\mu)Cr_1+(4\mu-2b_1)Cs_1 & \begin{array}{l}(4r_1/\varkappa)(1-\mu)Sr_1\\ \quad+(\varkappa b_1/s_1)(2\mu-b_1)Ss_1\end{array} & \mu(2-b_2)\\ \begin{array}{l}(\varkappa b_1^2/r_1)Sr_1+(\varkappa\mu b_1b_2/r_2)Cr_1\\ \quad-(4s_1/\varkappa)Ss_1-(2\varkappa\mu b_2/r_2)Cs_1\end{array} & \begin{array}{l}2b_1(Cr_1-Cs_1)\\ \quad+(\mu b_2/r_2)[2r_1Sr_1-(\varkappa^2b_1/s_1)Ss_1]\end{array} & \mu(2s_2/\varkappa-b_2\varkappa/r_2)\end{vmatrix}$$
$$=0. \qquad \ldots\ldots\ldots\ldots (2)$$

The derivation implies that $\varkappa\geqslant 0$, $c<\beta_1<\beta_2<\alpha_1<\alpha_2$, but real solutions also exist for $\beta_1<c<\beta_2$. In this case Cs_1 is real and Ss_1 imaginary; but in (2) s_1 always occurs as s_1Ss_1 or Ss_1/s_1, so that Δ remains real. When $c=\beta_1$, $s_1=0$ and there is a limiting case but no analytical difficulty arises.

III. NUMERICAL CALCULATIONS

For each given value of $\varkappa H$ equation (2) was solved for c using the Newton-Raphson iteration process. That is to say, if c_n is the nth iterate,

$$c_{n+1}=c_n-\Delta\Big/\frac{\partial\Delta}{\partial c_n}.$$

The process was terminated as soon as two successive values of c agreed to five decimal places, and generally only two or three iterations were necessary. This speed of convergence is comparable with that for more complicated matrix iterative methods (e.g. Haskell 1953).

In (2) c is a function of $\varkappa H$ so that the waves are dispersive. The group velocity C, given by

$$C=c+\varkappa\,\mathrm{d}c/\mathrm{d}\varkappa,$$

was calculated directly using

$$\varkappa\frac{\mathrm{d}c}{\mathrm{d}\varkappa}=-\varkappa H\frac{\partial\Delta}{\partial(\varkappa H)}\Big/\frac{\partial\Delta}{\partial c},$$

and the calculation time for each step was about 5 sec.

For each new value of $\varkappa H$ the first iterate to be used was found from the formula

$$c_0(\varkappa H+\delta(\varkappa H))=c(\varkappa H)-\delta(\varkappa H)\frac{\partial\Delta}{\partial(\varkappa H)}\Big/\frac{\partial\Delta}{\partial c},$$

where $\delta(\varkappa H)$ is the difference between the two values of $\varkappa H$. The partial derivatives required here and in the calculation of C were found by a numerical differentiation.

The value of c_0 for the first value of $\varkappa H$ used in any case was found by a subsidiary program which examined Δ for a set of values of c in a specified arithmetical progression for specified values of $\varkappa H$, printing whenever a change of sign occurred in Δ as c was increased.

In the main program $\varkappa H$ was printed at each step, followed by c, C, and the number of iterations required. All printing was in floating decimal form and the calculation time for each step was about 5 sec. Program tapes are available at the Department of Applied Mathematics, University of Sydney, for future calculations. The elastic parameters can be varied to suit different crustal models and still higher modes may be calculated if required.

IV. Discussion of the Solutions

Velocities for the fundamental and first higher mode (M_{21} or Sezawa mode) for the models A to K defined in Table 1 are tabulated in Tables 2 and 3.

A solution for the last case in Table 1, previously obtained using a desk machine (Haskell 1953) was used as a program check. Typical period-group velocity curves for the case $H=35$ km are shown in Figure 1.

Table 1

VELOCITIES (IN KM/SEC) AND THE DENSITY RATIOS DEFINING THE ELEVEN MODELS

Model	A	B	C	D	E	F	G	H	I	J	K	Haskell
α_1	*5·8*	6·0	*6·2*	6·0	6·0	6·0	6·0	6·0	6·0	6·0	6·0	6·14
β_1	3·6	3·6	3·6	*3·4*	*3·8*	3·6	3·6	3·6	3·6	3·6	3·6	3·39
α_2	8·2	8·2	8·2	8·2	8·2	8·2	8·2	*8·0*	*8·4*	8·2	8·2	8·26
β_2	4·8	4·8	4·8	4·8	4·8	4·8	4·8	4·8	4·8	*4·6*	*5·0*	4·65
ρ_2/ρ_1	1·296	1·296	1·296	1·296	1·296	*1·400*	*1·207*	1·296	1·296	1·296	1·296	1·111

Fundamental mode solutions exist for $0<\varkappa H<\infty$ and as $\varkappa H\rightarrow 0$, $c\rightarrow\beta_2$. The higher mode M_{21} has a cut-off period corresponding to $c=\beta_2$ and as $\varkappa H\rightarrow\infty$, $c\rightarrow\beta_1$.

There is always a well-defined minimum to the group velocity for both modes ; waves associated with these minima are designated Airy phases (Pekeris 1948).

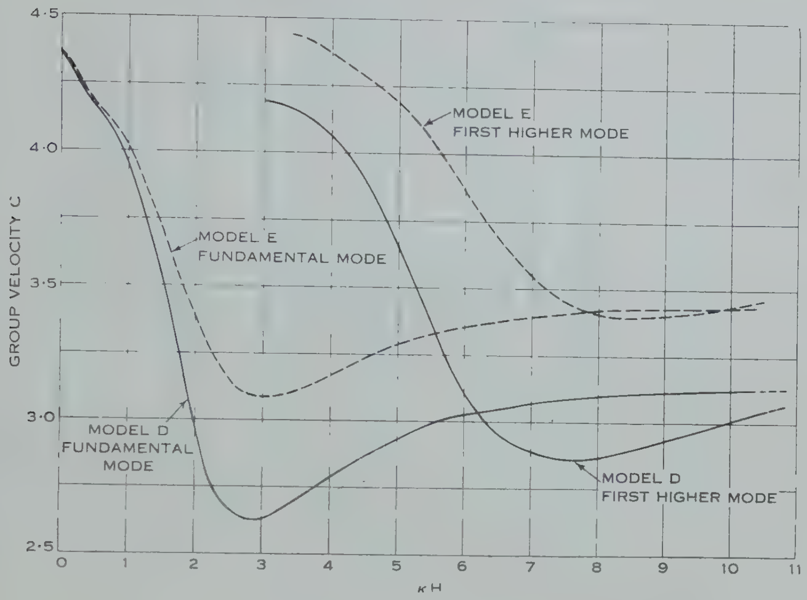

Fig. 1

The models indicate that the Airy wave velocity is sensitive mainly to β_1, the shear velocity in the upper layer. Of the 11 models, D has the minimum and E the maximum Airy wave velocity for both models. In general M_{21} is affected more by changes in β_1 than is the fundamental mode.

Table 2

PHASE AND GROUP VELOCITIES (IN KM/SEC) FOR THE ELEVEN MODELS: FUNDAMENTAL MODE

$\varkappa H$	Model A		Model B		Model C		Model D	
	c	C	c	C	c	C	c	C
0·10	4·36925	4·33570	4·37124	4·33995	4·37303	4·34376	4·36905	4·33573
0·20	4·33757	4·27786	4·34205	4·28772	4·34603	4·29643	4·33799	4·28025
0·40	4·28428	4·18898	4·29465	4·21185	4·30374	4·23155	4·28780	4·20051
0·60	4·24051	4·11804	4·25717	4·15332	4·27151	4·18304	4·24841	4·13952
0·80	4·20082	4·04330	4·22346	4·08879	4·24270	4·12649	4·21299	4·07070
1·00	4·16026	3·94839	4·18829	4·00162	4·21185	4·04537	4·17544	3·97379
1·50	4·03376	3·58409	4·07180	3·64295	4·10344	3·69182	4·04407	3·54222
2·00	3·86631	3·15691	3·90744	3·19540	3·94174	3·22796	3·84666	2·98114
2·50	3·69583	2·91036	3·73392	2·92586	3·76571	2·93846	3·63735	2·67553
3·00	3·55877	2·86055	3·59217	2·86729	3·61998	2·87221	3·47116	2·63439
3·50	3·46159	2·90469	3·49105	2·91063	3·51551	2·91493	3·35576	2·70060
4·00	3·39628	2·97465	3·42290	2·98242	3·44494	2·98834	3·27938	2·78922
4·50	3·35327	3·04225	3·37791	3·05217	3·39828	3·06021	3·22953	2·87016
6·00	3·29462	3·17795	3·31625	3·19259	3·33404	3·20454	3·16169	3·02553
7·00	3·28146	3·22227	3·30223	3·23867	3·31929	3·25238	3·14619	3·07506
8·00	3·27573	3·24613	3·29605	3·26435	3·31271	3·27934	3·13926	3·10288
10·00	3·271	3·271	3·292	3·283	3·308	3·298	3·135	3·123

Table 2 (*Continued*)

$\varkappa H$	Model E		Model F		Model G		Model H	
	c	C	c	C	c	C	c	C
0·10	4·37287	4·34302	4·37381	4·34502	4·36865	4·33483	4·35471	4·32365
0·20	4·34492	4·29268	4·34705	4·29744	4·33698	4·27781	4·32589	4·27255
0·40	4·29901	4·21820	4·30415	4·22995	4·28495	4·19322	4·27984	4·20023
0·60	4·26230	4·16058	4·27085	4·17933	4·24311	4·12648	4·24405	4·14543
0·80	4·22951	4·00978	4·24122	4·12273	4·20521	4·05402	4·21206	4·08405
1·00	4·19615	4·02208	4·21006	4·04316	4·16601	3·95981	4·17849	3·99952
1·50	4·09273	3·72703	4·10196	3·69011	4·04177	3·59920	4·06552	3·64642
2·00	3·95656	3·37662	3·93835	3·20921	3·87758	3·18431	3·90405	3·20160
2·50	3·81521	3·15273	3·75765	2·90646	3·71114	2·94398	3·73234	2·93056
3·00	3·69775	3·08952	3·60786	2·84067	3·57702	2·89221	3·59147	2·87000
3·50	3·61207	3·11527	3·50093	2·88809	3·48143	2·93213	3·49074	2·91196
4·00	3·55334	3·17110	3·42907	2·96536	3·41684	2·99865	3·42275	2·98304
4·50	3·51416	3·22942	3·38180	3·04015	3·37408	3·06412	3·37784	3·05251
6·00	3·46014	3·35244	3·31728	3·18843	3·31523	3·19682	3·31624	3·19291
7·00	3·44796	3·39308	3·30267	3·23694	3·30180	3·24109	3·30223	3·23855
8·00	3·44269	3·41526	3·29625	3·26243	3·29586	3·26470	3·29605	3·26449
10·00	3·439	3·432	3·292	3·285	3·292	3·286	3·292	3·283

$\varkappa H$	Model I		Model J		Model K	
	c	C	c	C	c	C
0·10	4·38563	4·35422	4·21602	4·18953	4·51961	4·48313
0·20	4·35618	4·30110	4·19144	4·14599	4·48544	4·42160
0·40	4·30771	4·22227	4·15220	4·08436	4·42939	4·33089
0·60	4·26880	4·16050	4·12169	4·03758	4·38469	4·26072
0·80	4·23363	4·09317	4·09441	3·98522	4·34454	4·18460
1·00	4·19705	4·00364	4·06580	3·91355	4·30292	4·08273
1·50	4·07744	3·63987	3·97039	3·61853	4·16585	3·66131
2·00	3·91049	3·18984	3·83482	3·24242	3·97327	3·14549
2·50	3·73534	2·92143	3·68830	2·99467	3·77421	2·86045
3·00	3·59281	2·86488	3·56491	2·92496	3·61585	2·81537
3·50	3·49134	2·90944	3·47475	2·95220	3·50507	2·87404
4·00	3·42304	2·98161	3·41300	3·01126	3·43136	2·95729
4·50	3·37798	3·05213	3·37179	3·07212	3·38313	3·03522
6·00	3·31626	3·19289	3·31466	3·19934	3·31759	3·18703
7·00	3·30224	3·23951	3·30156	3·24254	3·30280	3·23606
8·00	3·296	3·263	3·29576	3·26585	3·29630	3·26285
10·00	3·292	3·284	3·292	3·285	3·292	3·284

Variation in the density contrast between the media (as in Models F and G) has only a slight effect on the M_{21} curve but for $3 \cdot 7 < c < 4 \cdot 1$ km/sec a change in ρ_2/ρ_1 of $0 \cdot 2$ causes 15 per cent. displacement in the fundamental mode curve relative to M_{21}. The seismological implications of this point have been discussed by Oliver, Dorman, and Sutton (1959).

An important further inference from the solutions is that different combinations of elastic parameter values give very similar dispersion curves in both modes (e.g. models A and G). The main conclusion from a comparison is that observed Rayleigh wave dispersion alone cannot be used to give precise values to individual elastic parameters.

TABLE 3

PHASE AND GROUP VELOCITIES (IN KM/SEC) FOR THE ELEVEN MODELS: FIRST HIGHER MODE

$\varkappa H$	Model A		Model B		Model C		Model D	
	c	C	c	C	c	C	c	C
3·00	4·73368	4·33063	4·73399	4·33471	4·73427	4·33834	4·65065	4·19180
3·50	4·67200	4·27672	4·67321	4·28524	4·67426	4·29263	4·58331	4·15835
4·00	4·61882	4·21087	4·62110	4·22184	4·62309	4·23134	4·52516	4·06725
4·50	4·56798	4·10360	4·57133	4·11615	4·57423	4·12704	4·46595	3·90390
5·00	4·51395	3·94197	4·51824	3·95487	4·52198	3·96610	4·39814	3·65893
5·50	4·45254	3·72817	4·45755	3·73920	4·46191	3·74861	4·31771	3·36665
6·00	4·38253	3·49883	4·38787	3·50566	4·39251	3·51138	4·22733	3·11285
6·50	4·30691	3·31110	4·31220	3·31401	4·31678	3·31590	4·13487	2·95405
7·00	4·23119	3·19455	4·23619	3·19442	4·24049	3·19406	4·04753	2·88196
7·50	4·15999	3·14068	4·16459	3·13878	4·16854	3·13750	3·96901	2·86468
8·00	4·09571	3·12762	4·09990	3·12515	4·10350	3·12336	3·90025	2·87681
8·50	4·03901	3·13851	4·04281	3·13635	4·04607	3·13334	3·84082	2·90484
9·00	3·98959	3·16128	3·99303	3·15841	3·99598	3·15726	3·78972	2·93813
9·50	3·94677	3·19045	3·94987	3·18651	3·95254	3·18601	3·74585	2·97296
10·00	3·909	3·225	3·912	3·219	3·914	3·220	3·708	3·009
15·00	3·721	3·4	3·722	3·5	3·724	3·4	3·519	3·2

	Model E		Model F		Model G		Model H	
	c	C	c	C	c	C	c	C
3·00			4·72245	4·31980	4·74448	4·35152	4·73147	4·32609
3·50	4·74510	4·43259	4·66313	4·29467	4·68249	4·27572	4·67004	4·27940
4·00	4·70198	4·36900	4·61445	4·24651	4·62697	4·19597	4·61772	4·21799
4·50	4·66109	4·29493	4·56892	4·15446	4·57289	4·07662	4·56802	4·11449
5·00	4·61956	4·19071	4·52051	4·00431	4·51517	3·90599	4·51523	3·95598
5·50	4·57439	4·04808	4·46427	3·78974	4·45028	3·69187	4·45505	3·74317
6·00	4·52340	3·87328	4·39773	3·54141	4·37783	3·47400	4·38600	3·51136
6·50	4·46642	3·69478	4·32320	3·32741	4·30129	3·30201	4·31091	3·31930
7·00	4·40583	3·54929	4·24674	3·19175	4·22578	3·19715	4·23533	3·19863
7·50	4·34534	3·45600	4·17397	3·12796	4·15533	3·14823	4·16401	3·14120
8·00	4·28810	3·40963	4·10795	3·11294	4·09192	3·13726	4·09951	3·12704
8·50	4·23587	3·39548	4·04962	3·12319	4·03602	3·14822	4·04253	3·13763
9·00	4·18927	3·40119	3·99878	3·14714	3·98728	3·16862	3·99283	3·15998
9·50	4·14820	3·41636	3·95473	3·17593	3·94500	3·19656	3·94972	3·18784
10·00	4·111	3·443	3·916	3·215	3·908	3·232	3·912	3·223
15·00	3·924	3·6	3·722	3·4	3·721	3·5	3·722	3·5

Table 3 (*Continued*)

κH	Model I		Model J		Model K	
	c	C	c	C	c	C
3·00	4·73621	4·34247	4·58280	4·33042	4·86340	4·37757
3·50	4·67602	4·29048	4·53799	4·22874	4·79202	4·34387
4·00	4·62410	4·22530	4·49579	4·17135	4·73148	4·26216
4·50	4·57428	4·11765	4·45582	4·09594	4·67191	4·11676
5·00	4·52093	3·95383	4·41464	3·98539	4·60604	3·89748
5·50	4·45978	3·73546	4·36897	3·83207	4·52942	3·62456
6·00	4·38953	3·50057	4·31661	3·64609	4·44289	3·36702
6·50	4·31335	3·30895	4·25783	3·46294	4·35269	3·18887
7·00	4·23695	3·19085	4·19572	3·32289	4·26584	3·09738
7·50	4·16510	3·13632	4·13442	3·23896	4·18668	3·06728
8·00	4·10025	3·12350	4·07703	3·19963	4·11674	3·07172
8·50	4·04305	3·13463	4·02511	3·19233	4·05593	3·09614
9·00	3·99321	3·15767	3·97907	3·20278	4·00346	3·12762
9·50	3·95001	3·18687	3·93866	3·22118	3·95830	3·16210
10·00	3·912	3·223	3·903	3·244	3·918	3·205
15·00	3·722	3·5	3·720	3·4	3·724	3·4

V. References

Bolt, B. A., Doyle, H. A., and Sutton, D. J. (1958).—*Geophys. J. R. Astr. Soc.* **1** : 135.

Ewing, W. M., Jardetzky, W. S., and Press, F. (1957).—" Elastic Waves in Layered Media." (McGraw-Hill : New York.)

Haskell, N. A. (1953).—*Bull. Seismol. Soc. Amer.* **43** : 17.

Oliver, J., Dorman, J., and Sutton, G. (1959).—*Bull. Seismol. Soc. Amer.* **49** : 379.

Pekeris, C. L. (1948).—*Mem. Geol. Soc. Amer.* **27**.

Sezawa, K. (1927).—*Bull. Earthq. Res. Inst. Tokio* **3** : 1.

Stoneley, R. (1954).—*Mon. Not. R. Astr. Soc. Geophys. Suppl.* **6** : 610.

THE PHOTODISINTEGRATION OF RARE EARTH ELEMENTS

By H. H. Thies*† and B. M. Spicer*

[*Manuscript received March* 10, 1960]

Summary

The neutron yields from praseodymium, terbium, and holmium have been measured as a function of bremsstrahlung energy, and from these the shapes of the respective cross sections have been deduced. For terbium and holmium, the cross section for photon absorption shows two peaks, in agreement with the predictions of both the hydrodynamic model and the independent particle model of the nuclear photoeffect in non-spherical nuclei. The case of praseodymium was treated as a control experiment, since this nucleus is nearly spherical. Its photon absorption cross section has only one peak, in agreement with expectation for a spherical nucleus. The results are discussed in terms of both the hydrodynamic model and the independent particle model. Values of the deformation parameter are deduced from the photodisintegration data and are compared with values obtained by other methods.

I. Introduction

Both collective theory (Danos 1956, 1958; Okamoto 1956, 1958) and shell model theory (Wilkinson 1956, 1958) predict that in non-spherical heavy nuclei the photonuclear giant resonance is broadened and will show two maxima if the nuclear deformation is large enough. Known nuclear electric quadrupole moments indicate that the nuclear deformation increases from a negligible amount for elements of atomic mass near 140 to a maximum for A near 170, and decreases again to small values for A near 200. Thus, by systematically investigating the shape of the giant resonance for nuclei over this mass range, it should be possible to demonstrate experimentally any broadening and splitting effect in the giant resonance. This would then lead to the testing of theories on the subject, and possibly to the use of photodisintegration data for the evaluation of nuclear deformations and electric quadrupole moments.

In the heavy elements it is not practicable to observe the photonuclear absorption cross sections directly. However, to a fair degree of approximation, they can be derived from photoneutron cross sections for these elements. The approximation here arises because of the need to correct for multiple neutron emission. Because of the very high Coulomb barrier, the emission of charged particles gives negligible contribution.

If the photoneutrons are to be observed directly, only mono-isotopic or almost mono-isotopic elements may be used as targets if separated isotopes are not available. In the region of interest here these are all odd-mass nuclei, namely: ^{139}La, ^{141}Pr, ^{159}Tb, ^{165}Ho, ^{169}Tm, ^{175}Lu, ^{181}Ta, ^{197}Au, ^{209}Bi.

---

* Physics Department, University of Melbourne.

† Present address: Physics Department, University of Western Australia, Nedlands, W.A.

In a previous paper (Spicer *et al.* 1958) an experiment on the photonuclear giant resonance in ^{139}La and ^{181}Ta was reported. This experiment used direct neutron detection (BF_3-counters in a paraffin moderator). Simultaneously a similar very accurate experiment on ^{159}Tb, ^{181}Ta, ^{197}Au was performed independently by Fuller and Weiss (1958). In the present paper further direct neutron detection experiments on ^{141}Pr, ^{159}Tb, and ^{165}Ho are reported.

This type of experiment measures the total neutron production cross section

$$\sigma_{\gamma,\Sigma n}=\sigma_{\gamma,n}+2\sigma_{\gamma,2n}+3\sigma_{\gamma,3n}+. . .$$

The computation of the absorption cross section from $\sigma_{\gamma,\Sigma n}$ above the $(\gamma,2n)$ threshold requires a knowledge of the ratio $S=\sigma_{\gamma,n}/\sigma_{\gamma,2n}$. S may be estimated from statistical theory of nuclear reactions (Blatt and Weisskopf 1952). For the nucleus ^{165}Ho it was possible to determine S experimentally by combining the results from the direct neutron detection experiment with those from an independent activation experiment on the reaction $^{165}\mathrm{Ho}(\gamma,n)$.

The available experimental results on ^{139}La, ^{141}Pr, ^{159}Tb, ^{165}Ho, ^{181}Ta, and ^{197}Au will be discussed in the light of theoretical predictions.

II. Theoretical Description of the Photonuclear Effect

The predictions of the hydrodynamic theory have been discussed previously (Spicer *et al.* 1958) and lead to the result that the two eigenvalues are related by the equation

$$E_b/E_a=\hbar\omega_b/\hbar\omega_a=0\cdot911a/b+0\cdot089.$$

Here a refers to the semi-axis of rotational symmetry and b to the semi-axis perpendicular to a. If (E_b-E_a) is large enough, the positions of E_a and E_b will coincide approximately with the positions of the experimental maxima (E_1 and E_2). Frictional coupling between the two eigen-modes will tend to decrease (E_2-E_1) and flatten the minimum between E_1 and E_2.

Wilkinson (1958) used the Nilsson level scheme and computed photonuclear absorption cross sections for $140<A<210$. His results show that cross sections in non-deformed nuclei have one narrow maximum. This is broadened in deformed nuclei, and for $A=165$ the computed cross section is split into two separated maxima.

Wave functions and transition probabilities corresponding to the Nilsson Hamiltonian can be computed (see Nilsson 1955). They do, however, depend much more sensitively on the form of the chosen Hamiltonian than do the transition energies, and thus the computation of transition probabilities is not significant for excitation energies in the region 10–25 MeV. It is possible, however, to predict semiquantitatively the manner in which the nuclear deformation will affect electric dipole absorption cross sections, without actually knowing the strength of the $E1$ transitions individually. In the spheroidal nucleus, nuclear states are specified by different quantum numbers than in the spherical case. Thus, new selection rules (Alaga 1955, 1957) become increasingly effective with increasing nuclear deformation. In deformed nuclei, these selection rules separate the allowed electric dipole transitions into two groups. In transitions of group I, the excitation energy is used predominantly to add energy to the component of motion of one nucleon in the direction of *a*, the axis of rotational symmetry. In group II, the energy is added predominantly to the component of motion in a direction perpendicular to *a*.

The systematic shift of levels with deformation of a prolate type causes excitation energies for group I transitions to be smaller than for group II transitions, in general. (For an oblate spheroid, the opposite condition tends to hold.) Also, as a consequence of the selection rules, there are approximately twice as many allowed $E1$ transitions in group II as in group I. Thus the $E1$ absorption cross section will separate into two giant resonance components. These components will have mean energies of E_{I} and E_{II} respectively. This does not mean that the maxima in the composite cross section will occur at E_{I} and E_{II} (see Fig. 1). For deformations insufficient to give rise to separation of the peaks, a single broadened peak will result.

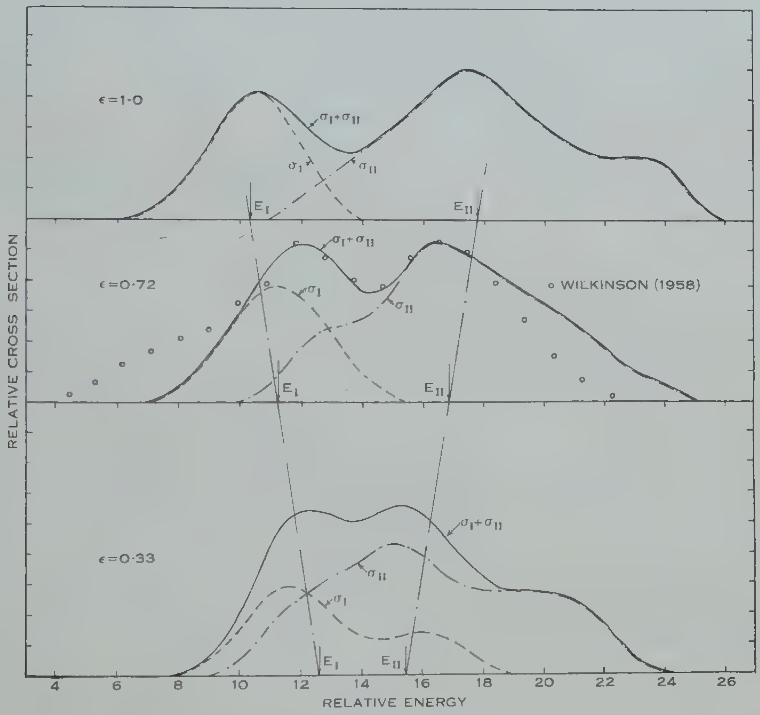

Fig. 1.—Cross section for photon absorption in ^{165}Ho computed from the Nilsson level scheme. The three cross sections are for different assumed nuclear deformations.

For particular nuclei, we investigated the broadening and splitting effect in the following manner. From the Nilsson level diagram (Nilsson 1955) the excitation energies of the electric dipole transitions allowed by the selection rules are found. In the first approximation, it is assumed that all the allowed transitions have equal strength. The corresponding absorption lines are given half-width Γ_{level}, and a Gaussian shape. Contributions from the various transitions are summed at a series of intervals. The value of Γ_{level} may be taken as 3 MeV, since this is an estimated value for non-deformed nuclei given by Wilkinson (1956). However, it is possible that this value may be less than 3 MeV for strongly deformed nuclei, as in this case the level degeneracies are reduced considerably. Component $E1$ cross sections σ_{I} and σ_{II}, corresponding to transitions in groups I and II, may be derived separately. Although the strengths of transitions may vary considerably from equality, these variations will not affect the shape and position of σ_{I} and σ_{II} significantly, as in this region of A the number of transitions is large. For example, for A near 160, there are 14 proton transitions in group I and 28 in group II. The cross sections σ_{I} and σ_{II}, and their sum σ_{abs}, for the nucleus ^{165}Ho are shown on Figure 1. The calculations were made for three values of the deformation.

It was found empirically from a number of diagrams similar to Figure 1 that the positions of E_{I} and E_{II}, the mean energies of σ_{I} and σ_{II}, follow the relationship

$$E_{\text{II}}/E_{\text{I}}=1+0\cdot 7\varepsilon. \quad \ldots\ldots\ldots\ldots\ldots\ldots \quad (1)$$

Here ε is the deformation parameter (Danos 1958) defined by

$$\varepsilon=(a^2-b^2)/R^2. \quad \ldots\ldots\ldots\ldots\ldots\ldots \quad (2)$$

It is related to the deformation parameter δ of Nilsson (1955) by the relationship

$$\varepsilon=2\delta(1+0\cdot 66\delta). \quad \ldots\ldots\ldots\ldots\ldots \quad (3)$$

R is the radius of a sphere having the same volume as the spheroid. ($R^3=ab^2=r_0^3A$. Throughout this paper, the value $r_0=1\cdot 2$ fermi is used (Ford and Hill 1955).) Thus the independent particle model predicts that the giant resonance is broadened in non-spherical nuclei, and, for large deformations, splits into two maxima in a manner similar to that predicted by the hydrodynamic model.

Using equation (2), the prediction of the hydrodynamic theory may be expressed in terms of an expansion in ε as follows

$$E_b/E_a=1+0\cdot 46\varepsilon+\text{terms of order } (\varepsilon^2). \quad \ldots\ldots\ldots \quad (4)$$

In view of the crudeness of the assumptions which led to (1) and (4), the predictions on the splitting effect from hydrodynamic theory and from independent particle model theory are in substantial agreement. This is so in spite of the very different assumptions in the two theories.

III. Experiments on Photoneutrons from ^{141}Pr, ^{159}Tb, and ^{165}Ho

Bremsstrahlung from the Melbourne 18 MeV electron synchrotron was used to irradiate the targets. Each target consisted of 10 g of a rare earth oxide in powder form (Pr_6O_{11}, Tb_4O_7, Ho_2O_3). The oxide was contained as a tablet in a polystyrene container. Sample impurities consisted of neighbouring rare earths, and were smaller than 1 per cent. in each case. The absorption of γ-rays in the target and the container lid was less than 3 per cent. in all cases, and was taken into account in the yield analysis.

With the exception of an activation experiment on the reaction ^{165}Ho(γ,n), the photoneutrons were detected by BF$_3$-counters embedded in a paraffin moderator. The arrangement of target, BF$_3$-counters, paraffin moderator, and concrete " house " was essentially the same as that described by Spicer *et al.* (1958). Four BF$_3$-counters, separated from the target by 12·5 cm of paraffin, were grouped as two pairs, and the counts from these were recorded through two independent electronic counting systems. The electronic counting loss in each system was determined experimentally and was kept less than 1·2 per cent. by limiting the yield rate of the synchrotron when necessary. Corrections were made for the counting loss. The neutron detection efficiency of each counting system was checked before and after each run by inserting a Ra-Be neutron source into an accurately reproducible position in the paraffin moderator and recording the counts obtained per minute. The number of neutrons counted in a given run was thereby corrected for the average deviation in neutron detection efficiency from a standard average value.

The γ-ray dose was measured by using a 25 r Victoreen thimble as a transmission ionization chamber. The leakage of this instrument was measured periodically and found to be negligible over several days. Each run was arranged so as to make the recorded dose approximately 10 r, thus effectively eliminating any relative error that would arise from a calibration error in the Victoreen scale. Temperature and pressure were recorded before and after each run and a temperature-pressure correction was applied to each dose reading.

The energy scale of the synchrotron had been calibrated previously by means of photoneutron threshold measurements (Spicer *et al.* 1958). This calibration was checked periodically by measuring the ^{55}Mn(γ,n) threshold.

For proper interpretation of the experimental results, the standard error in each yield point must be known. This error may be substantially greater than the purely statistical counting error. It can be estimated only inadequately from the reproducibility of neutron counts, γ-ray dose measurements, and energy settings of the accelerator, but can be obtained accurately if a yield ordinate has been measured many times at random time intervals during a complete experiment.

During each experiment, individual yield ordinates were measured in some instances up to 14 times, and it was found that the spread of values obtained at each energy setting followed a normal distribution within statistical accuracy. Experiments were performed with praseodymium, terbium, and holmium targets in position and background runs were made with the empty containers in the target position. The background remained unaltered when the empty polystyrene container was removed.

The contribution of photoneutrons from the oxygen content of the rare earth oxide samples was estimated. Under all circumstances its contribution to the total neutron production was less than 1 per cent.

Yield ordinates were measured at 0·25 MeV intervals from 7 to 18 MeV. These results are shown in Figures 2, 3, 4, for praseodymium, terbium, and holmium respectively. Smooth yield curves were drawn through each discrete set of ordinates, fitting by eye with minimum curvature curves. For the

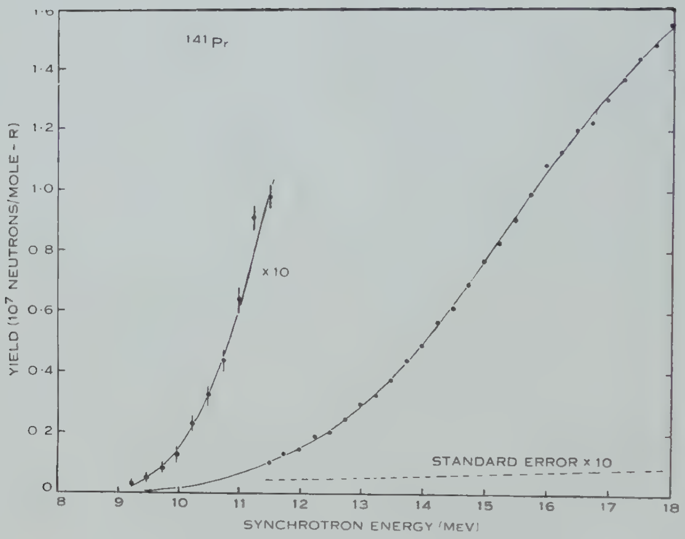

Fig. 2.—Total neutron yield from praseodymium.

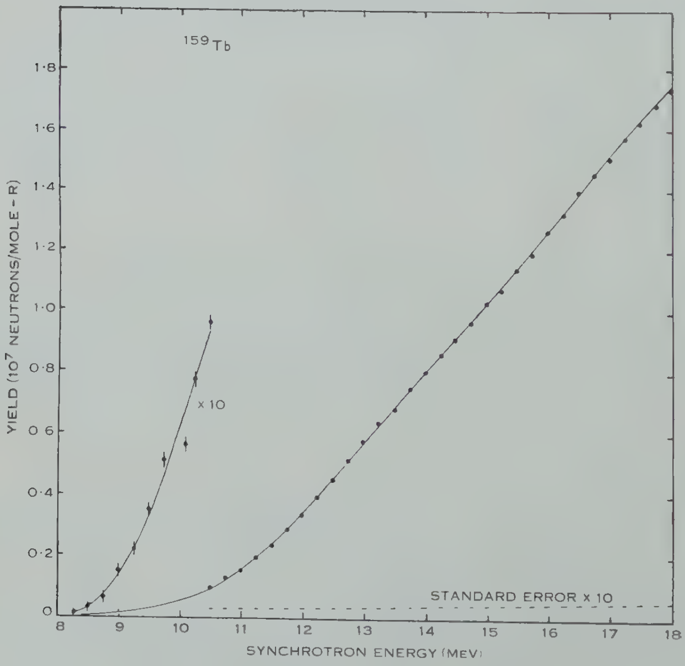

Fig. 3.—Total neutron yield from terbium.

transformation of yield data to cross sections for photoneutron production the tables of Penfold and Leiss (1958), having $\Delta E=1$ MeV, were used. Each set of measured yield ordinates was separated into four subsets, each subset having $\Delta E=1$ MeV. These subsets were then analysed separately, and the resultant cross sections were then combined to make a composite cross section. Thus, the cross section ordinates making up one "unsmoothed" cross section curve come from four interlaced and independent sets of "unsmoothed" cross section ordinates. Standard errors of unsmoothed cross section values were computed from standard errors of yield ordinates.

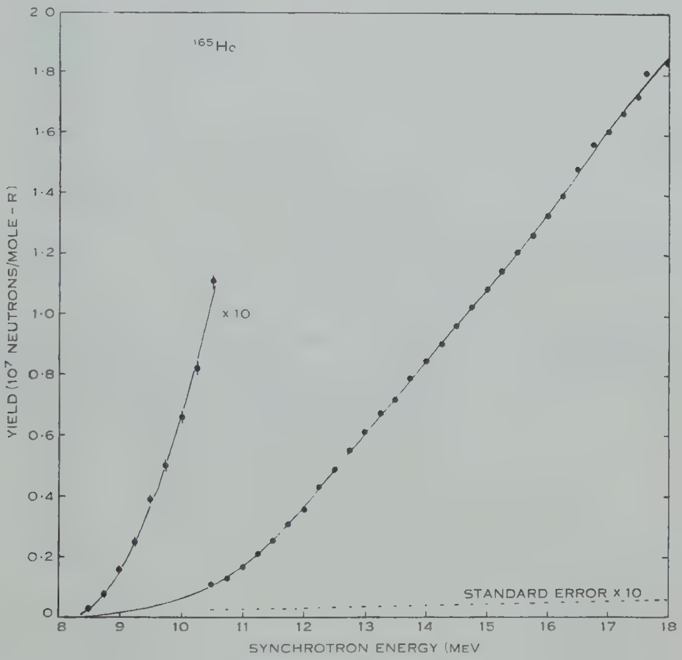

Fig. 4.—Total neutron yield from holmium.

The smooth cross sections shown were obtained from analysis of the smoothed yield curves as drawn through the experimental points. Values of the yield were read off this smooth curve and these were treated in the same manner as the unsmoothed yield points. The cross sections are shown in Figures 5 (^{141}Pr), 6 (^{159}Tb), and 7 (^{165}Ho). The results on terbium and holmium are the averages from two independent experiments. These results agreed within the standard errors and demonstrated the reproducibility of results. Note that these cross sections are the total neutron production cross sections.

To reconstruct the photon absorption cross section $\sigma_{\mathrm{abs}}=\sigma_{\gamma,n}+\sigma_{\gamma,2n}$ from the total neutron production cross section $\sigma_{\gamma,\Sigma n}=\sigma_{\gamma,n}+2\sigma_{\gamma,2n}$, allowance has to be made for neutron multiplicity above the $(\gamma,2n)$ threshold.

(γ,n) thresholds of some rare earths have recently been measured by Geller, Muirhead, and Halpern (Muirhead, personal communication 1959), and agree within less than 0·3 MeV with those calculated from the semi-empirical mass formula of Cameron (1957). Therefore this formula was used to calculate the values of (γ,2n) thresholds. The values obtained were 17·6 MeV for ^{141}Pr(γ,2n),

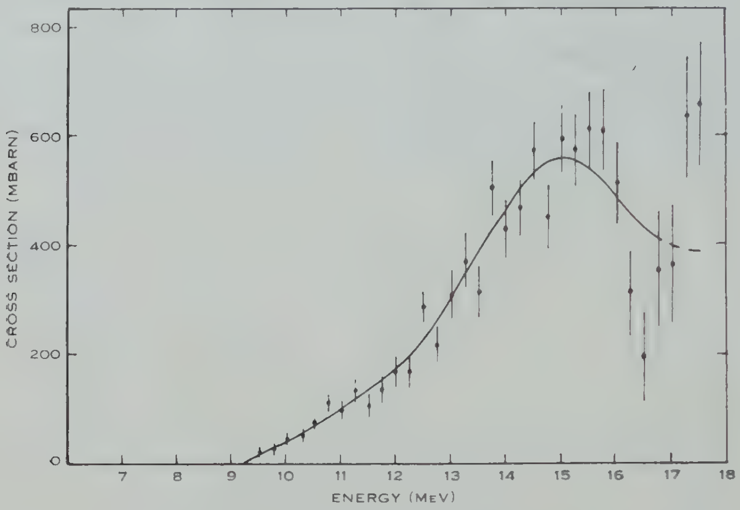

Fig. 5.—Total neutron production cross section for ^{141}Pr. The points are obtained by analysis using the experimental points. The smooth curve is obtained by analysis of a smooth yield curve drawn through the experimental points.

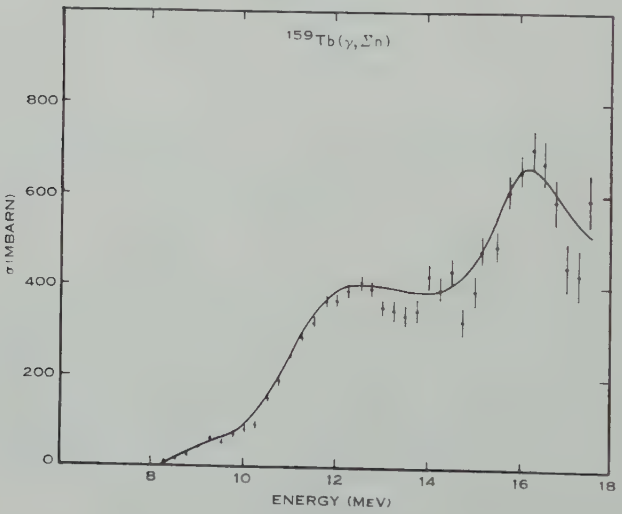

Fig. 6.—Total neutron production cross section for ^{159}Tb.

14·8 MeV for ^{159}Tb(γ,2n), and 14·4 MeV for ^{165}Ho(γ,2n). Thus, in the present experiment on ^{141}Pr, the neutron multiplicity need not be considered.

Blatt and Weisskopf estimated the neutron multiplicity using statistical theory of nuclear reactions. Applied to the present instance, this does not take account of the neutrons emitted in a direct photoeffect. This can be built in to the statistical theory estimate, which then becomes

$$\sigma_{\gamma,n}+\sigma_{\gamma,2n}=\frac{\sigma_{\gamma,n}+2\sigma_{\gamma,2n}}{1+(1-x)\{1-(1+k/\Theta)\mathrm{e}^{-k/\Theta}\}}. \quad \ldots\ldots\ldots \quad (5)$$

Here x is the fraction of direct events to total number of events, k is the energy difference between the incident photon energy and the $(\gamma,2n)$ threshold value,

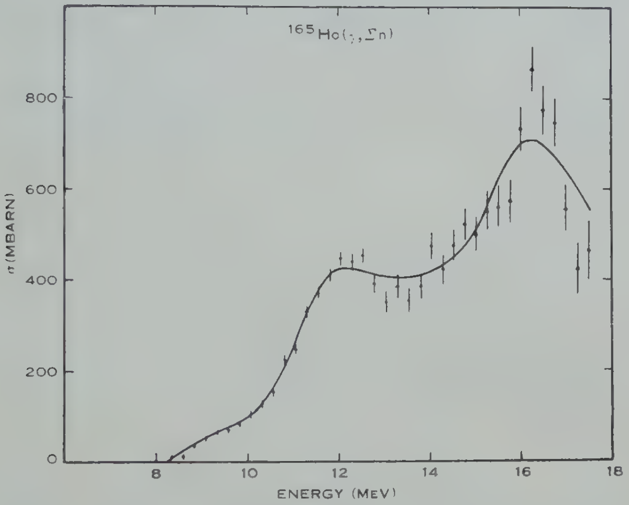

Fig. 7.—Total neutron production cross section for ^{165}Ho.

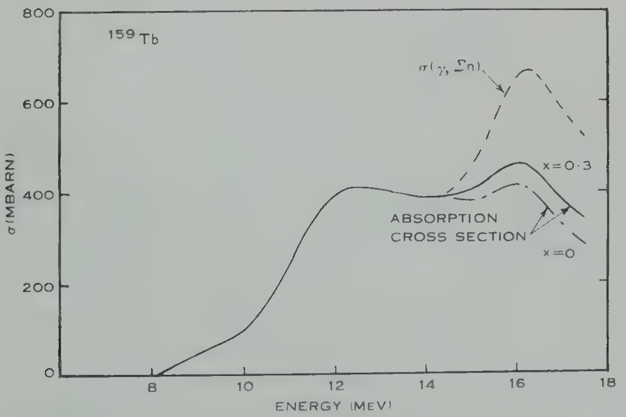

Fig. 8.—Cross section for photon absorption in ^{159}Tb, using statistical theory of nuclear reactions to correct for neutron multiplicity. The factor x is a measure of the probability that a direct photoeffect will occur.

and Θ MeV is the nuclear temperature of the target nucleus less one neutron. Values of Θ were obtained from Blatt and Weisskopf (1952).

Equation (5) can be brought into agreement with measured data on neutron multiplicities if a value of x between 0·3 and 0·4 is assumed. Experimental data considered are by Montalbetti, Katz, and Goldemberg (1953), Whalin and Hanson (1953), Berman and Brown (1954), Silva, Goldemberg, and Smith (1958), and Carver and Turchinetz (1959*a*, 1959*b*).

The cross sections in ^{159}Tb and ^{165}Ho, corrected for neutron multiplicity, are shown in Figures 8 and 9. Curves are drawn for values of x of zero and 0·3.

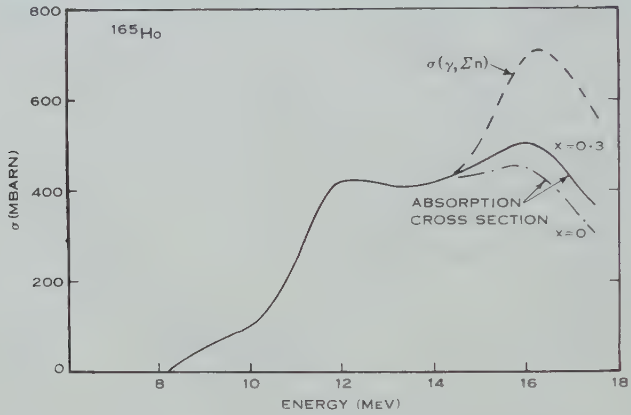

Fig. 9.—Cross section for photon absorption in ^{165}Ho. The correction for neutron multiplicity is applied using statistical theory.

IV. Activation Experiment

The (γ,n) cross section in ^{165}Ho was determined from a separate experiment by counting the β^--activity of the daughter nucleus ^{164}Ho. Brown and Becker (1954) give the half-life of this nuclide as 36·7 min. The β^--spectrum has a maximum energy of 0·99 MeV.

The Ho_2O_3 used in the BF_3-counter experiment was subdivided into nine samples of 1·050 g each. These were each pressed into tablet form (1·4 cm diameter by 0·18 cm) in identical polystyrene containers, and protected by 0·32 cm thick " Perspex " lids. The containers could be located accurately and reproducibly in a jig 30 cm from the synchrotron target. Dose measurements were made in the manner previously described. In this experiment the γ-ray beam traversed the target before striking the Victoreen thimble. The absorption of γ-rays in the target was therefore allowed for in the analysis.

The container lid was removed for counting the activity. This was commenced 5 min after the cessation of irradiation (to allow the ^{15}O 2-min activity to die out to some extent) and continued for 30 min. Only pure 37-min activity of ^{164}Ho could be detected. Allowance was made for the finite dead-time of the Geiger counting system, and the appropriate correction applied to the results.

A procedure was developed to allow for the decay of the activity during irradiation, and for variations in the yield rate of the synchrotron. The γ-ray beam, after traversing the dosemeter, was allowed to strike a 500 g lead sample. This was located in the " sample position " in the paraffin moderator plus BF_3-counter assembly that had been used for the direct neutron detection experiments. The counters therefore received copious photoneutrons from the lead sample. The number of neutrons recorded in any time interval is proportional to the γ-ray dose given in that time. The neutron counts were recorded at 2-min intervals and used as a relative measure of the dose which the holmium sample had received during that interval. The decay of the activity of the holmium sample during the 30 min irradiation period could then be calculated with due allowance for variations in dose rate.

Activation points were taken at four energies below the $(\gamma,2n)$ threshold, and at $0\cdot25$ MeV intervals above $14\cdot5$ MeV. Each point was repeated at least twice. A smooth curve was fitted to the measured points (see Fig. 10). This curve was normalized to the total neutron yield curve at the energies below the $(\gamma,2n)$ threshold at which the activity was measured. The (γ,n) cross section at energies above the $(\gamma,2n)$ threshold was computed from the yield curve in the manner previously described, and is shown as $\sigma_{\gamma,n}$ on Figure 11. On the same figure the total neutron cross section $\sigma_{\gamma,\Sigma n}$ is shown. It is to be noted that the yield curve for the ^{164}Ho activity has not been measured well enough for analysis using the experimental points to be useful. Consequently, all discussion of this cross section refers to the result of analysis of the smooth yield curve.

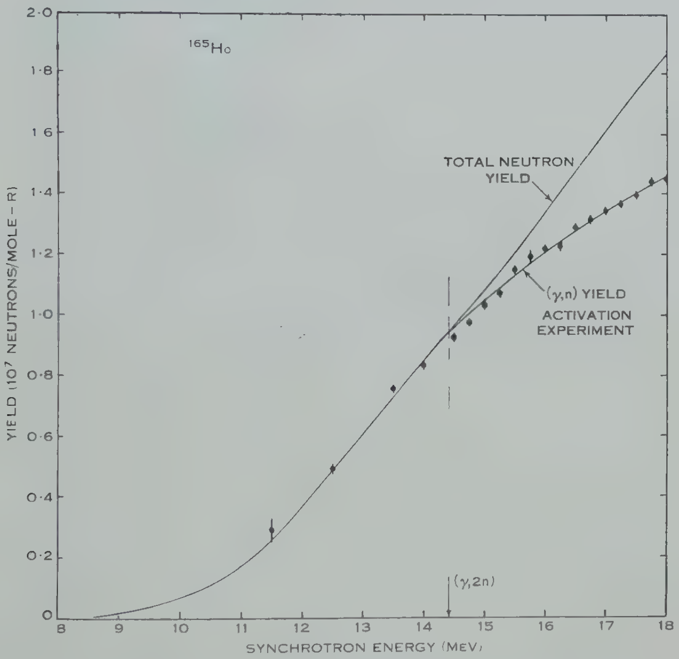

Fig. 10.—Yield curve for the ^{165}Ho$(\gamma,n)^{164}$Ho reaction, measured by counting the ^{164}Ho activity. It was normalized on to the total neutron yield curve for holmium below the $(\gamma,2n)$ threshold.

Using the total neutron cross section $\sigma_{\gamma,\Sigma n}$ given by the BF$_3$-counter experiment and the (γ,n) cross section of the activation experiment, the photon absorption cross section is given by

$$\sigma_{\text{abs}}=\sigma_{\gamma,n}+\sigma_{\gamma,2n}=\tfrac{1}{2}\{\sigma_{\gamma,\Sigma n}+\sigma_{\gamma,n}\}. \qquad \ldots\ldots\ldots\ldots (6)$$

The absorption cross section σ_{abs} computed with equation (**6**) is compared in Figure 12 with the absorption cross section computed using neutron multiplicity theory, using equation (**5**) with $x=0\cdot3$. The two cross sections are in agreement within statistical expectations, although a value of x as high as $0\cdot4$ would be equally suitable.

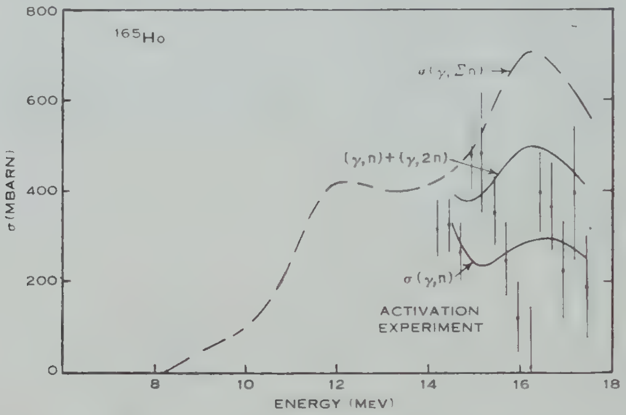

Fig. 11.—Result of analysis of the holmium activation experiment. Also plotted are the total neutron production cross section and the photon absorption cross section derived using the activation results.

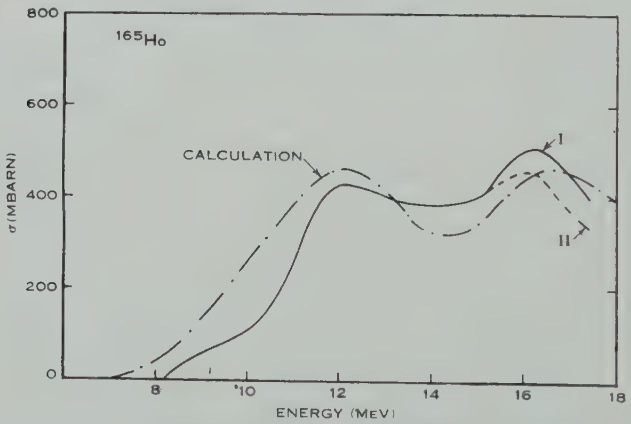

Fig. 12.—Comparison of the calculated cross section for photon absorption in ^{165}Ho with experimental measurements of the same quantity. Curve I has the neutron multiplicity correction applied using the activation experiment. Curve II has neutron multiplicity correction applied using statistical theory of nuclear reactions, with an assumed 30 per cent. direct photoeffect.

V. Results

The derived γ-absorption cross section for the undeformed nucleus ^{141}Pr showed one narrow giant resonance maximum, whereas in the strongly deformed nuclei ^{159}Tb and ^{165}Ho the predicted broadening and splitting effect was observed. These results are consistent with those obtained for the spherical nuclei ^{139}La and ^{197}Au, and the deformed ^{159}Tb and ^{181}Ta, by Fuller and Weiss (1958) and

Spicer *et al.* (1958). In both sets of experiments essentially the same experimental technique was used.

When comparing the experimental results on photonuclear absorption cross sections with theoretical predictions, the notation given below will be used. The component of the giant resonance will have maximum cross section $(\sigma)_{\text{max.}}$ at energy E. The width of the resonance will be discussed in terms of $\Gamma_{-\frac{1}{2}}$ and $\Gamma_{+\frac{1}{2}}$, which give the energy difference between E and the energy at which the cross section is half its maximum value below and above the energy E respectively. The total width of the resonance, Γ, is given by $(\Gamma_{-\frac{1}{2}}+\Gamma_{+\frac{1}{2}})$. The integrated cross section I is in good approximation proportional to the product of $(\sigma)_{\text{max.}}$ and Γ. Thus the ratio of the integrated cross sections under two component peaks of a split giant resonance is given by

$$\frac{I_2}{I_1}=\frac{(\sigma_2)_{\text{max.}}\Gamma_2}{(\sigma_1)_{\text{max.}}\Gamma_1}=\frac{(\sigma_2)_{\text{max.}}\Gamma_{2,+\frac{1}{2}}}{(\sigma_1)_{\text{max.}}\Gamma_{1,-\frac{1}{2}}}. \qquad \ldots\ldots\ldots\ldots\ (7)$$

The total width of a double-peaked giant resonance shall be defined by

$$\Gamma_{\text{G.R.}}=\Gamma_{1,-\frac{1}{2}}+\Gamma_{2,+\frac{1}{2}}+E_2-E_1. \qquad \ldots\ldots\ldots\ldots\ (8)$$

The giant resonance parameters for ^{139}La, ^{141}Pr, ^{197}Au, ^{159}Tb, ^{165}Ho, and ^{181}Ta are collected in Tables 1 and 2.

TABLE 1

GIANT RESONANCE PARAMETERS FOR NON-DEFORMED NUCLEI

Nucleus	^{139}La	^{141}Pr	^{197}Au
Reference . .	Spicer *et al.* (1958)	Present Paper	Fuller and Weiss (1958)
E (MeV)	14·9	15·1	13·5
$(\sigma)_{\text{max.}}$ (mbarn)	460	480	590
$2\times\Gamma_{-\frac{1}{2}}$ (MeV)	4·2	4·4	4
$\Gamma_{\text{G.R.}}$ (MeV)	4·2	—	4·2

TABLE 2

GIANT RESONANCE PARAMETERS IN DEFORMED NUCLEI

Nucleus . .	^{159}Tb		^{165}Ho	^{181}Ta	
Reference . .	Fuller and Weiss (1958)	Present Paper	Present Paper	Fuller and Weiss (1958)	Spicer *et al.* (1958)
$\Gamma_{\text{G.R.}}$ (MeV)	6·5	6·7±0·5	7±0·5	6·2±0·2	6·1
E_1 (MeV)	12·5	12·4±0·2	12·1±0·2	12·45	12·6
$(\sigma_1)_{\text{max.}}$ (mbarn)	260	410	420	308	500
Γ_1 (MeV)	2·4	3·3	2·8	2·3	2·0
E_2 (MeV)	16·3	16·0±0·2	16·2±0·2	15·45	15·3
$(\sigma_2)_{\text{max.}}$ (mbarn)	310	460	510	348	450
Γ_2 (MeV)	4·0	4·5	4·7	4·4	4·0
I_2/I_1 . .	2·0	2·0	2·0	2·16	1·8
E_2/E_1 . .	1·30	1·29±0·03	1·34±0·03	1·25±0·01	1·21±0·03

VI. Interpretation of Results

If the experimentally determined values of E_1 and E_2 are equated to the E_a and E_b respectively of the Danos-Okamoto theory, the nuclear deformation parameter may be calculated from equation (4) by inserting the relevant values from Table 2. These values are entered in Table 3.

The independent particle model theory may also be used to obtain values of the nuclear deformation. The shapes of the cross sections were calculated from the energy level diagram of Nilsson (1955), and the value of ε was estimated by comparing the computed cross sections with the experimental ones. The comparison for the case of ^{165}Ho is shown in Figure 12.

Table 3

NUCLEAR QUADRUPOLE MOMENTS AND DEFORMATION IN ^{159}Tb, ^{165}Ho, AND ^{181}Ta

Method	Nucleus	ε	Q_0 (barn)	Reference
Coulomb excitation . .	^{159}Tb	0·69	8·1	Martin, Marmier, and de Boer (1958)
Coulomb excitation . .		0·63	6·9	Alder *et al.* (1956)
Survey, low-lying levels . .		0·74	—	Mottelson and Nilsson (1959)
Photodisintegration (Danos)		0·63	7·0±0·7	Present paper
Photodisintegration (IPM)		0·72	8·0±0·8	Present paper
Paramagnetic resonance . .	^{165}Ho	0·4	+4·3	Baker and Bleaney (1955)
Coulomb excitation . .		0·69	8·0	Martin, Marmier, and de Boer (1958)
Coulomb excitation . .		0·67	7·8	Alder *et al.* (1956)
Survey, low-lying levels . .		0·72		Mottelson and Nilsson (1959)
Photodisintegration (Danos)		0·74	8·6±0·9	Present paper
Photodisintegration (IPM)		0·72	8·4±0·9	Present paper
Atomic spectroscopy . .	^{181}Ta	0·43	+5·8±0·5	Murakawa and Kamei (1957)
Coulomb excitation . .		0·41	5·6	Martin, Marmier, and de Boer (1958)
Coulomb excitation . .		0·50	6·8	Alder *et al.* (1956)
Survey, low-lying levels . .		0·53		Mottelson and Nilsson (1959)
Photodisintegration (Danos)		0·54	7·0	Fuller and Weiss (1958)
Photodisintegration . .		0·46	6·0	Spicer *et al.* (1958)

If the nuclear charge is assumed to be uniformly distributed throughout the nucleus, the values of ε obtained may be used to compute a value of Q_0, the intrinsic nuclear electric quadrupole moment. The quadrupole moment of a charge Ze uniformly distributed throughout a spheroid is given by

$$Q_0=0\cdot4Z(a^2-b^2). \qquad \ldots\ldots\ldots\ldots\ldots\ldots \quad (9)$$

The relation between ε and Q_0 is

$$\varepsilon=2\cdot5Q_0/r_0^2ZA^{\frac{2}{3}}, \qquad \ldots\ldots\ldots\ldots\ldots\ldots \quad (10)$$

using equation (2) and $R^3=r_0^3A$. In Table 3 the values of ε and Q_0 obtained from the photodisintegration data are set out. Also shown in Table 3 are values for ε and Q_0 obtained from measurements of atomic spectra, from Coulomb excitation measurements, and from a survey of the low-lying levels of deformed nuclei.

The theory of fast electric quadrupole transitions between low-lying levels (Coulomb excitation) and of the spacings of low-lying levels in deformed nuclei are based on the collective theory of nuclear rotational states (Bohr and Mottelson 1953). Both of these types of study give values of Q_0^2 directly in terms of the collective theory, and therefore do not specify the sign of Q_0. The accuracy of such Q-values is limited to some 20 per cent. still, due to the inherent difficulties in the absolute measurements necessary. To compute the deformation parameter ε, again some sort of assumption has to be made concerning the nuclear charge distribution. Again, we assume a uniform charge distribution.

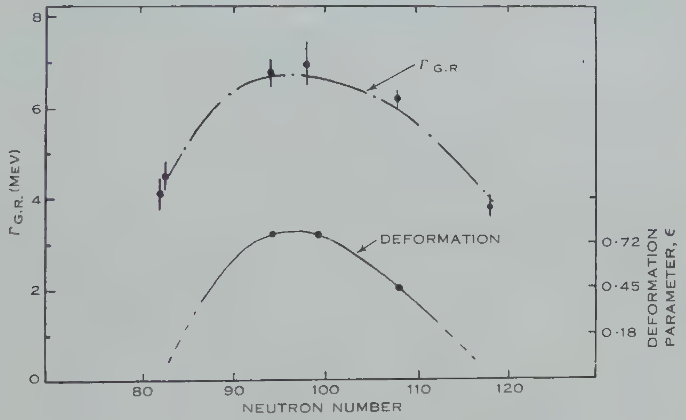

Fig. 13.—Plot of $\Gamma_{G.R.}$ and ε as a function of neutron number over the region of interest.

The atomic spectroscopy measurements do not give the value of Q_0 immediately. Rather they give a value of the quadrupole moment with respect to the nuclear angular momentum direction, say Q, which is less than the value of Q_0. Q_0 is the quadrupole moment relative to the direction of the nuclear axis of symmetry, which in strongly deformed nuclei is not necessarily in the same direction as the angular momentum vector. In the extreme case of strong coupling (Bohr and Mottelson 1953) Q and Q_0 are related by $Q = Q_0.P_I$, where

$$P_I = \frac{I(2I-1)}{(I+1)(2I+3)}$$

and I is the ground state spin. Okamoto (1958) has argued for the validity of the strong coupling approximation in the case of the nuclei ^{159}Tb, ^{165}Ho, ^{181}Ta.

It must be pointed out that the comparison of the above data with photodisintegration data should be treated with some caution. The three alternative methods of determining nuclear deformations which were mentioned are all concerned with nuclei in their ground state or in states very near it. In contrast, photodisintegration data concern transitions between the ground state and excited states 15–20 MeV above the ground state. Again, Okamoto (1958) has argued that the comparison made here is worth while, and the close agreement exhibited in Table 3 indicates that his argument may be correct.

It is to be noted that the ratios I_2/I_1 noted in Table 2 do approximately fulfil the theoretical prediction of the value 2 for that ratio.

On Figure 13 the values of ε and of $\Gamma_{\text{G.R.}}$ are plotted as a function of the neutron number N. It is seen that the broadening effect in the photonuclear giant resonance is dependent on nuclear deformation.

VII. Conclusion

The quantitative investigation of the broadening and splitting effect in the photonuclear giant resonance, in particular the latter effect, requires extremely accurate experiments. The splitting effect remained unobserved in earlier experiments because in those cases the experimental resolution was not sufficient.

The splitting effect was not observed in the (γ,n) cross sections of ^{139}La, ^{141}Pr, and ^{197}Au. This is in agreement with the prediction that the effect will not be present for non-deformed nuclei. This does not exclude the possibility of some fine structure in these cross sections, but merely states that the experimental resolution at present attainable is insufficient to detect it.

The experimental resolution in the experiments of Fuller and Weiss (1958), Spicer *et al.* (1958), and of the present work was sufficient to indicate that the splitting effect observed is real. A discussion of the resolution of bremsstrahlung experiments is given by Thies (to be published). The predictions on photonuclear absorption cross sections from hydrodynamic theory and from independent particle model theory are very much alike, and are in excellent agreement with observation. It was not possible to decide whether experimental cross sections favour either one of the two theories.

VIII. Acknowledgment

One of the authors (H.H.T.) held an I.C.I.A.N.Z. research fellowship during most of this work.

IX. References

Alaga, G. (1955).—*Phys. Rev.* **100** : 432.

Alaga, G. (1957).—*Nuclear Phys.* **4** : 625.

Alder, K., Bohr, A., Huus, T., Mottelson, B. R., and Winther, A. (1956).—*Rev. Mod. Phys.* **28** : 432.

Baker, J. M., and Bleaney, B. (1955).—*Proc. Phys. Soc.* A **68** : 1090.

Berman, A. I., and Brown, K. L. (1954).—*Phys. Rev.* **96** : 83.

Blatt, J. M., and Weisskopf, V. F. (1952).—" Theoretical Nuclear Physics." p. 379. (Wiley : New York.)

Bohr, A., and Mottelson, B. R. (1953).—*Math-fys. Medd.* **27**, No. 16.

Brown, H. N., and Becker, R. A. (1954).—*Phys. Rev.* **96** : 1372.

Cameron, A. G. W. (1957).—Atomic Energy of Canada Ltd. Report CRP 690.

Carver, J. H., and Turchinetz, W. (1959*a*).—*Proc. Phys. Soc.* **73** : 69.

Carver, J. H., and Turchinetz, W. (1959*b*).—*Proc. Phys. Soc.* **73** : 110.

Danos, M. (1956).—*Bull. Amer. Phys. Soc.* **1** : 135, 246.

Danos, M. (1958).—*Nuclear Phys.* **5** : 23.

Ford, K. W., and Hill, D. L. (1955).—*Annu. Rev. Nuclear Sci.* **5** : 25.

Fuller, E. G., and Weiss, M. S. (1958).—*Phys. Rev.* **112** : 560.

Martin, M., Marmier, P., and de Boer, J. (1958).—*Helv. Phys. Acta* **31** : 435.

Montalbetti, R., Katz, L., and Goldemberg, J. (1953).—*Phys. Rev.* **91** : 659.

Mottelson, B. R., and Nilsson, S. G. (1959).—*Math-fys. Medd.* **1**, No. 8.

Murakawa, K., and Kamei, T. (1957).—*Phys. Rev.* **105** : 671.

Nilsson, S. G. (1955).—*Math-fys. Medd.* **29**, No. 16.

Okamoto, K. (1956).—*Progr. Theor. Phys., Osaka* **15** : 75.

Okamoto, K. (1958).—*Phys. Rev.* **110** : 143.

Penfold, A. S., and Leiss, J. E. (1958).—" Analysis of Photo Cross Sections." (Physics Research Laboratory, University of Illinois : Champaign, Illinois.)

Silva, E., Goldemberg, J., and Smith, P. B. (1958).—*Nuovo Cim.* **1** : 18.

Spicer, B. M., Thies, H. H., Baglin, J. E., and Allum, F. R. (1958).—*Aust. J. Phys.* **11** : 298.

Whalin, E. A., and Hanson, A. O. (1953).—*Phys. Rev.* **89** : 324.

Wilkinson, D. H. (1956).—*Physica* **22** : 1039.

Wilkinson, D. H. (1958).—*Phil. Mag.* **3** : 567.

SOUTHERN HEMISPHERE METEOR SHOWER ACTIVITY IN JULY AND AUGUST

By A. A. Weiss*

[*Manuscript received March* 21, 1960]

Summary

Observations of the radiant positions and the activities of the δ-Aquarids and three minor showers of July and August, obtained with high resolution radio equipment at Adelaide from 1957 to 1959, are given in detail. Data for the δ-Aquarids are combined with similar observations in 1953 to obtain the radiant ephemeris

$$\alpha = 342\cdot3^\circ + 0\cdot76\ (\odot - 126\cdot0^\circ)$$
$$\delta = -16\cdot4^\circ + 0\cdot13\ (\odot - 126\cdot0^\circ).$$

The δ-Aquarid activity extends from July 20 to August 14, with a maximum near July 29. Minor shower activity, extending over and beyond the whole duration of δ-Aquarid activity, is identified as proceeding from three main centres already known visually: the Capricornids, the Pisces Australids, and the Cetids.

I. Introduction

The period from the beginning of July to the middle of August is one of high meteor shower activity in the southern hemisphere. The principal shower is the δ-Aquarids. Numerous minor showers with radiants south of the ecliptic have been detected by visual observations (McIntosh 1935). In addition, a previously unreported day-time shower, the Phoenicids, has been discovered by the Adelaide radio surveys.

With the exception of 1955, observations over July and August have been made each year from 1953 to 1959. The observations prior to 1956 have already been published (Weiss 1955, 1957), and all available data on the Phoenicid shower have been summarized in Weiss (1960). The present paper describes the remaining observations for 1957 to 1959, and summarizes the measurements, with high resolution equipment, of the radiant coordinates and echo rates for the δ-Aquarids and three of the more prominent of the minor showers. The observations for 1954 and 1956, made with the 27 Mc/s "wind" equipment, lack the resolution necessary for the separation of the δ-Aquarid from the minor shower activity, and have been excluded from this summary.

II. Equipment

The bulk of the observations have been made with the 67 Mc/s radiant survey equipment (Weiss 1955, 1960). This is a high resolution radar system with two narrow-beam aerials directed at low elevation along azimuths 35·5° S. of E. (termed the N aerial) and 14° N. of E. (S aerial). The line densities of electrons in the faintest trails detected by this equipment are close to 1×10^{11} electrons/cm, corresponding to visual magnitude $M_v \sim +7$. The method of

---

* Division of Radiophysics, C.S.I.R.O., at Department of Physics, University of Adelaide.

measuring radiant coordinates has been described adequately in the papers cited. The equipment operated at the same high sensitivity in 1957 and 1958, and at much lower sensitivity in 1953.

During 1959 the 67 Mc/s equipment was replaced by a new equipment operating at 61 Mc/s, the transmitter power of 50 kW remaining unchanged. The observations were made during the period of reconstruction with a temporary aerial system with only one receiving channel; the beam axis was directed due west at an elevation of 29°. Because of the temporary nature of the installation the geometry of this aerial system has not been investigated in detail. The resolving power of the system, however, is inferior to that of the 67 Mc/s array, and the detection threshold is $M_v \sim +6$.

III. The Phoenicid Shower

For the sake of completeness the following details of this day-time shower are given. The activity extends from July 5 to July 19, with a fairly sharp maximum at July 14, $\odot = 112°$, when the echo rate is 30/hr. Radiant coordinates for 1958, which are the most reliable determinations, are

$$\alpha = 31 \cdot 1° + 1 \cdot 05 \ (\odot - 109 \cdot 6°),$$
$$\delta = -47 \cdot 9° + 0 \cdot 54 \ (\odot - 109 \cdot 6°).$$

Data for the earlier years will be found in Weiss (1960).

IV. The δ-Aquarid Shower

(a) *Observations for 1957, 1958, and 1959*

The daily positions of the radiant, and the echo rates, are listed in Table 1. The times of detection of echoes at 700 km slant range, from which the radiants were determined, are plotted in Figure 1.

The shower appears to persist until about August 14, but near the emergence of the Earth from the stream the range-time plots show considerable scatter, presumably associated with a diffuse radiant. This, coupled with the low echo rate, precludes accurate measurement of the radiant. In 1957 echoes were received from N and S aerial channels on alternate days, and the radiants for individual days were determined by interpolation between times of passage separated by two days. Since only one channel was available in 1959, the radiant could not be measured to the same order of accuracy as in the previous years, and no data have been given.

The times for the 700 km echoes, plotted in Figure 1, were determined by maximizing the echo count within theoretical range-time envelopes. The main source of error is random grouping amongst both shower and sporadic meteors. We see from Figure 1 that except near the fringes of the stream the error in the measurement of these times probably does not exceed ±5 min; the consequent errors in radiant coordinates are: R.A. ±1°, declination ±3°. It is also evident from Figure 2, by comparison of the 1957 and 1958 data, that the interpolations which are necessary to derive radiant coordinates for the individual days of 1957 do not introduce appreciable errors. The overall uncertainty in an individual radiant determination should not exceed ±2° in R.A. and ±5° in declination.

The "envelope" echo rates of Table 1 for 1957 and 1958 are the actual numbers of shower echoes detected inside theoretical range-time envelopes for the appropriate radiant positions on the corresponding days. No attempt has been made to reduce these envelope rates to hourly rates. Theoretical envelopes have not been calculated for the 1959 aerial system, and an empirical envelope has been determined from the echo rates themselves. The "total" echo rate is the number of shower echoes detected each day over the following periods: 1957 and 1958, N aerial, 01–04 hr; S aerial, 02–05 hr; 1959, 22–02 hr. Small corrections have been applied to both sets of rates to allow for known variations in sensitivity over each run, assuming a mass-distribution parameter* $s \sim 1 \cdot 6$ for the δ-Aquarids and $s = 2 \cdot 0$ for sporadics. The value of $s \sim 1 \cdot 6$ has

Table 1

RADIANTS AND ECHO RATES FOR THE δ-AQUARID SHOWER 1957–1959

Date	Radiant Coordinates				Echo Rates					
	1957		1958		Envelope			Total		
	α	δ	α	δ	1957	1958	1959	1957	1958	1959
July 20 ..			332	—23		17			97	
21 ..	337	—18	336	—20	18	23	82	93	104	88
22 ..	337	—18	337	—18	27	45	118	99	144	96
23 ..	337	—17	337	—18	39	58	133	117	140	160
24 ..	338	—17	338	—18	50	52	184	107	126	216
25 ..	339	—16	339	—18	67	65	230	132	152	289
26 ..	340	—16	339	—18	95	110	242	158	218	280
27 ..	340	—16	—	—	92	—	242	220	—	264
28 ..	341	—15	—	—	111	—	292	271	—	322
29 ..	342	—15	—	—	140	—	296	319	—	342
30 ..	343	—15	343	—17	120	99	289	176	247	338
31 ..	343	—15	—	—	119	—	243	233	—	276
Aug. 1 ..	344	—15	344	—17	68	65	235	156	144	246
2 ..	345	—16	345	—17	68	56	209	171	148	228
3 ..	345	—16	345	—17	43	47	216	118	145	211
4 ..	346	—16	346	—17	65	35	217	144	111	252
5 ..	346	—17	—	—	38	—	160	116	—	175
6 ..	347	—17	347	—17	42	32	135	130	67	135
7 ..	347	—17			23	49	112	69	104	116
8 ..	348	—15			25	12	122	94	66	146
9 ..	350	—13			31	22	72	99	100	66
10 ..	351	—12			17	22		82	49	
11 ..						15			55	
12 ..						16			50	
13 ..						20			27	
14 ..						17			35	

---

* This parameter is the exponent in the differential law for the distribution of meteor masses, namely, $\nu_m dm = \text{const.}\, m^{-s} dm$.

been determined (in 1959) from a comparison of the echo rates in two receiver channels held at different sensitivities. The high echo rates in 1959, relative to 1957 and 1958, are due to the increased aperture of the aerial system used in 1959, and do not necessarily indicate a higher shower activity.

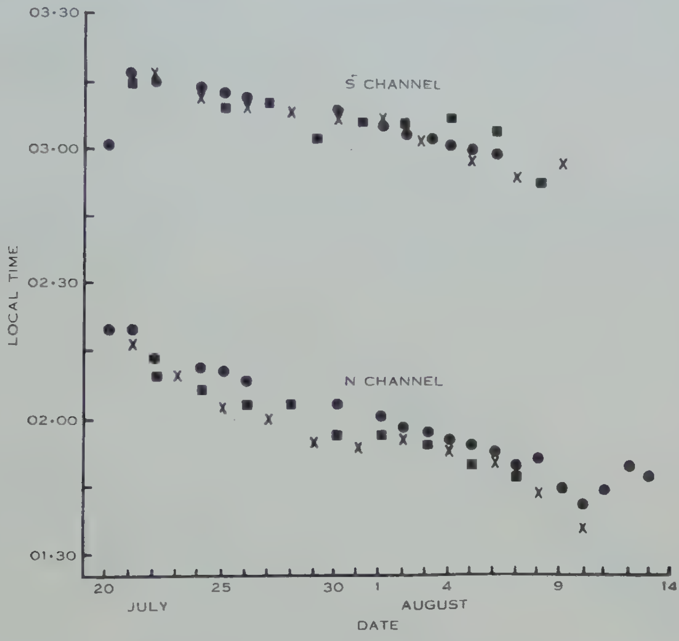

Fig. 1.—Times of detection of echoes at 700 km slant range, δ-Aquarids. 1953, ■; 1957, ×; 1958, ●.

(b) *Radiant*

Radiant positions on individual days are plotted in Figure 2. The radiant ephemeris estimated by the method of least squares is

$$\alpha = 342 \cdot 2^\circ + 0 \cdot 77 \ (\odot - 126 \cdot 0^\circ),$$
$$\delta = -16 \cdot 6^\circ + 0 \cdot 19 \ (\odot - 126 \cdot 0^\circ).$$

These daily motions in α and δ are considerably smaller than those, namely, 0·96° in α, 0·41° in δ, determined by a different method by McIntosh (1934) from the New Zealand visual observations. It is evident from Figure 2 that McIntosh's daily motion in δ is not incompatible with the radio determination. This is, however, not the case for the daily motion in α, nor can the discrepancy be attributed to the two different methods used in determining the ephemeris. The ephemeris was formed by McIntosh by reducing all radiant coordinates to apparent ecliptical latitude β and the difference in longitude, $\lambda - A$, between the apparent radiant λ and the apex of the Earth's way, A, taking the mean position of the whole and translating it back to the α,δ coordinate system. β and $\lambda - A$ have been termed apparent coordinates because corrections for zenith attraction and diurnal aberration have not been applied. These corrections are small, however, and barely exceed 0·5°. The data used by McIntosh are plotted in Figure 3, and it is seen that there is, for the visual observations, no systematic dependence of $\lambda - A$ and of β on the longitude of the apex, A. Similar treatment of the radio data, on the other hand, reveals systematic changes in both $\lambda - A$ and in β with the age of the shower. These, when translated back to the α,δ system, yield the daily motions sketched in Figure 2. The corresponding ephemeris, which differs only slightly from the least squares ephemeris, is

$$\begin{aligned}\alpha &= 342{\cdot}3^\circ + 0{\cdot}76\ (\odot - 126{\cdot}0^\circ),\\ \delta &= -16{\cdot}4^\circ + 0{\cdot}13\ (\odot - 126{\cdot}0^\circ).\end{aligned}$$

The Adelaide radiant coordinates have not been corrected to epoch 1950, to which the longitude of the Sun is referred, because the probable errors far exceed the corrections. The corrections required to reduce the radio and visual observations, separated by over 20 years, to common epoch will be appreciable, but as the reference epoch for the visual observations is not stated, no corrections have been applied. An error not exceeding 0·5° may thus have to be taken into account in comparing mean radiants; the daily motions, of course, will not be affected.

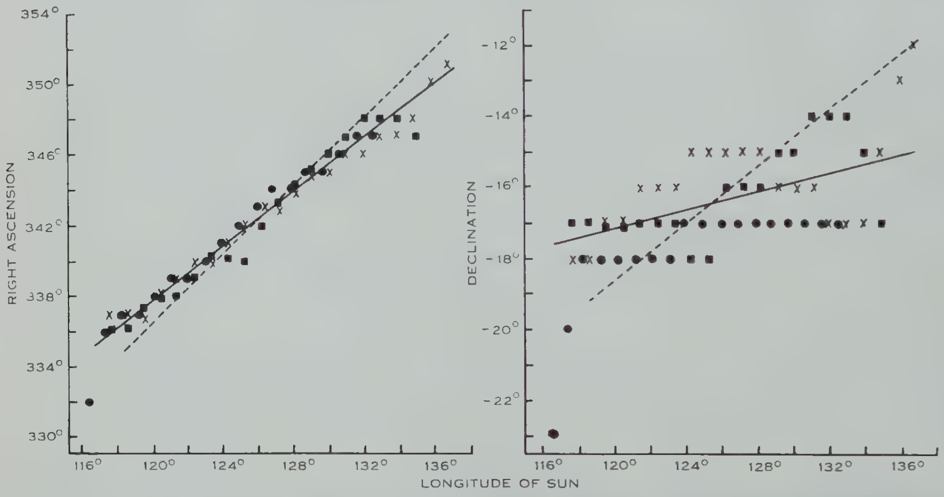

Fig. 2.—Right Ascension and declination of the δ-Aquarid radiant. Determinations for individual days: 1953, ■; 1957, ×; 1958, ●. The full lines are the best fits to the radio data determined through ecliptical coordinates in the manner indicated in Section IV (*b*) of the text. The dashed lines are similar fits to visual data for 1926 to 1933 (after McIntosh).

That these systematic changes in $\lambda - A$ and β are real can be seen from the following argument. A constant value of $\lambda - A$ implies that the time of transit of the radiant changes by only a few minutes over the duration of the shower; any change in the time of passage of the shower radiant through the aerial collecting sectors is thus produced almost entirely by a shift in the declination of the radiant. Now, for radiants whose declinations lie in the range $0^\circ > \delta > -20^\circ$, the time of passage for the S aerial is extremely insensitive to the declination (see, e.g. Figure 1 of Weiss 1955), and if $\lambda - A$ is constant the time of passage through the S aerial collecting sector should change by a few minutes at most. In actual fact we find (Fig. 1) for the S aerial an advance of 18 min from July 22 to August 6, which is identical for each of the three years for which observations are available. Since a change of this magnitude is quite outside the experimental error in the measurement of times of passage, we may conclude that $\lambda - A$, at least, cannot be constant for the duration of the shower. Further consideration of the times of passage for the N aerial then indicates that β also is not constant for the duration of the shower.

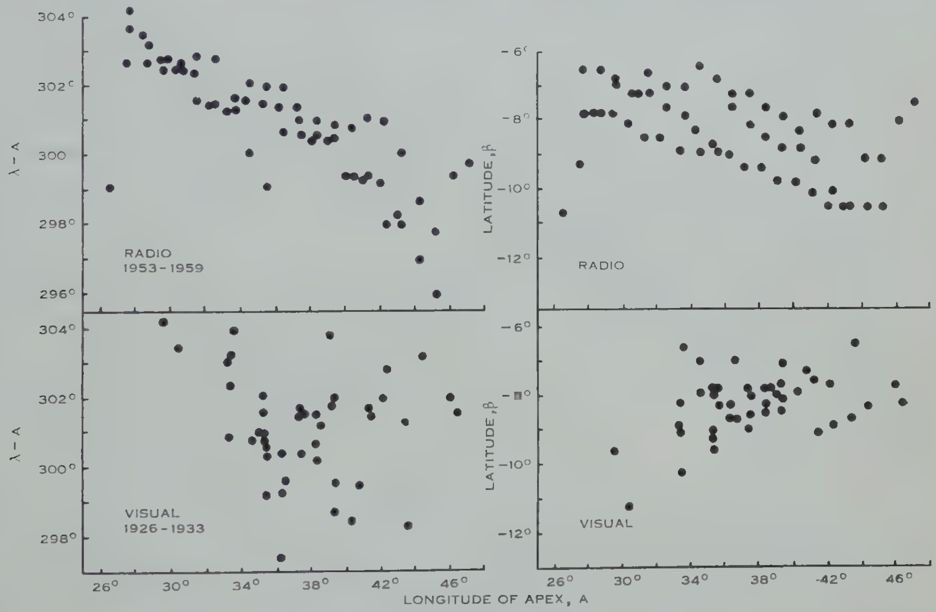

Fig. 3.—Comparison in ecliptical coordinates of the New Zealand visual radiant and the Adelaide radio radiant for the δ-Aquarids. Corrections for zenith attraction and diurnal aberration have not been applied, and coordinates are not reduced to common epoch.

Although it is possible that the discrepancy between the visual and the radio ephemerides could be due to incomplete separation of the minor showers from the δ-Aquarids in the Adelaide observations, this explanation is unlikely in view of the excellent agreement between the mean positions of the radiant as found from the two sets of data.

(c) *Radiant Diameter*

It is not possible to measure the radiant diameter because two of the minor showers cannot be fully resolved from the δ-Aquarid radiant. The large variations in radiant diameter attributed to the δ-Aquarid stream on the basis of the 1953 observations (Weiss 1955) are now recognized as largely due to the intermittent nature of the minor shower activity.

(*d*) *Activity*

The shower is first detectable on July 20 and persists until August 14. This duration agrees with the visual observations.

An overall picture of the dependence of shower activity on solar longitude has been determined by multiplying the envelope rates for 1953 and 1959 by factors of $3 \cdot 2$ and $0 \cdot 30$ respectively, and then combining these with the 1957 and 1958 data. Echo rates so obtained are plotted in Figure 4. The activity is slightly asymmetrical about a flat maximum between $\odot = 124^\circ$ and $\odot = 125^\circ$.

Variations in equipment sensitivity have been so large that no conclusions can be drawn regarding variations from year to year in the activity of the δ-Aquarid stream.

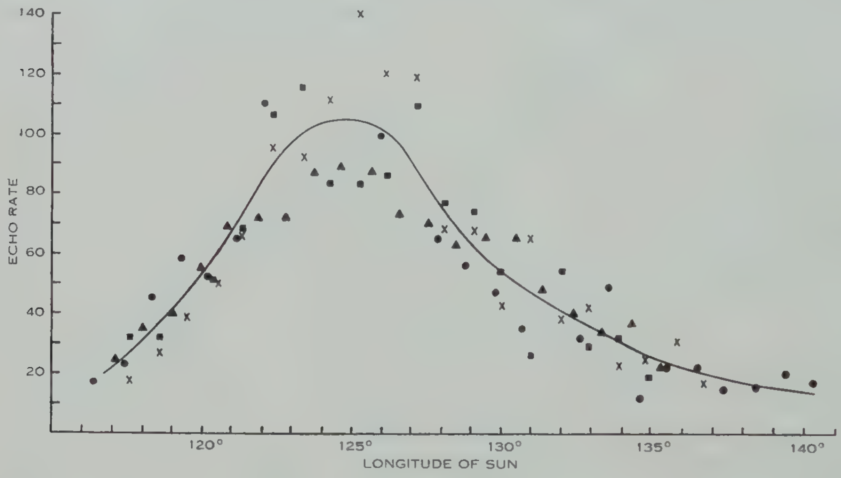

Fig. 4.—The rate of shower echoes falling inside range-time envelopes for the δ-Aquarids. Echo rates for 1953 and 1959 have been reduced to the 1957/1958 level of activity. 1953, ■; 1957, ×; 1958, ●; 1959, ▲.

V. The Minor Showers

The period from mid July to mid August is one of remarkably high minor shower activity in the southern hemisphere. It can be seen from Table 1 that after excluding sporadic activity the total echo rates for 1957 and 1958 in 3 hr centred on the time of peak δ-Aquarid activity exceed the envelope rates by a factor usually exceeding 2. A similar excess was noted in 1953 when the equipment operated at much lower sensitivity. Some at least of the excess echoes are to be attributed to δ-Aquarid meteors which fall outside the theoretical envelopes, which are computed for a point radiant, but the majority are associated with minor stream activity.

At the higher sensitivity of 1957 and 1958, three main centres of activity could be recognized. The times of occurrence of echoes at 700 km range in each of the two aerial channels are plotted in Figure 5. The large scatter in each set of points is due to the low echo rates of these minor showers, which rarely ever exceed the sporadic rate. Radiants have been determined by drawing straight lines through these plots. In addition, day-by-day radiants were computed from the 1958 data, in which information was available on most days (see Table 2). In general, the quality of the individual radiant determinations is poor, again because of the low echo rates ; a radiant classified as A is probably accurate to 3°, but the quality of the radiant deteriorates rapidly for the B and C classifications. The radiant ephemerides, and the 1958 measurements for individual days, are plotted in Figure 6.

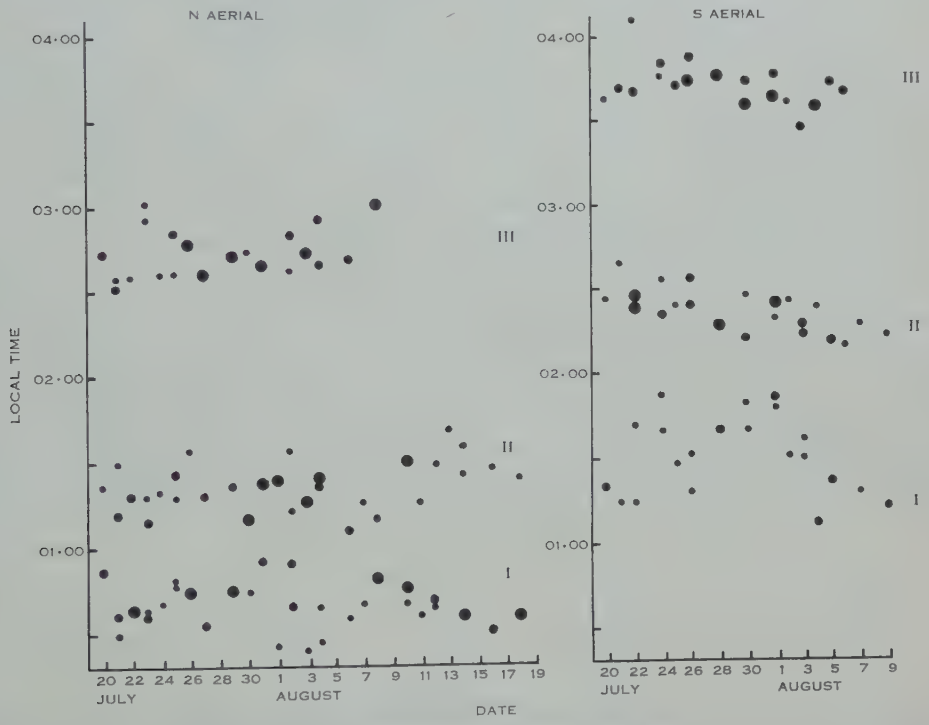

Fig. 5.—Times of detection of echoes at 700 km slant range, minor showers 1957 and 1958. Large dots represent determinations of good accuracy, and small dots, determinations of low accuracy. I, Capricornids ; II, Pisces Australids ; III, Cetids.

The identification of the Cetid radiant is beyond doubt. It corresponds closely with a visual radiant at 352°/11°, −18° active from July 19 to August 1, reported by McIntosh (see, e.g., southern hemisphere finding list compiled by Ellyett and Roth (1955)).

Although the times of passage of the other two centres through the N and S collecting areas are fixed with reasonable precision, there is some uncertainty in the way in which they are to be paired for the determination of the radiants. The criterion adopted was the relative strengths of the activities in each aerial channel on the same days, which indicated that the 00·39 passage through the N aerial is linked with the 01·31 passage through the S aerial, and 01·22 (N aerial) with 02·31 to 02·05 (S aerial). This grouping also gave the best agreement with the visual results, according to which the minor shower activity is confined to

Table 2

radiants of the minor showers 1958

Date	Capricornids			Pisces Australids			Cetids		
	α	δ	Class	α	δ	Class	α	δ	Class
July 20	307	—26	B	322	—17	C	341	—20	C
21	306	—22	C	326	—10	C	342	—16	B
22	313	—17	B	324	—16	A	343	—17	C
24	314	—18	C	325	—18	C	347	—15	C
25	313	—23	C	327	—18	C	346	—17	C
26	315	—21	B	330	—18	C	348	—19	A
30	320	—19	C	332	—13	B	350	—20	B
Aug. 1	321	—12	C	333	—19	B	—	—	—
2	321	—20	C	335	—14	C	353	—18	C
3	322	—17	C	333	—19	A	—	—	—
4	319	—26	C	337	—18	C	355	—19	A

only two radiants other than the Cetids—see Table 3. Although there are some discrepancies between the visual and radio radiants, the visual nomenclature has been retained to avoid confusion.

The strengths of all three showers vary irregularly from day to day. The Pisces Australids are the most active of the three; and the Cetids, which are resolved from the δ-Aquarid shower only with difficulty, are the weakest. The onset of all three showers occurs prior to July 20, the date from which the detailed analysis was made; the Capricornids and the Pisces Australids persist beyond the middle of August, but the Cetid activity was not detected after August 8.

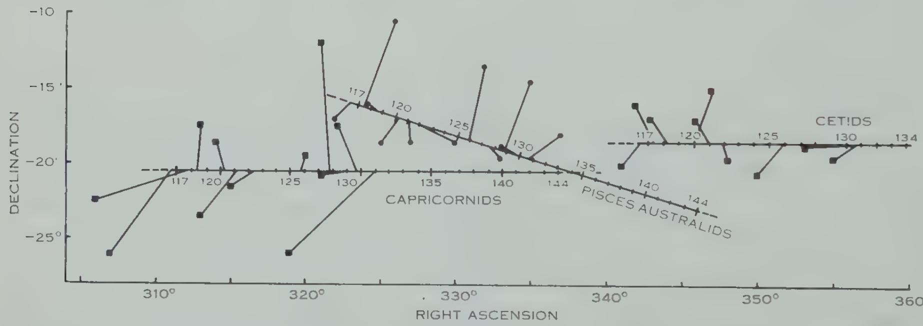

Fig. 6.—Ephemerides for the minor streams of July and August. The three straight lines, which are averages for 1957 and 1958, indicate the mean positions of the respective radiants in Right Ascension and declination as functions of the longitude of the Sun, whose value is marked along the lines. Individual radiants shown are for 1958; each is joined to the point on the mean radiant path corresponding to the longitude of the Sun at which it was determined.

The comparatively small excess of the total rates (in 4 hr) over the envelope rates for 1959 is thought to be misleading and not a true measure of the minor shower activity. As already mentioned, the resolving power of the 1959 aerial system is lower than that used in previous years and the activity from only one of the three recognized minor radiants can be resolved completely from the main δ-Aquarid activity. The envelopes used in the analysis of the 1959 data were determined empirically from the observations, and it is almost certain that a considerable fraction of the Cetid and Pisces Australid activity has been included in the envelope activity for the δ-Aquarids. There are, however, in the range-time plots some excess echoes whose range changes with time in the manner expected of shower activity and which precede the main δ-Aquarid activity by 130 min. These are identified as proceeding from the Capricornid radiant. In fact, this time difference of 130 min gives for the Capricornid radiant in 1959 a Right Ascension which agrees better with the visual radiant than the 1957 and 1958 determinations.

TABLE 3

COMPARISON OF RADIO AND VISUAL RADIANTS

Shower	Adelaide Radio			Visual†		
	Dates of Activity	Radiant		Dates of Activity	Radiant	
		α	δ		α	δ
Capricornids	July 20*–Aug. 18*	311/337	—20	July 10–Aug. 5	300/325	—10/—19
Pisces Australids	July 20*–Aug. 18*	323/346	—16/—23	July 14–Aug. 22	330/339	—30
				July 26–Aug. 8	337/350	—30/—33
δ-Aquarids	July 20 –Aug. 14	335/353	—14/—19	July 22–Aug. 15	331/351	0/—17
Cetids ..	July 20*–Aug. 8	342/0	—18	July 19–Aug. 1	352/11	—18

* Shower may commence before, or terminate after, these dates.

† From Ellyett and Roth (1955).

VI. REFERENCES

ELLYETT, C. D., and ROTH, K. W. (1955).—*Aust. J. Phys.* **8** : 390.

McINTOSH, R. A. (1934).—*Mon. Not. R. Astr. Soc.* **94** : 583.

McINTOSH, R. A. (1935).—*Mon. Not. R. Astr. Soc.* **95** : 709.

WEISS, A. A. (1955).—*Aust. J. Phys.* **8** : 148.

WEISS, A. A. (1957).—*Aust. J. Phys.* **10** : 299.

WEISS, A. A. (1960).—*Mon. Not. R. Astr. Soc.* (In press.)

METEOR HEIGHT DISTRIBUTIONS AND THE FRAGMENTATION HYPOTHESIS

By A. A. Weiss*

[*Manuscript received April* 19, 1960]

Summary

This paper is concerned with a comparative study of the incidence of fragmentation amongst bright and faint meteors, as disclosed by photographic measurements of heights and light curves of brighter meteors (visual magnitudes $<+4$), and by measured radio-echo height distributions of faint meteors (visual magnitudes $\sim+6$). The discussion is based on photometric and height data for sporadic and shower meteors obtained by Harvard and Canadian observers, and on radio-echo height distributions measured at Jodrell Bank. Mean photographic light curves are shorter than predicted by evaporation theory, and there is a large residual scatter in the heights of maximum brightness after reduction to standard meteor velocity and brightness. Trail length is independent of reduced height, and also of velocity if this exceeds 25 km/sec; for slower meteors trail lengths shorten rapidly. The radio-echo height distribution as a function of trail length is calculated for a simple model which incorporates these features of the ablation process for brighter meteors. Comparison with radio height measurements indicates that meteors below the photographic threshold show a closer approach to the predictions of the evaporation theory than meteors bright enough to record photographically.

I. Introduction

The photographic recording of meteor trails has demonstrated that the process of trail formation amongst visual meteors is not correctly described by the evaporation theory (Herlofsen 1948), which treats the interaction of a solid particle with the atmosphere. Thus, Hawkins and Southworth (1958), in a discussion of basic data for sporadic meteors, conclude that the observed lengths of meteor trails are considerably shorter than predicted by the evaporation theory and appear to depart from the theory in a random fashion. They refer to a suggestion by Jacchia (1955) that this discrepancy can be accounted for by the phenomenon of fragmentation of the meteoroid. Jacchia, Kopal, and Millman (1950) had already advanced this explanation to account for their observation of exceptionally short trajectories and abnormally great heights of the 1946 Draconid (Giacobinid) meteors.

These are direct measurements, and the inapplicability of the evaporation theory is inescapable. It is more difficult to ascertain the extent to which the evaporation theory fails to describe the ionization curves of the fainter meteors accessible to radio equipments, because a radio equipment responds to only a short segment of the individual meteor trail. This question, however, is of some importance, not only in its own right but also because radio measurements of the heights of echoing points, of the echo rate, and of echo durations have been

---

* Division of Radiophysics, C.S.I.R.O., at Department of Physics, University of Adelaide.

applied by Browne *et al.* (1956), and other workers, to the determination of the distribution of the masses of meteors whose brightnesses extend down to visual magnitude $M_v \sim +7$, and Evans (1954, 1955) has derived values of the atmospheric pressure and scale height from the height distributions. In all these applications the assumption has been made that the ablation of a meteoroid is correctly described by the evaporation theory. Unless the nature of the ablation process changes significantly over a range of meteor brightness of only two or three magnitudes, this assumption would appear to be unwarranted.

An indirect approach to the measurement of ionization curves of radio meteors has been made by Greenhow and Neufeld (1957). These workers compared echo amplitudes at two rather ill-defined points on an individual meteor trail, and from a statistical analysis of a large number of echo amplitude ratios they concluded that the mean ionization curve of these fainter meteors $(+6 < M_v < +8)$ is shorter than predicted by evaporation theory.

Apart from second-order effects introduced chiefly by the finite aperture of the aerial system and the celestial spread in radiant points of sporadic meteors, the width (r.m.s. deviation) of the sporadic radio-echo height distribution depends on four main factors. These are (*a*) the mass distribution of the meteoroids; (*b*) the atmospheric scale height and its variation with height; (*c*) the mean ionization curve of the meteor trails; (*d*) the dependence of the height of maximum ionization on the mass of the meteoroid. The mass distribution for sporadic meteors is known (Kaiser 1954*b*). If one assumes the evaporation theory, (*c*) and (*d*) are prescribed and hence the width of the radio-echo height distribution can be computed as a function of the atmospheric scale height Kaiser (1954*a*, 1954*b*; Weiss 1959). It was by comparing with his actual height measurements theoretical height distributions computed under this set of assumptions that Evans (1954, 1955) was able to study the properties of the atmosphere. The atmospheric scale height, however, is sufficiently well known to justify an alternative treatment of the height measurements, which is rendered more appropriate by the doubts which have arisen over the validity of the evaporation theory. In the absence of a physical theory of fragmentation the mean ionization curve (as regards both length and profile) and the dependence of the height of the trail on meteoroid mass may be regarded as free parameters. A comparison of the measured width of the radio-echo height distribution with the width computed with the above-mentioned trail characteristics (*c*) and (*d*) as free parameters should then lead to an estimate of the extent of the fragmentation amongst the sample of meteors measured.

The necessity for retention of two free parameters, and the possibility of random departures of individual meteors from the mean behaviour, are complications which effectively preclude the direct application of this procedure to the radio meteors. The random variations are important simply because a radio equipment responds only to a short segment of the meteor trail. A measurement of the height of a single echoing point tells us nothing about the height of the point of maximum brightness of the trail, the shape of the ionization curve, or the maximum brightness of the trail. This compels us to analyse the radio height data on a statistical basis, with the possibility of erroneous conclusions unless the causes of random variations and errors are scrutinized. Random departures of individual meteors from the mean height of maximum ionization may well be decisive; random fluctuations in the shape of the ionization curve are of much less consequence.

For these reasons, it would obviously be desirable to have prior knowledge of the behaviour of these characteristics amongst the brighter photographic meteors, where the incidence of fragmentation is beyond dispute. Neither the Harvard nor the Canadian workers carried the analysis of their photographic data to this point; they went little further than establishing that, for their samples of meteors, the trails were shorter than predicted by the evaporation theory, occurred at abnormally great heights, and were subject to random fluctuations. As already mentioned, Evans's approach to the radio-echo data was to assume the validity of the evaporation theory and then to proceed to the evaluation of the atmospheric parameters; his numerical values were qualified by the remark that if fragmentation were widespread it seemed surprising that scale height results which were at all reasonable should be obtained.

The present paper is a comparative study of the incidence of fragmentation amongst bright and faint meteors, based on a more detailed analysis and rediscussion of the observational material obtained by Jacchia, Kopal, and Millman (1950), Evans (1954, 1955), and Hawkins and Southworth (1958). The photographic data are first analysed in detail, as regards light curves, trail lengths and heights, with particular emphasis on scatter about the mean behaviour. This is followed by the theoretical derivation of the height distribution which would be observed, by radio techniques, for a model group of meteors which exhibited these characteristics, including the scatter. This model height distribution is then compared with the actual observations of radio-echo height distributions of faint meteors. This comparison suggests that fragmentation is less marked amongst the fainter meteors.

II. PHENOMENOLOGICAL DESCRIPTION OF THE ABLATION PROCESS FOR PHOTOGRAPHIC METEORS

In this section we derive a tentative phenomenological description of the observed lengths, light curves, and heights of photographed meteor trails. The analysis is based on photometric and height data for 286 sporadic and 74 shower meteors, with brightnesses extending down to a little below $M_v = +4$, as tabulated by Hawkins and Southworth (1958); and for 150 Draconid shower meteors, with brightnesses down to $M_v \sim +1$, measured by Jacchia, Kopal, and Millman (1950). These samples are taken to be representative of the brighter meteors.

It should be emphasized at this juncture that this description may not be suitable as the basis for a theory of fragmentation of meteoroids. Rather, the analysis is intended to enumerate those characteristics of photographed meteor trails which are relevant to the calculation of the corresponding radio-echo height distribution. These characteristics are not necessarily those which one would choose to examine preliminary to a discussion of the physical causes and consequences of fragmentation of the meteoroid.

(*a*) *Mean Light and Ionization Curves*

The data given are insufficient to define light curves for individual meteors, but by reducing all meteors to the same arbitrary height at maximum brightness a mean light curve may be determined. Photographic magnitude M_p is converted into intensity I by the simple relation

$$M_p = \text{constant} - 2{\cdot}5 \log I. \quad \ldots\ldots\ldots\ldots\ldots \quad (1)$$

Mean light intensity curves so obtained are sketched in Figure 1; the profiles are normalized so that plate limit corresponds to $I/I_{\text{max.}} = 1$. The light curve for the sporadic meteors is designated BB, and that for the Draconid shower meteors, CC. For the sporadic meteors the level of maximum brightness above plate limit has been tabulated by Hawkins and Southworth. This quantity was not given for the Draconids, but since the observations extended over only 5 hr, plate threshold has been assumed constant and some $\frac{1}{2}$ magnitude below the faintest measured meteor.

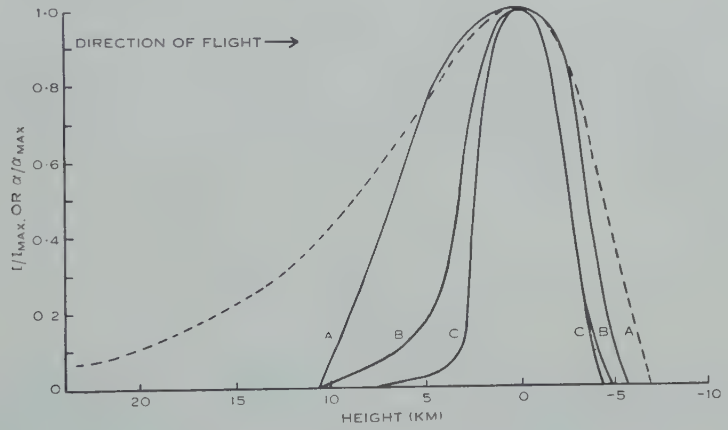

Fig. 1.—Ionization and light curves for sporadic and shower meteors. Curve AA, ionization curve proposed by Greenhow and Neufeld for faint sporadic meteors; BB, mean light curve for photographed sporadic meteors; CC, mean light curve for Draconid meteors; dashed curve, light and ionization curves predicted by evaporation theory with atmospheric scale height 6·4 km. In each case the height scale has been adjusted to height of maximum brightness as zero.

The mean ionization curve proposed by Greenhow and Neufeld (1957) for faint sporadic meteors ($+6 < M_v < +8$) is also reproduced in Figure 1 (curve AA). It will be seen that the ionization curve is somewhat longer than the light curve for the photographic sporadic meteors, which are about three magnitudes brighter, but that both profiles are a good deal shorter than the prediction of the evaporation theory, namely,

$$I/I_{\text{max.}} = \alpha/\alpha_{\text{max.}} = (9/4)(\rho/\rho_{\text{max.}})(1 - \tfrac{1}{3}\rho/\rho_{\text{max.}})^2 \quad \ldots\ldots \quad (2)$$

(Herlofsen 1948). ρ is the atmospheric density and α the electron (ion) line density. The subscript " max." refers to the point of maximum electron density (and light intensity) on the trail.

The small sample of shower meteors tabulated by Hawkins and Southworth also have light curves which are shorter than predicted by (**2**). There also seem to be systematic differences between the light curves of meteors belonging to different showers. In particular, the Taurid meteors show the closest approach to the evaporation theory and the Quadrantids the largest deviations from it. However, the samples are far too small for these to be other than hints of important differences in the characteristics of meteoroids belonging to different showers.

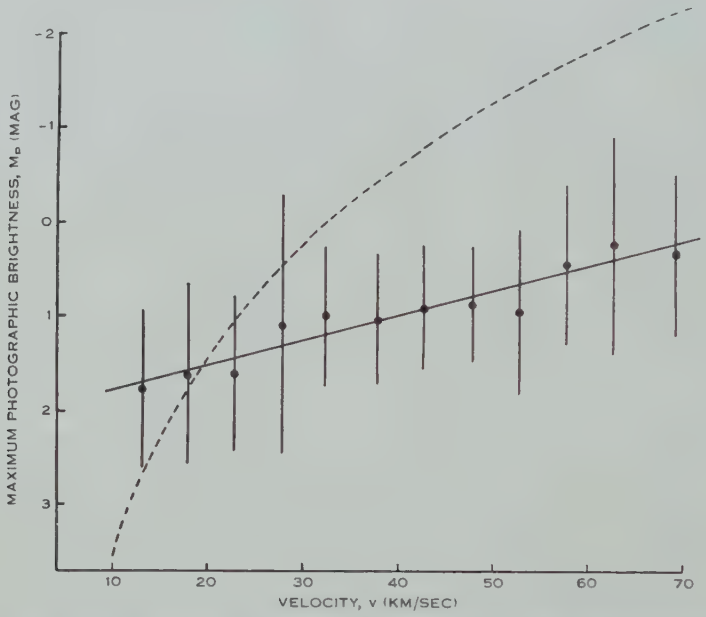

Fig. 2.—The relation between meteor velocity and photographic absolute magnitude at maximum brightness, for sporadic meteors. Vertical lines give the r.m.s. deviations of the mean brightnesses for velocity groups. The full line is the regression line for the weighted means, and the dashed curve the relation (**11**) predicted by the evaporation theory, to an arbitrary zero.

(*b*) *Heights of Maximum Brightness*

On the assumption that corrections to the observed heights of maximum brightness, $h_{\text{max.}}$, for velocity and for brightness are independent, these heights have been reduced to standard velocity and standard brightness.

For sporadics the standards are: velocity, 40 km/sec; absolute brightness 0·0 mag. The following empirical relations were determined during the course of the reduction to reduced height $h'_{\text{max.}}$ in kilometres,

$$h_{\text{max.}}=47\cdot 4+12\cdot 76\ln v, \qquad \ldots\ldots\ldots\ldots\ldots \quad (3)$$

$$M_p= 2\cdot 04- 0\cdot 025v, \qquad \ldots\ldots\ldots\ldots\ldots \quad (4)$$

$$h_{\text{max.}\,v}=93\cdot 6+ 1\cdot 22M_{pv}. \qquad \ldots\ldots\ldots\ldots\ldots \quad (5)$$

Here v is in km/sec, a prime indicates an observed quantity reduced to standard velocity and brightness, and the subscript v denotes reduction to standard velocity only. M_p is the absolute photographic magnitude at maximum intensity.

Relation (**3**) is given by Hawkins and Southworth. The data leading to (**4**) are summarized in Figure 2, in which individual points are the mean brightnesses for narrow velocity ranges and the regression line is determined from the weighted means. The regression coefficient in (**5**) was derived in a similar manner from the data presented in Figure 3 ; the individual points are now mean heights for narrow ranges of M_{Pv}.

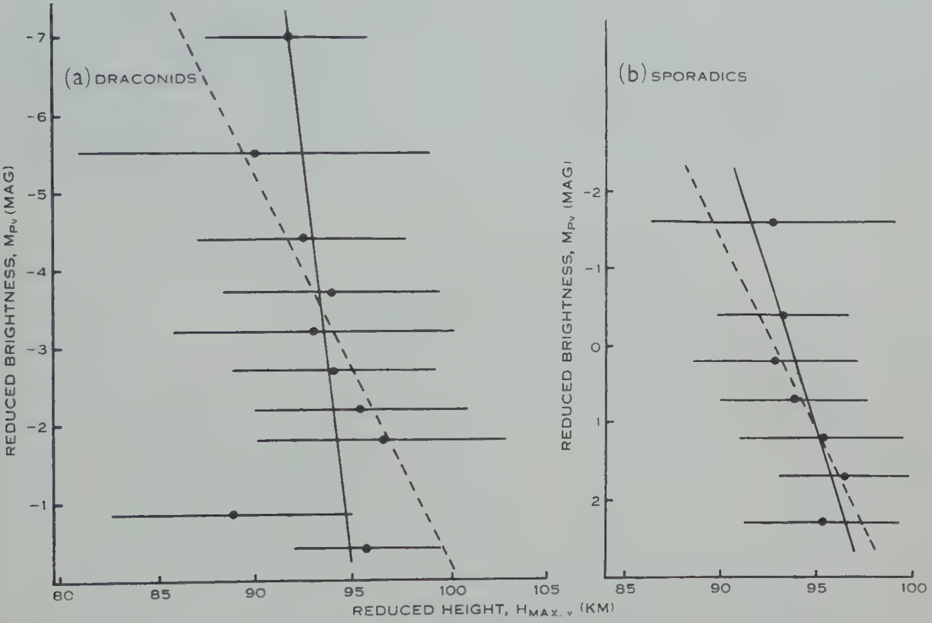

Fig. 3.—The relation between height and maximum brightness. For sporadic meteors both parameters have been reduced to the standard velocity of 40 km/sec ; for the Draconids reduction to standard velocity is unnecessary. Horizontal lines are r.m.s. deviations of the means. Full lines are regression lines for the weighted means, and the dashed lines are the relation (**12**) predicted by the evaporation theory, to an arbitrary zero.

For the Draconids (Fig. 3),

$$h_{\mathrm{max.}\,v}=95\cdot 0+0\cdot 48M_{Pv}. \qquad \ldots\ldots\ldots\ldots\ldots\ldots \quad (\mathbf{6})$$

The above notation is retained although, in this case, no velocity corrections are necessary. As before, the standard brightness is 0·0 mag, with the proviso that the different type of plate used here may give rise to a small difference between standard brightnesses for sporadics and for the Draconids.

It is well to stress here that the empirical relations (**3**)–(**6**) apply only to the samples of photographic meteors analysed in this paper, but they are expected to be typical. After reduction to standard velocity and brightness there remains a considerable scatter in the heights of maximum brightness, whose distribution is illustrated in Figure 4. There is no dependence of this residual scatter on velocity or maximum brightness. Although such a spread is to be expected as a consequence of fragmentation, three possible causes of a spurious scatter immediately come to mind. They are : (*a*) imperfect reduction to the standard, arising from uncertainty in the regression lines in Figures 2 and 3; (*b*) the adoption of M_P as a basis for reduction to a standard meteoroid. Physically it would be more acceptable to reduce all heights to a standard mass. The distribution of trail lengths found in Section II (*c*) implies that there is no one-to-one correspondence between M_P and meteoroid mass; (*c*) a systematic change in the form of the light curve with trail length. (*a*) is proved to be negligible by the fact that the scatter in $h'_{\text{max.}}$ for the Draconids is unchanged if the theoretical relation (**12**), instead of the empirical relation (**6**), is used in the reductions. (*b*) is probably responsible for the largest errors in reduction. These errors would be minimized if the integrated absolute magnitude were to be used instead of M_P. However, the Draconid data (Fig. 7) suggest that the reduction in the scatter in $h'_{\text{max.}}$, which would ensue if this substitution in basic data were possible, cannot be very large. The spread in M_P for given integrated absolute magnitude only slightly exceeds 1 mag, which is to be compared with a total range in M_P of 8 mag. If the spread in M_P for sporadic meteors is no larger than for the Draconids, most of the residual scatter in $h'_{\text{max.}}$ is undoubtedly real, and as such is characteristic of the ablation process. Figure 7 of Jacchia, Kopal, and Millman (1950), in which beginning, maximum, and end heights for individual Draconid meteors are plotted, leaves one in no doubt as to the reality of the scatter in this case.

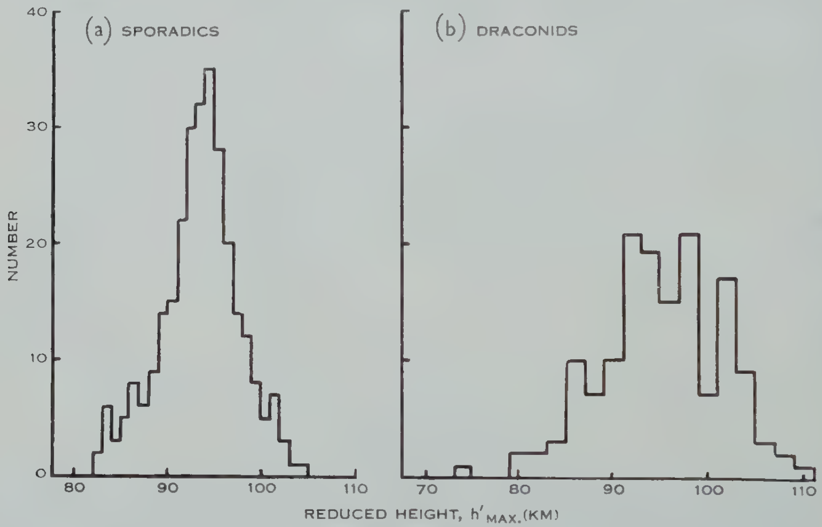

Fig. 4.—The distribution of the heights of maximum brightness, after reduction to standard velocity and standard brightness ($M_P=0$). For sporadics the standard velocity is 40 km/sec; for the Draconids reduction to standard velocity is unnecessary.

The mean reduced height for the Draconids, 95·0 km, is close to the 93·6 km found for sporadics. The Draconid geocentric velocity (23 km/sec) is lower than the sporadic standard velocity (40 km/sec). We find using (**3**) that Draconid trails are formed, on the average, 9 km higher than sporadics of comparable brightness.

(c) *Lengths of Trails*

Observed distributions of trail lengths, defined as beginning height—end height,* are plotted in Figure 5. The abscissa is the ratio of observed length to the length expected, from the mean photographic light curves BB and CC of Figure 1, for the appropriate brightness above plate limit. This quantity will be termed the relative length of the trail. The light curve has been assumed to be independent of velocity, although this is known not to hold for the brightest meteors. Distributions for sporadics and for the Draconids are very similar, if the low velocity tail of the former is disregarded. Scatter diagrams reveal that relative trail length and reduced height $h'_{\text{max.}}$ are only weakly correlated. There is a slight tendency for relatively shorter trails to form at greater heights, but for practical purposes it is sufficient to regard these two properties of the trail as independent. For velocities exceeding 25 km/sec the distribution of relative trail length is independent of velocity, but as the velocity decreases below 25 km/sec the trails shorten rapidly (see Fig. 6). This may imply that extreme departures from the evaporation theory are a consequence of a long time of flight of the meteoroid, and that, on the dustball hypothesis, severe fragmentation occurs only after an appreciable time-lag, perhaps associated with thermal effects.

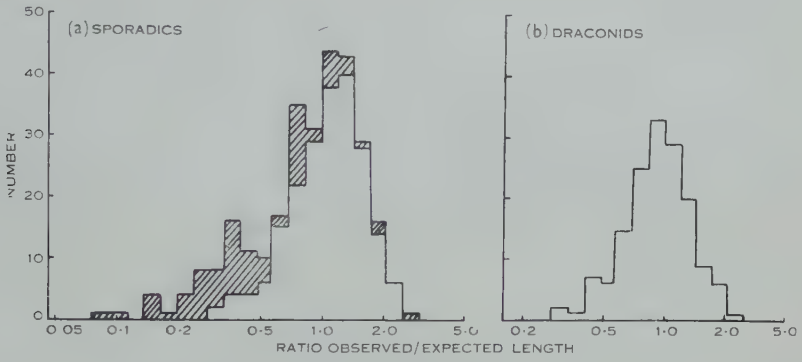

Fig. 5.—The distribution of the observed relative lengths of meteor trails. The observed relative length is the ratio of the observed length to the length expected, from the mean light curves BB or CC of Figure 1, for the appropriate brightness above plate limit. Sporadic meteors with velocities $\leqslant 20$ km/sec are indicated by cross-hatching.

For the Draconids there is no correlation between relative trail length and the ratio $(h_b - h_{\text{max.}})/(h_{\text{max.}} - h_e)$ (b=beginning, e=end of trail), which suggests that there is no systematic relation between relative trail length and the form of the light curve. For sporadics, on the other hand, there is a tendency for relatively short trails to have the comparatively short, steep rise to maximum brightness which is to be expected in cases of extreme fragmentation. This

---

* Assuming that the light curve profile is independent of the zenith angle χ of the radiant, the true length of the trail is found by multiplication by sec χ.

discrepancy between the two groups of meteors may be real or it could be due to the small number of segments in the Draconid trails, which in many cases makes the position of maximum brightness rather uncertain.

(*d*) *Integrated Absolute Brightness of Draconid Meteors*

In addition to apparent photographic magnitude at maximum brightness (which is readily converted to absolute magnitude M_P), Jacchia, Kopal, and Millman have tabulated for the Draconids the integrated absolute magnitude, $M_i=-2\cdot5\log\int I dt$, to an arbitrary zero. Figure 7 is a plot of M_P versus M_i, in which trails longer and shorter than the mean length have been distinguished. Since we are dealing with a homogeneous velocity group of meteors, the influence of velocity on brightness does not come into consideration. If the integrated absolute magnitude M_i is taken as a measure of meteoroid mass, this diagram implies that, for given mass and velocity, a short trail is accompanied by a larger maximum brightness (smaller M_P) than a long trail.

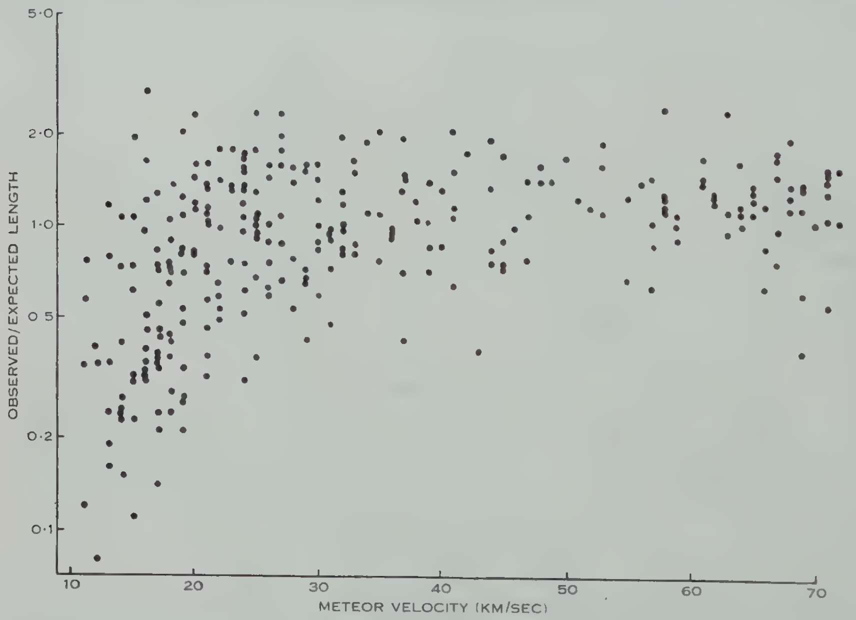

Fig. 6.—Scatter diagram of the relative trail length *v.* meteor velocity, for sporadic meteors.

This relation can be given a definite numerical form. Neglecting deceleration, the above definition of M_i implies that for given M_i, $\int I dh$=constant. If the shape of the light curve varies with the relative trail length l in such a way that the difference in height between any two points of equal light intensity is proportional to l, it follows that $lI_{\text{max.}}$=constant for given M_i. This restriction on the shape of the light curve is artificial, but we may still expect that in general $lI_{\text{max.}}\simeq$constant for given M_i. We see from Figure 5 (*b*) that for the great majority of trails $0\cdot4\leqslant l\leqslant2\cdot0$, i.e. l varies by a factor of 5. Now a ratio of 5 in $I_{\text{max.}}$ corresponds to a difference of 1·75 mag in M_P. This agrees closely with the spread actually found in M_p (Fig. 7). We conclude that almost the entire spread in M_p for given M_i is to be attributed to variations in the trail length, and that, for given mass and velocity, $\int I dh$ is independent of $I_{\max.}$.

The spread in M_p amongst the two classes of meteor, those with $l>1$ and those with $l<1$, is rather larger than expected, especially amongst the brightest meteors. This scatter could well be due to irregularities (flares) in the individual light curves, and to minor variations in the shape of the light curves for given l and M_i. It is not, however, the controlling feature in the spread of M_p for given M_i.

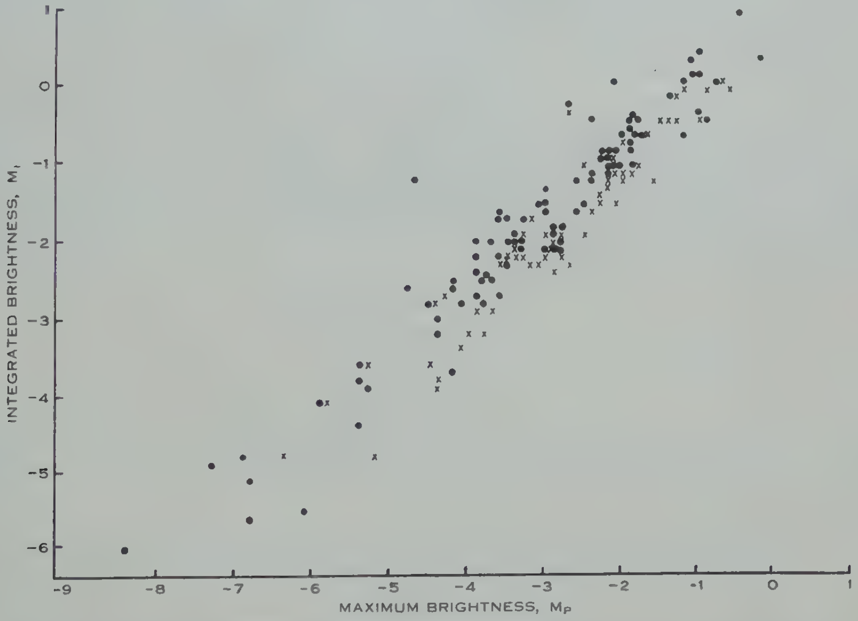

Fig. 7.—The relation between the absolute magnitude at maximum brightness, M_p, and the integrated absolute magnitude, M_i (to an arbitrary zero), Draconid meteors. ×, Trail lengths longer than the mean value for given M_p ; ●, trail lengths shorter than the mean.

(e) *Remarks on the Analysis*

In their original discussions of the photographic data, both Jacchia, Kopal, and Millman, and Hawkins and Southworth stressed two aspects of the light curves, namely, the shortness of the trails and the random fluctuations which occur. The present analysis supplements the earlier conclusions and indicates the extent of the departures by individual meteors from the mean behaviour. Perhaps the most interesting new feature is the large scatter in the reduced height at maximum brightness ; this is so large that it assumes considerable importance in the computation of the radio-echo height distributions for fragmenting meteoroids.

The main features of the ablation process, described above, apply equally well to sporadic meteors and to the Draconids, despite the different physical structure of the meteoroids involved. The major limitation arises from the lack of light curves of individual meteors, with the result that it has been possible to obtain only a rough qualitative estimate of the dependence of the form of the light curve on trail length. Nevertheless, it is reasonable to conclude that this description should not be modified in any essential detail by more refined observational data.

III. COMPARISON WITH EVAPORATION THEORY

The empirical relations (**3**)–(**6**) are now compared with the predictions of the evaporation theory. If the deceleration of the meteoroid is neglected, the equations describing the relevant results of the theory for an isothermal atmosphere (see e.g. Hawkins and Southworth for a summary) are

$$\rho_{\mathrm{max.}} \propto m^{\frac{1}{3}} v^{-2}, \quad \ldots\ldots\ldots\ldots\ldots\ldots\ldots \quad (\mathbf{7})$$

$$I_{\mathrm{max.}} \propto m^{\frac{2}{3}} \rho_{\mathrm{max.}} v^{5} \tau. \quad \ldots\ldots\ldots\ldots\ldots\ldots \quad (\mathbf{8})$$

$\rho_{\mathrm{max.}}$ is the atmospheric density and $I_{\mathrm{max.}}$ the luminous intensity at maximum brightness, m and v are the initial mass and velocity of the meteoroid, and τ is the luminous efficiency of an evaporated meteor atom. In an isothermal atmosphere of scale height H,

$$\rho_{\mathrm{max.}} = \rho_0 \exp \{(h_{\mathrm{max.}} - h_0)/H\},$$

and (**7**) becomes, for constant mass,

$$h_{\mathrm{max.}} = \mathrm{constant}^* + 2H \ln v. \quad \ldots\ldots\ldots\ldots\ldots \quad (\mathbf{9})$$

Hawkins and Southworth, who adopted the value of $H = 6 \cdot 38$ km established by the Rocket Panel (1952), found that (**9**) gave good agreement with their observational data.

Writing in (**8**) $\tau = \tau_0 v^{\eta}$ where $\eta \sim -0 \cdot 3$ (Weiss 1957) and using Opik's relation between visual magnitude M_v and intensity I,

$$M_v = 24 \cdot 6 - 2 \cdot 5 \log I, \quad \ldots\ldots\ldots\ldots\ldots \quad (\mathbf{10})$$

we obtain, again for constant mass,

$$M_v = \mathrm{constant}^* - 6 \cdot 75 \log v. \quad \ldots\ldots\ldots\ldots \quad (\mathbf{11})$$

This is to be compared with (**4**), with M_v replaced by M_P, subject to the uncertainties associated with colour index. According to Jacchia (1957) colour index increases from $-1 \cdot 8$ mag for $M_P < -3$ to $-1 \cdot 0$ mag for $M_P = +2$, but the change in colour index is largely if not entirely physiological in origin. In any case, the discrepancy between (**4**) and (**11**) is so wide (see Fig. 2) that there is little doubt that the evaporation theory fails completely to describe the observed relation between meteor brightness and velocity.

---

* These constants can be evaluated from the evaporation theory if the parameters of the atmosphere and the meteoroid are specified. Their absolute values do not concern us here. With the exception of (**12**), these constant terms are a function of the mass. Since meteor mass and velocity are independent, the relations (**9** and (**11**) will still apply to the mean values of $h_{\mathrm{max.}}$ and M_v, provided the constant is replaced by an appropriate average over all detectable meteor masses.

Eliminating the meteoroid mass from (**7**) and (**8**) gives, for constant velocity,

$$\ln I_{\text{max.}}=\text{constant}^*-3h_{\text{max.}}/H,$$

which in the notation of (**5**) and (**6**) becomes

$$h_{\text{max.}\,v}=\text{constant}^*+1\cdot 96\ M_{Pv}. \quad \ldots\ldots\ldots\ldots \quad (\mathbf{12})$$

The observed gradients are less than required by (**12**), but comparison of this relation with Figure 3 shows that, for both sporadic and Draconid meteors, the central more populous points are not inconsistent with (**12**).

The basic equations (**7**) and (**8**) are unchanged if an atmosphere in which the scale height increases linearly with height is substituted for the assumed isothermal atmosphere (Weiss 1959). The former is a good approximation to the actual atmosphere in the meteor region. Hence the only modification required to obtain, for the actual atmosphere, the relations corresponding to (**9**), (**11**), and (**12**) is to replace H in (**9**) and (**12**) by the local scale height. Although significant, these alterations are not so large as to invalidate the conclusions drawn from the comparisons already made between the observations and the predictions of the evaporation theory in an isothermal atmosphere.

IV. RADIO HEIGHT MEASUREMENTS AND THE FRAGMENTATION OF FAINT METEORS

We now proceed to evaluate the width of the radio-echo height distribution which would be measured for the sample of brighter sporadic meteors analysed in Section II, and to compare it with actual radio measurements of the heights of echoing points of fainter meteors. The observational data used in this comparison are the radio measurements, segregated into velocity groups, made at Jodrell Bank by Evans (1954, 1955) on sporadic meteors with $M_v \sim +6$. Evans has applied corrections for an expected error of ±1 km in the individual height measurements, and also for the finite range of velocities included in each group.

The sample of meteors examined by Evans is very different from the samples of photographic meteors which have hitherto been considered. They are a good deal fainter and are restricted to those meteors for which both velocity and height of the echoing point could be measured. Assuming the theory of evaporation in an isothermal atmosphere, Evans deduced values of the scale height increasing from 6·2 km at a height of 85 km to 7·8 km at a height of 107 km, and atmospheric densities which agreed well with the density profile from rocket and photographic measurements of meteors obtained in New Mexico.

Since in the actual atmosphere the scale height increases with height across the meteor region, the scale heights deduced by Evans are too large. This comes about because the scale height determined for each velocity group of meteors is really an average taken over the whole spread of the heights of the echoing points of the meteors within the group. The scale height gradient, which is not considered in the isothermal theory, is thus a cause of a small additional spread in the height distributions.

---

* See previous footnote.

The theory of the radio-echo height distribution in a non-isothermal atmosphere, in which the evaporation theory and a linear variation of scale height with height in the atmosphere have been assumed, has been given by the author (Weiss 1959). With the aid of this theory, a reinterpretation of Evans's measurements leads to the scale height

$$H=6\cdot1+0\cdot06(h-95\cdot0)\text{ km} \quad \ldots\ldots\ldots\ldots \quad (\mathbf{13})$$

for the range of heights h from 85 to 105 km. This agrees well with the ARDC 1956 Model Atmosphere, which in the height range 90–105 km is represented approximately by the linear relation

$$H=6\cdot4+0\cdot09(h-95\cdot0)\text{ km.} \quad \ldots\ldots\ldots\ldots \quad (\mathbf{14})$$

The agreement is probably better than this, since in deriving (**13**) no allowance has been made for loss of echoes due to diffusion of the meteor trail. Diffusion will limit the number of echoes measurable in the higher height ranges, thereby reducing the measured r.m.s. deviations and mean heights for the higher velocity groups. Both mean height and height gradient in (**13**) are therefore lower limits.

Table 1

R.M.S. DEVIATIONS OF THE RADIO-ECHO HEIGHT DISTRIBUTIONS

R.M.S. Deviation	Dependence of $\rho_{\text{max.}}$ on Meteoroid Mass	γ				
		0·0*	0·2	1·0	2·0	∞†
Elementary, δx_1 ..	$m^{\frac{1}{3}}$	1·01	0·72	0·54	0·48	0·33
	m^0	1·17	0·65	0·31	0·19	0·00
Complete, δx ..	$m^{\frac{1}{3}}$	1·10	1·07	0·96	0·92	0·86
	m^0	—	0·93	0·78	0·74	0·71

* Evaporation theory.

† Trails of zero length.

Were it not for the scatter in the reduced height $h'_{\text{max.}}$ for the photographic meteors, there would be no reason to doubt that the samples of fainter meteors examined by Evans obey the evaporation theory. This scatter is, however, so large (r.m.s. deviation $\pm4\cdot2$ km) that if it is present amongst the samples measured by Evans it cannot fail to make a significant contribution to the observed r.m.s. deviations. The conclusion that the ablation of the fainter radio meteors is correctly described by the evaporation theory therefore cannot be accepted without further scrutiny.

Details of the calculation of the r.m.s. deviation of the radio-echo height distribution as a function of the length of the ionized trail will be found in Appendix I. The definition of trail length already given in Section II, namely, beginning height—end height, is retained. A parameter γ is introduced, in terms of which the length of the trail between the two heights where the line density $\alpha=0$ is $H\ln(1+3/\gamma)$. The complete r.m.s. deviations δx, with which the observations are compared directly, are listed in the last two lines of Table 1, for several values of γ. δx as tabulated includes the scatter in the reduced height $h'_{\text{max.}}$.

For a trail with $\gamma=1\cdot0$, which corresponds to the mean photographic light curve BB of Figure 1, and an assumed scale height of $6\cdot4$ km, we see from Table 1 that the calculated r.m.s. deviation of the radio height distribution, δx, is $6\cdot1$ km. This is some 15 per cent. lower than the $7\cdot2$ km found by Evans (1955). This is for the case where $\rho_{\text{max.}}\propto m^{\frac{1}{3}}$; if height is independent of mass, the deficiency of the calculated below the measured r.m.s. deviation is increased to 30 per cent. Since the photographic data suggest that the real dependence of height on mass falls between these two extremes, we may expect that the calculated r.m.s. deviation of the radio-echo height distribution corresponding to meteors brighter than $M_v\sim+4$ will fall some 20 per cent. below that actually measured for meteors with $M_v\sim+6$.

There are, however, two deficiencies in the representation of the actual photographic light curves by simplified models which will tend to reduce this discrepancy. Firstly, the value of $\gamma=1\cdot0$ was arrived at by equalizing the integrals $\int(\alpha/\alpha_{\text{max.}})\mathrm{d}h$ corresponding to the mean light curve BB of Figure 1 and to the adopted model (**18**). The differences in shape of the two ionization curves are not insignificant, and this may result in a slight understatement of the calculated r.m.s. deviation. Secondly, the radio height measurements do not include meteors with speeds less than 20 km/sec. It is seen from Figure 6 that about half of these very slow meteors have abnormally short trails, and consequently the adopted mean value of $\gamma=1\cdot0$ may be a little high. Against these two factors must be offset any contribution to the residual scatter in the reduced height $h'_{\text{max.}}$ for photographic meteors which arises from irregularities and random variations in the shapes of the light curves; and also any loss of echoes by diffusion.

One other factor requires consideration. The values of δx_1 given in Table 1 were computed for an isothermal atmosphere. In fact, as we have seen, the meteor region is one in which the scale height increases quite rapidly with height. If the real gradient is approximated by the linear function (**14**), we find (Weiss 1959) that for $\gamma=0$ (evaporation theory) δx_1 should be increased from $1\cdot01$ to $1\cdot07$, i.e. by 6 per cent. For $\gamma>0$, δx_1 will require increases of approximately this same magnitude, but the increases in δx will be much less, 1 or 2 per cent. at most, because of the large correction terms in (**21**), all of which are insensitive to the scale height gradient.

Although the precise numerical evaluation of some of these corrections is difficult, not one of them is large. Collectively they seem quite inadequate to influence the first impression that the width of the radio-echo height distribution computed for sporadic meteors brighter than $M_v\sim+4$ falls considerably below that measured for fainter meteors, $M_v\sim+6$. Measured radio-echo r.m.s. deviations can be brought into agreement with predictions based on the photographic model only by assuming that the errors in the measurement of heights of individual echoing points have been grossly underestimated, by a factor of at least 4. Since this seems improbable, we may conclude that the ablation process which is typical of bright (photographic) meteors is not applicable to fainter (radio) meteors.

V. Discussion

The conclusion that the consequences of fragmentation are less marked amongst the fainter meteors is supported by other radio evidence. It is unfortunate, however, that the only radio data which might confirm the photographic evidence for fragmentation amongst bright meteors are limited and inconclusive.

On the reasonable assumption that a grouping of meteors by line densities at the reflection points is also, on the average, a grouping by absolute brightness, the variation of the height distribution with meteor brightness has been ascertained for a sample of meteors measured at Adelaide by radio techniques. In September 1953 heights and line densities were measured for 482 meteors. These have been divided into three groups, with line densities at the reflection points of $2–9\times10^{11}$, $1\cdot0–1\cdot9\times10^{12}$, and $\geqslant2\times10^{12}$ electrons/cm. Mean heights for the three groups are respectively $90\cdot6$, $91\cdot7$, and $92\cdot6$ km ; r.m.s. deviations from the means are $5\cdot9$, $6\cdot8$, and $6\cdot9$ km. The increase of mean height with increasing brightness is not inconsistent with the hypothesis of an increasing severity of fragmentation, but the increase in the r.m.s. deviation is unexpected.

Evans (1955) has pointed out that estimates, by radio techniques, of the deceleration for meteoroids in the same range of brightness as those to which his height distributions apply seem to be little, if any, greater than the theoretically expected values for a solid particle.

Finally, the ionization curve of Greenhow and Neufeld (Fig. 1), although shorter than predicted by the evaporation theory, is almost twice as long as the mean light curves deduced from the samples of photographic meteors under discussion.

A difference in physical structure between fainter and brighter (and therefore more massive) meteoroids is an obvious explanation of the closer approach to the predictions of the evaporation theory shown by the former. If this is so, small meteoroids must be regarded essentially as solid particles. But this is not the only possible interpretation, and indeed it is less attractive than the alternative which is now considered.

If it is postulated that the physical structure of large and small meteoroids is identical and that they differ only in the number of particles of which they are aggregates, the difference between the ablation processes for the two classes of meteoroids may be apparent rather than real. The crumbling of a small meteoroid, composed of relatively few fragments, will be completed at a much earlier point on the flight path through the atmosphere than the fragmentation of a large meteoroid. The time-lag in the onset of fragmentation, which we have noticed as a characteristic of very slow meteors, supports this view.

The fragments into which the meteoroid is divided are individually expected to obey the evaporation theory. As is shown in Appendix I, this still implies a shortening of the ionization curve, which is the more marked the higher the density of the atmosphere at the point on the flight path where the evaporation of the fragment commences. Consequently, a small meteoroid, which fragments early in its flight, will produce a light and ionization curve conforming closely to the evaporation theory for a solid particle; the large departures from this theory shown by a massive meteoroid follow from the longer time which is required for fragmentation to be completed.

This alternative explanation requires that the individual particles composing the meteoroid be sufficiently minute.

VI. REFERENCES

BROWNE, I. C., BULLOUGH, K., EVANS, S., and KAISER, T. R. (1956).—*Proc. Phys. Soc.* B **69**: 83.

EVANS, S. (1954).—*Mon. Not. R. Astr. Soc.* **114**: 63.

EVANS, S. (1955).—"Meteors." (Ed. T. R. Kaiser.) p. 86. (Pergamon Press: London.)

GREENHOW, J. S., and NEUFELD, E. L. (1957).—*Mon. Not. R. Astr. Soc.* **117**: 359.

HAWKINS, G. S., and SOUTHWORTH, R. B. (1958).—*Smithson. Contr. Astrophys.* **2**: 349.

HAWKINS, G. S., and UPTON, E. K. L. (1958).—*Astrophys. J.* **128**: 727.

HERLOFSEN, N. (1948).—*Rep. Prog. Phys.* **11**: 444.

JACCHIA, L. G. (1955).—*Astrophys. J.* **121**: 521.

JACCHIA, L. G. (1957).—*Astr. J.* **62**: 358.

JACCHIA, L. G., KOPAL, Z., and MILLMAN, P. M. (1950).—*Astrophys. J.* **111**: 104.

KAISER, T. R. (1954*a*).—*Mon. Not. R. Astr. Soc.* **114**: 39.

KAISER, T. R. (1954*b*).—*Mon. Not. R. Astr. Soc.* **114**: 52.

ROCKET PANEL (1952).—*Phys. Rev.* **88**: 1027.

WEISS, A. A. (1957).—*Aust. J. Phys.* **10**: 397.

WEISS, A. A. (1959).—*Aust. J. Phys.* **12**: 54.

APPENDIX I

The Radio-Echo Height Distribution as a Function of Trail Length

In this appendix we derive the characteristics of the radio-echo height distribution as a function of the length of the ionized trail. Since light and ionization curves are proportional, it would be desirable to carry through these calculations using a functional representation of the mean light curves of Figure 1. This has been attempted, but the resulting mathematics is intractable. Instead, anticipating that the height distribution will be much more sensitive to the length than the shape of the ionization curve, the height distributions have been calculated for a simple model of a fragmenting meteoroid. Since our object is to compute the width of the radio-echo height distribution corresponding to the picture of a fragmenting meteoroid derived in Section II, the scatter in the reduced height $h'_{\max.}$ has been incorporated into our model.

It can be shown that a particle of mass m_0 inserted at speed into an isothermal atmosphere, at a level where the density is ρ_0, produces by evaporation a trail whose maximum electron line density is

$$\alpha_{\max.}=\frac{4}{9}(\beta/\mu H)m_0(1+\gamma/3)^3\cos\chi. \qquad \ldots\ldots\ldots\ (15)$$

This maximum occurs at the level $\rho_{\max.}$ specified by

$$\rho_{\max.}=\rho_1+\rho_0/3=\rho_1(1+\gamma/3). \qquad \ldots\ldots\ldots\ (16)$$

Here we have written $\gamma=\rho_0/\rho_1$. ρ_1 is the density at the height of maximum ionization for the same particle entering the Earth's atmosphere from outside ($\rho=0$). It is given by

$$\rho_1=\frac{8}{3}\left(\frac{3}{4\pi}\right)^{\frac{1}{3}}\frac{\rho_m^{\frac{2}{3}}l\cos\chi}{Hv^2\Lambda}m^{\frac{1}{3}} \quad \ldots\ldots\ldots\ldots\ldots \quad (\mathbf{17})$$

for a spherical particle ; if the particle is not spherical, a shape factor of order unity must be included in (**17**). The meaning of the symbols employed is as follows :

ρ_m=density of meteor particle,
v=meteor velocity,
μ=mass of individual meteor atom,
χ=zenith angle of meteor radiant,
H=scale height of isothermal atmosphere,
β=ionizing efficiency of an evaporated meteor atom,
l=latent heat of evaporation of the meteoroid,
Λ=heat transfer coefficient.

The usual assumptions, that the deceleration of the particle is negligible, and that $v^2 \gg 12l$, have been made. These are valid for all but the slowest meteors.

The ionization curve generated by this particle is

$$\left.\begin{aligned}\alpha&=0, && \rho<\gamma\rho_1\\ &=(\beta/\mu H)\cos\chi\, m_0\frac{\rho}{\rho_1}\left(1+\frac{\gamma}{3}-\frac{\rho}{3\rho_1}\right)^2, && \gamma\rho_1\leqslant\rho\leqslant(3+\gamma)\rho_1.\end{aligned}\right\} \quad \ldots \quad (\mathbf{18})$$

Provided that the particle mass m_0 is replaced by the meteoroid mass m, expressions (**15**)–(**18**) will describe the simple case of a meteoroid for which ablation is negligible until the meteoroid fragments, at the level specified by ρ_0, into a number of particles, all of mass m_0, which individually obey the evaporation theory.

The length of the meteor trail, defined as the difference in height between the two points where $\alpha=0$, is $H\ln(1+3/\gamma)$, independent of the zenith angle χ. The total number of ions generated by the meteoroid is independent of the length of trail, as may be verified by evaluating the integral

$$\int_{-H\ln(3+\gamma)}^{-H\ln\gamma}\alpha\, dh=\frac{\beta m}{\mu}.$$

The ionization curve (**18**) exhibits a progressive shift of the position of maximum ionization towards the end of the trail as the trail shortens. These last two properties are characteristic of the observed photographic light curves.

Consider now the case of a homogeneous velocity group of meteors proceeding from a point radiant. Using the ionization curve (**18**) and following through the analysis of Kaiser (1954*a*), we find for the elementary height distribution υ^*, measured within a narrow angular sector of the echo plane,

$$\upsilon^*=\left(\frac{3}{2z^{-\frac{1}{2}}+z}\right)^{3(s-1)}-\left(\frac{3\gamma}{(3+\gamma)z}\right)^{3(s-1)}, \quad \ldots\ldots\ldots \quad (\mathbf{19})$$

with

$$z=\rho/\rho_1\geqslant(2\gamma/3)^{\frac{2}{3}}.$$

s is the mass distribution parameter, assuming a differential law $n_m dm \propto m^{-s} dm$ for the distribution of meteoroid masses. The first term of (**19**) is identical with the elementary height distribution according to the evaporation theory. The second term is introduced by the finite length of the trail, since for any given height there is now a maximum detectable mass as well as a minimum detectable mass.

Alternatively, we may consider the case in which the ionization curve is described by (**18**), but with $\rho_{\text{max.}}$=constant replacing $\rho_{\text{max.}} \propto m^{\frac{1}{3}}$. The elementary height distribution then becomes

$$\upsilon^* = \left\{ z^{1/2}\left(1+\frac{\gamma}{3}\right) - \frac{z^{3/2}}{3} \right\}^{2(s-1)}, \quad \gamma \leqslant z \leqslant 3+\gamma. \qquad \ldots\ldots \ (\mathbf{20})$$

Let us now introduce the new height variable

$$x_1 = -\ln z = (h-h_1)/H,$$

h_1 being the height corresponding to the density ρ_1. R.M.S. deviations δx_1 of the height distributions (**19**) and (**20**) have been computed for $s=2\cdot0$, which is the accepted value for fainter sporadic meteors (Kaiser 1954*b*). This value of s is probably a lower limit, since Hawkins and Upton (1958) found $s=2\cdot34$ for the sample of photographic meteors analysed in Section II. These values of δx_1 are listed in Table 1 for several values of γ. $\gamma=0\cdot2$ and $\gamma=2\cdot0$ correspond roughly to the longest and shortest trails measured photographically for meteors with velocities greater than 20 km/sec. This cut-off in velocity has been imposed to conform to the lowest velocity group studied by Evans.

Before these r.m.s. deviations can be compared with the observations, corrections are necessary for (*a*) the spread in heights introduced by the finite aperture of the aerial, (*b*) the distribution of radiants over the celestial sphere, and (*c*) the scatter in the reduced heights (Fig. 4), which is approximately Gaussian. The complete r.m.s. deviation δx is found from

$$(\delta x)^2 = (\delta x_1)^2 + C_A + C_\varphi + C_\chi + R^2. \qquad \ldots\ldots\ldots\ldots \ (\mathbf{21})$$

C_A and C_φ are the corrections for aerial polar diagram in azimuth and in elevation. They are given respectively by expressions (**16**) and (**20**) of Kaiser (1954*b*). In the present case they have been computed for a double Gaussian aerial beam ; with $s=2\cdot0$, $C_A=C_\varphi=0\cdot06$. For the height distribution (**20**), of course, the aerial aperture can contribute no additional spread, and these corrections vanish. C_χ is the correction from a point radiant to the uniform distribution of radiants which is simulated by observation over an extended period. It is given by expression (**9**) of Kaiser (1954*b*) ; again with $s=2\cdot0$, $C_\chi=0\cdot08$. The r.m.s. deviation of the residual scatter in reduced height (Fig. 4 (*a*)) is 4·2 km, and with $H=6\cdot4$ km, $R=0\cdot66$.

Complete r.m.s. deviations δx are also listed in Table 1. These are the values with which the observations are to be compared. The corrections for aerial polar diagram and for the radiant distribution are sufficiently small that uncertainty in these geometrical factors is of little account.

ON THE IDENTIFICATION OF EXTRAGALACTIC RADIO SOURCES

By B. Y. Mills*

[*Manuscript received March* 22, 1960]

Summary

Identifications of radio sources with galaxies and clusters of galaxies have been sought systematically in a limited region of the sky. The optical data have been taken principally from the National Geographic Society–Palomar Observatory Sky Atlas and a catalogue of clusters of galaxies prepared by Abell (1958) from the same Atlas. The radio data are taken from results obtained with the Sydney cross-type radio telescope, supplemented at times with additional information from a recent Cambridge Catalogue (3C). A total of 46 possible identifications with galaxies are listed and 55 possible identifications with clusters of galaxies, the great majority of which are new. Most of these galaxies are double systems, but no other common features could be recognized: it seems probable that many galaxies of completely normal appearance are very strong radio emitters. The possible nature of the double galaxies is discussed briefly and attention is drawn to a corresponding duplicity in the radio brightness distribution observed in some strong radio sources. In many cases the emission from clusters appears to be associated with a single galaxy or pair of galaxies in the cluster; evidence for the existence of radiation of intergalactic origin is inconclusive. A selection of the possible galaxy identifications has been used to derive a provisional radio luminosity function; it appears probable that there is no distinct class of " radio galaxies ", but all radio luminosities appear to be represented, the numbers of radio sources in a given volume of space falling rapidly with increasing luminosity. A radio luminosity function of the form derived is capable of accounting for a substantial number of the radio sources of small size observed at high galactic latitudes; the remainder could be accommodated by the uncertainty in the data. It is found that, at the levels to which source counts can currently be taken, cosmological effects are likely to be small, although the most distant sources are markedly affected.

I. Introduction

To understand the physical significance of radio astronomical observations it is necessary to identify the types of objects in which the radiation originates. A number of such objects are known; at galactic distances these include hydrogen emission nebulae, supernova remnants, and the whole Galaxy itself; extragalactic objects include other spiral and irregular galaxies radiating in much the same way as our own, large clusters of galaxies, and very rare types of galaxies radiating many orders of magnitude more than the average. However, the great majority of detectable radio sources remain unidentified.

The galactic radio sources are rare objects concentrated very close to the plane; they may be identified only when there is fortuitously a " window " through the general dust clouds in their direction, or else when they are very close. A high proportion of identifications is therefore not expected. At high galactic latitudes, however, obscuration is low and the lack of identification must be related to the types of objects causing the emission; if these are galaxies they must be very distant.

---

* Division of Radiophysics, C.S.I.R.O., University Grounds, Chippendale, N.S.W.; present address: School of Physics, University of Sydney.

The need is evident for a systematic comparison of a large and homogeneous sample of radio sources with an equally homogeneous sample of galaxies. In the present investigation such a comparison has been made and many new possible identifications of " radio galaxies " and clusters found. It has also proved feasible to take the first steps in the derivation of a radio luminosity function for galaxies which is consistent with the existing observational results.

II. OBSERVATIONAL DATA

The radio data have been taken principally from a recent catalogue of sources between declinations +10° and −20° observed with the Sydney cross-type radio telescope at a wavelength of 3·5 m (Mills, Slee, and Hill 1958). For the optical data, the basic source has been the original plates of the National Geographical Society–Palomar Observatory Sky Atlas in the same region. These have been supplemented by additional radio data at more southerly declinations and a recent Cambridge catalogue of radio sources (3C) which has been made available in advance of publication ;* also many plates taken with the larger telescopes of the Mount Wilson and Palomar Observatories have been examined.

The basic catalogue of radio sources includes 1159 within the declination limits of +10° and −20°. The Cambridge 3C catalogue used for supplementary information includes 112 sources in the same area, of which about 85 can be recognized in the Sydney catalogue. The great majority of the 3C sources which could not be recognized were weak sources close to the galactic plane where the situation is confused by the existence of a high concentration of extended non-thermal and thermal sources, so that different types of instruments might be expected to yield different results. When a source was listed in both catalogues, it was found that the Right Ascension listed in the Sydney catalogue could usually be improved substantially by use of the 3C data. This possibility arose because the latter catalogue was prepared using an interferometer which gave quite precise values for the time of transit across a fictitious meridian inclined at a few degrees to the true meridian, but subject to possible lobe ambiguities. Once the correct lobe had been identified (about 30 per cent. required lobe shifts to bring them into coincidence with the Sydney position) and the Sydney declination adopted (because very large apparent errors in some of the 3C declinations caused uncertainty as to how they should be applied), the most probable Right Ascension was then determined giving the 3C data some three or four times the weight of the Sydney values. For the stronger sources it is estimated that the probable error in Right Ascension due to this procedure is of the order of ½ min of arc, compared with an average probable error of about 3 min in declination. These errors would be roughly doubled for the weaker sources included in the 3C catalogue. When the 3C data are not available, the accuracy in Right Ascension is only slightly better than in declination.

The angular sizes of radio sources having possible identifications were also measured at the same wavelength when this was feasible. The instrument used is described elsewhere (Goddard, Watkinson, and Mills 1960); briefly, it consists of two interferometers of identical sensitivity but different spacings between aerials, one of 30λ and the other 3000λ. By measuring the ratio of responses on each spacing a crude estimate of the angular size of a radio source is possible. The sizes quoted later in this paper were derived on the assumption that the brightness distribution across a radio source is circularly symmetric and has a Gaussian distribution. On this assumption the angle between half-brightness points is given by

---

* This catalogue has now been published with some slight modifications (Edge *et al.* 1959).

$$\theta_0 \approx 37\cdot 4(\ln X)^{\frac{1}{2}} \text{ seconds of arc,}$$

where X is the ratio, response at 30λ/response at 3000λ. When X is large, greater than 3 or 4, fine structure in the distribution is likely to dominate and lead to a low estimate for the size. As X approaches unity, measurement errors become important and limit the size which can be measured to something greater than 10–30 sec of arc, depending on the intensity of the source. Because the sensitivity of the angular size interferometer is less than that of the radio telescope used in preparing the original catalogue, not all the selected radio sources could be measured.

Finally, comparisons were made between the radio sources and a very homogeneous collection of data on clusters of galaxies prepared by Abell (1958). Abell's catalogue, being prepared from the plates of the Palomar Sky Survey, is based on the same material as the other optical data used.

III. Analysis of the Data

A preliminary inspection of the Sky Survey plates showed the futility of any attempt to identify all the radio sources. The positional uncertainties of the weakest sources are so large that numerous galaxies are contained within their limits, and one can only consider seriously coincidences with the very bright galaxies which had been investigated earlier (Mills, Slee, and Hill 1958). Also, near the galactic plane, the obscuration is so heavy and the star density so high that the search appeared hopeless. Accordingly, only a limited sample of sources was inspected; this sample was chosen from the Sydney catalogue as follows.

(i) All Class II sources (i.e. sources having $|b| > 12\frac{1}{2}°$) with flux densities 2×10^{-25} Wm^{-2} (c/s)$^{-1}$ or higher. The catalogue is reasonably complete in this category.

(ii) Fainter sources, or sources with lower latitude, recognized in the 3C catalogue.

(iii) All sources, not included above, in two areas at high latitudes selected because of their low radio background emission and freedom from any obvious clustering of bright galaxies. These areas are defined by the Sky Survey plates centred on $09^{h}\,36^{m}$ to $11^{h}\,12^{m}$, $-18°$ to $0°$; and $23^{h}\,12^{m}$ to $23^{h}\,36^{m}$, $-18°$ to $0°$.

A total of about 400 positions was examined, made up of about 230 in category (i), 20 in category (ii), and the remaining 150 in category (iii).

Initially, the source positions were plotted approximately on the Sky Survey prints using offsets from catalogued stars. The area within three probable errors of the position was searched for the presence of single galaxies brighter than $m_p \approx 16$, or double systems brighter than about magnitude 19. All such coincidences were then investigated more closely on the original plates. Here positions were plotted to an accuracy of about $\frac{1}{2}$ min of arc and coincidences taken to be significant only when the discordance was less than two probable errors (unless the object showed great peculiarity). The fainter sources in category (iii) received slightly different treatment as the listed errors were ignored and coincidences sought within 10 min of arc of their positions: only galaxies showing some peculiarity, or double systems were noted.

A total of 46 coincidences were considered to be worth recording. The angular sizes of 38 of these have subsequently been measured.

In categories (i) and (ii) (containing 250 sources) there were 39 coincidences, of which 19 were with single galaxies and 20 with apparently double or multiple systems. To check the possibility of chance coincidences, a number of randomly selected positions was examined. Out of 200 positions, each with an associated area of 50 square minutes (corresponding roughly to the mean positional uncertainties), 4 coincidences were found with single galaxies of magnitude 16 or brighter, and 2 with very faint double systems of about magnitude 19. The number of chance coincidences with galaxies brighter than magnitude 16 to be expected from the data of Hubble (1936) is 6, in agreement with the above result. Thus it appears safe to conclude that the majority of coincidences, particularly with the double galaxies, are significant. The angular size data have proved very useful in making individual decisions: they also indicate that a very high proportion of the double galaxies are likely to be real identifications.

Among the radio sources in category (iii), seven coincidences were found, comprising six double galaxies and one peculiar single system. On the basis of the above statistical tests, about half a dozen coincidences might be expected with faint double systems due to chance, so that little weight can be given to the coincidences.

A different procedure has been adopted in making comparisons with Abell's catalogue of clusters. In this case the clusters are often very extended objects so that precise positions are of little use. Accordingly, all the 1159 radio sources in the Sydney catalogue have been compared with the 877 clusters listed in the area of the radio catalogue. Coincidences have been noted for positions agreeing within 1 min in Right Ascension and 20 min of arc in declination, a compromise based on the desire to exclude as many chance coincidences as possible without eliminating many real identifications. A total of 55 coincidences were noted. The chance coincidences were estimated by comparing the radio positions of 1950 epoch with the cluster positions of 1855 epoch given in Abell's catalogue. These totalled 16 so that the majority of the 55 coincidences are likely to be real identifications.

IV. POSSIBLE IDENTIFICATIONS

The data relating to observed coincidences have been collected in Tables 1, 2, and 3. Tables 1 and 2 include coincidences observed with single or double galaxies during examination of the Sky Survey plates, and Table 3, the

TABLE 1

COINCIDENCES BETWEEN RADIO SOURCES AND GALAXIES IN WHICH THE ANGULAR SIZE MEASUREMENT IS CONSISTENT WITH AN IDENTIFICATION

When bracketed the angular size measurement is doubtful. Sources marked with an asterisk are included in the 3C catalogue

Radio Source			Galaxy Position (1950)		Flux Densities (10^{-26} Wm^{-2} (c/s)$^{-1}$)	Angular Size ″	Notes
Ref. No.	Adopted Position (1950) R.A. h m s	Adopted Position (1950) Dec. ° ′	R.A. h m s	Dec. ° ′			
00+02*	$0\ 10\ 00^4$	$+0\ 37^5$	0 10 03	+0 34	20	(~30)	A faint galaxy which appears double with the 200 in. telescope.† The magnitude of the combined systems is 18: giving $m_{1\cdot 9}—m_p=—9$:. The size is admissible for an identification but needs checking. Another somewhat peculiar galaxy is at $0^h\ 10^m\ 08^s$, +0° 24′, but the position is too discordant
00—04	$0\ 17\ 48^{12}$	$—02\ 51^4$	0 17 49	—02 56	23	(⩾30)	A faint double galaxy, one component has magnitude 17: the other 19:. The size is admissible but needs checking. $m_{1\cdot 9}—m_p=—8$. A normal Sc galaxy of magnitude 16 is at $0^h\ 17^m\ 42^s$, —02° 56′
00—18	$0\ 16\ 12^{12}$	$—10\ 46^5$	0 16 20	—10 39	23	(>30)	A distorted Sc ($m_p=14\frac{1}{2}$) with an early type companion ($m_p=16$) about 1′ south. The size needs checking but at present appears to support the identification. $m_{1\cdot 9}—m_p=-5\frac{1}{2}$
00—015*	$0\ 51\ 39^3$	$—3\ 42^4$	0 51 39	—3 43	23	⩾35	A close double galaxy with some distortion in the outer parts. The combined magnitude is about 17. This appears a very likely identification with $m_{1\cdot 9}—m_p=—8$
01+04	$01\ 23\ 06^{18}$	$+01\ 22^5$	01 22 57	+01 30	20	>30	NGC533 ($m_p=12\cdot 5$) a normal E3 galaxy. The size measurement is consistent with the identification. $m_{1\cdot 9}—m_p=—3\cdot 4$

01—05*	01 23 33^2	—01 35^2	01 23 28	—01 36	88	~45	NGC545/547. A pair of elliptical galaxies each of magnitude 13, giving $m_{1\cdot9}-m_p=-5\cdot7$. The position given is that of the centroid of the system. The radio position appears closer to that of NGC547 and the size measurement indicates that the whole system is not radiating uniformly. The galaxies are in a loose cluster, A194
02—110	02 35 24^6	—19 43^3	02 35 18	—19 41	44	~30	A faint double galaxy ($m_p=18$:) or a close conjunction of a star and galaxy. The angular size is consistent with the identification and a photograph with the 200 in. telescope would be useful to decide on the nature of the object. The galaxy appears to be a member of a distant cluster, A367. We have $m_{1\cdot9}-m_p\approx-10$
02—011*	02 40 06^4	—00 09^3	02 40 06	—00 14	35	(>30)	NGC1068, a well-known identification and one of the class of galaxies with strong and broad emission lines in the nucleus. The angular size needs checking. Taking $m_p=9\cdot6$, we have $m_{1\cdot9}-m_p=-1\cdot1$
02+010*	02 55 07^4	+05 53^4	02 55 02	+05 50	51	(~40)	A pair of elliptical galaxies each with $m_p=15\frac{1}{2}$, separation about 15″ NS. Using the combined magnitudes we have $m_{1\cdot9}-m_p=-7$. The galaxies are in a loose cluster and an angular size of 5′ is given in the 3C catalogue. Possibly there is some radiation from the cluster as a whole, or another member of the cluster
02+011*	02 59 02^4	+01 35^5	02 59 02	+01 43	27	(>30)	A close double galaxy of about magnitude 17, giving $m_{1\cdot9}-m_p=-8$. The declination agreement is not particularly good and needs checking but is acceptable. The size measurement is consistent but also needs checking. The double galaxy may be associated with the cluster A409
03+03*	03 05 50^3	+03 50^5	03 05 48	+03 56	34	>40	NGC1218, an So of normal appearance and magnitude 15, giving $m_{1\cdot9}-m_p=-6\frac{1}{2}$. The angular size is consistent. There is an interesting double galaxy about 12^s following, but this appears too far away

---

† Minkowski suggests that this object is a close conjunction of a foreground star and a single galaxy.

TABLE 1 (*Continued*)

Radio Source			Galaxy Position (1950)		Flux Densities (10^{-26} Wm^{-2} (c/s)$^{-1}$)	Angular Size ″	Notes
Ref. No.	Adopted Position (1950)						
	R.A. h m s	Dec. ° ′	R.A. h m s	Dec. ° ′			
03—03*	03 31 44^3	—01 25^4	03 31 45	—01 28	64	35	A very faint double galaxy ($m_p \approx 19$–20). It could not be considered but for the angular size measurement. However, there are some 18 magnitude galaxies of normal appearance quite close so that the identification is uncertain. We have $m_{1\cdot 9} - m_p \approx -11$
05—11*	05 02 37^6	—10 13^5	05 02 31	—10 19	20	>30	A rather interesting Sb of magnitude about 15½. It displays heavy obscuration in the spiral arms and has strong λ3727 emission, but otherwise a normal spectrum. We have $m_{1\cdot 9} - m_p = -6\frac{1}{2}$
05+02*	05 10 55^3	+01 02^6	05 10 56	+01 08	38	(>30)	An Sab galaxy of magnitude about 16, giving $m_{1\cdot 9} - m_p = -7\frac{1}{2}$. There is a superimposed star suggesting a double galaxy on the Sky Survey plates. However, with the 200 in. telescope the star is separated and a heavy absorption lane is visible around the nucleus. The angular size is consistent with the identification, but needs checking
08+03*	08 19 54^4	+06 07^4	08 19 50	+05 55	125 (60)	~30 + extended component	A double S, each component having a magnitude of 17½. Taking the combined magnitudes we have $m_{1\cdot 9} - m_p = -8\frac{1}{2}$. An identification of the galaxy pair with the small source appears quite possible. The discrepancy in declination could then be explained by radiation from the extended source, which might be associated with a coincident loose cluster of galaxies

09—14*	09 15 43^{3}	—11 52^{2}	09 15 42	—11 53	690	~50	An earlier identification which now appears practically certain. A very close double E galaxy with a combined magnitude of 15·9 in the cluster A780. The galaxy shows some emission lines, λ3727, the nebulium lines and Hβ. $m_{1\cdot9}$—m_p=—10½
10—018	10 46 18^{12}	—02 33^{5}	10 46 30	—02 36	20	(~30)	A double galaxy, or else perhaps a galaxy with superimposed star each of about magnitude 17. Since the positional agreement is not particularly good and the nature of the object in doubt, this coincidence cannot be given much weight. The angular size also needs checking. $m_{1\cdot9}$—m_p=—7
11—08	11 16 54^{12}	—02 46^{3}	11 16 34	—02 48	31	>30	A pair of faint galaxies both of magnitude about 18 separated by about 10″ arc. The size is consistent and the agreement in R.A. poor but acceptable. There is another pair about 2 magnitudes brighter separated by ½′ arc at 11^{h} 16^{m} 51^{s}, —2° 49′. The separation is rather large but these could also be the radio source. There are no other likely candidates nearby. The selected pair have $m_{1\cdot9}$—m_p=—7½
12+04	12 14 48^{12}	+04 00^{6}	12 14 36	+03 58	30	>40	NGC4234, an Irregular galaxy of magnitude 12·4. This is one of Haro's blue galaxies. The spectrum shows λ3727 in emission but has no other peculiarities. The size is consistent with an identification. $m_{1\cdot9}$—m_p=—3·7
12+05*	12 16 51^{4}	+05 59^{5}	12 16 50	+06 07	100	~55	NGC4261, an apparently normal E2 of m_p=10·9, giving $m_{1\cdot9}$—m_p=—3·5. The declination agreement is rather poor but acceptable. NGC4264, which appears somewhat peculiar, is 5′ further north, too far for serious consideration
12—118*	12 52 03^{6}	—12 19^{4}	12 52 00	—12 18	53	>50	NGC4782/4783, a pair of very similar So galaxies, each of magnitude 12·7 and about 1′ arc apart in a common envelope. This appears to be a very likely identification with $m_{1\cdot9}$—m_p=—3·8. The galaxy position is that of the centroid of the double system

TABLE 1 (*Continued*)

Ref. No.	Radio Source		Galaxy Position (1950)		Flux Densities (10^{-26} Wm^{-2} $(c/s)^{-1}$)	Angular Size ″	Notes
	Adopted Position (1950)						
	R.A. h m s	Dec. ° ′	R.A. h m s	Dec. ° ′			
14—*019*	14 55 30^{18}	—00 54^{7}	14 55 48	—00 54	19	(>30)	A normal SBc galaxy of magnitude 11·7, giving $m_{1\cdot9}—m_p = —2\cdot5$. There are no other galaxies in the vicinity likely to have large radio size. However, the size needs to be checked
15+05*	15 14 17^{5}	+07 11^{6}	15 14 20	+07 12	140	∼40	Two Eo galaxies, of magnitudes 15½ and 16, separated by 1′ arc in a small cluster. The position and size fit the brighter member better. Taking the combined magnitudes, we have $m_{1\cdot9}—m_p = —8$
16+*010**	16 48 44^{4}	+05 04^{2}	16 48 49	+05 02	890	∼55	The radio source is Hercules A, which previously had been identified with the double galaxy noted of magnitude 17½. However, this identification has now been queried and is possibly incorrect: it is discussed in the text. $m_{1\cdot9}—m_p = —12\frac{1}{2}$. The size given in 3C is 2′·3: there is undoubtedly fine structure in a quite large source
17—*23*	17 09 24^{12}	—23 18^{5}	17 09 25	—23 15	45	⩾40	A very obscured field; but a cluster of galaxies is visible, the brightest member being close to the radio position as noted. The apparent magnitude is 17 but because of the obscuration it is undoubtedly very much brighter. $m_{1\cdot9}—m_p = —9$

17—06*	17 18 00^{3}	—00 55^{3}	17 17 59	—00 54	475	~50	Again a very obscured field with the brightest member of a cluster close to the radio position. The apparent magnitude is 17, but it is intrinsically very much brighter. $m_{1\cdot9}-m_p \geqslant -11$. The 3C catalogue gives the size as 3′·5, which would be consistent with the identification and with our measurement assuming the existence of some fine detail in the brightness distribution. Boischot gives 6′, which is difficult to reconcile, but perhaps there is some additional radiation from the cluster. In the Sydney catalogue the possible presence of an extended source is noted
20+*010**	20 45 46^{4}	+06 57^{7}	20 45 41	+06 50	22	(<30)	A pair of very red galaxies each of magnitude 18½ and with separation 5″. The object appears interesting and the size is admissible although uncertain. The galaxies appear to be associated with a very distant cluster. $m_{1\cdot9}-m_p=-9$
21—*21*	21 04 36^{12}	—25 36^{3}	21 04 32	—25 38	50:	⩾50	A close pair of elliptical galaxies, each of magnitude 16½, in a small cluster containing two other early type pairs. Using the combined magnitude, we have $m_{1\cdot9}-m_p=-7$
22—09*	22 21 23^{5}	—02 18^{3}	22 21 29	—02 23	60	~45	A rather peculiar galaxy of magnitude 17. With the 200 in. telescope it appears as an edge-on spiral with dense nucleus and a bright concentration on one edge. The overall size is nearly ½′, which is consistent with the radio size, but the positional agreement is not particularly good. $m_{1\cdot9}-m_p=-9$
23+03*	23 09 20^{4}	+09 16^{8}	23 09 19	+09 16	*51* (29)	>40	An apparently normal So of magnitude 15½ in a loose cluster (Pegasus II). The fact that the source is observable with the Cambridge interferometer indicates that a source of small size must be involved. The observations are consistent with radiation from the single galaxy noted plus radiation from the cluster. $m_{1\cdot9}-m_p=-7$:

TABLE 2

COINCIDENCES BETWEEN RADIO SOURCES AND GALAXIES IN WHICH NO ANGULAR SIZE DATA ARE AVAILABLE OR IN WHICH THE SIZE DOES NOT SUPPORT THE IDENTIFICATION

Radio Source			Galaxy Position (1950)		Flux Densities (10^{-26} Wm^{-2} (c/s)$^{-1}$)	Angular Size ″	Notes
Ref. No.	Adopted Position (1950)						
	R.A. h m s	Dec. ° ′	R.A. h m s	Dec. ° ′			
00—*06*	00 21 30^{24}	—08 14^{6}	00 21 28	—08 19	24	~25	An So galaxy of normal appearance and magnitude 16:. The angular size is rather small but not impossible. However, there are several fainter galaxies within the area of uncertainty which would fit the size better
00—*017**	00 54 24^{6}	—01 39^{2}			*90* (72)	>45	This source is probably a blend of a moderately small source and an extended source. One interpretation of the data would give radiation in almost equal amounts from a small cluster (A119) and an Eo galaxy of normal appearance and magnitude 16:
01—*06**	01 29 00^{8}	—07 03^{6}	01 28 52	—07 07	19	~30	NGC584. A normal E3 galaxy of magnitude 11·2. The angular size appears too small for this identification. Probably the coincidence is a chance one
02—*15**	02 13 10^{4}	—13 19^{3}	02 13 01	—13 17	42	~20	An apparently normal Sc of magnitude 15½. The size appears to be rather too small and, since there are numerous very faint galaxies within the position uncertainty, probably the rather poor positional coincidence is the result of chance
04+*014**	04 58 15^{6}	+01 24^{6}	04 58 20	+01 18	15	—	An early type spiral of magnitude 16½ which displays very heavy absorption in the spiral arms. The flux density is too low for a measurement of size

08—02*	08 03 09^{4}	—00 30^{6}	08 03 06	—00 49	15	—	A very interesting multiple galaxy with at least 2 and perhaps 3 components. The brightest has magnitude 16. The declination is rather far off, but the 3C declination is off by an equal amount on the other side : examination of the original Sydney records reveals some ambiguity due to confusion effects and the galaxy position is admissible. The system possibly belongs to a distant cluster, A623, and radiation from this may be causing difficulties. An angular size measurement would be very desirable but the flux is too low
09—*16*	09 31 24^{18}	—16 47^{6}	09 31 29	—16 46	13	—	An Sb showing either a double nucleus, or a star superimposed on the nucleus. A photograph with the 200 in. telescope might disclose the nature of the object.
09—1*10*	09 42 42^{18}	—19 33^{6}	09 42 36	—19 30	12	—	An interesting pair of spirals, each of magnitude 16½: and about 0′·8 apart. Similar galaxies are not radio sources and this coincidence may be chance
09—1*14*	09 54 00^{18}	—13 36^{6}	09 54 18	—13 31	14	—	The brightest galaxy in the vicinity, of magnitude 15, it has a peculiar concentration at one edge. However, there are several fainter galaxies which cannot be eliminated
10—0*3*	10 08 06^{18}	—07 25^{6}	10 08 18	—07 37	17	(∼40)	A close pair of galaxies each of magnitude 17. The declination is rather far off but admissible. There are several fainter galaxies in the vicinity, however, and the size measurement is rather uncertain
10—0*10*	10 25 24^{18}	—07 20^{6}	10 24 40	—07 18	10	—	A close pair of galaxies each of magnitude 18. The agreement in R.A. is poor but admissible
21+0*10*	21 49 36^{24}	+07 52^{8}	21 49 45	+08 00	23	(<30)	A very close double galaxy with a combined magnitude of 17. There are several fainter galaxies nearby. The size needs checking but at present suggests an association with one of the fainter galaxies

TABLE 2 (*Continued*)

Radio Source			Galaxy Position (1950)		Flux Densities $(10^{-26}$ $\mathrm{Wm}^{-2}\,(\mathrm{c/s})^{-1})$	Angular Size ″	Notes
Ref. No.	Adopted Position (1950)						
	R.A. h m s	Dec. ° ′	R.A. h m s	Dec. ° ′			
22—17*	22 11 55^{5}	—17 11^{4}	22 11 45	—17 14	127	~35	A spiral of normal appearance and magnitude 16, perhaps associated with a small cluster. The size is somewhat low but acceptable; however, there are several fainter galaxies within the limits of uncertainty which fit the size better
23—*08*	23 15 36^{18}	—02 29^{7}	23 16 13	—02 36	9·8	—	A double galaxy of combined magnitude 18: and separation 5″. The position agreement is rather poor but acceptable
23—1*12*	23 22 36^{12}	—12 29^{5}	23 22 43	—12 25	30	<20	An So with a very bright nucleus and magnitude = 16. The small size counts against the identification and, as there are numerous galaxies of magnitude 19–20 within the positional uncertainty, the coincidence is probably chance
23—0*15*	23 38 00^{18}	—00 08^{6}	23 38 25	—00 11	11	–	A rather distorted double galaxy of late type and combined magnitude about 17. This is an interesting-looking object but the size of the source cannot be measured

TABLE 3

COINCIDENCES BETWEEN RADIO SOURCES AND THE CLUSTERS OF GALAXIES IN ABELL'S CATALOGUE

The photographic magnitude given is that of the tenth brightest cluster member

Radio Source				Cluster			
Ref. No.	Position (1950)		Flux Density (10^{-26} Wm^{-2} (c/s)$^{-1}$)	Ref. No.	Position (1950)		m_p
	R.A. h m	Dec. ° ′			R.A. h m	Dec. ° ′	
00—*14*	00 05·6^{3}	—19 58^{6}	17	2	00 58·8	—19 54	17·3
00+*03*	00 14·2^{3}	+06 48^{7}	12	16	00 14·1	+06 30	17·0
00—1*11*	00 25·3^{4}	—13 10^{7}	13	36	00 25·1	—13 03	17·6
00+*07*	00 30·8^{3}	+05 53^{5}	25	55	00 31·3	+06 05	17·2
00—0*17*	00 54·5^{1}	—01 39^{2}	90 (72)	119†	00 53·8	—01 31	15·0
01—*14*	01 08·2^{4}	—14 33^{6}	16	157	01 08·5	—14 40	16·9
01—*05*	01 23·5^{1}	—01 35^{2}	88	194†	01 23·0	—01 45	13·9
01—1*13*	01 36·9^{4}	—17 49^{6}	10	235	01 37·7	—17 40	17·5
02—*09*	02 29·4^{3}	—04 55^{5}	12	362	02 29·1	—05 05	17·7
02+0*10*	02 55·1^{1}	+05 53^{4}	51	400†	02 54·9	+06 01	13·9
03—*11*	03 03·5^{3}	—12 21^{5}	18	415	03 03·4	—12 14	16·3
03—*12*	03 05·4^{4}	—16 44^{6}	17	416	03 04·9	—16 55	17·7
04—*05*	04 09·5^{3}	—01 50^{5}	15	477	04 09·6	—02 00	17·5
04—1*12*	04 32·0^{2}	—13 26^{5}	38	496	04 31·3	—13 21	15·3
04—0*16*	04 46·8^{3}	—09 55^{5}	16	513	04 45·8	—09 48	17·5
04+0*11*	04 51·5^{4}	—02 33^{6}	10	520	04 51·6	+02 53	17·4
04+0*13*	04 56·3^{3}	+05 20^{8}	10	526	04 57·1	+05 24	16·4
05—*14*	05 13·0^{3}	—15 56^{8}	11	538	05 12·9	—15 45	17·4
08—*02*	08 03·1^{3}	—00 30^{6}	15	623†	08 03·1	—00 49	16·9
08+0*10*	08 55·0^{4}	+03 36^{8}	9·0	732	08 55·2	+03 22	17·7
09—*02*	09 06·5^{3}	—09 38^{6}	17	754	09 06·4	—09 27	15·2
09—*14*	09 15·7^{1}	—11 53^{2}	690	780†	09 16·0	—12 04	16·6
09+*05*	09 41·8^{3}	+09 57^{7}	32	862	09 42·1	+09 44	17·7
09+*06*	09 43·0^{3}	+02 21^{5}	7	869	09 43·6	+02 36	17·4
10—0*21*	10 59·8^{2}	—00 52^{5}	23	1148	10 59·8	—00 48	17·6
11+*09*	11 38·4^{4}	+05 43^{8}	8·2:	1346	11 38·5	+05 58	16·8
11—1*13*	11 47·1^{3}	—11 47^{6}	17	1391	11 47·3	—12 02	18·0
12—*01*	12 01·8^{3}	—04 36^{6}	12	1453	12 01·0	—04 23	17·8
				1458	12 01·5	—04 48	17·3
12—*08*	12 15·9^{3}	—04 47^{7}	16	1517	12 16·5	—04 45	16·6
12—1*11*	12 34·0^{3}	—14 13^{7}	9·6	1572	12 34·1	—14 26	17·3
12—1*13*	12 37·3^{5}	—15 38^{6}	14^{+}	1583	12 37·8	—15 42	17·8
12—0*19*	12 48·0^{2}	—01 36^{6}	14	1620	12 47·1	—01 20	17·2
13+*09*	13 40·3^{4}	+02 20^{9}	13	1773	13 39·6	+02 29	15·6
13—1*17*	13 59·1^{2}	—11 35^{5}	13	1836	13 58·9	—11 24	17·7
14+*01*	14 01·6^{3}	+09 22^{7}	28	1850	14 01·0	+09 22	17·5
14—0*18*	14 53·5^{2}	—05 44^{4}	16	1994	14 53·6	—05 39	17·7
15+*03*	15 08·6^{2}	+06 08^{6}	24	2029	15 08·4	+05 57	16·0
15+*06*	15 14·4^{5}	+00 18^{8}	16	2050	15 13·7	+00 17	17·1
15+*05*	15 14·2^{2}	+07 11^{6}	140	2052†	15 14·2	+07 11	15·0

---

† Coincidences with single or double galaxies in these clusters are noted in Tables 1 and 2.

TABLE 3 (*Continued*)

Radio Source				Cluster			
Ref. No.	Position (1950)		Flux Density (10^{-26} Wm^{-2} $(c/s)^{-1}$)	Ref. No.	Position (1950)		m_p
	R.A. h m	Dec. ° ′			R.A. h m	Dec. ° ′	
15+0*11*	15 $37\cdot4^{3}$	+06 08^{8}	22	2109	15 38·1	+06 11	17·4
15—0*12*	15 $38\cdot1^{5}$	—01 54^{6}	37 (21)	2103	17 37·3	—02 01	17·1
20—1*11*	20 $45\cdot0^{3}$	—18 20^{7}	15	2328	20 45·4	—18 00	16·4
21—1*20*	21 $48\cdot7^{3}$	—15 54^{7}	8·8	2382	21 49·3	—15 53	16·0
21—1*21*	21 $48\cdot9^{3}$	—19 53^{7}	18^{+}	2384	21 49·5	—19 47	15·9
22—0*12*	22 $29\cdot2^{4}$	—08 33^{6}	15	2448	22 29·1	—08 42	16·0
22—1*15*	22 $35\cdot8^{2}$	—17 36^{6}	17	2462	22 36·4	—17 38	16·2
22—0*14*	22 $36\cdot9^{3}$	—04 13^{6}	16	2464	22 36·6	—04 14	17·8
22+0*15*	22 $57\cdot2^{4}$	+09 43^{8}	15	2512	22 57·0	+09 50	17·1
23—1*3*	23 $07\cdot7^{3}$	—10 45^{7}	7·6	2544	23 07·6	—11 05	17·2
23+02	23 $08\cdot2^{3}$	+07 28^{6}	22	2551	23 09·0	+07 38	17·5
23—1*4*	23 $09\cdot6^{3}$	—12 54^{6}	11	2549	23 08·7	—13 05	17·0
23—08	23 $15\cdot6^{3}$	—02 29^{7}	9·8	2571†	23 16·0	—02 33	17·6
23—1*12*	23 $22\cdot6^{2}$	—12 29^{5}	30	2597†	23 22·7	—12 24	16·6
23—1*16*	23 $27\cdot6^{2}$	—18 47^{6}	13	2612	23 28·3	—18 56	17·7
23—0*15*	23 $38\cdot0^{3}$	—00 08^{6}	11	2644†	23 38·5	—00 12	16·6

coincidences with clusters in Abell's catalogue. Photographic magnitudes given in Tables 1 and 2 have been taken, where possible, from Humason, Mayall, and Sandage (1956), de Vaucouleurs (1957), or Holmberg (1958). Where the galaxy is too faint for inclusion by these authors, estimates have been made using a comparison sequence of images of galaxies calibrated in photo-red magnitudes and kindly made available by Dr. G. O. Abell. The red magnitudes have then been transformed to photographic, using the data of Abell (1958) and Holmberg (1958); it is expected that the accuracy is about 1 magnitude. In several cases photographs with the 200-in. Hale telescope have been referred to; this unpublished material was kindly made available by Dr. R. L. Minkowski. Also, several of the coincidences noted in the tables had been recognized by Dr. Minkowski in an earlier unpublished investigation of a portion of the area examined here, using essentially the same data.

In Table 1 are collected those coincidences for which the available angular size data are consistent with an identification. Criteria for such consistency are by no means well established and, in general, considerable latitude has been allowed. From an examination of known and well-established identifications it has been concluded that, with the present aerial spacings, a radio galaxy of photographic magnitude 19 would have an expected equivalent angular size of $\frac{1}{2}$ min of arc, with an uncertainty of about a factor of 2 or 3. It has also been borne in mind that intrinsically strong radio sources are likely to have a greater extent in space than intrinsically weak sources. A number of coincidences excluded from Table 1 because of inappropriate sizes are given in Table 2, along with those coincidences in which the radio source is too faint for a size measurement. Since all the faint sources and all those with incompatible sizes are included in Table 2, it is possible that not many of the coincidences are significant. In all, there are 30 sources in Table 1 and 16 sources in Table 2. In recording the difference of radio and photographic magnitudes the estimated radio magnitude at 1·9 m wavelength is quoted, based on the magnitude system of Hanbury Brown and Hazard, together with scale and spectrum adjustments described before (Mills 1959). The relation used is $m_{1\cdot 9}=-53\cdot 4-2\cdot 5\log S_{3\cdot 5}+0\cdot 8$. In this scale a flux density of 10^{-25} $\mathrm{Wm^{-2}\,(c/s)^{-1}}$ at 3·5 m wavelength corresponds to a magnitude of 9·9.

A brief discussion of each coincidence is given in the " notes " column and some of their common features are examined in Section VI. One coincidence, however, that with the source 16+0*10* (Hercules A) needs detailed discussion. This source had earlier been identified by Minkowski (1957) with the highly peculiar double galaxy noted in the table. This identification, together with others, has been used to derive a collimation error for the 3·5 m Cross; the position of the source given by Mills, Slee, and Hill (1958) includes the derived correction of $+4^s$ Right Ascension and agrees quite well with the galaxy position. However, the more accurate Right Ascension of the 3C position appears incompatible with an identification agreeing precisely with the uncorrected Sydney position. A new determination has been attempted at Sydney, basing the collimation correction on the positions of two well-established identifications, Virgo A and Hydra A, closely straddling the source Hercules A in declination. However, the result was essentially the same, the indicated correction being $+3^s$; this position is quite compatible either with the 3C position or the galaxy position, and doubt concerning the identification arises because of the claimed accuracy of the former. However, inspection of the Sky Survey and 200-in. telescope plates shows that there are no galaxies in the immediate vicinity bright enough to suggest a radio size as great as that measured, except the system noted, and even this is somewhat faint. One possibility is that here we have a close blend of radio sources, the dominant one being associated with the double system, the weaker with one of numerous faint galaxies in a north preceding direction; examination with an instrument of very high resolving power in both coordinates seems necessary to clarify the situation.

Coincidences between radio sources and clusters are listed in Table 3. Of the 55 coincidences noted, it was shown that the chance expectation is 16 so that the probability of a selected coincidence being significant is not so high as in Table 1. In every case the apparent radio emission is considerably more than anticipated from the integrated emission of " normal " galaxies in the cluster. Several of these radio sources have, however, also been listed in Tables 1 and 2, indicating that, in these cases at least, the radiation is more likely to be originating in a single peculiar system within the cluster than in the cluster as a whole; such cases are marked by a dagger in Table 3. It is not possible to decide at present whether the remaining significant coincidences are similar or whether one has examples of " radio clusters " where radiation from the intergalactic material reaches abnormally high values.

V. THE RADIO LUMINOSITY FUNCTION

Interpretation of statistical analyses connected with the distribution of radio sources requires, as a starting point, some knowledge of the radio luminosity function, that is, knowledge of the number of radio sources in a given volume of space as a function of their emission. Since there is, at present, no reliable way of determining directly the distance of a radio source by radio means, one must proceed by identification of the sources and the application of optical criteria of distance. In the following analysis identifications with galaxies only are considered.

There are sufficient possible identifications resulting from the present investigation to take the first step in determining the radio luminosity function. Thus, if it be assumed that this function is constant throughout the volume of space accessible to the present observations, then we determine at the outset the probability of a galaxy, chosen at random, having a specified ratio of radio to optical emission. The result obtained with the present material can only be regarded as provisional, to be improved when better determined positions and angular sizes become available ; in particular, the operation of selection effects, necessarily imposed by the quality of the data, allows the existence of distant unidentified sources of high radio emission.

In the next step, absolute values for radio emission and space density may be obtained from optically derived properties of the galaxies. However, the latter step is not taken explicitly here because the optical data are at present inadequate. Instead, some statistical properties of the radio sources are deduced from the probability function above, and compared directly with observation, making some appropriate simplifying assumptions where necessary.

For simplicity, also, the initial assumption will be made that red-shift effects are negligible over the range in which identifications have been sought. A later analysis in which these are considered indicates that errors will be small compared to those arising from the uncertainties in identification and small-number statistics.

(*a*) *Derivation*

We shall for brevity define the ratio of radio to optical emission of a galaxy by $\underline{m}=m_{1\cdot 9}-m_p$. Then we may write $P_{\underline{m}}\cdot\Delta\underline{m}$ as the probability that a galaxy chosen at random has $\underline{m}$ between $\underline{m}-\frac{1}{2}\Delta\underline{m}$ and $\underline{m}+\frac{1}{2}\Delta\underline{m}$. Now the area searched systematically for identifications is very close to 10^4 square degrees so that the number of galaxies brighter than m_p in the chosen area can be obtained from Hubble's (1936) relation, on ignoring the red-shift correction, as

$$\log N=0\cdot 6m_p-9\cdot 2+4\cdot 0=0\cdot 6m_p-5\cdot 2,$$

whence

$$\log P_{\underline{m}}\cdot\Delta\underline{m}=\log n_{\underline{m}}\cdot\Delta\underline{m}-0\cdot 6m_p+5\cdot 2, \qquad \dots\dots\dots \quad (1)$$

where $n_{\underline{m}}\cdot\Delta\underline{m}$ is the number of identifications with galaxies brighter than m_p having $\underline{m}$ lying between $\underline{m}-\frac{1}{2}\Delta\underline{m}$ and $\underline{m}+\frac{1}{2}\Delta\underline{m}$.

Restricting attention to identifications with $m_{1{\cdot}9}$ brighter than $9{\cdot}2$ ($S_{3{\cdot}5}>2\times10^{-25}$ Wm^{-2} (c/s)$^{-1}$), which have been looked for systematically, it is evident that we can have a complete set of identifications only with galaxies brighter than

$$m_p=9{\cdot}2-\underline{m}.$$

Substituting this in (**1**) we have for this set of identifications

$$\log P_{\underline{m}}\cdot\Delta\underline{m}=\log n_{\underline{m}}\Delta\underline{m}+0{\cdot}6\underline{m}-0{\cdot}3. \quad \ldots\ldots\ldots\ldots \quad (\mathbf{2})$$

For single galaxies which have been investigated systematically only to magnitude 16 this expression is correct for $\underline{m}$ greater than $-6{\cdot}8$. For double galaxies investigated to $m_p=19$ the limiting value of $\underline{m}$ is about $-9{\cdot}8$. It is evident that, for single galaxies with $\underline{m}<-6{\cdot}8$ and for double galaxies with $\underline{m}<-9{\cdot}8$, N is a constant defined by the limiting photographic magnitude. Thus for single galaxies with $\underline{m}<-6{\cdot}8$

$$\begin{aligned}\log P_{\underline{m}}\cdot\Delta\underline{m}&=\log n_{\underline{m}}\cdot\Delta\underline{m}+0{\cdot}6\times-6{\cdot}8-0{\cdot}3\\&=\log n_{\underline{m}}\cdot\Delta\underline{m}-4{\cdot}4, \quad \ldots\ldots\ldots\ldots\ldots\ldots \quad (\mathbf{3})\end{aligned}$$

and similarly for double galaxies with $\underline{m}<-9{\cdot}8$

$$\log P_{\underline{m}}\cdot\Delta\underline{m}=\log n_{\underline{m}}\cdot\Delta\underline{m}-6{\cdot}2. \quad \ldots\ldots\ldots\ldots\ldots\ldots \quad (\mathbf{4})$$

To construct the probability function the data of Table 1 have been used. It is not suggested that all coincidences listed in this Table are real identifications, or that all identifications in the area are included, but it appears to be an adequate sample for making a preliminary analysis. The photographic magnitudes of two galaxies in heavily obscured regions (coinciding with the sources 17–06 and 17–23) have been corrected by 4 magnitudes and the sources 14–019 and 22–09 have been omitted because they do not fit into the scheme used in deriving equations (**2**), (**3**), and (**4**) ; the former has too low a flux density, the latter an associated galaxy which is too faint. In order to obtain sufficient numbers in each magnitude interval, $\Delta\underline{m}$ has been taken as 2 magnitudes ; because of this large interval the equations are no longer exactly correct, but the uncertainties in the data do not warrant alteration. Likewise, the numbers are too few to differentiate between single and double galaxies, and in Table 4, where the results are tabulated, they are lumped together. When equations (**3**) and (**4**) had to be applied the probabilities were computed separately and then added.

The probability function is plotted in Figure 1, where it is evident that, between $\underline{m}=+1$ and $\underline{m}=-13$, the straight line defined by

$$\log P_{\underline{m}}=-1{\cdot}0+0{\cdot}42\underline{m} \quad \ldots\ldots\ldots\ldots\ldots \quad (\mathbf{5})$$

gives a reasonable approximation to the observed points. The point marked by a cross at $\underline{m}=+1$ has been derived from the data on normal galaxies (Mills 1959) ; about 50 per cent. of spirals representing about 25 per cent. of all galaxies had values for $\underline{m}$ between $+0{\cdot}5$ and $+1{\cdot}5$, leading to $P_{+1}\simeq\frac{1}{4}$.

(*b*) *Applications of the Luminosity Function*

Let us now consider in a general way the flux densities and numbers of the radio sources predicted by a law of this form and compare them with the actual observations. Initially we will ignore cosmological effects; later they will be taken into account.

TABLE 4

DERIVATION OF THE PROBABILITY FUNCTION FROM THE OBSERVED COINCIDENCES

The interval Δm is taken as 2 magnitudes

$\underline{m}$	$n_{\underline{m}}\cdot\Delta\underline{m}$	$\log P_{\underline{m}}$
+1	—	—
—1	1	—1·2
—3	4	—1·8
—5	3	—3·1
—7	9	—3·8
—9	7	—5·1
—11	3	—6·0
—13	1	—6·5

Substituting equation (5) in equation (1), we find the following relationship between $n_{\underline{m}}$, $\underline{m}$, and m_p

$$\log n_{\underline{m}} = -6\cdot 2 + 0\cdot 42\underline{m} + 0\cdot 6m_p,$$

or, if we take $\mathcal{N}_{\underline{m}}$ as the total number of sources over the whole sky in an interval $\Delta\underline{m}=2$, we have

$$\begin{aligned}\log \mathcal{N}_{\underline{m}} &= -5\cdot 3 + 0\cdot 42\underline{m} + 0\cdot 6m_p\\ &= -5\cdot 3 - 0\cdot 18\underline{m} + 0\cdot 6m_{1\cdot 9}. \qquad \ldots\ldots\ldots\ldots (6)\end{aligned}$$

In defining a family of uniformly distributed radio sources, the most convenient parameter is the flux density of the first "average" source, S_0 (Mills and Slee 1957). This may be derived for each value of $\underline{m}$ by putting $\mathcal{N}_{\underline{m}}=1$ in equation (6), and converting $m_{1\cdot 9}$ to flux density at $3\cdot 5$ *m* using the formula in the preceding section, thus

$$S_{0,\underline{m}} = \text{antilog}\,(-24\cdot 60 - 0\cdot 12\underline{m}). \qquad \ldots\ldots\ldots\ldots (7)$$

Thus we have

$$\begin{aligned}S_{0,-13} &= 9\cdot 0\times 10^{-24}\ \text{Wm}^{-2}\ (\text{c/s})^{-1}\\ S_{0,-11} &= 5\cdot 3\times 10^{-24}\ \text{Wm}^{-2}\ (\text{c/s})^{-1},\\ S_{0,-9} &= 3\cdot 0\times 10^{-24}\ \text{Wm}^{-2}\ (\text{c/s})^{-1},\ \text{etc.}\end{aligned}$$

To obtain the flux density S_0 of the first "average" source of the whole population, we note that the total number of sources with flux densities greater than S is given by

$$\begin{aligned}\mathcal{N} &= (S_{0,+1}/S)^{3/2} + (S_{0,-1}/S)^{3/2} + (S_{0,-3}/S)^{3/2} + \ldots\\ &= (S_0/S)^{3/2},\end{aligned}$$

whence

$$S_0^{3/2} = S_{0,+1}^{3/2} + S_{0,-1}^{3/2} + S_{0,-3}^{3/2} + \ldots\ .$$

If the population is limited to $\underline{m}=-13$, which represents the greatest radio emission recognized, we may perform the sum and find that

$$S_0=1\cdot3\times10^{-23}\ \mathrm{Wm}^{-2}\ (\mathrm{c/s})^{-1}.$$

From the direct counting of observed sources Mills and Slee (1957) concluded that $S_0=2\cdot1\times10^{-23}\ \mathrm{Wm}^{-2}\ (\mathrm{c/s})^{-1}$. Since it was also found that a substantial proportion of the sources were of large apparent size and therefore not represented by the present class of identifications, it would appear that, within the uncertainty of the data, the agreement is good. However, cosmological effects have been ignored and before a definite conclusion can be reached it is necessary to examine the results in a more realistic universe.

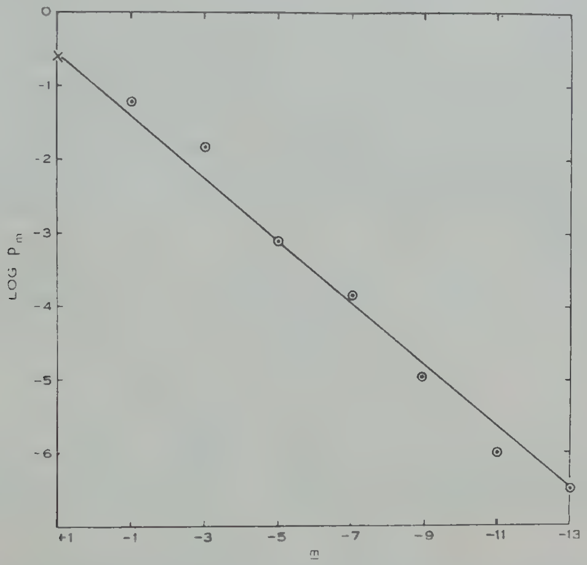

Fig. 1.—The probability that a galaxy chosen at random has radio emission defined by $\underline{m}$, where $\underline{m}$ is the difference between the radio and photographic magnitudes of the galaxy $(m_{1\cdot9}-m_p)$.

No attempt will be made to decide between different cosmologies, but one particular type will be worked out in detail to illustrate the kind of effects expected. The Einstein-de Sitter universe is chosen as a model; it is the simplest of the "exploding" models and is characterized by the absence of curvature and cosmological constant. If the assumption is made that the total number of radio sources of any given emission has remained unaltered during the evolution of the universe it turns out that the number counts may be expressed by a very simple relation, which is derived in Appendix I. Thus, for a class of source of fixed emission we have the relation

$$S=\frac{S_0}{\mathcal{N}^{\frac{2}{3}}}\left[1-\left(\frac{\mathcal{N}}{\mathcal{N}_0}\right)^{\frac{1}{3}}\right]^{4+2\gamma}, \qquad \ldots\ldots\ldots\ldots\ldots\ldots (8)$$

where $\mathcal{N}$ is the number of sources with flux density greater than S, $\mathcal{N}_0$ is the total number of such sources in the observable universe, and the spectrum of the sources is of the form

$$S\propto\lambda^{\gamma}.$$

The correction to the normal source count relation is given by the bracketed term. $\mathcal{N}_0$ is derived fundamentally from the measured red-shifts of identified galaxies, but for clarity we will assume a particular value of Hubble's constant, namely, $H=100$ km/s/megaparsec, and calculate the space density of the various source classes and their absolute luminosities. The final source counts, however, are independent of the value chosen for H.

It is first assumed that all identified galaxies have the same absolute photographic magnitude. Some such assumption is necessary to proceed because of the present inadequate data ; it is not unreasonable as shown by Dewhirst (1959), at least for those galaxies of the highest radio emission which dominate the source counts and for which cosmological corrections are required. The mean, absolute photographic magnitude of six identified galaxies listed by Dewhirst is $M_p=-20\cdot5$, also using $H=100$ km/s/megaparsec. This value will be adopted in the present calculations although it may eventually prove to be too luminous, because of selection effects. Thus the absolute radio luminosity of a source is given by

$$\begin{aligned}L_{\underline{m}}&=4\pi(3\cdot09\times10^{17})^2\text{ antilog }-0\cdot4(52\cdot6+M_p+\underline{m})\text{ W (c/s)}^{-1}\\&=1\cdot7\times10^{23}\text{ antilog }-0\cdot4\underline{m}\text{ W (c/s)}^{-1}\text{ at }3\cdot5\text{ m wavelength,}\end{aligned}$$

for example,

$$L_{13}=2\cdot7\times10^{28}\text{ W (c/s)}^{-1}.$$

It is readily shown, by consideration of the number of sources in a given spherical volume, that the space density, $\rho_{\underline{m}}$, is given by the relation

$$\rho_{\underline{m}}=6\sqrt{\pi}\cdot(S_{0,\underline{m}}/L_{\underline{m}})^{3/2}, \quad \ldots\ldots\ldots\ldots\ldots \quad (9)$$

where $S_{0,\underline{m}}$ is obtained as in (**7**). It is also shown in Appendix I that

$$\mathcal{N}_0=36\pi\rho_2(cT)^3,$$[*]

where T is the reciprocal of Hubble's constant, whence

$$\begin{aligned}\mathcal{N}_{0,\underline{m}}&=216\pi^{3/2}(cT)^3(S_{0,\underline{m}}/L_{\underline{m}})^{3/2}\\&=1\cdot8\times10^{9}\text{ antilog }0\cdot42m, \quad \ldots\ldots\ldots\ldots \quad (\mathbf{10})\end{aligned}$$

for example,

$$\mathcal{N}_{0,-13}=6\cdot4\times10^{3}.$$

In Figure 2 the source counts expected from equations (**8**) and (**10**) have been plotted for values of $\underline{m}$ between +1 and −13. The assumption is made that $\gamma=+1\cdot0$ for all sources. Also shown are the combined counts and those obtained from direct observation. The latter have been obtained from the known strong sources in the whole sky (open circles) and the catalogue of Mills, Slee, and Hill (1958) covering about 3 steradians (solid circles). The standard errors in the numbers due to statistical fluctuations are indicated by vertical wings. To obtain the best estimate of the true source count, corrections are necessary at low flux densities; these have been calculated at 10^{-25} Wm^{-2} (c/s)$^{-1}$ and 2×10^{-25} Wm^{-2} (c/s)$^{-1}$ using the data of Mills and Slee (1957), plus an additional small correction for a type of error discovered subsequently. This error arises from the systematic over-estimation of flux densities not very much above the sensitivity limit; it is a partially subjective effect, but very similar between different observers. It will be discussed in a later publication. The corrected points are indicated by crosses, and a straight line drawn through these represents the true source counts as closely as possible with the present data.

---

[*] The symbol ρ_2 is used in Appendix I to denote the space density of objects at the present time, i.e. it is equivalent to $\rho_{\underline{m}}$ above.

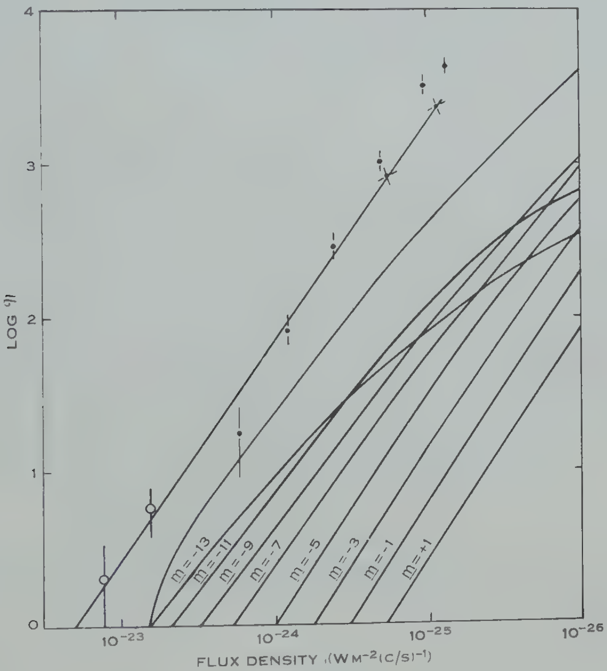

Fig. 2.—Comparison of the observed source counts with those predicted by the derived radio luminosity function. The observational points are shown as dots or crosses, depending on their origin, having vertical wings indicating the standard error due to statistical fluctuation. Two points corrected for the instrumental effects which occur at low flux densities are indicated by crosses. Expected counts for each class of source are labelled with the corresponding value of $\underline{m}$; the total expected count which is the sum of these is also shown.

It appears that the numbers derived from Table 1 are too low by a factor of about 3 to account for all the observed sources. However, substantial numbers of the sources appear to be of large size, possibly irregularities in the galactic corona or relatively close blends (e.g. two or more radio galaxies in a cluster); these would not appear in Table 1 and would not contribute to the radio luminosity function. They comprise about 30 per cent. of listed sources having flux density near 5×10^{-25} Wm^{-2} (c/s)$^{-1}$ and, perhaps, as indicated by preliminary results with the Sydney angular size interferometer, an even greater proportion of fainter sources. One is therefore left with a discrepancy of a factor of 2 which, in view of the uncertainty in the data, is barely significant. However, there are several possible additional identifications between strong sources and galaxies of apparently normal appearance which are too faint for inclusion in Table 1 although the radio sizes are admissible. These could quite well raise the probability function at high emissivities sufficiently to counteract any deficiency. They are clearly a subject for future investigation both at radio and optical wavelengths. A further possibility, that there is a *significant* number of sources having $\underline{m}<-13$, does not, at present, appear very likely, since these would drastically alter the form of the source counts.

One of the most striking features of the computed curve is the small influence of cosmological effects. There is no appreciable curvature above about 10^{-25} Wm^{-2} (c/s)$^{-1}$ where the mean slope is about $-1\cdot3$, and between 10^{-25} and 10^{-26} Wm^{-2} (c/s)$^{-1}$ the slope decreases to only about $-1\cdot0$, although the sources of highest emission show very marked effects in this region. The reason, of course, is the dilution by the intrinsically weaker sources, which being closer, show little effects and indeed initially tend to increase the numerical value of the slope. The difference between various cosmologies would also be masked in this way and, since this difference is unlikely to be large in the first place (e.g. Hoyle 1959), the simple counting of observed sources is unlikely to be a very sensitive test. However, suitable angular size data could prove very valuable by allowing the separation of the various classes of source.

Finally, one may compute the integrated extragalactic emission from the class of radio sources defined by Figure 1. It is shown in Appendix I that the equivalent brightness temperature of the integrated background in an Einstein-de Sitter universe is given by

$$T_{\underline{m}}=\frac{L_{\underline{m}}\rho_{\underline{m}}\lambda^2cT}{4\pi k(5+2\gamma)}. \qquad \ldots\ldots\ldots\ldots\ldots\ldots\ldots \quad (\mathbf{11})$$

Making the assumptions as before we find

$$T_{\underline{m}}=3\cdot1 \text{ antilog } 0\cdot02\underline{m} \text{ degK}$$

whence

$$T=\sum_{\underline{m}=+1}^{\underline{m}=-13} T_{\underline{m}}=20\ {}^{\circ}\mathrm{K}.$$

This is a lower limit for two reasons: (*a*) it is probable that the derived radio luminosity function does not include all extragalactic sources, as shown above, and (*b*) in deriving the luminosity function it was assumed that all galaxies identifiable as radio emitters had an absolute magnitude of $-20\cdot5$. While this value is probably appropriate for deriving the cosmological correction to the counts of sources of high emission, for which it was used originally, it is inappropriate for calculating the integrated emission of the "normal" spiral galaxies which have the greatest weight in determining T; these would have a smaller emission, a higher space density, and a greater integrated temperature. As an example, if we put $M_p = -16\cdot 5$ (Hubble's mean value corrected for the new value of H) instead of $-20\cdot 5$, the integrated emission is increased by 2 magnitudes (equations (**9**) and (**11**)) to 125 °K. Shain (1959) has concluded that the most probable value of the extragalactic contribution to the observed temperatures near the Galactic poles is about one-third of the total, or about 250 °K, but he stated that it could be very much less.

VI. DISCUSSION

It follows from the results presented in the last section that the Class II sources of small angular size are likely to be extragalactic. Analysis suggests that these sources can be substantially represented by a class defined by the possible identifications in Table 1, possibly with the addition of a class of apparently normal galaxies of relatively high radio emission.

There is less information about the sources of large size. In a few cases these may be identified with clusters of galaxies, either representing radiation from the intergalactic material in the cluster or from two or more strongly emitting galaxies. However, few of the sources coinciding with clusters in Table 3 are listed as " extended " or " perhaps extended " in the Sydney catalogue and, conversely, extended Class II sources do not show a significantly higher correlation with clusters. It is therefore concluded that rich clusters of the type listed by Abell are not associated with the majority of the extended radio sources. The most likely explanation appears to be that these sources are mainly galactic irregularities and/or blends of closely spaced " radio galaxies ". Angular size data which are being collected at present should throw more light on this problem and it will not be discussed here any further.

It is perhaps appropriate to consider a possibility which arises because of the apparently continuous nature of the radio luminosity function. If radio galaxies are formed only with the highest emission by a rare cataclysmic process and thereafter the emission slowly decays to a normal value, the number of galaxies having a luminosity between L and $L+\mathrm{d}L$ will be inversely proportional to $\mathrm{d}L/\mathrm{d}t$. Assuming a luminosity function of the form derived in the preceding section, it is easily shown that this would require a decay law approximately of the form

$$L \simeq L_0/(1+At),$$

where A is a constant and t the time after the outburst. However, the synchrotron mechanism does not easily lend itself to a decay law of this kind. For example, if the outburst produces a spectrum of relativistic electrons defined by the power law, $n\mathrm{d}E \propto (1/E^{\beta})\mathrm{d}E$ (where $\beta \approx 3$), the subsequent decay of the luminosity due to radiation losses at a fixed frequency and in a constant magnetic field is readily shown to be

$$L = L_0(1-Bt)^{\beta-2},$$

where B is a constant related to the frequency chosen and the magnetic field. While it appears that a suitably varying magnetic field could produce the decay law suggested by observation, in fact no physically plausible variation has been found which will do so. Also, other features are expected in a decaying source, namely, a change in the radio spectrum with age (i.e. with absolute radio luminosity) and a high frequency cut-off in the radiation which is also a function of age. Present observational evidence does not appear to support the existence of these features and it seems that the luminosity function is probably not formed as the result of such a process. If a radio galaxy is a transient phenomenon, the luminosity function would appear to be determined primarily by the peak value of the emission rather than the decay law.

Let us now consider the galaxies listed in Table 1, which are the most likely to be real identifications. These galaxies have no obvious common feature, as all types of system are represented ; they do, however, separate into two distinct classes, single galaxies and double galaxies. Members of these same classes have already been recognized in identifying the strongest radio sources ; e.g. the radio sources Virgo A and Fornax A are identified with single galaxies and Cygnus A, Hydra A, Hercules A, and Perseus A with doubles ; the source Centaurus A is a possible member of the latter class also.

Identifications with single galaxies are in general uncertain, for there appears to be no reliable optical clue which indicates excess radio emission. The galaxy NGC4486, identified with Virgo A, has, it is true, a very blue " jet " extending from the nucleus. However, this is recognizable only because the galaxy is so close ; similar features would not be visible usually in the single galaxies of Table 1 and, in fact, no abnormal features were noted. In Table 2 one galaxy, associated with the source 04+0*14*, displays heavy absorption in the spiral arms, but it is not known if this is a significant form of abnormality. One cannot hope to derive much useful information from optical studies of the single galaxies listed.

The double galaxies are rather more interesting. If these are real identifications, as appears likely in the majority of cases, they must be physical rather than optical doubles. The question arises whether they are colliding (Baade and Minkowski), separating (Ambartsumian), or orbiting. The first two possibilities can be separated from the third on a statistical basis by measurement of the radial velocities of the two components, and it is hoped that this information will be available before long.

The collision hypothesis does not appear to stand up to a close examination ; the numbers of colliding galaxies in the Universe are expected to be quite small, in fact quite negligible outside the centres of dense clusters, as shown by Spitzer and Baade (1951), and, if the further limitation is imposed that only giant colliding galaxies produce markedly excess radio emission (to agree with the absolute luminosities of identified radio galaxies), the interpretation is completely inadequate. The ideas of Ambartsumian (1956) are hard to understand, since he suggests that some of the double galaxies may be recently formed systems, separating and forming two nuclei ; the application of these ideas to very old galaxies containing a high proportion of Population II stars, as some of the identified galaxies appear to be, does not appear legitimate. However, there is some observational support for the suggestion in an earlier identification made with the system associated with NGC6166. Dewhirst (1959) describes this as containing within a common envelope two or possibly three nuclei in addition to the main system with a velocity difference between the brightest components of about 1500 km/s.

In contrast to the general implausibility of these suggestions it appears that two closely orbiting galaxies are quite likely to build up strong magnetic fields as a result of interaction of the surrounding very tenuous gas The presence of a normal concentration of relativistic electrons could then lead to an abnormally high radio emission. There is no real evidence that this sort of process occurs, however, and NGC6166 could certainly not be explained in this way. Since none of these possibilities appears plausible in all cases, perhaps a radio source can be associated with any of the three.

Of particular interest to the double galaxy situation are the results on the distribution of radio emission across a galaxy. Here again we appear to have evidence of duplicity. The Cygnus A source, with its two concentrations on either side of a double galaxy, is now well established, and recently Wade (1959) has shown that the extended corona of the Centaurus A source also appears to consist of two symmetrically situated concentrations with about the same apparent spatial separation as Cygnus A. The situation in Centaurus A is complicated by the existence of a small central source responsible for about 25 per cent. of the total emission and apparently coinciding with the band of dust crossing NGC5128 (Mills 1953). A more detailed study of this small source by Twiss, Carter, and Little (in press) shows that it, too, is a double system. The possibility that these are all toroidal sources is not supported by the detailed distributions given, and the present evidence does appear to suggest that they are real doubles.

In view of the scanty data it is rather profitless to speculate about the processes by which optical and radio double galaxies are formed. Rather, it is necessary to collect a great deal more information both at optical and radio wavelengths, particularly about the coincidences listed in Table 1. In this way it may be possible to separate the basic factors from a mass of probably irrelevant detail.

VII. Acknowledgments

Examination of the original plates of the National Geographic Society–Palomar Observatory Sky Atlas was carried out during a two-month period at the California Institute of Technology, supported financially by a grant from the National Science Foundation.

The author is indebted to Dr. D. W. Dewhirst and Professor M. Ryle for making available material prior to publication, and, in particular, to Dr. R. L. Minkowski whose advice and freely given unpublished data helped very materially.

VIII. References

Abell, G. O. (1958).—*Astrophys. J. Suppl. Ser.* **3** : 211.

Ambartsumian, V. A. (1956).—Proceedings of the 5th Conference on questions of cosmogony (Radioastronomy), Moscow, p. 413.

Bondi, H. (1952).—" Cosmology." (Cambridge Univ. Press.)

Dewhirst, D. (1959).—" Paris Symposium on Radio Astronomy." (Ed. R. N. Bracewell.) p. 507. (Stanford Univ. Press.)

Edge, D. O., Shakeshaft, J. R., McAdam, W. B., Baldwin, J. E., and Archer, S. (1959).—*Mem. R. Astr. Soc.* **68** : 37.

Goddard, B. R., Watkinson, A., and Mills, B. Y. (1960).—An interferometer for the measurement of radio source sizes. *Aust. J. Phys.* **13** (4). (In press.)

Holmberg, E. (1958).—*Medd. Lunds. Astr. Obs.* Ser. II, No. 136.

Hoyle, F. (1959).—"Paris Symposium on Radio Astronomy." (Ed. R. N. Bracewell.) p. 529. (Stanford Univ. Press.)

Hubble, E. (1936).—*Astrophys. J.* **84** : 517.

Humason, M. L., Mayall, N. V., and Sandage, A. R. (1956).—*Astr. J.* **61** : 97.

Mills, B. Y. (1953).—*Aust. J. Phys.* **6** : 452.

Mills, B. Y. (1959).—"Handbuch der Physik." Vol. 53, p. 239. (Springer-Verlag : Berlin.)

Mills, B. Y., and Slee, O. B. (1957).—*Aust. J. Phys.* **10** : 162.

Mills, B. Y., Slee, O. B., and Hill, E. R. (1958).—*Aust. J. Phys.* **11** : 360.

Minkowski, R. L. (1957).—"Radio Astronomy, Symposium No. IV of the International Astronomical Union." p. 107. (Cambridge Univ. Press.)

Shain, C. A. (1959).—"Paris Symposium on Radio Astronomy." (Ed. R. N. Bracewell.) p. 328. (Stanford Univ. Press.)

Spitzer, L., and Baade, W. (1951).—*Astrophys. J.* **113** : 413.

Twiss, R. Q., Carter, A. W. L., and Little, A. G. (1960).—Brightness distribution over some strong sources at 1427 Mc/s. *Observatory.* (In press.)

de Vaucouleurs, G. (1957).—*Ann. Obs. Houga* II, No. 1.

Wade, C. M. (1959).—*Aust. J. Phys.* **12** : 471.

APPENDIX I

Relations in an Einstein-de Sitter Universe

This relativistic model universe is characterized by absence of curvature and cosmological constant. It is well known (e.g. Bondi 1952) that the appropriate metric is given by

$$ds^2 = dt^2 - R^2(dr^2 + r^2 d\theta^2 + r^2 \sin^2 \theta d\theta^2),$$

where

$$R = ct^{\frac{2}{3}}.$$

Denoting properties at the time of emission of the radiation by subscript 1, and at the time of reception by subscript 2, we may write down the following relations, using conventional notation.

The present time $t_2 = T^{\frac{2}{3}}$, where $T = 1/H$.

If $z = \Delta\lambda/\lambda_0$,

$$1 + z = R_2/R_1 = (t_1/t_2)^{-\frac{2}{3}}.$$

The luminosity distance

$$q_1 = cr_1R_2 = cR_2 \int_{t_1}^{t_2} dr/R = 3ct_2[1 - (t_1/t_2)^{\frac{1}{3}}].$$

The number of sources of space density ρ_2 within q_1 is then given by

$$\mathcal{N} = \frac{4}{3}\pi\rho_2 q_1^3 = 36\pi\rho_2 c^3 t_2^3 [1 - (t_1/t_2)^{\frac{1}{3}}]^3. \quad \ldots\ldots\ldots\ldots \quad \textbf{(A1)}$$

Whence the total number of sources in the observable universe is obtained by putting $t_1=0$, thus

$$\mathcal{N}_0=36\pi\rho_2c^3t_2^3=36\pi\rho_2c^3T^3. \quad \ldots\ldots\ldots\ldots\ldots \quad \textbf{(A2)}$$

The flux density of a source of luminosity L_1, at a distance q_1, is given by

$$S=L_1/4\pi q_1^2(1+z)^2.$$

With a spectrum of the form $L\propto\lambda^\gamma$, and in the absence of evolutionary changes in L we may write

$$L_2=L_1(\upsilon_2/\upsilon_1)$$

or

$$S=L_2/4\pi q_1^2(1+z)^{2+\gamma}. \quad \ldots\ldots\ldots\ldots\ldots \quad \textbf{(A3)}$$

From (**A1**), (**A2**), and (**A3**), we have

$$S=\frac{L_2\rho^{\frac{2}{3}}}{6^{\frac{2}{3}}\pi^{\frac{1}{3}}}\,\frac{[1-(\mathcal{N}/\mathcal{N}_0)^{\frac{1}{3}}]^{4+2\gamma}}{\mathcal{N}^{\frac{2}{3}}},$$

which, on using the relation $\rho=6\sqrt{\pi}.(S_0/L)^{3/2}$ (equation (**9**)), becomes

$$S=(S_0/\mathcal{N}^{\frac{2}{3}})[1-(\mathcal{N}/\mathcal{N}_0)^{\frac{1}{3}}]^{4+2\gamma}. \quad \ldots\ldots\ldots\ldots \quad \textbf{(A4)}$$

Consider now the sources in unit solid angle at distance q_1. These contribute a flux $\mathrm{d}B$, given by

$$\mathrm{d}B=S\mathrm{d}n=\frac{\rho_2L_2}{4\pi(1+z)^{2+\gamma}}\mathrm{d}q_1$$

and the brightness temperature

$$T=\frac{\lambda^2}{2k}\int\mathrm{d}B=\frac{L_2\rho_2\lambda^2}{8\pi k}\int_{z=0}^{z=\infty}\frac{\mathrm{d}q}{(1+z)^{2+\gamma}}$$

$$=\frac{L_2\rho_2\lambda^2}{4\pi k(5+2\gamma)}\cdot cT. \quad \ldots\ldots\ldots\ldots \quad \textbf{(A5)}$$

FREE PATH FORMULAE FOR THE COEFFICIENT OF DIFFUSION D AND VELOCITY OF DRIFT W OF IONS AND ELECTRONS IN GASES

By L. G. H. Huxley*

[*Manuscript received May 24, 1960*]

Summary

In derivations of formulae for D and W for electrons by the method of free paths (Huxley 1957*a*, 1957*b*) the assumption was made that along a number of successive free paths an electron travels at essentially the same speed c. As this assumption is not true of ions it would not be legitimate to apply the formulae to the motion of ions in gases without further discussion. However, the formulae are in fact valid for ionic motion and in what follows they are established in a more general form.

I. Coefficient of Diffusion D

Consider a large number p of free paths $x_1, x_2, \ldots, x_n$ all traversed at the same speed c by the ion or electron, but not necessarily consecutively.

If l_0 is the mean free path then

$$pl_0 = \sum_1^n x_k.$$

Let $\bar{g}$ be the mean speed of the ion (with speed c) relative to the molecules which move at random and let N be the number of molecules in unit volume.

The sum of the times spent in traversing the paths x_k is $t=pl_0/c$, that is to say, $p=ct/l_0$. But $p=\bar{g}tN\pi\sigma^2$, consequently $l_0=(c/\bar{g})N\pi\sigma^2=l_0(c)$. For electrons $\bar{g}=c$; $l_0=1/N\pi\sigma^2$. σ is the limiting value of the impact parameter beyond which deflections of the ions are unimportant.

Consider a diffusing group of n electrons or ions. In the absence of an electric or magnetic field the rate of increase of the mean of the squares of the distance of the n particles from a fixed origin is given by the well-known formula $\mathrm{d}\overline{r^2}/\mathrm{d}t=6D$.

In time t let the kth particle traverse a succession of free paths $\mathbf{x}_{k,m}$ so that its vector position changes from $\mathbf{r}_{0k}$ at time $t=0$ to $\mathbf{r}_k$ at time t. That is,

$$\mathbf{r}_k = \mathbf{r}_{0k} + \sum_{m=1} \mathbf{x}_{k,m}.$$

Also, if $\mathbf{r}_0$ is the position of the centroid of the group,

$$n\mathbf{r}_0 = \sum_{k=1}^{n} \mathbf{r}_k = \sum_{k=1}^{n} \mathbf{r}_{0k}\,; \qquad \sum_{k=1} \sum_{m=1} \mathbf{x}_{k,m} = 0,$$

$$\sum_{k=1} r_k^2 = \sum_k \mathbf{r}_k \cdot \mathbf{r}_k = \sum_{k=1} r_{0k}^2 + 2\mathbf{r}_0 \sum_{k=1} \sum_{m=1} \mathbf{x}_{k,m} + \Big(\sum_{k=1} \sum_{m=1} \mathbf{x}_{k,m}\Big) \cdot \Big(\sum_{k=1} \sum_{m=1} \mathbf{x}_{k,m}\Big).$$

---

* Commonwealth Scientific and Industrial Research Organization, Melbourne.

The total increment in the squares of the distances r_k is, therefore, since the middle term on the right-hand side is zero in the mean,

$$\Delta r^2 = \sum_{k=1}^{n} (r_k^2 - r_{0k}^2) = \Big(\sum_{k=1} \sum_{m=1} \mathbf{x}_{k,m}\Big)\cdot\Big(\sum_{k=1} \sum_{m=1} \mathbf{x}_{k,m}\Big)$$
$$= \sum_{k=1} \Big\{ \sum_{m=1} x_{k,m}^2 + 2 \sum_{m=1} x_{k,m}(x_{k,(m+1)} \cos(\theta_1)_{k,m} + x_{k,(m+2)} \cos(\theta_2)_{k,m} + \ldots +)\Big\},$$

where $(\theta_j)_{k,m}$ is the angle between the mth free path and the $(m+j)$th free path of the kth particle.

Of the total number T of free paths $\mathbf{x}_{k,m}$ let the proportion of those traversed at speeds lying between c and $(c+\mathrm{d}c)$ be $f\mathrm{d}c$.

The contribution of such free paths to

$$\sum_{k=1} \sum_{m=1} x_{k,m}^2$$

is $T2l_0^2 f\mathrm{d}c$, where, as explained above,

$$l_0 = l_0(c) = \left(\frac{c}{\bar{g}}\right)\left(\frac{1}{N\pi\sigma^2}\right), \text{ and } \int_0^\infty f\mathrm{d}c = 1.$$

Their contribution to

$$2 \sum_{k=1} \sum_{m=1} x_{k,m}(x_{k,m+1} \cos(\theta_1)_{k,m} + x_{k,m+2} \cos(\theta_2)_{k,m} + \ldots)$$

is $(Tf\mathrm{d}c)2l_0S$; where S is the mean value of the sum in the bracket, namely,

$$\Big[\overline{\sum_{j=1} x_{k,m+j} \cos(\theta_j)_{k,m}}\Big]_c,$$

associated with those free paths x_m traversed at speed c. In general the free paths $x_{k,m+j}$ in S are not traversed at speed c.

Thus the contribution to Δr^2 by those free paths traversed at speed c is $\Delta r_0^2 = (Tf\mathrm{d}c)2l_0(l_0+S)$, and the average increment over a free path of that quantity is $2l_0(l_0+S)$. Since the average time spent over a free path is l_0/c, the mean rate of increase is $2c(l_0+S)$ from each particle moving at speed c. It follows that the rate of increase of the mean of the squares of the distances r_k taken over the distribution of velocities over the whole group of n particles is

$$\frac{\mathrm{d}}{\mathrm{d}t}\overline{r^2} = \overline{2c(l_0+S)} = 6D.$$

Thus

$$D = \tfrac{1}{3}\overline{(l_0+S)c} = \tfrac{1}{3}\overline{lc}, \qquad \ldots\ldots\ldots\ldots\ldots\ldots \quad (1)$$

where

$$l = l_0 + S\,; \quad l_0 = \left(\frac{c}{\bar{g}}\right)\left(\frac{1}{N\pi\sigma^2}\right); \quad \text{and } S = \Big[\overline{\sum_{j=1} x_{k,m+j} \cos(\theta_j)_{k,m}}\Big]_c \equiv S(c).$$

The evaluation of S is simplified in the case of diffusing electrons because, if the free path $x_{k,m}$ is traversed at speed c, the succeeding paths $x_{k,m+j}$ are also traversed at almost the same speed.

Thus $S = l_0(\overline{\cos\theta_1} + \overline{\cos\theta_2} + \ldots + \overline{\cos\theta_j} + \ldots)$, where $\overline{\cos\theta_j}$ is the mean value of the cosine of the angles θ_j between a free path traversed at speed c and its jth succession.

Consider $\overline{\cos\theta_2}$; if the angle between the second and third free paths is α, then $\theta_2 = (\theta_1 + \alpha)$, and $\cos\theta_2 = \cos\theta_1 \cos\alpha - \sin\theta_1 \sin\alpha$, and $\overline{\cos\theta_2} = (\overline{\cos\theta_1})(\overline{\cos\alpha}) = (\overline{\cos\theta_1})^2$, the term in the sines disappearing in the mean. Proceeding thus, it follows that $(\overline{\cos\theta_j}) = (\overline{\cos\theta_1})^j$.

Consequently, $S = l_0\,\overline{\cos\theta_1}/(1 - \overline{\cos\theta_1})$ and

$$D = \tfrac{1}{3}(\overline{lc}) \text{ with } l = l_0/(1 - \overline{\cos\theta_1}) \text{ and } l_0 = 1/N\pi\sigma^2. \qquad \ldots\ldots \ (2)$$

If the ions and electrons are scattered isotropically, then $\overline{\cos\theta_j} = 0$ for all values of j.

It may be remarked that S is also the mean value of the corresponding sum for the free paths preceding a free path $x_{k,m+j}$ traversed at speed c, since the reversed sequence is dynamically possible.

II. VELOCITY OF DRIFT IN A UNIFORM AND CONSTANT ELECTRIC FIELD

In the absence of an electric field the number of free paths in a large group of n_0 free paths all traversed at speed c, whose lengths lie between x and $x+\mathrm{d}x$, is (with $NA_0(c) = 1/l_0 = (N\pi\sigma^2)\bar{g}/c$)

$$\mathrm{d}n_1 = -n_0 N A_0(c) \exp\left(-NA_0(c)x\right)\mathrm{d}x = -NA_0(c) n_1 \mathrm{d}x,$$

where $n_1 = n_0 \exp(-NA_0 x)$.

When, however, an electric field $\mathbf{E}$ is present the velocity of the ions or electrons changes over the course of a free path and at a distance x along a free path the velocity has become $c + \Delta c(x)$ where $\Delta c(x)$ is proportional to E. In what follows it will be assumed that $\Delta c(x)/c \ll 1$ and terms dependent on E^2 are rejected.

Thus at the end of a free path of length x, the collisional cross section has become $A_0(c) + \{\mathrm{d}A_0(c)/\mathrm{d}c\}\Delta c(x)$. Consequently,

$$\frac{\mathrm{d}n_1}{\mathrm{d}x} = -\left[NA_0(c) + N\frac{\mathrm{d}A_0}{\mathrm{d}c}\Delta c(x)\right] n_1,$$

so that the number of free paths that exceed x in length is

$$n_1 = n_0 \exp\left[-NA_0 x - N\frac{\mathrm{d}A_0}{\mathrm{d}c}\int_0^x \Delta c(x)\mathrm{d}x\right],$$

and the number of free paths whose lengths lie between x and $x+\mathrm{d}x$ becomes

$$\mathrm{d}n_1 = n_0\left[NA_0 + N\frac{\mathrm{d}A_0}{\mathrm{d}c}\Delta c(x)\right]\left[\exp\left(-NA_0 x - N\frac{\mathrm{d}A_0}{\mathrm{d}c}\int_0^x \Delta c(x)\mathrm{d}x\right)\right]\mathrm{d}x.$$

Consequently,

$$\frac{\mathrm{d}n_1}{n_0} \doteqdot \left\{NA_0 + N\frac{N\mathrm{d}A_0}{\mathrm{d}c}\left(\Delta c(x) - NA_0\int_0^x \Delta c(x)\mathrm{d}x\right)\right\} \exp(-NA_0 x)\cdot\mathrm{d}x. \qquad \ldots\ldots\ldots\ldots \ (3)$$

In terms of the mean free path $l_0=1/NA_0$ equation (**3**) becomes

$$\frac{\mathrm{d}n_1}{n_0}=\exp\left(-\frac{x}{l_0}\right)\left\{\frac{1}{l_0}+\frac{1}{l_0^2}\cdot\frac{\mathrm{d}l_0}{\mathrm{d}c}\left(\frac{1}{l_0}\int_0^x \Delta c(x)\mathrm{d}x-\Delta c(x)\right)\right\}\mathrm{d}x. \quad \ldots\ldots\ldots \quad (\mathbf{4})$$

Consider a group of n ions or electrons moving in a steady state of motion and let the number whose speeds lie between c and $c+\mathrm{d}c$ be $\mathrm{d}n_c=nf(c)\mathrm{d}c$. In the course of each free path the ion or electron is displaced by the field **E** by a small amount in the direction of **E** so that the centroid of the group drifts with a velocity **W**.

In travelling at speed c at an angle θ to **E** along a free path of length x, an ion is deflected a distance $\frac{1}{2}(Ee/m)(x/c)^2 \sin\theta$ at right angles to the direction θ and is on this account advanced a distance $\frac{1}{2}(Ee/m)(x\sin\theta/c)^2$ in the direction of the force **E**e.

In addition it travels the distance $x\cos\theta$ as in free flight without **E**. The increment in speed due to **E** is $\Delta c(x)=(Ee/m)(x/c)\cos\theta$ in the direction θ, the proportion of those free paths that begin in direction θ and are terminated between x and $x+\mathrm{d}x$ is obtained by substituting this value of $\Delta c(x)$ in equation (**4**).

The mean displacement along a single free path of an ion of the group $\mathrm{d}n_c$ taken over all directions θ and free paths x is, therefore,

$$\frac{1}{2}\int_0^\pi\int_0^\infty\left\{\frac{Ee}{2m}\left(\frac{x}{c}\right)^2\sin^2\theta+x\cos\theta\right\}\left\{\frac{1}{l_0}+\frac{1}{l_0^2}\frac{\mathrm{d}l_0}{\mathrm{d}c}\left(\frac{x}{2l_0}-1\right)x\cos\theta\cdot\frac{Ee}{mc}\right\}$$
$$\times\exp\left(-\frac{x}{l_0}\right)\sin\theta\mathrm{d}\theta\mathrm{d}x$$
$$=\frac{2}{3}\frac{Ee}{m}\left(\frac{l_0}{c}\right)^2+\frac{1}{3}\frac{Ee}{m}\frac{l_0}{c}\frac{\mathrm{d}l_0}{\mathrm{d}c}=\frac{1}{3}\frac{Ee}{m}\frac{l_0}{c}\frac{1}{c^2}\frac{\mathrm{d}}{\mathrm{d}c}(l_0c^2). \quad \ldots\ldots\ldots\ldots\ldots\ldots \quad (\mathbf{5})$$

The average time taken to traverse a single free path at speed c is l_0/c, consequently the mean speed of drift of the centroid of the $\mathrm{d}n_c$ electrons of the group n is

$$W_c=\frac{1}{3}\frac{Ee}{m}\frac{1}{c^2}\frac{\mathrm{d}}{\mathrm{d}c}(l_0c^2).$$

It remains to consider the contribution to W_c of the equivalent mean extension of the free paths x that arises when the scattering of ions or electrons in encounters with molecules is not isotropic so that $\overline{\cos\theta_1}$ is not zero. This extension was defined in Section I and was denoted by $S=S(c)$.

In effect, the displacement in the direction of **E** of an ion traversing a free path x between encounters at an angle θ with **E** is increased from $x\cos\theta$ to $(x+S)\cos\theta$, but this quantity vanishes in the mean taken over all directions θ. Nevertheless, the extension S is responsible for an addition to the mean displacement as given in expression (**5**). The field **E** produces a change in direction of the velocity **c** at the end of a free path x, of an amount $\Delta\theta=(Ee/m)(x/c^2)\sin\theta$ and an increase in the speed by an amount $\Delta c(x)=(Ee/m)(x/c)\cos\theta$. Thus S is increased to $S+(\mathrm{d}S/\mathrm{d}c)\Delta c(x)$, and through the operation of the field **E** along x the ion or electron receives an additional displacement $\{S+(\mathrm{d}S/\mathrm{d}c)\Delta c(x)\}\Delta\theta\cdot\sin\theta$

in the direction of $\mathbf{E}$. The mean value of this displacement for all free paths of length x and direction θ is

$$\tfrac{1}{2}\int_0^\pi \int_0^\infty \left\{S\,\frac{Ee}{m}\,\frac{x}{c^2}\sin^2\theta+\frac{\mathrm{d}S}{\mathrm{d}c}\,\frac{Ee}{m}\,\frac{x}{c}\cos\theta\,\sin\theta\right\}\frac{1}{l_0}\exp\left(-\frac{x}{l_0}\right)\sin\theta\mathrm{d}\theta\mathrm{d}x$$

$$=\tfrac{1}{3}\frac{Ee}{m}\,\frac{l_0}{c}\left(\frac{2S}{c}+\frac{\mathrm{d}S}{\mathrm{d}c}\right)=\tfrac{1}{3}\frac{Ee}{m}\,\frac{l_0}{c}\,\frac{1}{c^2}\,\frac{\mathrm{d}}{\mathrm{d}c}(Sc^2). \qquad \dots\dots\dots\dots\dots\dots\dots (6)$$

The total mean displacement of an electron or ion traversing a free path at speed c is the sum of the final terms in expressions (**5**) and (**6**), namely,

$$\tfrac{1}{3}\frac{l_0}{c}\,\frac{Ee}{m}\,\frac{1}{c^2}\,\frac{\mathrm{d}}{\mathrm{d}c}\{(l_0+S)c^2\}=\tfrac{1}{3}\frac{l_0}{m}\,\frac{Ee}{m}\,\frac{1}{c^2}\,\frac{\mathrm{d}}{\mathrm{d}c}(lc^2),$$

where $l=l_0+S$ as defined in equation (**1**). The mean time to traverse a free path is (l_0/c), consequently the speed of drift of the centroid of those ions or electrons moving at speeds c is

$$W_c=\tfrac{1}{3}\frac{Ee}{m}\,\frac{1}{c^2}\,\frac{\mathrm{d}}{\mathrm{d}c}(lc^2).$$

Consequently, the velocity of the centroid of the group as a whole is,

$$\mathbf{W}=\tfrac{1}{3}\frac{\mathbf{E}e}{m}\,\overline{\frac{1}{c^2}\,\frac{\mathrm{d}}{\mathrm{d}c}(lc^2)}=\tfrac{1}{3}\frac{\mathbf{E}e}{Nm}\,\overline{\frac{1}{c^2}\,\frac{\mathrm{d}}{\mathrm{d}c}\left(\frac{c^2}{A}\right)}, \qquad \dots\dots\dots (7)$$

where the equivalent collisional cross section is $A=1/Nl$ and the average is taken with respect to the distribution of speeds c (Huxley 1957*a*, where the derivation of the formula is restricted to the motions of electrons).

From the expressions for the coefficient of diffusion D and velocity of drift $\mathbf{W}$ (equations (**1**) and (**7**)) it can be seen that the ratio W/D is given by

$$\left.\begin{aligned}\frac{W}{D}&=\frac{Ee}{m}\left(\overline{c^{-2}\frac{\mathrm{d}}{\mathrm{d}c}(lc^2)}\right)/(\overline{lc})\\&=\frac{Ee}{\frac{1}{2}m\overline{c^2}}\left\{\frac{\overline{c^2}}{2}\cdot\overline{c^{-2}\frac{\mathrm{d}}{\mathrm{d}c}(lc^2)}/(\overline{lc})\right\}\\&=\frac{Ee}{\frac{1}{2}m\overline{c^2}}F.\end{aligned}\right\} \qquad \dots\dots\dots\dots (8)$$

Consider the expression $\overline{c^{-2}\mathrm{d}(lc^2)/\mathrm{d}c}$ in the special case in which the speeds of agitation of the ions or electrons are distributed according to the law of Maxwell, that is to say, $\mathrm{d}n_0/n=(4/\alpha^3\sqrt{\pi})\exp(-c^2/\alpha^2)c^2\mathrm{d}c$.

The mean value required is, therefore,

$$\frac{4}{\alpha^3\sqrt{\pi}}\int_0^\infty \exp\left(-\frac{c^2}{\alpha^2}\right)\frac{\mathrm{d}}{\mathrm{d}c}(lc^2)\mathrm{d}c=\frac{4}{\alpha^3\sqrt{\pi}}\,\frac{2}{\alpha^2}\int_0^\infty \exp\left(-\frac{c^2}{\alpha^2}\right)lc^3\mathrm{d}c$$

$$=(2/\alpha^2)(\overline{lc})$$

$$=3(\overline{lc})/\overline{c^2}.$$

The formula for W/D in this case reduces to

$$\frac{W}{D}=\frac{3}{2}\left(\frac{Ee}{\frac{1}{2}m\overline{c^2}}\right). \qquad \text{(9)}$$

Suppose instead, that the dependence $l(c)$ of l upon c is of the form $l\propto c$ (inverse fifth power interaction), then the factor F also reduces to 3/2 and equation (**9**) is again valid. In general, however, equation (**9**) is not exact since F assumes values other than 3/2 when the law of distribution is not that of Maxwell or $l(c)$ is not proportional to c. In general, for electronic motion, $F\neq 3/2$.

III. REFERENCES

HUXLEY, L. G. H. (1957*a*).—*Aust. J. Phys.* **10**: 118.
HUXLEY, L. G. H. (1957*b*).—*Aust. J. Phys.* **10**: 240.

HETEROGENEOUS NUCLEATION BY AGGREGATES OF PARTICLES

By R. B. HEAD* and K. L. SUTHERLAND*†

[*Manuscript received May* 17, 1960]

Summary

The induction of a new phase by fine particles of a nucleating substance is complicated not only by variation in sizes but also by aggregation. The general effect of aggregation is to decrease the total number of particles but to reduce the supercooling (or supersaturation) necessary for growth of a new phase. Point contacts appear to be more fruitful than do line contacts, although both may be able to cause a substance to be more active than a large flat surface of the substrate. If the contact between particles is not a specially favoured position for nucleation, the aerosol as a whole appears to contain a higher proportion of active particles because of the persistence of initially active particles and the loss of less active ones.

I. INTRODUCTION

The nucleation of supersaturated solutions and vapours and of supercooled liquids by foreign particles depends upon the size and composition of the particles. Fletcher (1958) has related the extent of supersaturation or supercooling to the radii of spherical nuclei and the contact angle between the phases formed on their surfaces. In any practical work involving aerosols, particularly in the laboratory, it is necessary to use such concentrations that particles coagulate. Thus typical aerosols of silver iodide used in other studies in this laboratory contained 10^5 particles cm^{-3} (approximate mean radius 10^{-6} cm), the concentration of which would fall by coagulation and by diffusive loss to the walls of the containing vessel to about one-third in an hour. Frequently it was necessary to study aerosols over periods longer than this when the effectiveness of the nuclei are being altered by the action of chemicals or of light. This paper examines theoretically the effect of coagulation.

II. FORM OF AGGREGATES

If the particles are spherical and of equal size, the aggregates form simple chains or structures with point contacts (Fig. 1 (*a*)). We shall confine this portion of our discussion to dimers. If the particles are crystals then the form of the aggregates is more complex. Only one situation will be examined: that of two crystals forming a step (Fig. 1 (*b*)).

At edges or points of contact between surfaces the growth of a new phase will usually be enhanced by capillary condensation because of the favourable curvature of the surface of the phase being formed. If, however, the growing phase is crystalline then its fit on both of the surfaces forming the aggregate may become dominant. Thus in Figure 1 (*b*) it may be imagined that the substrate

---

* Division of Physical Chemistry, Chemical Research Laboratories, C.S.I.R.O., Melbourne.

† Present address: Colonial Sugar Refining Co., Sydney.

for crystal nucleation may be suitable on the horizontal surface but unsuitable on the vertical surface. Under these conditions the aggregate may exhibit the characteristics only of the more active member of the pair. Such an aggregate shall be defined as " not in registry ". For the formation of a liquid phase the surfaces are always in registry.

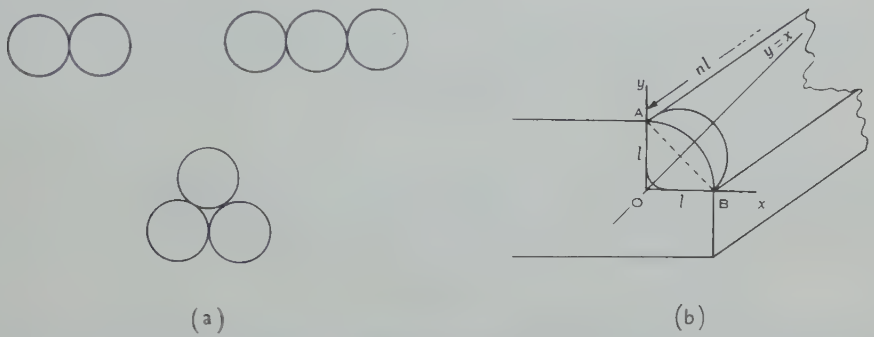

Fig. 1.—Forms of aggregates. (*a*) Aggregates from spheres, (*b*) stepped aggregates from plates.

III. Properties of Aggregates not in Registry

Consider an aerosol containing p single particles in each of n classes. These classes may be determined experimentally by lowering the temperature or increasing the supersaturation by measured amounts, the less active particles acting only under the greater driving force. At a given time we shall want to know how many monomers, dimers, trimers, etc. are present and to classify these aggregates on their probable composition. If a polymer contains at least one particle from class 1 (the most active), then it shall continue to belong to class 1. If, however, the most active particle in the polymer belongs to class r then the aggregate belongs to class r. Aggregation therefore decreases the total number of particles and eliminates the least active classes.

The kinetics of coagulation under Brownian movement was formulated by Smoluchowski (1916, 1917) on the basis that all particles are the same size and that all aggregates are regarded as having the same size and diffusion constant as the single particles.

The rate of removal of particles is given by

$$-\mathrm{d}\nu/\mathrm{d}t=k\nu^2, \quad \ldots\ldots\ldots\ldots\ldots\ldots\ldots \quad (1)$$

where k, the velocity constant, is defined in terms of the viscosity of the gas, the radius of particle, its sphere of influence, and the temperature (see Green and Lane 1957).

The total number of aggregates and single particles after a time t is

$$\Sigma\nu=np\{1/(1+T)\}, \quad \ldots\ldots\ldots\ldots\ldots\ldots \quad (2)$$

where T is $knpt$ and $\Sigma\nu$ is the sum of single particles (ν_1), dimers (ν_2), trimers (ν_3), m-mers (ν_m). The number of m-mers is

$$\nu_m=npT^{m-1}/(1+T)^{m+1}. \quad \ldots\ldots\ldots\ldots\ldots \quad (3)$$

We now require the composition of each aggregate in terms of the probable most active monomer in it. Suppose we select m particles at random to form an m-mer. Since there are np particles, the number of different choices is

$$\binom{np}{m}.$$

The number of choices containing only particles from classes $r+1, r+2, \ldots, n$ is

$$\binom{np-rp}{m}$$

and the number containing only particles from classes $r, r+1, \ldots, n$, is

$$\binom{np-rp+p}{m}.$$

Thus the number containing only particles from groups $r, r+1, \ldots, n$, *and at least one particle from group* r is the difference of these numbers, is

$$\binom{np-rp+p}{m}-\binom{np-rp}{m}.$$

Since these and only these choices form m-mers which belong to class r, the fraction of the m-mers which belongs to class r is

$$F_{mr}=\left\{\binom{np-rp+p}{m}-\binom{np-rp}{m}\right\}\Big/\binom{np}{m}. \quad \ldots\ldots\ldots\ldots \quad (4)$$

In any experiment the total number of particles within any one class is large and the number of particles within an aggregate small. Under these conditions

$$\binom{q}{m}\simeq\frac{q^m}{m!}$$

so that (4) becomes

$$F_{nr}=\frac{(np-rp+p)^m/m!-(np-rp)^m/m!}{(np)^m/m!}$$
$$=\frac{(n-r+1)^m-(n-r)^m}{n^m}. \quad \ldots\ldots\ldots\ldots\ldots\ldots \quad (5)$$

Equation (3) gives the number of each polymer at a given time and the total number of particles active in a given temperature class r is then

$$A_r=\nu_1F_{1r}+\nu_2F_{2r}+\nu_3F_{3r}+\ldots+\nu_mF_{mr}. \quad \ldots\ldots\ldots \quad (6)$$

A sample is considered containing five classes and their distribution between classes 1 to 5 (expressed as a percentage of the current number of particles) is shown in Figure 2. The percentage active at any temperature step for aggregates up to 16 particles is shown in Figure 3, which illustrates the steady march of the sample into the most active class. When the total concentration of the sample has decreased to 20 per cent. of its original value ($T=4$, Fig. 2) the first temperature class has increased from 20 to 55 per cent.

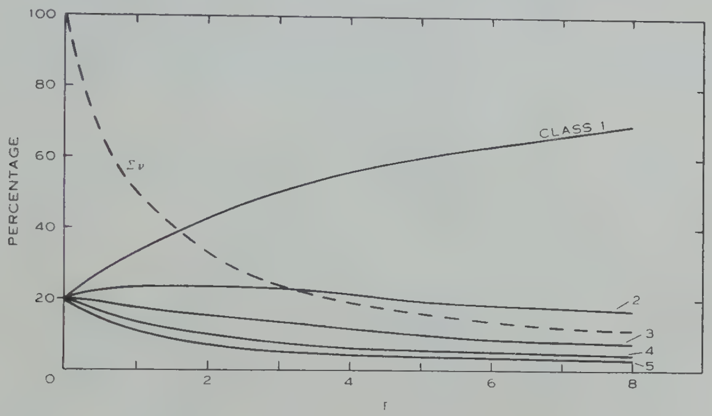

Fig. 2.—The variation with time ($T=knpt$) of the total number of particles and of their distribution between classes 1–5 (expressed as a percentage of the current number of particles).

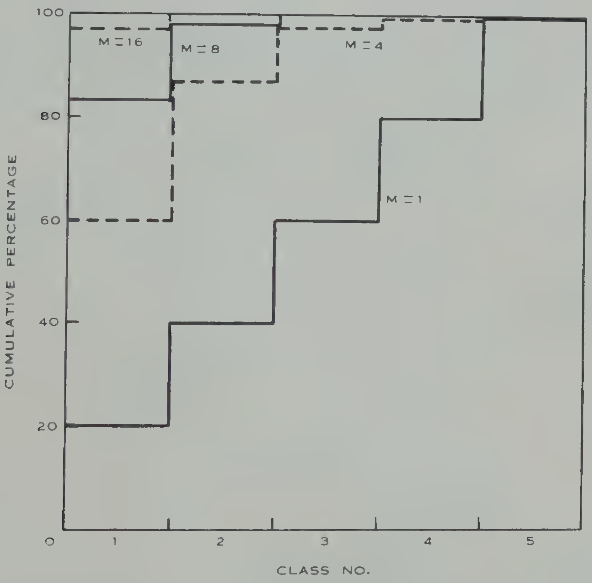

Fig. 3.—The percentage active at given temperature ranges for aggregates containing m particles. Any particle active at the higher temperature (e.g. class 1) will also be active at a lower temperature (e.g. class 5).

IV. PROPERTIES OF SPHERICAL DIMERS IN REGISTRY

Let the aerosol consist of particles each of two spheres of radius R (Fig. 4). Let the surface of the condensed phase lying between the spheres be generated by a function $y=f(x)$. We require that the surface free energy be a minimum for a given volume V of condensed phase. Let the angle of contact, measured through the condensed phase, be θ. Then the difference in free energy between the system with and without a volume V of condensed phase is

$$\Delta G = V\Delta G_V + S_{12}\gamma_{12} - S_{23}\gamma_{13} + S_{23}\gamma_{23}, \quad \dots\dots\dots\dots \quad (7)$$

where the S and γ are the surface areas and surface energies between the phases 1, 2, 3 as indicated. ΔG_V is the free energy of transformation from one phase to another. The relation between contact angle and interfacial energies is assumed to be

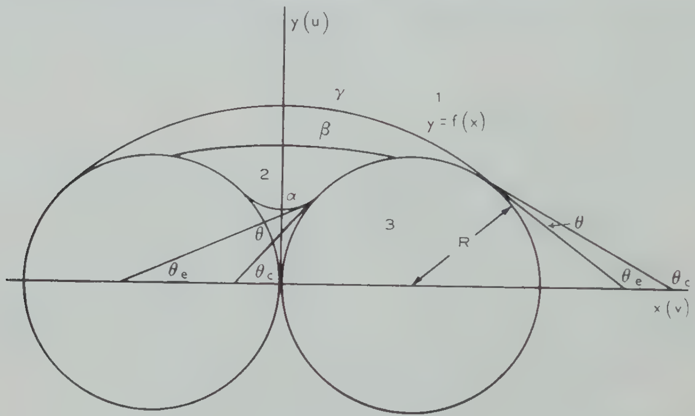

Fig. 4.—Formation of a new phase (2) from the initial (1) on a nucleus (3) formed from two particles each of radius R. θ=contact angle; $\tan\theta_c$=tangent to the generating circle; $\tan\theta_e$=tangent to the generating curve $y=f(x)$.

α: a minimum at $x=0$, $\tan\theta_c>0$, $\tan\theta_e>0$;
β: a maximum at $x=0$, $\tan\theta_c>0$, $\tan\theta_e<0$;
γ: a maximum at $x=0$, $\tan\theta_c<0$, $\tan\theta_e<0$.

$$\gamma_{12}\cos\theta = \gamma_{13} - \gamma_{23}. \quad \dots\dots\dots\dots\dots\dots \quad (8)$$

The volume and surface areas are

$$\left.\begin{aligned} V &= 2\pi\int_0^{x_0} y^2\mathrm{d}x - \tfrac{2}{3}\pi x_0^2(3R - x_0), \\ S_{12} &= 4\pi\int_0^{x_0} y(1+y_x^2)^{\frac{1}{2}}\mathrm{d}x, \\ S_{23} &= 4\pi R x_0, \end{aligned}\right\} \quad \dots\dots\dots\dots \quad (9)$$

where y_x is $\mathrm{d}y/\mathrm{d}x$.

Hence we require that ΔG, given by

$$\Delta G = 2\pi\int_0^x [\Delta G_V(y^2 - 2xR + x^2) + 2\gamma_{12}\{y(1+y_x^2)^{\frac{1}{2}} - R\cos\theta\}]\mathrm{d}x \quad \dots\dots\dots\dots \quad (10)$$

shall be a minimum. This condition is obtained from

$$\frac{\partial K}{\partial y} - \frac{\mathrm{d}}{\mathrm{d}x}\frac{\partial K}{\partial y_x} = 0, \quad \dots\dots\dots\dots\dots\dots \quad (11)$$

where K is the integrand of equation (**10**).

This leads to

$$y_{xx}(1+y_x^2)^{-3/2}-y^{-1}(1+y_x^2)^{-\frac{1}{2}}=\Delta G_V/\gamma_{12}=\zeta, \qquad \ldots\ldots \quad (12)$$

which is equivalent to

$$-\frac{\mathrm{d}}{\mathrm{d}y}\{y(1+y_x^2)^{-\frac{1}{2}}\}=\zeta y,$$

that is,

$$(1+y_x^2)^{-\frac{1}{2}}=1/\xi y-\tfrac{1}{2}\zeta y, \qquad \ldots\ldots\ldots\ldots \quad (13)$$

where ξ, the integration constant, is determined from the condition that

$$\left.\begin{array}{l} y_x=0 \text{ at } x=0 \quad (y=y_0), \\ \xi=1/y_0(1+\zeta y_0). \end{array}\right\} \qquad \ldots\ldots\ldots\ldots\ldots \quad (14)$$

The solution of (**13**) must be written in several forms depending upon the value of ζ.

Case (i) $\zeta>0$ (*subsaturation*)

The gradient of the generating curve is everywhere positive and the curve has a minimum at $x=0$. Equation (**14**) requires $\xi>0$ since ζ, $y_0>0$. Integration of equation (**13**) gives

$$\int_{y_0}^{y}\frac{\mathrm{d}y}{\{\xi^2y^2/(1-\xi\zeta y^2)^2-1\}^{\frac{1}{2}}}=\int_0^{x_0}\mathrm{d}x, \qquad \ldots\ldots\ldots\ldots \quad (15)$$

where y_0, the value of y for $x=0$, is found by solving equation (**13**) with y_x equal to zero, that is,

$$y_0=\{-\xi+(\xi^2+4\xi\zeta)^{\frac{1}{2}}\}/2\zeta\xi. \qquad \ldots\ldots\ldots\ldots \quad (16)$$

This equation transforms to

$$(ab)^{\frac{1}{2}}\cdot v=\int_f^{Rz/(ab)^{\frac{1}{2}}}\frac{(1-z^2)\mathrm{d}z}{\sqrt{\{(e^2-z^2)(z^2-f^2)\}}}, \qquad \ldots\ldots\ldots\ldots \quad (17)$$

where

$$\left.\begin{array}{l} v=x/R,\ z=(ab)^{\frac{1}{2}}y, \\ e^2=(b/2a+1)+(b^2/4a^2+b/a)^{\frac{1}{2}}, \\ f^2=(b/2a+1)-(b^2/4a^2+b/a)^{\frac{1}{2}}, \\ a=\zeta R,\ b=\xi R. \end{array}\right\} \qquad \ldots\ldots\ldots\ldots \quad (18)$$

This may be evaluated in terms of elliptic integrals

$$\left(\frac{ab}{e^2}\right)^{\frac{1}{2}}v=\frac{1}{e^2}\{F(k,\tfrac{1}{2}\pi)-F(k,\varphi)\}-\{E(k,\tfrac{1}{2}\pi)-E(k,\varphi)\}, \qquad \ldots\ldots \quad (19)$$

where $F(k,\frac{1}{2}\pi)$, $E(k,\frac{1}{2}\pi)$ are the complete elliptic integrals of the first and second kinds, $F(k,\varphi)$, $E(k,\varphi)$ are incomplete elliptic integrals, and

$$\left.\begin{array}{c} \sin\varphi=(1/k)(1-abu^2/e^2), \\ k^2=(e^2-f^2)/e^2, \\ u=y/R. \end{array}\right\} \qquad \ldots\ldots\ldots\ldots \quad (20)$$

The parameter b is determined from the condition that the curve shall intersect the circles (see Fig. 4, curve α) at an angle θ (the contact angle). If $\tan\theta_e$ is the gradient to the elliptic curve and $\tan\theta_c$ that to the circle, then $\theta_e=\theta_c-\theta$, and

$$\tan\theta_e=y_x=\{b^2u_i^2/(1-abu_i^2)^2-1\}^{\frac{1}{2}}=\tan\overline{\theta_c-\theta}$$
$$=\frac{(1-v_i)/u_i-\tan\theta}{1+(1-v_i)\tan\theta/u_i}=\varepsilon, \quad \ldots\ldots\ldots\ldots\ldots\ldots \quad (\mathbf{21})$$

where (u_i, v_i) is the point of intersection of the generating curve. Therefore

$$b=(\varepsilon^2+1)^{\frac{1}{2}}/\{u_i+au_i^2(\varepsilon^2+1)^{\frac{1}{2}}\}. \quad \ldots\ldots\ldots\ldots \quad (\mathbf{22})$$

Case (ii) $\zeta=0$ (*saturation*)

Reverting to equation (**12**) then

$$y_{xx}(1+y_x^2)^{-1}-y^{-1}=0, \quad \ldots\ldots\ldots\ldots\ldots\ldots \quad (\mathbf{23})$$

the solution to which is

$$u=(1/b)\cosh b\iota, \quad \ldots\ldots\ldots\ldots\ldots\ldots\ldots\ldots \quad (\mathbf{24})$$

where

$$b=(1/v_i)\operatorname{arsinh}(1/\varepsilon), \quad \ldots\ldots\ldots\ldots\ldots \quad (\mathbf{25})$$

and ε is defined in equation (**21**).

Case (iii) $\zeta<0$ (*supersaturation*)

Put $a=-c$ where $c>0$. It may be shown that b must be greater than 0. Three cases arise, shown in Figure 4, and equation (**17**) becomes

$$(ac)^{\frac{1}{2}}v=\int\frac{(1+z^2)dz}{\sqrt{\{(e^2-z^2)(z^2-f^2)\}}}. \quad \ldots\ldots\ldots\ldots \quad (\mathbf{26})$$

(α) A minimum at $x=0$, $\tan\theta_c>0$ (Fig. 4, curve α).

The solution is

$$\left(\frac{bc}{e^2}\right)^{\frac{1}{2}}v=\left(\frac{1}{e^2}\right)\{F(k,\tfrac{1}{2}\pi)-F(k,\varphi)\}+\{E(k,\tfrac{1}{2}\pi)-E(k,\varphi)\}, \quad \ldots \quad (\mathbf{27})$$

where

$$\left.\begin{aligned}
e^2&=(b/2c-1)+(b^2/4c^2-b/c)^{\frac{1}{2}},\\
f^2&=(b/2c-1)-(b^2/4c^2-b/c)^{\frac{1}{2}},\\
k^2&=(e^2-f^2)/e^2,\\
\sin\varphi&=\frac{1}{k}\left(1-\frac{bc}{e^2}u^2\right)^{\frac{1}{2}}\\
&=\left\{\frac{b^2u_i^2}{(1+bcu_i^2)^2}-1\right\}^{\frac{1}{2}}=\frac{(1-v_i)/u_i-\tan\theta}{1+(1-v_i)\tan\theta/u_i},\\
b&=\frac{(\varepsilon^2+1)^{\frac{1}{2}}}{bcu_i^2(\varepsilon^2+1)^{\frac{1}{2}}-u}.
\end{aligned}\right\} \quad \ldots\ldots \quad (\mathbf{28})$$

When φ is close to $\frac{1}{2}\pi$ the differences of the tabulated functions cease to be accurate. The differences are then expanded by Taylor's theorem about $\frac{1}{2}\pi$

(β) A maximum at $x=0$ and $\tan\theta_c>0$ (Fig. 4, curve β).

The equation to be solved is

$$(bc)^{\frac{1}{2}}v=-\int\frac{(1+z^2)\mathrm{d}z}{\sqrt{\{(e^2-z^2)(z^2-f^2)\}}}, \qquad \ldots\ldots\ldots\ldots \quad (29)$$

and the solution is

$$\left(\frac{bc}{e^2}\right)^{\frac{1}{2}}v=\frac{1}{e^2}F(k,\varphi)+E(k,\varphi), \qquad \ldots\ldots\ldots\ldots \quad (30)$$

where the various symbols are given by equation (**28**).

(γ) A maximum at $x=0$ and $\tan\theta_c<0$ (Fig. 4, curve γ).

The solution is given by equations (**30**) and (**28**).

Case (iv)

A special case arises when $\theta_e=0$. The curve becomes a straight line given by

$$u=(bc)^{-\frac{1}{2}}. \qquad \ldots\ldots\ldots\ldots \quad (31)$$

Case (v)

A special case arises when b becomes infinite, i.e. if the intersection of curve and circle is given by $1-cu(\varepsilon^2+1)^{\frac{1}{2}}=0$. The curve becomes a circle given by

$$u^2+v^2=1/c^2. \qquad \ldots\ldots\ldots\ldots \quad (32)$$

(*a*) *Calculation of the Form of the Liquid Surface*

The calculations are confined to the substances silver iodide and water. The contact angle for AgI/Liquid H_2O/H_2O (vap.) is 10°. It is assumed, following Fletcher, that this angle applies whether the phases are ice/vapour or ice/water, although this is very doubtful. It does, however, enable a comparison to be made with the curve for spherical particles obtained by Fletcher's method (1958).

We are interested in supersaturated conditions so that no calculations were made in the under-saturation region. The procedure in calculation was to take a point (u_i, v_i) on the generating circle representing the particle and then to determine c by successive approximations from either of equations (**27**) or (**30**). Equations (**24**), (**31**), and (**32**) enable three curves to be calculated explicitly and give a guide to choice of c values for the approximative methods. The results of calculation are shown in Figure 5. It will be noticed that the c values rise to a maximum and then fall: there are two surfaces for each c value $(-\Delta G_V/\gamma_{12})$.

(*b*) *The Free Energy of Embryos*

The theory of nucleation of a new phase on a substrate requires that transient groups of molecules (embryos) form on the surface. The relatively large free surface energies of the smaller embryos cause these to be unstable: the number present of each size at a given temperature and supersaturation may then be determined from Boltzmann's law. With increasing size the free energy barrier rises to a maximum and once an embryo exceeds a critical size, it grows without

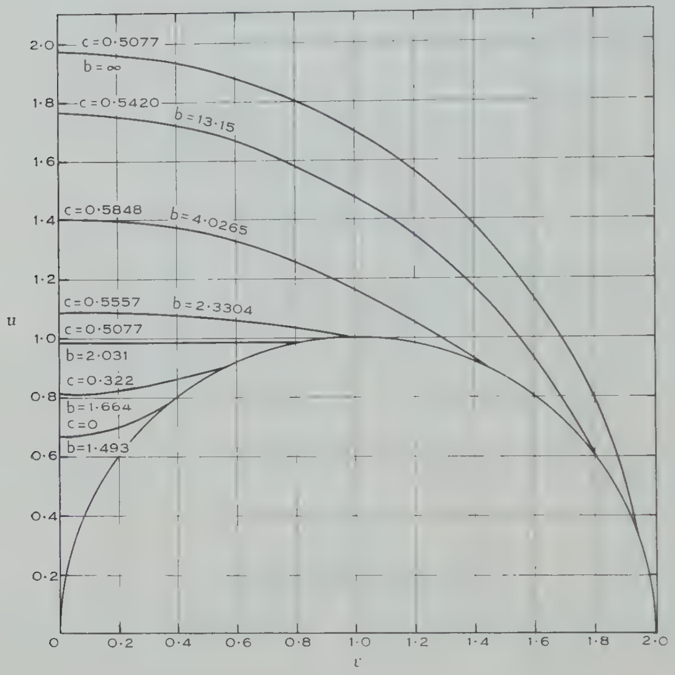

Fig. 5.—Shapes of the menisci from saturation ($c=0$) through increasing supersaturation (c increasing): $\theta=10°$, generating circle of unit radius.

limit. Equation (**10**) expresses the contributions of the free energy changes due to surface and to phase transformation and may be rewritten as

$$\begin{aligned}\Delta G=&2\pi\Delta G_V R^3\int_0^{v_i} u^2\mathrm{d}v-\tfrac{2}{3}\pi\Delta G_V R^3 v_i^2(3-v_i)\\&+4\pi\gamma_{12}R^2\int_0^{v_i} u(1+u_v^2)^{\frac{1}{2}}\mathrm{d}v-4\pi\gamma_{12}R^2 v_i\cos\theta\\=&-\tfrac{2}{3}\pi\Delta G_V R^3 v_i^2(3-v_i)-4\pi\gamma_{12}R^2 v_i\cos\theta\\&+2\pi\Delta G_V R^3\int_{u_0}^{u}\frac{u^2}{u_v}\mathrm{d}u\\&+4\pi\gamma_{12}R^2\int_{u_0}^{u}\frac{u(1+u_v^2)^{\frac{1}{2}}}{u_v}\mathrm{d}u. \qquad \ldots\ldots\ldots\ldots\ldots\ (\mathbf{33})\end{aligned}$$

Since u_v is known as a function of u only (equation (**13**)), the solution may be obtained.

The integrals may be written into a combination of the forms

$$\int\frac{\mathrm{d}z}{\sqrt{\{(e^2-z^2)(z^2-f^2)\}}}\quad\int\frac{z^2\mathrm{d}z}{\sqrt{\{(e^2-z^2)(z^2-f^2)\}}}\quad\int\frac{z^4\mathrm{d}z}{\sqrt{\{(e^2-z^2)(z^2-f^2)\}}}.$$

The first of these integrals gives an elliptic integral of the first kind; the second integral gives an elliptic integral of the second kind. The third integral is reduced by using the relation

$$z\sqrt{Z}=\int\frac{\mathrm{d}z}{\sqrt{Z}}-2(1+k^2)\int\frac{z^2}{\sqrt{Z}}\mathrm{d}z+3k^2\int\frac{z^4}{\sqrt{Z}}\mathrm{d}z, \quad \ldots\ldots \quad (34)$$

where Z is the denominator in the integrals above and k is the modulus of the elliptic integral (defined in equations (**20**) and (**28**)).

The final expressions for the free energies are:*

Case (ii): $a=0$

$$\Delta G=-\tfrac{2}{3}\pi\Delta G_V R^3v^2(3-v)-4\pi\gamma_{12}R^2v\cos\theta$$
$$+\{\pi\gamma_{12}R^2/b^2-\pi\Delta G_V R^2/2b^3\}(2vb+\sinh 2vb). \quad \ldots \quad (35)$$

Case (iiiα): $a=-c$, minimum at $x(v)=0$

$$\Delta G=-\tfrac{2}{3}\pi\Delta G_V R^3v^2(3-v)-4\pi\gamma_{12}R^2v\cos\theta$$
$$+2\pi\Delta G_V R^3\frac{e}{(bc)^{3/2}}\Bigg[-\frac{e^2k^2}{3}\sin\varphi\cos\varphi\,(1-k^2\sin^2\varphi)^{\frac{1}{2}}$$
$$-\frac{f^2}{3}\{F(k,\tfrac{1}{2}\pi)-F(k,\varphi)\}+\left\{1+\frac{2(e^2+f^2)}{3}\right\}\{E(k,\tfrac{1}{2}\pi)-E(k,\varphi)\}\Bigg]$$
$$+4\pi\gamma_{12}R^2\frac{eb}{(cb)^{3/2}}\{E(k,\tfrac{1}{2}\pi)-E(k,\varphi)\}. \quad \ldots\ldots\ldots\ldots\ldots\ldots \quad (36)$$

Case (iiiβ): $a=-c$, maximum at $x(v)=0$

$$\Delta G=-\tfrac{2}{3}\pi\Delta G_V R^3v^2(3-v)-4\pi\gamma_{12}R^2v\cos\theta$$
$$+2\pi\Delta G_V R^3\frac{e}{(bc)^{3/2}}\Bigg[\frac{e^2k^2}{3}\sin\varphi\cos\varphi(1-k^2\sin^2\varphi)^{\frac{1}{2}}$$
$$-\frac{f^2}{3}F(k,\varphi)+\left\{1+\frac{2(e^2+f^2)}{3}\right\}E(k,\varphi)\Bigg]$$
$$+4\pi\gamma_{12}R^2\frac{eb}{(cb)^{3/2}}E(k,\varphi). \quad \ldots\ldots\ldots\ldots\ldots\ldots\ldots\ldots \quad (37)$$

Case (iv): $\theta_c=0$

$$\Delta G=2\pi\Delta G_V R^3v\{u^2-\tfrac{1}{3}v(3-v)\}+4\pi\gamma_{12}R^2v\{u-\cos\theta\}. \quad \ldots\ldots \quad (38)$$

Case (v): $b\doteq\infty$

$$\Delta G=\tfrac{2}{3}\pi\Delta G_V R^3\left\{\frac{2}{c^3}-\left(2-\frac{1}{c}\right)^2\left(\frac{3}{c}-2+v\right)-v^2(3-v)\right\}$$
$$+4\pi\gamma_{12}R^2\left\{\frac{1}{c^2}-\frac{1}{c}(2-v)-v\cos\theta\right\}. \quad \ldots\ldots\ldots\ldots \quad (39)$$

These equations may all be written in the form

$$\Delta G=\Delta G_V R^3E+R^2F. \quad \ldots\ldots\ldots\ldots\ldots\ldots \quad (40)$$

The values of E and F were tabulated for the values of a and c shown in Figure 5.

---

* The subscript i in v_i is dropped beyond this point.

(c) *Calculation of Relation between* R *and Supersaturation*

It is usual to calculate the supersaturation at which the rate of nucleation becomes appreciable. For a spherical particle the rate, per particle, is

$$J = 4\pi 10^{25} R^2 \exp\left(-\Delta G^*/kT\right), \qquad \ldots\ldots\ldots\ldots \quad \textbf{(41)}$$

where ΔG^* is the free energy of the critical embryo. The pre-exponential term is only known to within a factor of 100, but this is relatively unimportant as the rate increases very rapidly when the free energy of the embryo is in the neighbourhood of ΔG^*. It will be clear from the curves which follow that the critical supersaturation may be readily obtained graphically without direct recourse to an equation of the type of (**41**) which requires $\Delta G^* \simeq 60kT$ to satisfy it (Fletcher 1960).

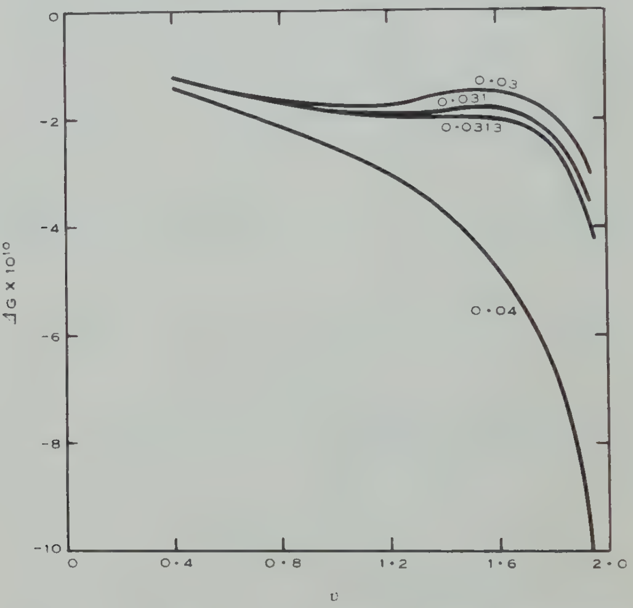

Fig. 6.—The variation in free energy of a liquid embryo with size. The ordinate gives the point of intersection of the generating curves (see Fig. 4). $R = 10^{-6}$ cm; $\theta = 10°$; temperature 0 °C; the curves are labelled with the values of $\log_{10} P/P_s$, the value 0·0313 being critical.

(i) *Condensation.*—If P is the partial pressure of water vapour in the gas and P_s that of the saturated vapour at the same temperature, then

$$\Delta G_V = -(RT/V_L) \ln (P/P_s), \qquad \ldots\ldots\ldots\ldots \quad \textbf{(42)}$$

where V_L is the molar volume of water, R the gas constant, and T the absolute temperature. We shall adopt the same values as did Fletcher for $\gamma_{12} = 75 \cdot 6$ erg cm^{-2} at 0° C. Using $\theta = 10°$, the variation of ΔG, at a given radius for a monomer particle, is calculated as a function of v_i, i.e. as the embryo increases in volume the meniscus will move around the sphere. Figure 6 shows the curves obtained at four different supersaturations. At $\log_{10} P/P_s = 0 \cdot 04$ the embryo grows spontaneously even from the smallest size. At 0·03 a hump has appeared in the curve and at this supersaturation the difference in free energy between the minimum (spontaneous capillary condensation) and the maximum is so large that the nucleation rate is infinitesimally small. A free energy barrier (the hump in the curve) for the required nucleation rate is 2×10^{-12} ergs per embryo, so that for an appreciable rate of nucleation only a plateau will be apparent, on the scale shown. This is found at $\log_{10} P/P_s=0\cdot0313$ for dimers of particle radius 10^{-6} cm.

Figure 7 compares the variation of P/P_s with the radii of the particles forming a dimer to that for monomer particles. It is only for particle radii between 10^{-6} and 10^{-7} cm that appreciable differences appear.

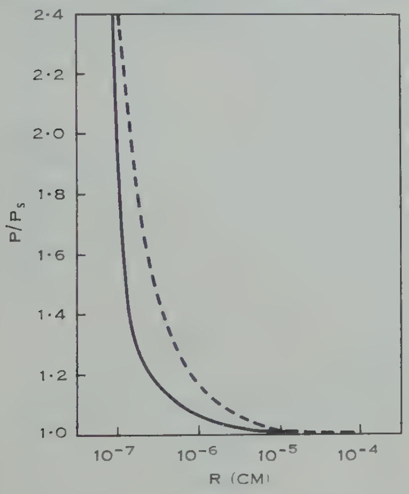

Fig. 7

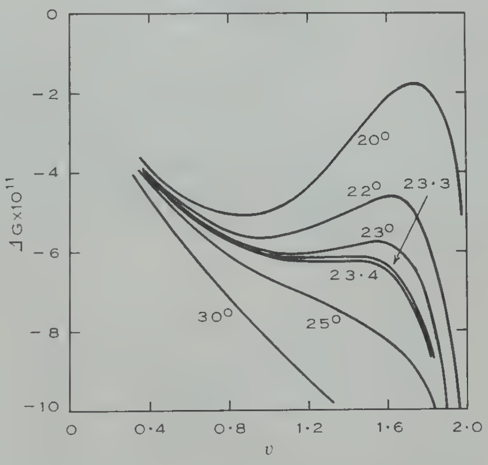

Fig. 8

Fig. 7.—The supersaturation, P/P_s, at which water condenses on a dimer consisting of particles of radius R. Temperature 0 °C ; contact angle 10°. The broken curve is for a monomer of radius R.

Fig. 8.—The variation in free energy with size of embryos formed by sublimation at different supersaturations; $R=10^{-6}$ cm; $\theta=10°$; curves are labelled with the values of ΔT (the supercooling), the value 23·4 °C being critical.

(ii) *Sublimation.*—The motive free energy is given by

$$\Delta G_V=-(RT/V_s)\ln(P_L/P_I), \qquad \ldots\ldots\ldots\ldots (43)$$

where V_s is the molar volume of ice, P_L is the vapour pressure of a flat water surface, and P_I that of a flat ice surface. Again, as treated by Fletcher (1958), we shall neglect effects of disregistry and lattice strain except insofar as these are included in the contact angle relating the surface free energies. The vapour pressure P_L may be related to the supercooling ($\Delta T=273-T°$) necessary for nucleation by

$$\log_{10}(P_L/P_I)=\alpha\Delta T, \qquad \ldots\ldots\ldots\ldots\ldots (44)$$

where $\alpha=0\cdot00972$/degC. A value of 100 erg cm^{-2} (Fletcher 1958) is assumed for γ_{12}. Figure 8 shows the variation in free energy for the growth of an embryo on a dimer consisting of particles of 10^{-6} cm radius. Figure 9 compares the supercooling required for different radii of monomer and dimer. It is apparent that the disability conferred on a particle by a finite contact angle is removed by the formation of dimers. There is, in principle, a considerable gain in the use of dimers formed by spheres in the useful range (10^{-6} to 10^{-5} cm) of sizes where a number of particles can be produced per unit weight of seeding material.

(iii) *Freezing.*—A similar calculation to that for sublimation is made for the process of nucleation by a dimer suspended in supercooled water. Here the γ_{12} value for the ice-water interface is taken as 20 erg cm^{-2} (Fletcher 1958) and the results are shown in Figure 10. Again there appears to be considerable advantage in the use of dimers or polymers.

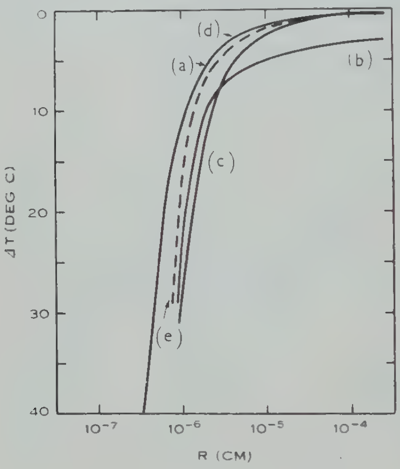

Fig. 9

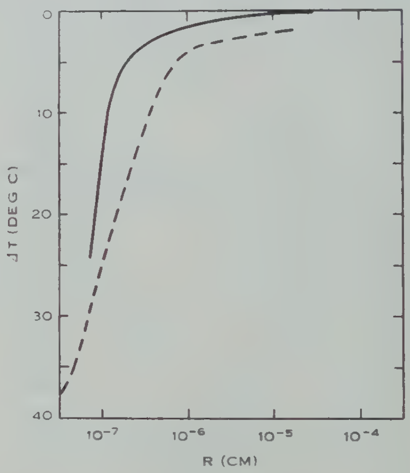

Fig. 10

Fig. 9.—The supercooling ΔT at which ice is formed by sublimation on : (*a*) a dimer consisting of spherical particles of radius R ; (*b*) a monomer (spherical particles) of radius R ; (*c*) a ledge of width and height l, and length l ; (*d*) a ledge of width and height l, and length $5l$; (curves (*a*) and (*d*) are superimposed). Contact angle 10° for (*a*), (*b*), (*c*), (*d*). (*e*) A monomer (spherical particles) of radius R but contact angle 0°.

Fig. 10.—The supercooling ΔT at which ice is formed by freezing on a dimer consisting of particles of radius R. Contact angle 10°. The broken curve is for a monomer of radius R.

V. Properties of a Ledge formed by Plate Dimers

If the aerosol of silver iodide is formed by evaporation, the particles are usually crystalline hexagonal plates. Suppose that a dimer forms by one plate lying partially over another. For simplicity consider a ledge, such as that shown in Figure 1 (*b*), in which the height and width are equal to l and its length is nl. For the calculation n will be chosen as 1 and 5.

It will be assumed that the embryo is contained by a cylindrical surface and having two ends cut square. This form of surface will *not* be that giving the minimum free surface energy and consequently the dimers will be more effective than we calculate. At undersaturations the embryo lies within the step and if the contact angle is greater than $\frac{1}{4}\pi$, Wylie (1952) has shown that it rests in the ledge as a segment of a sphere. At or near saturation the embryo meets the ledge edges A, B and during further growth the contact angle θ is indeterminate until the embryo forms the angle θ with the surfaces outside the ledges, when it may again move over the surface.

As long as the centres of the circles forming the embryo surface lie below AB, the curvature is convex, and the embryo is constrained between AB, the free surface energy is given by

$$\begin{aligned}\Delta G=\Delta G_V\omega\left\{\rho^2 \operatorname{arsin}\frac{l}{(\sqrt{2})\rho}+\tfrac{1}{2}l^2-\tfrac{1}{2}(2\rho^2-l^2)^{\frac{1}{2}}\right\}\\ +2\gamma_{12}\left\{\omega\left(\operatorname{arsin}\frac{l}{(\sqrt{2})\rho}-l\cos\theta\right)+\rho^2\operatorname{arsin}\frac{l}{(\sqrt{2})\rho}\right.\\ \left.-\tfrac{1}{2}(2\rho^2-l^2)^{\frac{1}{2}}+\tfrac{1}{2}l^2\right\}, \quad \ldots\ldots\ldots\ldots \quad \textbf{(45)}\end{aligned}$$

where ω, the length of the embryo, is less than or equal to nl and ρ is the radius of the surface. For the cylindrical surface taken, it may be shown that, provided the contact angle is less than 34°, the embryo fills the whole length of the ledge, i.e. $\omega=nl$, even at the maximum curvature of the surface. For surfaces of small curvature, like the flat surface joining AB, the contact angle may be as high as $\frac{1}{4}\pi$ before the embryo segments.

(*a*) *Calculation of the Relation between Size of Ledge and Nucleation*

Calculations were confined to sublimation nuclei using the constants of Section IV (*c*) (ii) and a value of $n=1$ and 5. The most rapid process was to plot the variations of ΔG with the volume of the embryo (the term attached to ΔG_V in equation (**45**)). The curves are similar in shape to Figure 8; Figure 9 shows the variation of supercooling with step height and length. The dimer forming a ledge, of height and width l, is not as effective as a dimer formed from spheres of radius R but most of this difference will arise from the choice of a free surface energy which is not minimal (see preceding section). The dimer formed with step lengths of $5l$ are apparently more effective but to form a step of length $5l$ the particles must have dimensions of at least $5l$ by l by l or more probably $5l$ by $5l$ by l, i.e. to the equivalents of particles of $1{\cdot}71R$ and $2{\cdot}92R$ respectively. Plotting the curve for the ledge dimer $5l$ using either of these values of R practically superimposes it on the ledge curve for a step l, i.e. the activity at a given ledge height per unit volume of dimer is constant. It is likely that ledge dimers of all sizes are as effective as dimers formed from spheres. It is certain that ledges are advantageous when the particles are large, for then the effect of a finite contact angle is almost removed.

VI. CONCLUSIONS

An aerosol allowed to aggregate will show a decrease in the total number of active particles but with an increasing proportion of particles active at higher temperatures. Where point contacts or ledges form (and, by inference, corners) these are likely to be very active in two senses. They generally raise the temperature at which nucleation is possible on a given substrate. This is of considerable importance since the number of natural clouds at temperatures close to 0° C exceeds those at the more usual temperature (−10 °C) where nucleation with silver iodide is effective. For a given mass of silver iodide it might well be more effective to dispense slightly coagulated smokes. If the particles in the smokes are tabular there may not be any advantage in coagulation, except for very coarse smokes, which are probably uneconomic in application anyway. Methods of producing monodisperse aerosols are being studied so that the various models may be differentiated.

VII. References

Fletcher, N. F. (1958).—*J. Chem. Phys.* **29**: 572.

Fletcher, N. F. (1960).—*Aust. J. Phys.* **13**: 408.

Green, H. L., and Lane, W. R. (1957).—"Particulate Clouds: Dusts, Smokes and Mists." pp. 126–66. (Spon Ltd.: London.)

von Smoluchowski, M. (1916).—*Phys. Z.* **17**: 557, 585.

von Smoluchowski, M. (1917).—*Z. Phys. Chem.* **92**: 129.

Wylie, R. G. (1952).—*Aust. J. Sci. Res.* A **5**: 618.

SHORT COMMUNICATIONS

THERMALLY ACTIVATED FERROMAGNETIC DOMAIN WALL MOTION*

By F. D. STACEY†

The properties of small ferromagnetic domains are influenced strongly by thermal agitation if the energies involved in transitions between different states of magnetization (rotations and domain wall movements) are only a few times kT (k being Boltzmann's constant and T the absolute temperature). The study of such small-scale magnetic phenomena, now known as " micromagnetics " (see, for example, Brown 1959*a*), has developed rapidly in recent years in response to commercial interests in fine powder permanent magnets and thin film memory cores. The possibility of observing directly thermally induced domain wall movements is therefore a matter of some interest. It appears that Olmen and Mitchell (1959) have made such an observation, although they did not specifically claim to have done so. The purpose of this note is to present an elementary theory of thermally activated domain wall motion and to show that the results reported by Olmen and Mitchell are in agreement with it.

The delayed response of magnetic domains to changes in external field is termed " magnetic viscosity " but some ambiguity has arisen from the two different physical processes involved. Domain wall velocities have been observed in metals by Sixtus and Tonks (1931, 1932) and in ferrites by Galt (1954). In both cases the velocity v in a field H is

$$v = G(H - H_0),$$

H_0 being a critical field (static coercive force) and G is a constant of the order 10^4 cm sec^{-1} oersted^{-1}. In metals the velocity is limited principally by eddy currents. Galt explained the velocities observed in ferrites in terms of the dissipation of anisotropy energy during ionic reordering in moving walls. Galt (1954) and George (1959) have referred to this latter process as magnetic viscosity.

The expression is also used for much slower changes in magnetic domains, such as were observed by Street and Woolley (1949) in " Alnico " and subsequently recognized as important phenomena in rock magnetism (e.g. by Néel 1955). This longer period magnetic viscosity is controlled by thermal activation, which must be invoked to explain the slow domain wall motion observed by Olmen and Mitchell.

Consider a domain wall crossing a sequence of potential barriers, which will be assumed for simplicity to have equal heights E_0. In the presence of a field H in the direction of the expanding domain, the energy which must be supplied to the wall in order to impel it across a barrier is

$$E = E_0 - \alpha H, \qquad \dots\dots\dots\dots\dots\dots\dots\dots \quad (1)$$

---

* Manuscript received March 22, 1960.

† Geophysics Department, Australian National University, Canberra.

where energy (αH) is supplied by the field during penetration of or " climbing up " the barrier. The wall can move freely only if $E \leqslant 0$, but if $E > 0$, movement can be induced thermally. The probability P of the wall acquiring in unit time sufficient thermal energy to cross a barrier is

$$P = C \exp\,(-E/kT). \qquad \ldots\ldots\ldots\ldots\ldots\ldots\ldots \quad (2)$$

Alternatively, P is the number of occasions per second on which the wall acquires thermal energy E which could impel it across the barrier. There are several calculations of the frequency factor C. Néel (1955) suggested 10^9 to 10^{10} sec^{-1} ; Stacey (1959*a*) obtained $C = 6 \times 10^{12}$ sec^{-1} at room temperature, but this must be regarded as an upper limit, as it expresses the probability of sufficient energy becoming instantaneously available rather than the probability that the wall will move sufficiently rapidly to make use of it (Stacey 1959*b*). A completely different formula for specific application to single domains has been given by Brown (1959*b*). In the following calculation two alternatives are assumed : (i) C is a large but arbitrary constant with negligible dependence upon parameters such as temperature. This leads to equations (**5A**) and (**6A**). (ii) C is proportional to T, as suggested by Stacey (1959*a*). This leads to the alternative equations (**5B**) and (**6B**). The difference is not very significant in the present case.

If the average separation of potential barriers in the direction of motion is d, then, assuming that the delay of the wall at each barrier is much greater than the time taken to move between barriers, the wall velocity v is given by

$$v = Pd = Cd \exp\,\{-(E_0 - \alpha H)/kT\}. \qquad \ldots\ldots\ldots\ldots \quad (3)$$

Putting $Cd = A$, $\alpha/k = B$, and $E_0/k = BH_0$, we obtain a simpler form

$$v = A \exp\,\{(B/T)(H - H_0)\}. \qquad \ldots\ldots\ldots\ldots\ldots\ldots \quad (4)$$

Equation (**4**) has the exponential dependence of wall velocity upon applied field which is required by the observations of Olmen and Mitchell. It must be noted that $H - H_0$ is necessarily negative in the range of interest as A is a large constant.

The temperature range of the observations was too limited to allow detailed comparison with (**4**) but the variation of v with T can be used to estimate the constant H_0, which is the field required to move the wall at 0 °K, or to move it very rapidly at any temperature. By differentiating equation (**4**) we obtain

$$\mathrm{d}(\ln v)/\mathrm{d}T = -B(H - H_0)/T^2 \qquad \ldots\ldots\ldots\ldots \quad (\mathbf{5A})$$

if the frequency factor C is independent of T, or

$$\mathrm{d}(\ln v)/\mathrm{d}T = -B(H - H_0)/T^2 + 1/T \qquad \ldots\ldots\ldots \quad (\mathbf{5B})$$

if C is proportional to T.

Examination of the data of Olmen and Mitchell shows that for their film $\mathrm{d}(\ln v)/\mathrm{d}T = 0 \cdot 09$ degC^{-1} at $T = 320$ °K and $H = 4 \cdot 0$ oersteds and that $B/T = 8 \cdot 8$ oersted^{-1}, so that from (**5A**) $H_0 = 7 \cdot 3$ oersteds, and from (**5B**) $H_0 = 7 \cdot 1_6$ oersteds. It is not possible to distinguish experimentally between these alternatives but, as the coercive force of the film when measured at 60 c/s was 7 oersteds and would therefore be slightly higher still at even more rapid switching, this must be regarded as an excellent agreement with the theoretical estimates of H_0.

Having determined H_0, the absolute values of measured velocity may be used to estimate A. From Olmen and Mitchell's data, at 4·0 oersteds switching field and 320 °K., spike velocity is 3×10^{-2} cm/sec. Taking true wall velocity as one-seventh of this, as noted by Olmen and Mitchell, we find

$$A = Cd = 1 \cdot 7 \times 10^{10} \text{ cm/sec} \qquad \ldots\ldots\ldots\ldots \quad \textbf{(6A)}$$

if C is independent of T, or

$$A = Cd = 0 \cdot 5 \times 10^{10} \text{ cm/sec} \qquad \ldots\ldots\ldots\ldots \quad \textbf{(6B)}$$

if C is proportional to T.

At this point an inadequacy of the simple theory must be noted. It has been assumed that the wall is inflexible and that it only meets one barrier at a time, neither of which can be true. Rather we should expect the wall to encounter a more or less straight line of elementary barriers and tend to fold round each of the barriers, making individual jumps past them. In this case the wall would effectively be divided into a large but unknown number of semi-independent sections, each opposed by a single elementary barrier. This allows a physically reasonable interpretation of the constant α in equation (**3**), since we may put

$$\alpha = 2atI_s,$$

where I_s is the saturation magnetization of the film, a is the average wall area of each effectively independent section of wall, and t is the effective half-thickness of the elementary potential barriers. However, this does not alter the foregoing equations, since we can consider the wall velocity of each section of wall separately in terms of the same equations.

If a direct microscopic observation could be made of the individual jumps of a slow-moving domain wall, so that d would be measured, the fundamental constant C could be estimated from equations (**6**). It may be noted as a preliminary result that a value of C as low as 10^{10} sec^{-1} does not appear to be consistent with the above figures, as it gives much too large a value of d. Taking the theoretical upper limit, $C = 6 \times 10^{12}$ sec^{-1} (at room temperature) we would expect to find $d \sim 10^{-3}$ cm. It therefore appears possible that such an observation could be made.

The helpfulness of suggestions by Dr. P. Gaunt of Sheffield University and Dr. W. A. Rachinger of the Aeronautical Research Laboratories, Melbourne, is gratefully acknowledged.

References

Brown, W. F. (1959*a*).—*J. Appl. Phys.* **30** : 62S.
Brown, W. F. (1959*b*).—*J. Appl. Phys.* **30** : 130S.
Galt, J. K. (1954).—*Bell Syst. Tech. J.* **33** : 1023.
George, R. G. (1959).—*Nature* **183** : 245.
Néel, L. (1955).—*Advanc. Phys.* **4** : 191.
Olmen, R. W., and Mitchell, E. N. (1959).—*J. Appl. Phys.* **30** : 258S.
Sixtus, K. J., and Tonks, L. (1931).—*Phys. Rev.* **37** : 930.
Sixtus, K. J., and Tonks, L. (1932).—*Phys. Rev.* **42** : 419.
Stacey, F. D. (1959*a*).—*Proc. Phys. Soc.* **73** : 136.
Stacey, F. D. (1959*b*).—*Phil. Mag.* **4** : 594.
Street, R., and Woolley, J. C. (1949).—*Proc. Phys. Soc.* A **62** : 562.

ON THE RELATION BETWEEN LUMINOSITY DISTANCE AND DOPPLER SHIFT IN RELATIVISTIC COSMOLOGY*

By R. VAN DER BORGHT†

Introduction

An approximate relation between luminosity distance D and Doppler shift δ in cosmology is usually obtained by a succession of complicated expansions in series.

In the present paper it is shown that an expression for D, even to a higher approximation in δ, can be obtained in a much simpler way.

The relation between luminosity distance D and red-shift δ commonly used in relativistic cosmology is (McVittie 1956)‡

$$D=\frac{c\delta}{h_1}\left(1+\frac{h_1^2+h_2}{2h_1^2}\delta\right), \qquad \ldots\ldots\ldots\ldots\ldots\ldots \quad (1)$$

where

$$h_1=\dot{R}(t_0)/R(t_0)=\dot{R}_0/R_0, \text{ i.e. the Hubble constant,} \qquad \ldots\ldots\ldots\ldots \quad (2)$$

and

$$h_2=\ddot{R}_0/R_0, \qquad \ldots\ldots\ldots\ldots\ldots\ldots\ldots\ldots \quad (3)$$

R being a function of t.

The exact expression for D is

$$D=\frac{R_0^2}{R}\,\frac{r}{1+\alpha r^2/4}, \qquad \ldots\ldots\ldots\ldots\ldots\ldots \quad (4)$$

where r is a function of R given by the null-geodesic equation

$$c\int_t^{t_0}\frac{\mathrm{d}t}{R(t)}=\int_0^r\frac{\mathrm{d}r}{1+\alpha r^2/4}. \qquad \ldots\ldots\ldots\ldots\ldots\ldots \quad (5)$$

The constant $\alpha=+1$ for an elliptic space,
$=0$ for a flat space,
$=-1$ for a hyperbolic space.

The left-hand side of (5) could be written

$$c\int_t^{t_0}\frac{\mathrm{d}t}{R(t)}=c\int_R^{R_0}\frac{\mathrm{d}R}{R\dot{R}},$$

and therefore

$$\int_0^r\frac{\mathrm{d}r}{1+\alpha r^2/4}=\psi, \qquad \ldots\ldots\ldots\ldots\ldots\ldots \quad (6)$$

---

* Manuscript received March 30, 1960.

† Visiting Fellow, A.N.U., Mount Stromlo Observatory, Canberra.

‡ McVittie, G. C. (1956).—"General Relativity and Cosmology." (Chapman & Hall: London.)

where

$$\psi = c\int_R^{R_0} \frac{\mathrm{d}R}{R\dot{R}}. \qquad \ldots\ldots\ldots\ldots\ldots\ldots\ldots \quad (7)$$

If $\alpha = +1$ it follows from (6) that

$$r = 2\tan\tfrac{1}{2}\psi,$$

and substituting this in (4) we have the following expression for the luminosity distance

$$D = (R_0^2/R)\sin\psi. \qquad \ldots\ldots\ldots\ldots\ldots\ldots \quad (8)$$

It is also easily seen that:

if $\alpha = 0$,
$$D = (R_0^2/R)\psi, \qquad \ldots\ldots\ldots\ldots\ldots\ldots\ldots\ldots \quad (9)$$

if $\alpha = -1$,
$$D = (R_0^2/R)\sinh\psi. \qquad \ldots\ldots\ldots\ldots\ldots \quad (10)$$

Elliptic and Hyperbolic Spaces

For these spaces

$$D = (R_0^2/R)F(R), \qquad \ldots\ldots\ldots\ldots\ldots\ldots\ldots \quad (11)$$

where

$$F(R) = \genfrac{}{}{0pt}{}{\sin}{\sinh}\left(c\int_R^{R_0}\frac{\mathrm{d}R}{R\dot{R}}\right), \qquad \ldots\ldots\ldots\ldots\ldots \quad (12)$$

the *sin* corresponding to the elliptic space and *sinh* to the hyperbolic one.

Using a Taylor expansion for F, we have

$$F(R) = F(R_0) + \left(\frac{\mathrm{d}F}{\mathrm{d}R}\right)_{R_0}(R-R_0) + \left(\frac{\mathrm{d}^2F}{\mathrm{d}R^2}\right)_{R_0}\frac{(R-R_0)^2}{2} + \left(\frac{\mathrm{d}^3F}{\mathrm{d}R^3}\right)_{R_0}\frac{(R-R_0)^3}{6} + \ldots, \qquad \ldots\ldots\ldots\ldots \quad (13)$$

where, firstly, $F(R_0) = 0$,

secondly,

$$\frac{\mathrm{d}F}{\mathrm{d}R} = -c\genfrac{}{}{0pt}{}{\cos}{\cosh}\left(c\int_R^{R_0}\frac{\mathrm{d}R}{R\dot{R}}\right)\frac{1}{R\dot{R}},$$

that is,

$$\left(\frac{\mathrm{d}F}{\mathrm{d}R}\right)_{R_0} = \frac{-c}{R_0\dot{R}_0}, \qquad \ldots\ldots\ldots\ldots\ldots\ldots\ldots\ldots\ldots \quad (14)$$

thirdly,

$$\frac{\mathrm{d}^2F}{\mathrm{d}R^2} = \pm c^2\genfrac{}{}{0pt}{}{\sin}{\sinh}\left(c\int_R^{R_0}\frac{\mathrm{d}R}{R\dot{R}}\right)\frac{-1}{R^2\dot{R}^2} - c\genfrac{}{}{0pt}{}{\cos}{\cosh}\left(c\int_R^{R_0}\frac{\mathrm{d}R}{R\dot{R}}\right)\frac{\mathrm{d}}{\mathrm{d}R}\left(\frac{1}{R\dot{R}}\right). \qquad \ldots\ldots \quad (15)$$

But

$$\frac{\mathrm{d}}{\mathrm{d}R}\left(\frac{1}{R\dot{R}}\right) = \frac{\mathrm{d}}{\mathrm{d}t}\left(\frac{1}{R\dot{R}}\right)\frac{\mathrm{d}t}{\mathrm{d}R} = -\frac{\dot{R}^2 + R\ddot{R}}{R^2\dot{R}^3}. \qquad \ldots\ldots\ldots\ldots \quad (16)$$

Substituting this in (15),

$$\frac{\mathrm{d}^2F}{\mathrm{d}R^2} = \mp c^2\genfrac{}{}{0pt}{}{\sin}{\sinh}\left(c\int_R^{R_0}\frac{\mathrm{d}R}{R\dot{R}}\right)\frac{1}{R^2\dot{R}^2} + c\genfrac{}{}{0pt}{}{\cos}{\cosh}\left(c\int_R^{R_0}\frac{\mathrm{d}R}{R\dot{R}}\right)\frac{\dot{R}^2 + R\ddot{R}}{R^2\dot{R}^3}, \qquad \ldots\ldots \quad (17)$$

and

$$\left(\frac{\mathrm{d}^2F}{\mathrm{d}R^2}\right)_{R_0}=c\frac{\dot{R}_0^2+R_0\ddot{R}_0}{R_0^2\dot{R}_0^3}. \qquad \ldots\ldots\ldots\ldots\ldots\ldots\ldots\ldots \quad \mathbf{(18)}$$

Fourthly,

$$\begin{aligned}\frac{\mathrm{d}^3F}{\mathrm{d}R^3}=&\mp c^3\begin{matrix}\cos\\ \cosh\end{matrix}\left(c\int_R^{R_0}\frac{\mathrm{d}R}{R\dot{R}}\right)\frac{-1}{R^3\dot{R}^3}\\ &\mp c^2\begin{matrix}\sin\\ \sinh\end{matrix}\left(c\int_R^{R_0}\frac{\mathrm{d}R}{R\dot{R}}\right)(-2R^{-3}\dot{R}^{-1}-2R^{-2}\dot{R}^{-3}\ddot{R})\frac{1}{\dot{R}}\\ &\pm c^2\begin{matrix}\sin\\ \sinh\end{matrix}\left(c\int_R^{R_0}\frac{\mathrm{d}R}{R\dot{R}}\right)\frac{\dot{R}^2+R\ddot{R}}{R^3\dot{R}^4}\\ &+c\begin{matrix}\cos\\ \cosh\end{matrix}\left(c\int_R^{R_0}\frac{\mathrm{d}R}{R\dot{R}}\right)\left(-\frac{2}{R^3}-\frac{2\ddot{R}}{R^2\dot{R}^2}+\frac{\dddot{R}}{\dot{R}^3R}-\frac{3\ddot{R}^2}{R\dot{R}^4}\right)\frac{1}{\dot{R}},\end{aligned}$$

and

$$\left(\frac{\mathrm{d}^3F}{\mathrm{d}R^3}\right)_{R_0}=\pm\frac{c^3}{R_0^3\dot{R}_0^3}+\frac{c}{\dot{R}_0}\left\{-\frac{2}{R_0^3}-\frac{2\ddot{R}_0}{R_0^2\dot{R}_0^2}+\frac{\dddot{R}_0}{\dot{R}_0^3R_0}-\frac{3\ddot{R}_0^2}{R_0\dot{R}_0^4}\right\}. \quad \ldots \quad \mathbf{(19)}$$

Substituting (**14**), (**18**), and (**19**) in (**13**) we have

$$\begin{aligned}F(R)=&-\frac{c}{R_0\dot{R}_0}(R-R_0)+c\frac{\dot{R}_0^2+R_0\ddot{R}_0}{R_0^2\dot{R}_0^3}\,\frac{(R-R_0)^2}{2}\\ &+\left\{\pm\frac{c^3}{R_0^3\dot{R}_0^3}+\frac{c}{\dot{R}_0}\left[-\frac{2}{R_0^3}-\frac{2\ddot{R}_0}{R_0^2\dot{R}_0^2}-\frac{3\ddot{R}_0^2}{R_0\dot{R}_0^4}+\frac{\dddot{R}_0}{\dot{R}_0^3R_0}\right]\right\}\frac{(R-R_0)^3}{6}.\end{aligned}$$

$$\ldots\ldots\ldots\ldots \quad \mathbf{(20)}$$

Substituting this in (**11**) and remembering that

$$1-R_0/R=-\delta,$$

and

$$R=R_0/(1+\delta)=R_0(1-\delta+\delta^2-\delta^3\ .\ .\ .),$$

we have

$$\begin{aligned}D=&-\frac{cR_0}{R}(-\delta)+c\frac{\dot{R}_0^2+R_0\ddot{R}_0}{\dot{R}_0^3}R_0(1-\delta+\delta^2-\delta^3\ .\ .\ .)\frac{(-\delta)^2}{2}\\ &+\left\{\pm\frac{c^3}{R_0\dot{R}_0^3}+\frac{c}{\dot{R}_0}\left[-\frac{2}{R_0}-\frac{2\ddot{R}_0}{\dot{R}_0^2}+\frac{\dddot{R}_0R_0}{\dot{R}_0^3}-\frac{3\ddot{R}_0^2R_0}{\dot{R}_0^4}\right]\right\}\frac{(-\delta)^3}{6}R_0^2(1-\delta+\delta^2\ .\ .\ .)^2,\end{aligned}$$

or, after a few reductions,

$$\begin{aligned}D=&\frac{c}{h_1}\delta+c\frac{h_1^2+h_2}{2h_1^3}\delta^2\\ &-\left\{\frac{c}{6}\,\frac{h_1^2+h_2}{h_1^3}+\frac{c}{6h_1}\left[\frac{h_3}{h_1^3}-3\frac{h_2^2}{h_1^4}\right]\pm\frac{c^3}{6R_0^2h_1^3}\right\}\delta^3. \quad \ldots\ldots \quad \mathbf{(21)}\end{aligned}$$

This is the luminosity distance–red-shift relation, correct to the third order in δ. The plus sign in the last term is used for elliptic spaces and the minus sign for hyperbolic ones.

Flat Spaces

In this case the luminosity distance is given by

$$D=\frac{R_0^2}{R}c\int_R^{R_0}\frac{dR}{R\dot{R}},\quad \text{i.e.}\quad F=C\int_R^{R_0}\frac{dR}{R\dot{R}}. \qquad \text{(22)}$$

Then, firstly,

$$\left(\frac{dF}{dR}\right)_{R_0}=-\frac{c}{R_0\dot{R}_0}, \qquad \text{(23)}$$

secondly,

$$\left(\frac{d^2F}{dR^2}\right)_{R_0}=c\frac{\dot{R}_0^2+R_0\ddot{R}_0}{R_0^2\dot{R}_0^3}, \qquad \text{(24)}$$

thirdly,

$$\left(\frac{d^3F}{dR^3}\right)_{R_0}=\frac{c}{\dot{R}_0}\left(-\frac{2}{R_0^3}-\frac{2\ddot{R}_0}{R_0^2\dot{R}_0^2}-\frac{3\ddot{R}_0^2}{R_0\dot{R}_0^4}+\frac{\dddot{R}_0}{\dot{R}_0^3R_0}\right). \qquad \text{(25)}$$

It is evident, by comparison of (**14**), (**18**), (**19**) and (**23**), (**24**), (**25**) that the luminosity distance–red-shift relation is

$$D=\frac{c}{h_1}\delta\left\{1+\frac{h_1^2+h_2}{2h_1^2}\delta-\frac{1}{6}\left[\frac{h_1^2+h_2}{h_1^2}+\left(\frac{h_3}{h_1^3}-3\frac{h_2^2}{h_1^4}\right)+\frac{\alpha c^2}{R_0^2h_1^2}\right]\delta^2\right\}, \qquad \text{(26)}$$

where $\alpha=+1$ for an elliptic space,
$\alpha=0$ for a flat space,
$\alpha=-1$ for a hyperbolic space,

and

$$h_3=\dddot{R}_0/R_0.$$

The first two terms in (**26**) give

$$D=\frac{c}{h_1}\delta+c\frac{h_1^2+h_2}{2h_1^3}\delta^2, \qquad \text{(27)}$$

which is the formula commonly used in relativistic cosmology and which does not distinguish between the three types of spaces.

STUDY OF THE FLARE–SURGE EVENT OF SEPTEMBER 7, 1958*†

By KAREN M. LOWMAN‡ and D. E. BILLINGS‡

Giovanelli and McCabe (1958) indicate that, while most flare-surges appear dark against the solar disk throughout the greater part of their existence, it is not uncommon for a surge in its earliest stages, just as it leaves the flare, to be bright. Rapidly moving material that remains bright against the solar disk for a longer time is much less frequently observed. Of the cases of longer lasting bright surges that have been reported as exceptional events by Dodson and Hedeman (1949, 1952), Ellison (1950), Dodson and McMath (1952), Bray, Loughhead, Burgess, and McCabe (1957), and Reid (1959), those reported by Dodson and McMath, by Bray *et al.*, and by Reid appear to be detached and rapidly moving portions of flares, whereas the remainder did not attain flare brightness.

The surge event of September 7, 1958 remained bright against the solar disk for several minutes, but was clearly less bright than the flare from which it appeared to originate. A somewhat unusual programme of filming rate and exposure times used by the Climax observers contributed significantly to the detail with which the progress of the surge could be followed. During the early stages of the surge, four photographs were made per minute with an exposure time adapted to bring out the features on the solar disk, while a fifth exposure each minute was sufficiently long to show prominence features beyond the limb. About 4 min after flare maximum the exposure rate was increased to two frames every 2 sec, one timed to bring out disk features, the other to bring out limb features. There were several frames that were exposed for an extra-long time, probably as a result of faulty shutter operation. On these very long exposures faint features in the surge could be detected that otherwise would have gone unnoticed.

Immediately after flare maximum, bright surge material was observed tracing a path across the Sun's disk, from the edge of the flare to the limb, then beyond the limb. Some material seemed to part from the main mass and drift more nearly radially toward the limb, while the main body of the surge intersected a tangent to the limb at an angle of approximately 50°.

In order to study the motion of the surge, we measured the radial distance of the leading edge of the surge from the limb, both before and after it crossed the limb. These measurements of radial distance, plotted against time, are shown in Figure 1, the velocity in the early stages being 470 km/sec.

---

* The research reported in this paper was supported by the National Academy of Sciences as part of the International Geophysical Year Programme, with the assistance of a grant from the Ford Foundation.

† Manuscript received December 23, 1959.

‡ The High Altitude Observatory of the University of Colorado, Boulder, Colorado, U.S.A.

The surge crossed the limb at 1452 U.T. through a low prominence which had appeared on the limb about 1 hr earlier. Figure 2, which is a composite of 29 sketches of the leading edge of the surge, chosen at 30 sec intervals, gives a representation of the trajectory of the surge. Preceding the main body of the surge was a more diffuse and less well defined, slightly slower-moving mass of material which rose even higher, to over 100,000 km beyond the limb.

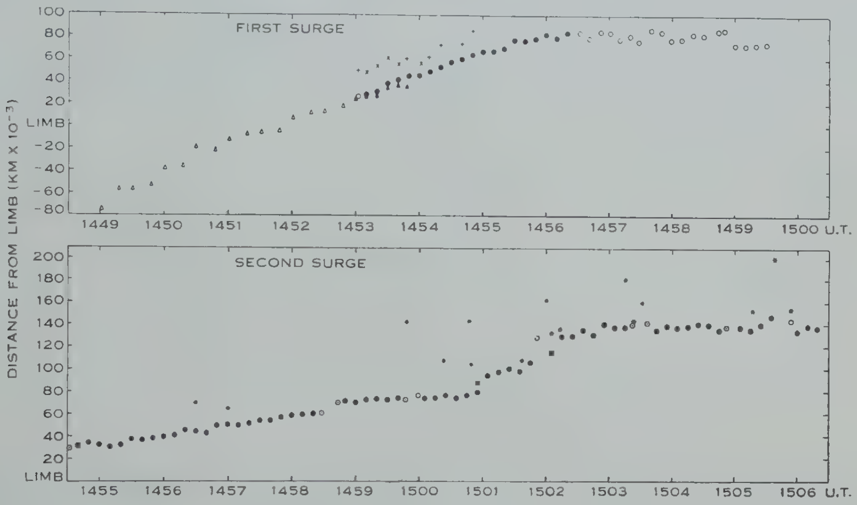

Fig. 1.—Variation of surge position with time; surge of September 7, 1958, at P.A. 72°.

Number of exposures on which point is based:	1	2 or 3	4 or 5
Intense feature seen on normal (disk) exposures	△		▲
Intense feature seen beyond limb	○	⊙	●
Diffuse forerunner seen beyond limb	*	+	×

At about 1454 : 30–1455 U.T., $2\frac{1}{2}$–3 min after the first surge crossed the limb, a second, somewhat larger and more spectacular surge began building up gradually beyond the limb, slightly north of the first, and rising essentially perpendicular to the limb.

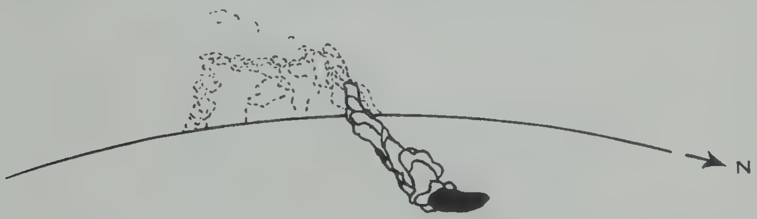

Fig. 2.—Composite sketch showing the flare at 1449 U.T. (black area) and the trajectory of the first surge from 1449 U.T. until 1502 U.T., with positions of the leading edge drawn at 30 second intervals. The solid outline is from normal exposures; the dotted outline from longer exposures.

The initial motion of this second surge was slow and the surge itself difficult to distinguish from a pre-existing prominence on the limb. In its earlier phase this surge was arch-shaped, with a strikingly bright knot of emission located within the centre of the top of the arch. The arch gradually took on a more columnar shape with an enlarged top containing the bright knot. This " column " rose between the above-mentioned prominence and the first surge. As it rose the arch-like characteristics of the lower levels disappeared and the prominence assumed its former outline on the limb.

Six minutes after the first suggestion of this slow-starting second surge, some very fast material seemed to break through it and speed upward with a velocity (between 1500 : 30 and 1502 : 19 U.T.) of nearly 520 km/sec. Thereafter, at about 130,000 km from the limb, it slowed down but continued to move, ultimately reaching a distance of more than 140,000 km. A few extra-long exposed frames of the film show material in the region between 170,000 and 200,000 km beyond the limb. Figure 3 is a composite of 15 sketches of the leading edge of the second surge, at 1-min intervals.

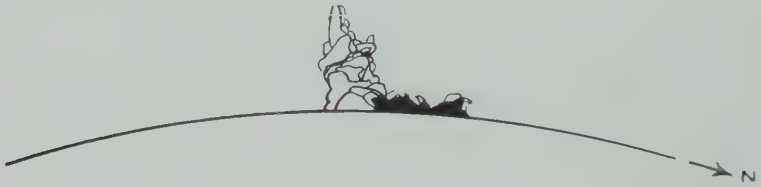

Fig. 3.—Composite sketch of the leading edge of the second surge at 60 second intervals, between 1452 and 1506 U.T. Darkened outline shows the initial stable prominence.

We next examined the flare around 1455 : 30 U.T., which should have been the time that material would have left the flare, at 520 km/sec, in order to appear at the limb at 1458 : 15 U.T. However, no noticeable special event within the flare could be found on the photographs. The only direct evidence found to connect this second surge with the flare were slight traces of dark and bright material apparently extending from the flare into the base of the surge.

Table 1

DEDUCED ELECTRON DENSITIES

Height above the Chromosphere (km)	Electron Density (cm^{-3})
40,000±10,000	$4{\cdot}2\times10^{8}$
70,000	$2{\cdot}5\times10^{8}$
80,000	$1{\cdot}9\times10^{8}$

Of the various solar radio noise emission features that were reported as beginning about the time of the maximum phase of the flare by Boulder, Cornell, Ottawa, and Fort Davis, an unclassified burst of intensity 1, having some features of a type II burst, and lasting from 1449·7–1455 U.T., appeared to be the most likely to be associable with either surge. This burst was recorded at Fort Davis in the 100–580 Mc/s frequency range, along with a small group of moderate intensity type III bursts at 1449–50 U.T. of the type described by Giovanelli (1958), and an unclassified burst of slight intensity at 1457 U.T.

By comparing Figure 1 with a reproduction of the Fort Davis sweep-frequency record kindly furnished us by Dr. Alan Maxwell, we have been able to deduce a rough correspondence between the optically determined position of the front of the first surge and the frequency of maximum emission in the simultaneous unclassified burst. Then, by equating the second harmonic of plasma frequency to the observed burst frequency, in accordance with the March 1, 1957 observation of Giovanelli and Roberts (1958), and estimating the height of the surge above the chromosphere by the distance, measured normal to the limb, from the centre of the flare to the front of the surge, we deduce the electron densities given in Table 1.

These densities, and the corresponding scale height of approximately 56,000 km, seem quite reasonable for a region in the corona overlying a large amount of solar activity.

References

Bray, R. J., Loughhead, R. E., Burgess, V. R., and McCabe, Marie K. (1957).—*Aust. J. Phys.* **10** : 319.

Dodson, Helen W., and Hedeman, Ruth E. (1949).—*Astrophys. J.* **110** : 242.

Dodson, Helen W., and Hedeman, Ruth E. (1952).—*Observatory* **72** : 30.

Dodson, Helen W., and McMath, R. R. (1952).—*Astrophys. J.* **115** : 78.

Ellison, M. A. (1950).—*Publ. R. Obs. Edinb.* **1** (4) : 61.

Giovanelli, R. G. (1958).—*Aust. J. Phys.* **11** : 350.

Giovanelli, R. G., and McCabe, Marie K. (1958).—*Aust. J. Phys.* **11** : 191.

Giovanelli, R. G., and Roberts, J. A. (1958).—*Aust. J. Phys.* **11** : 353.

Reid, J. H. (1959).—*Observatory* **79** : 96.

DISTRIBUTION OF AURORAS IN THE SOUTHERN HEMISPHERE*

By F. R. Bond† and F. Jacka†

Several attempts to delineate the southern zone of maximum frequency of visibility of auroras have led to widely discrepant results. That of White and Geddes (1939) suffered through lack of observations ; that of Vestine and Snyder (1945) was based on observed relations between morphology of geomagnetic disturbance and auroras in the northern hemisphere, and application to the southern hemisphere using very limited geomagnetic data. It may be, too, that the distribution of auroras changes slowly with solar activity.

The data obtained in Antarctica during the International Geophysical Year 1957–58 offer the possibility of a new study of the geographic distribution of auroras around the epoch of solar activity maximum. To be entirely satisfactory this study must take into account a number of factors not yet considered even in relation to the now extensive body of northern hemisphere data. The geographic distribution is different for different auroral forms ; there is a marked diurnal variation in latitude and a strong dependence of latitude on level of world-wide magnetic disturbance (Jacka 1953). It is also desirable that the distribution of auroras be specified with a resolution in latitude much less than the width of the curve of frequency of occurrence versus latitude.

As a first step in such a study I.G.Y. data from the Australian National Antarctic Research Expeditions' (ANARE) stations Mawson and Macquarie Island have been used to make a tentative estimate of the location of the isoaurore of maximum frequency of occurrence of auroras with discernible lower borders.

From measured angles of elevation and azimuth to points on the auroral lower borders, assumed at a constant height of 105 km, the positions of all auroras were plotted on synoptic maps at 15 minute intervals. From these maps the frequency of occurrence versus geomagnetic latitude was determined on a number of geomagnetic meridians. The frequency distributions all have a mode within a few degrees of the observer's latitude. Because some faint auroras observable overhead may not be observable at lower elevations it is possible that the observed modal latitude is shifted a little towards the observer's latitude. We have therefore taken as our estimate of the latitude of the mode, the mid point of the range in which the frequency exceeds 2/3 the maximum observed frequency. These estimated positions are marked by crosses in Figure 1.

These data are very meagre, so we tentatively introduce the hypothesis that the isoaurores are symmetrical about the geomagnetic meridian through the magnetic dip pole. Guided by the Mawson and Macquarie Island data and

---

* Manuscript received April 4, 1960.

† Antarctic Division, Department of External Affairs, Melbourne.

this hypothesis the full line curve on Figure 1 was drawn as a tentative representation of the isoaurore of maximum frequency of occurrence of auroras with discernible lower borders.

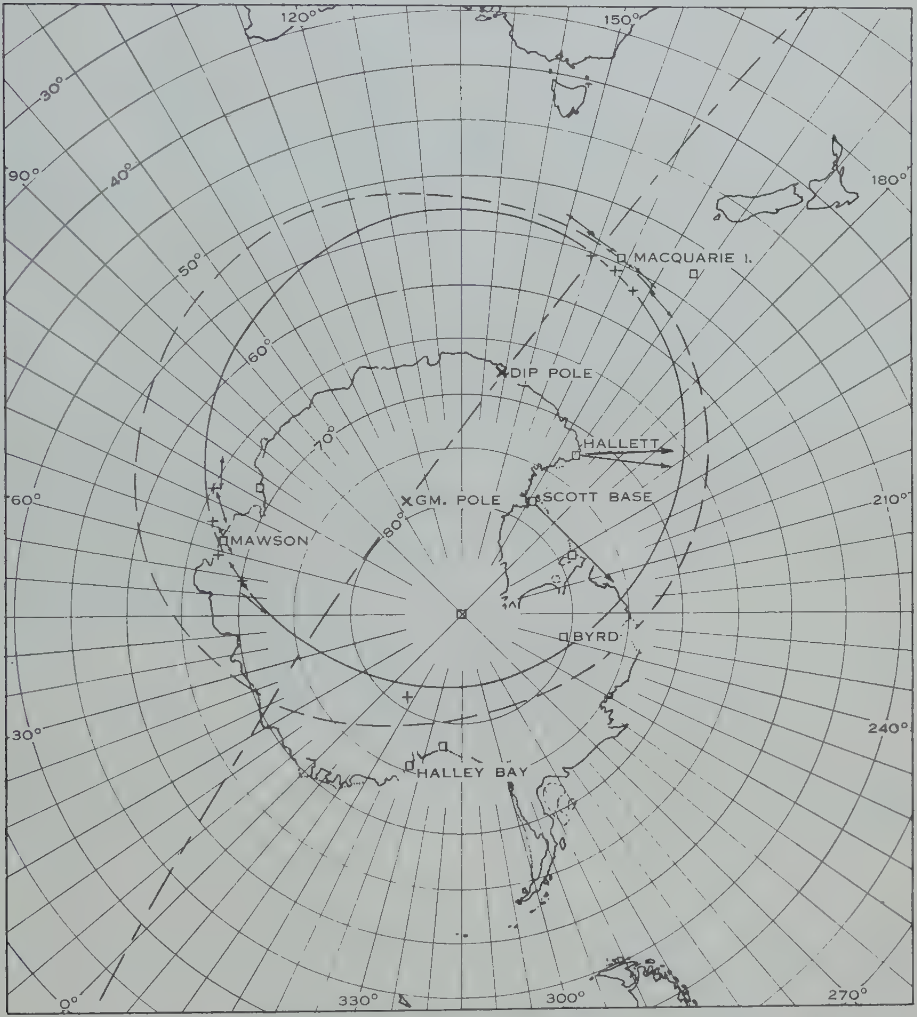

Fig. 1.—Full line curve : estimate of the isoaurore of maximum frequency of occurrence of auroras with discernible lower borders based on observed positions denoted by crosses in the regions of Macquarie Island and Mawson and assuming symmetry about the geomagnetic meridian through the dip pole. Dashed curve : Hultqvist's projection from 5·6 Earth radii in the geomagnetic equatorial plane.

The cross near geographic longitude 345° E. indicates the position of most frequent occurrence of auroral arcs estimated from the data summarized by Evans and Thomas (1959) for Halley Bay. This point is in reasonable agreement with our curve.

If Figure 1 is not grossly in error, there is one other I.G.Y. station (Byrd) from which the maximum frequency isoaurore should be observed at high elevation and several (marked by squares on Figure 1) from which it might be observed at low elevation and consequently low reliability.

The synoptic maps also permit the measurement of orientation of auroras relative to the meridians. The orientation angles show a small diurnal variation but the frequency distribution of angles is fairly narrow and roughly symmetrical. The mean orientations of arcs and simply shaped bands on a number of meridians near Mawson and Macquarie Island are indicated by short double-ended arrows on Figure 1. These are approximately parallel with the estimated isoaurore. We expect then that the mean value of azimuth (taking values 180° apart as equivalent) to the nearest (greatest elevation) point of arcs is perpendicular to the isoaurores. Two such azimuths (from data of Hatherton and Salmon (1959)) are indicated by arrows from Scott Base and Hallett in Figure 1. Agreement with our estimated isoaurore is reasonable.

In the region well inside the maximum frequency isoaurore, even the general form of the geographical distribution of auroras is uncertain. There is, however, mounting evidence for the existence of an inner zone of maximum frequency.

At this stage it is perhaps desirable to seek some correspondence with northern hemisphere data. Hultqvist (1958, 1959) has shown that projections from circles in the geomagnetic equatorial plane, along the actual magnetic field lines, onto the Earth's surface, produce oval curves which very closely parallel the auroral isochasms in the northern hemisphere. Using Hultqvist's data, we find that a circle of $5 \cdot 6$ Earth radii projects onto the dashed curve in Figure 1. The discrepancy between the curve and our maximum frequency isoaurore is so great as to cast doubts on the soundness of this approach to the problem of revealing a correspondence between the two hemispheres. On the other hand, Hultqvist's projections are based on geomagnetic field data of epoch 1945 which were very scanty in high latitudes, especially in the southern hemisphere.

The authors are now seeking data from other antarctic stations to enable more comprehensive study of the distribution and morphology of auroras in the southern hemisphere.

References

EVANS, S., and THOMAS, G. M. (1959).—*J. Geophys. Res.* **64** : 1381.

HATHERTON, T., and SALMON, K. J. (1959).—Antarctic Symposium, Buenos Aires.

HULTQVIST, B. (1958).—*Ark. Geofys.* **3** (4) : 63.

HULTQVIST, B. (1959).—*Nature* **183** : 1478.

JACKA, F. (1953).—*Aust. J. Phys.* **6** : 219.

VESTINE, E. H., and SNYDER, E. J. (1945).—*Terr. Magn. Atmos. Elect.* **50** : 105.

WHITE, F. W. G., and GEDDES, M. (1939).—*Terr. Magn. Atmos. Elect.* **44** : 367.

THE STRESS FIELDS AROUND SOME DISLOCATION ARRAYS*

By A. K. HEAD†

The stress fields around some edge dislocation arrays have been calculated using the approximation of Leibfried (1951) that the discrete dislocations are replaced by a continuous dislocation density. Haasen and Leibfried (1954) have calculated one such stress distribution (corresponding to (ii) below) via the stress function which they evaluated as a superposition integral over the dislocation distribution of the stress function of an infinitesimal dislocation. The results given here were evaluated directly as the superposition of the stress fields of the infinitesimal dislocations making up the distribution. Like most of the integrals which occur in this approximation, they can be evaluated most readily by contour integration (Haasen and Leibfried 1954). A multiple coordinate system is used and is such that the results can be written compactly and approximations and limiting cases can be easily obtained.

(i) Blocks at $x=\pm a$ with n positive dislocations between $x=b$ and $x=a$ and n negative dislocations between $x=-b$ and $x=-a$ which are held apart by an applied shear stress σ (Head and Louat 1955 (vi)).

The components of stress at a point $P(x,y)$ are

$$\sigma_{xx}=\sigma\left(\frac{\rho_1\rho_2}{r_1r_2}\right)^{\frac{1}{2}}\left[\frac{Ry}{\rho_1\rho_2}\cos\{\eta-\tfrac{1}{2}(\varphi_1+\varphi_2+\theta_1+\theta_2)\}-\frac{Ry}{r_1r_2}\cos\{\eta+\tfrac{1}{2}(\varphi_1+\varphi_2)-\frac{3}{2}(\theta_1+\theta_2)\}+2\sin\tfrac{1}{2}(\varphi_1+\varphi_2-\theta_1-\theta_2)\right], \quad \ldots\ldots\ldots\ldots (1)$$

$$\sigma_{yy}=\sigma\left(\frac{\rho_1\rho_2}{r_1r_2}\right)^{\frac{1}{2}}\left[-\frac{Ry}{\rho_1\rho_2}\cos\{\eta-\tfrac{1}{2}(\varphi_1+\varphi_2+\theta_1+\theta_2)\}+\frac{Ry}{r_1r_2}\cos\{\eta+\tfrac{1}{2}(\varphi_1+\varphi_2)-\frac{3}{2}(\theta_1+\theta_2)\}\right], \quad \ldots (2)$$

$$\sigma_{xy}=\sigma\left(\frac{\rho_1\rho_2}{r_1r_2}\right)^{\frac{1}{2}}\left[-\frac{Ry}{\rho_1\rho_2}\sin\{\eta-\tfrac{1}{2}(\varphi_1+\varphi_2+\theta_1+\theta_2)\}+\frac{Ry}{r_1r_2}\sin\{\eta+\tfrac{1}{2}(\varphi_1+\varphi_2)-\frac{3}{2}(\theta_1+\theta_2)\}+\cos\tfrac{1}{2}(\varphi_1+\varphi_2-\theta_1-\theta_2)\right], \quad \ldots\ldots\ldots\ldots (3)$$

where (R,η), (r_1,θ_1), (r_2,θ_2), (ρ_1,φ_1), (ρ_2,φ_2) are polar coordinates, as shown in Figure 1. The expression (3) for the shear stress is the total shear stress including the applied shear stress σ.

---

* Manuscript received February 12, 1960.

† Division of Tribophysics, C.S.I.R.O., Melbourne.

(ii) Haasen and Leibfried (1954) have considered the special case of (i) for $b=0$. This can be derived from (i) by putting $R=\rho_1=\rho_2$, $\eta=\varphi_1=\varphi_2$, and then (**1**)–(**3**) are equivalent to their result.

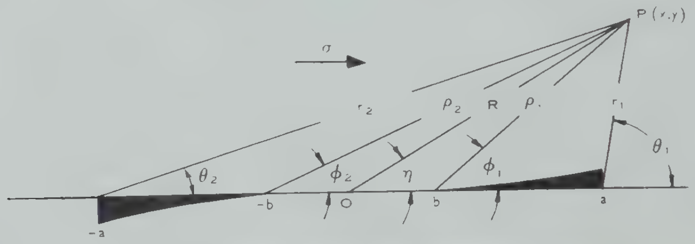

Fig. 1.—Coordinate system for equations (**1**)–(**3**).

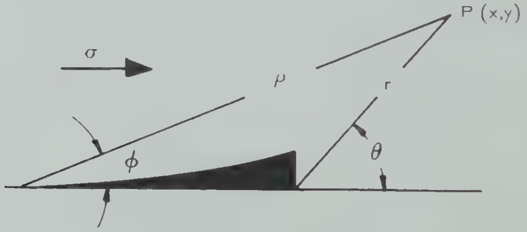

Fig. 2.—Coordinate system for equations (**4**)–(**6**).

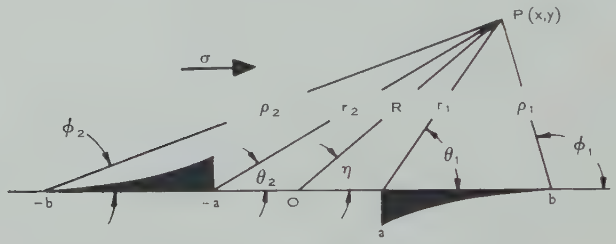

Fig. 3.—Coordinate system for Section (iv).

(iii) If the negative dislocations in (i) are removed to infinity by putting $r_2=\rho_2=2R=\infty$, $\varphi_2=\eta=\theta_2=0$, we are left with Figure 2, a group of positive dislocations forced against a block by a shear stress σ (Head and Louat 1955 (iv)), and (**1**)–(**3**) become

$$\sigma_{xx}=\tfrac{1}{2}\sigma(\rho/r)^{\frac{1}{2}}\left[\frac{y}{\rho}\cos\tfrac{1}{2}(\theta+\varphi)-\frac{y}{r}\cos\tfrac{1}{2}(\varphi-3\theta)+4\sin\tfrac{1}{2}(\varphi-\theta)\right], \quad \ldots \ (4)$$

$$\sigma_{yy}=\tfrac{1}{2}\sigma(\rho/r)^{\frac{1}{2}}\left[-\frac{y}{\rho}\cos\tfrac{1}{2}(\theta+\varphi)+\frac{y}{r}\cos\tfrac{1}{2}(\varphi-3\theta)\right], \quad \ldots\ldots\ldots\ldots \ (5)$$

$$\sigma_{xy}=\tfrac{1}{2}\sigma(\rho/r)^{\frac{1}{2}}\left[\frac{y}{\rho}\sin\tfrac{1}{2}(\theta+\varphi)+\frac{y}{r}\sin\tfrac{1}{2}(\varphi-3\theta)+2\cos\tfrac{1}{2}(\varphi-\theta)\right]. \quad \ldots \ (6)$$

The stresses near the head of the pile-up will be given approximately by putting

$$\rho\simeq L,\ \varphi\simeq 0,\ r\ll L,\ y=r\sin\theta$$

(where L is the length of the pile-up). Equations (**4**)–(**6**) then become the approximate expressions derived by Stroh (1954) from consideration of a pile-up of discrete dislocations.

(iv) Figure 3 is example (vii) from Head and Louat (1955) with n positive dislocations beyond $x=-a$ and n negative dislocations beyond $x=a$, driven together by a shear stress σ but prevented from coalescing by blocks at $x=\pm a$. The stress field in this case is also given by (**1**)–(**3**) if the symbols are reinterpreted as in Figure 3.

References

Haasen, P., and Leibfried, G. (1954).—*Nachr. Akad. Wiss. Göttingen* No. 2, 31.
Head, A. K., and Louat, N. (1955).—*Aust. J. Phys.* **8**: 1.
Leibfried, G. (1951).—*Z. Phys.* **130**: 214.
Stroh, A. N. (1954).—*Proc. Roy. Soc.* A **223**: 404.

THE OPTIMUM LINE WIDTH FOR A REFLECTION CAVITY MASER*

By G. J. Troup†

Introduction

It has been pointed out previously (Troup 1959, hereinafter referred to as I) that there is an optimum line width for the transition used in a reflection cavity maser and that this optimum line width gives maximum bandwidth for a given gain. However, it was not explicitly deduced in I that this optimum line width actually gives the maximum value of $(\text{Gain})^{\frac{1}{2}}\times$Bandwidth product for a given cavity maser system. This note makes the appropriate deduction.

The Line Width for Maximum $(Gain)^{\frac{1}{2}}\times$Bandwidth Product

Commencing with equation (**3**) of I, we have that the gain G of a reflection cavity maser is given to a good approximation by

$$G\simeq(|Q_m|+Q_L)^2(|Q_m|-Q_L)^{-2}, \qquad \ldots\ldots\ldots\ldots (1)$$

where Q_L is the loaded Q of the cavity and $|Q_m|$ is the modulus of the negative molecular Q.

The bandwidth B of a reflection cavity maser, assuming a Lorentz line shape for the amplifying transition, is given by (equation (**4**) of I)

$$B\simeq\delta[(|Q_m|/Q_L)-1][1+\delta|Q_m|/f]^{-1}, \qquad \ldots\ldots\ldots (2)$$

where δ is the line width of the amplifying transition and f is the centre frequency of both cavity and molecular responses.

Using equations (**1**) and (**2**), we get

$$G^{\frac{1}{2}}B\simeq\delta[(|Q_m|/Q_L)+1][1+\delta|Q_m|/f]^{-1}. \qquad \ldots\ldots\ldots\ldots (3)$$

---

* Manuscript received April 29, 1960.

† Weapons Research Establishment, Salisbury, S. Aust.

Now for reasonably large gains ($G>10$ say) $|Q_m|\simeq Q_L$, so that

$$G^{\frac{1}{2}}B\simeq 2\delta(1+\delta\,|Q_m|/f)^{-1}. \qquad \text{(4)}$$

Now the molecular Q, Q_m, is of the form (equation (**2**) of I)

$$|Q_m|=K\delta/N^*, \qquad \text{(5)}$$

where K is a constant for the particular active material and cavity system, and N^* is the number density of excess molecules in the emissive state.

Using equation (**5**), we rewrite equation (**4**) as

$$G^{\frac{1}{2}}B\simeq 2\delta[1+(K\delta^2/N^*f)]^{-1}. \qquad \text{(6)}$$

Differentiation of this expression with respect to δ shows that $G^{\frac{1}{2}}B$ has a maximum value

$$(G^{\frac{1}{2}}B)_{\text{max.}}=(K/N^*f)^{-\frac{1}{2}}, \qquad \text{(7)}$$

when $\delta=(K/N^*f)^{-\frac{1}{2}}=\delta_{\text{opt.}}$. The quantity $\delta_{\text{opt.}}$ is identical with the value of δ deduced in I to give maximum bandwidth at a given gain. This means that suitable adjustment of the transition line width δ, keeping all other parameters constant, can maximize the (Gain)$^{\frac{1}{2}}$ ×Bandwidth product.

Conclusion

In the paramagnetic maser, the simplest way of adjusting δ is clearly to use a magnetic field deliberately made inhomogeneous. This of course requires that $\delta<\delta_{\text{opt.}}$ initially. The discovery of the narrowness of the lines of Fe^{3+} in Ti_2O_3 (Butcher and Gill 1959; Low 1960) makes the technique described above particularly applicable to this material. Moreover, Townes *et al.* at Columbia have obtained a (Gain)$^{\frac{1}{2}}$ ×Bandwidth product of 250 Mc/s at 4500 Mc/s using ruby (Cr^{3+} in Al_2O_3) as the active medium, by the use of magnetic field inhomogeneity (Butcher and Gill 1959). This latter result is taken as experimental confirmation of the existence of an optimum line width for a given maser system. It also confirms that the use of an inhomogeneous magnetic field is a practicable way of adjusting the line width.

Note added in Proof.—Maiman (1960) has come to the same conclusions regarding optimum line width, and has pointed out some of the consequences for paramagnetic masers.

The author is indebted to Dr. J. E. Houldin, Physics Department, Chelsea Polytechnic, London, for encouraging the submission of this note for publication. Permission to publish has been granted by the Chief Scientist, Research and Development Branch, Department of Supply, Australia.

References

Butcher, P. N., and Gill, J. C. (1959).—Report on the Conference on Quantum Electronics, New York September 1959 : Royal Radar Establishment Memorandum No. 1667.

Low, W. (1960).—Paramagnetic substances suitable for maser operation in the millimeter range. " Proceedings of the Symposium on Millimeter Waves." p. 45. (Polytechnic Institute of Brooklyn Press : New York.)

Maiman, T. H. (1960).—Temperature and concentration effects in a ruby maser. *In* " Quantum Electronics." (Ed. C. H. Townes.) p. 324. (Columbia Univ. Press.)

Troup, G. J. (1959).—*Aust. J. Phys.* **12** : 218.

PHOTOPROTONS FROM TANTALUM*

By J. H. CARVER,† R. B. TAYLOR,† and W. TURCHINETZ†

Photoproton emission from tantalum has been studied by measuring the yield of the 5·5 hr isomer of ^{180}Hf produced in the $^{181}\mathrm{Ta}(\gamma,p)^{180\mathrm{m}}\mathrm{Hf}$ reaction. The experimental arrangements were similar to those used in a previous investigation (Carver and Turchinetz 1958) of the photodisintegration of tantalum, except that the shielding of the scintillation counter, a $1\frac{1}{2}$ in. diameter by 2 in. long NaI(Tl) crystal, has now been improved along the lines described by Pringle, Turchinetz, and Funt (1955). Larger quantities of tantalum (65 g) were used in the present experiments and, with these improvements, it was possible to separate the 5·5 hr ^{180}Hf activity from the similar, and more abundant, 2·1 hr ^{178}Ta activity produced in the $^{181}\mathrm{Ta}(\gamma,3n)^{178}\mathrm{Ta}$ reaction.

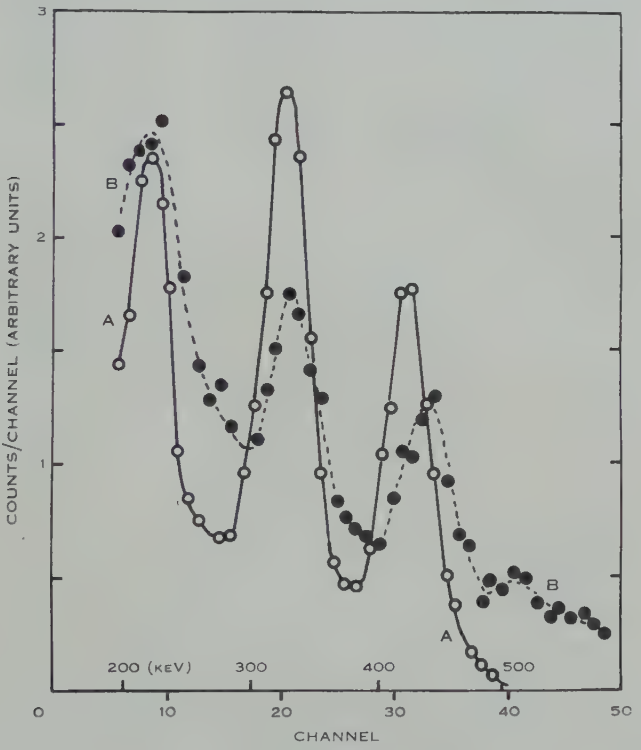

Fig. 1.—γ-Ray spectra of 5·5 hr ^{180}Hf and 2·1 hr ^{178}Ta. Spectrum B was measured 20 hr after spectrum A and corresponds mainly to ^{180}Hf.

In the energy region from 200 to 500 kV ^{180}Hf has γ-ray lines at 216, 332, 443, and 501 keV, and ^{178}Ta has lines at 214, 326, 332, and 427 keV (Strominger,

---

* Manuscript received May 23, 1960.

† Research School of Physical Sciences, Australian National University, Canberra.

Hollander, and Seaborg 1958). At lower energies the γ-ray spectrum is dominated by 8·15 hr ^{180}Ta produced in the ^{181}Ta(γ,n)^{180}Ta reaction. The difference between the γ-ray spectra of ^{180}Hf and ^{178}Ta is illustrated in Figure 1, which shows two of the observed spectra. Spectrum B of Figure 1 was measured 20 hr after spectrum A and corresponds mainly to ^{180}Hf. An analysis of the decay of these γ-ray lines, an example of which is shown in Figure 2, indicates that there are two components with half-lives of 5·5 and 2·1 hr, corresponding to ^{180}Hf and ^{178}Ta respectively. It is interesting to note that the half-life of ^{178}Ta obtained in this way is the same as that measured by Wilkinson (1950), whereas if no correction is made for the 5·5 hr component a value of 2·5 hr is obtained (Carver and Turchinetz 1958). In this analysis a small correction has been made for the bremsstrahlung produced by the β-particles of 8·15 hr ^{180}Ta which is produced in the ^{181}Ta(γ,n) reaction. This correction was made by irradiating a tantalum sample at 15 MeV, where there is no yield of ^{178}Ta or ^{180}Hf, and normalizing the bremsstrahlung tail to the intensity of the 55 keV X-ray peak.

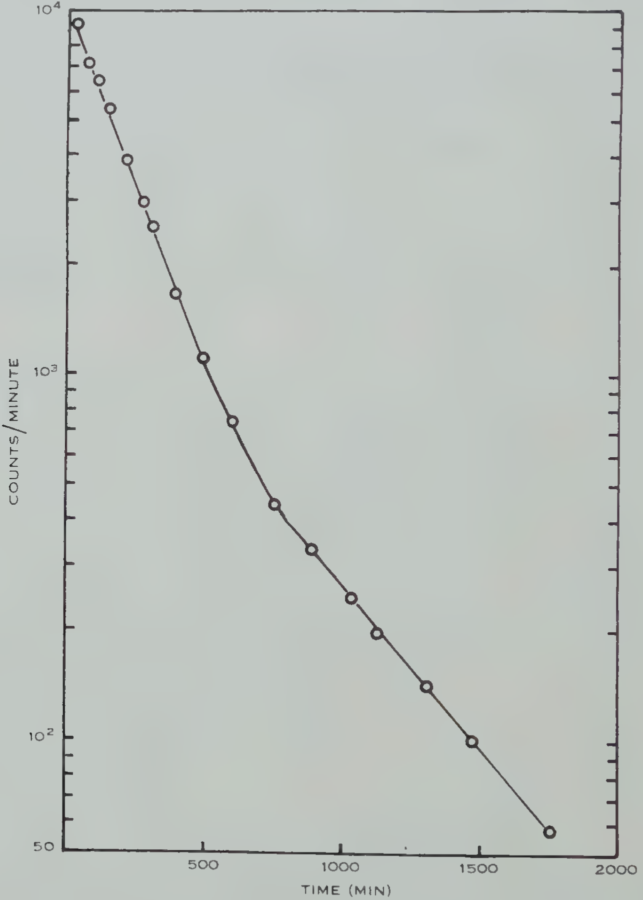

Fig. 2.—Decay curve for the 5·5 hr ^{180}Hf and 2·1 hr ^{178}Ta γ-rays of Figure 1.

The measured yield function and the derived cross-section curve for the ^{181}Ta(γ,p)^{180m}Hf reaction are shown in Figure 3. The points on the yield function were obtained from a least squares analysis of the 5·5 hr ^{180}Hf plus 2·1 hr ^{178}Ta γ-rays. The absolute cross-section scale was derived by comparison of these yields with the 10 min ^{62}Cu activity induced in copper foils using the absolute ^{63}Cu(γ,n) cross-section data of Berman and Brown (1954). This method is similar to that previously used to determine the (γ,n), (γ,$2n$), and (γ,$3n$) cross sections in ^{181}Ta (Carver and Turchinetz 1958).

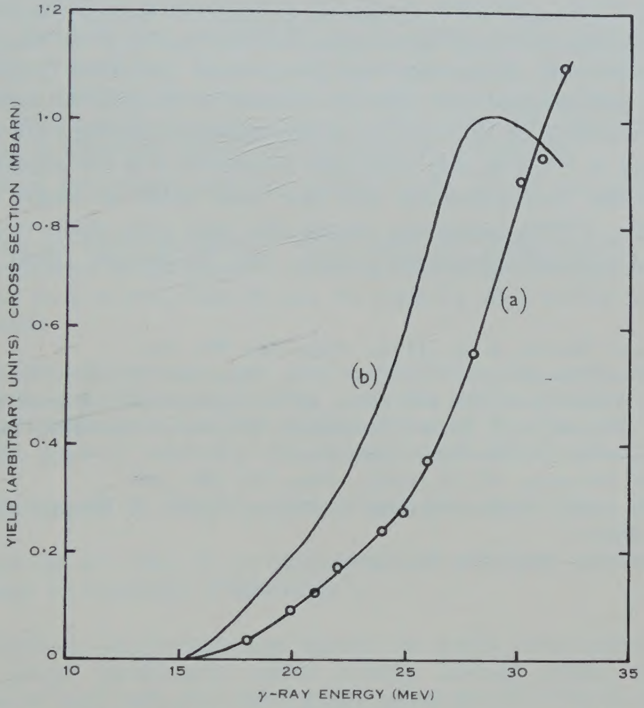

Fig. 3.—(*a*) The yield curve and (*b*) the derived cross section for the ^{181}Ta(γ,p)^{180m}Hf reaction.

The threshold for the ^{181}Ta(γ,p) reaction is 6·7 MeV (Wapstra 1958), but owing to the effect of the Coulomb barrier there is no appreciable yield below a γ-ray energy of ~16 MeV. The ^{181}Ta(γ,p) reaction leading to the 5·5 hr isomer of ^{180}Hf has a peak cross section of 1·0 mbn at a γ-ray energy of 28 MeV and an integrated cross section to 32 MeV of (10 ± 2) MeV mbn* which corresponds to 0·3 per cent. of the total integrated γ-ray absorption cross section. Owing to the difference between the shapes of the (γ,p) and the total γ-ray cross section the yield for the (γ,p) reaction leading to the isomeric state is 0·1 per cent. of the total yield for all γ-ray processes. Most of the previous data about (γ,p) cross sections in the heavy nuclei have been obtained with 23 MeV bremsstrahlung (e.g. Toms and Stephens 1955). The present results, together with those obtained for caesium and iodine by Taylor (1960) in this laboratory, indicate that higher energy γ-rays make a considerable contribution to the photoproton emission.

---

* Approximately equal contributions to the error come from the analysis of the decay curves and from the comparison of the ^{180}Hf plus ^{178}Ta yields with the ^{62}Cu yield. There is a smaller error, 6 per cent., in Berman and Brown's (1954) estimate of the integrated ^{63}Cu(γ,n) cross section on which the present determination is based.

Toms and Stephens (1955) used photographic plates to measure the total photoproton yield from tantalum for 23 MeV bremsstrahlung. Combining their result with the present measurements suggests that at 23 MeV the $5 \cdot 5$ hr isomeric state is populated in $\sim$10 per cent. of the (γ,p) disintegrations. The spin of the $5 \cdot 5$ hr level of ^{180}Hf is probably 9 and the ground states of ^{180}Hf and ^{181}Ta have spins 0 and 7/2 respectively (Strominger, Hollander, and Seaborg 1958), so that the present results are consistent with the general rule that in the production of an isomeric pair the member with spin closest to that of the target nucleus is favoured. If the bulk of the (γ,p) reactions proceeds through direct transitions leading to states in ^{180}Hf of only moderate excitation it is not surprising that the magnitude of the preference for the low spin state is larger than in the $^{181}\mathrm{Ta}(\gamma,3n)^{178}\mathrm{Ta}$, $^{178\mathrm{m}}$Ta reactions, where the high spin state is populated in 30 per cent. of the disintegrations (Carver and Turchinetz 1958).

References

Berman, A. I., and Brown, K. L. (1954).—*Phys. Rev.* **96** : 83.

Carver, J. H., and Turchinetz, W. (1958).—*Proc. Phys. Soc.* **71** : 613, 618.

Pringle, R. W., Turchinetz, W., and Funt, B. L. (1955).—*Rev. Sci. Instrum.* **26** : 859.

Strominger, D., Hollander, J. M., and Seaborg, G. T. (1958).—*Rev. Mod. Phys.* **30** : 585.

Taylor, R. B. (1960).—*Nuclear Phys.* (In press.)

Toms, M. E., and Stephens, W. E. (1955).—*Phys. Rev.* **98** : 626.

Wapstra, A. H. (1958).—" Encyclopaedia of Physics." (Ed. S. Flugge.) Vol. 38/1, p. 1. (Springer : Berlin.)

Wilkinson, G. (1950).—*Phys. Rev.* **80** : 495.

CORRIGENDA

VOLUME 13, NUMBER 2A, PAGES 451–9

" *Susceptibility of Chromium-based Alloys of Transition Elements* "

Pages 451, 453, and 458 : *For* Neel *read* Néel.

Page 453, line 20 : The expression within the braces should read :

$$\left\{\frac{1}{kT}\,\mathrm{sech}^2\frac{\Delta}{kT}+\frac{2}{\Delta}\tanh\frac{\Delta}{kT}\right\}.$$

Page 453, line 22 : *Insert* as proportional *before* to.

AUSTRALASIAN MEDICAL PUBLISHING CO. LTD.
SEAMER AND ARUNDEL STS., GLEBE, SYDNEY

NOTICE TO CONTRIBUTORS

1. GENERAL.—Papers will be considered for publication irrespective of the organization to which the authors are attached. Intending contributors, in preparing papers for submission, should follow the general style adopted in this Journal. A " Guide to Authors " may be obtained on application to the Editor.

   Papers, which should be written as concisely as possible, should be double-space typed on one side of the paper only and with liberal side margins. Every page, including those carrying tables and illustrations, should be numbered. Lengthy manuscripts should be accompanied by a table of contents with headings appropriately numbered. The organization to which the author is attached should be indicated in a footnote.

   The original typescript and one carbon copy should be forwarded.

2. SUMMARY.—A short summary, which may be paragraphed, should precede the introduction to the paper. It should be of an informative character and written in such a way that it can be used by abstracting journals without amendment.

3. REFERENCES.—References are to be cited in the text by the year of publication, e.g. Thomson (1948), and are to be arranged alphabetically, giving the author's name and initials followed by the year of publication, title of the paper (if desired), title of the periodical, volume, and pages, thus :

   Thomson, G. P. (1948).—*Proc. Phys. Soc. Lond.* **61** : 403–16.

   Abbreviations of titles of periodicals should conform to those used in " A World List of Scientific Periodicals ".

4. ILLUSTRATIONS.—Line drawings should be made with indian ink on white drawing paper (preferably bristol board), tracing paper, or graph paper. Only blue or very pale grey ruled graph paper should be used as yellow, green, and red lines are difficult to screen out. Blue linen should not be used. Lines should be sufficiently thick and symbols sufficiently large to allow of reduction to a page size of 7¾ by 5 in. (or less). It is suggested that figures be drawn approximately twice the width at which they are to be printed. Lettering and numbering should only be pencilled on the drawings as the appropriate type will be substituted before the blocks are made. Original drawings should be submitted but, where possible, photographic copies or blue-prints of the originals should also be forwarded.

   Half-tone photographs, which should be included only where essential, should be on glossy paper and show as much contrast as possible.

5. REPRINTS.—Individual authors receive 40 copies of each paper free, two authors receive 30 each, and three or more authors receive 20 each, but additional copies may be purchased.

CONTENTS

PAGE

The Constant Flux Problem in Non-uniform Exponential Media. By P. R. Wilson 461

Magnetic Bays at Macquarie Island. By C. S. Robertson 470

Motion of the Aurora and Magnetic Bays. By F. R. Bond 477

A Dynamo Theory of the Aurora and Magnetic Disturbance. By K. D. Cole 484

Rayleigh Wave Dispersion for a Single Layer on an Elastic Half Space. By B. A. Bolt and J. C. Butcher 498

The Photodisintegration of Rare Earth Elements. By H. H. Thies and B. M. Spicer 505

Southern Hemisphere Meteor Shower Activity in July and August. By A. A. Weiss 522

Meteor Height Distributions and the Fragmentation Hypothesis. By A. A. Weiss 532

On the Identification of Extragalactic Radio Sources. By B. Y. Mills .. 550

Free Path Formulae for the Coefficient of Diffusion D and Velocity of Drift W of Ions and Electrons in Gases. By L. G. H. Huxley .. 578

Heterogeneous Nucleation by Aggregates of Particles. By R. B. Head and K. L. Sutherland 584

Short Communications

Thermally Activated Ferromagnetic Domain Wall Motion. By F. D. Stacey 599

On the Relation between Luminosity Distance and Doppler Shift in Relativistic Cosmology. By R. Van der Borght 602

Study of the Flare-Surge Event of September 7, 1958. By Karen M. Lowman and D. E. Billings 606

Distribution of Auroras in the Southern Hemisphere. By F. R. Bond and F. Jacka 610

The Stress Fields around some Dislocation Arrays. By A. K. Head .. 613

The Optimum Line Width for a Reflection Cavity Maser. By G. J. Troup 615

Photoprotons from Tantalum. By J. H. Carver, R. B. Taylor, and W. Turchinetz 617

Corrigenda 620

AUSTRALASIAN MEDICAL PUBLISHING CO. LTD.
SEAMER AND ARUNDEL STS., GLEBE, SYDNEY